Alma Mater Studiorum – Università degli Studi di Bologna

DOTTORATO DI RICERCA IN SCIENZE BIOMEDICHE E NEUROMOTORIE

Ciclo XXX

Settore Concorsuale di afferenza: 05/D1

Settore Scientifico disciplinare: BIO/09

"PHARMACOTHERAPIES TARGETED TO NEUROGENESIS IN ORDER TO RESCUE COGNITIVE PERFORMANCE IN DOWN SYNDROME"

Dr. Andrea Giacomini

Coordinatore Dottorato

Prof. Lucio Cocco

Relatore

Prof.ssa Renata Bartesaghi

Esame finale anno 2018

Abstract

Down syndrome (DS) is a genetic condition caused by the triplication of chromosome 21 (HSA21). DS has a worldwide incidence of 1:700-1000 live births. The most invalidating feature of DS is intellectual disability (ID). ID, that lifelong affects DS individual, is mainly due to neurodevelopment alterations, characterized by reduced neurogenesis and defects in neuron maturation. These defects are already present during early fetal life stages. The molecular mechanisms that are at the basis of these phenotypic alterations of DS have not been fully understood so far, due to the extremely complicated genetic imbalance of trisomy 21. In the last decade, scientists have exploited DS mouse models in order to clarify the molecular mechanisms whereby gene triplication leads to the trisomy-linked brain phenotype and design possible interventions. The most studied DS model is the Ts65Dn mouse whose phenotype largely mimics the human condition. However, despite intense efforts of scientific community, **there are currently no therapies for DS**. Considering the time course of brain development, pharmacotherapies should be carried as early as possible during the lifespan. But is it possible to pharmacologically rescue the neurodevelopmental defects of DS? Our group has recently found that neonatal treatment with fluoxetine, an antidepressant belonging to the selective serotonin reuptake inhibitor class, resulted in the restoration of neurogenesis and behavioral deficits in Ts65Dn mice. These results showed for the first time that the trisomy-linked brain defects are reversible, provided that therapy is administered very early during the lifespan. Clinical trials are necessary in order to establish whether fluoxetine has the same positive impact in children with DS as in neonate Ts65Dn mice. Since we cannot take for granted that a molecule that is effective in mouse models is similarly effective in humans, it is important to establish whether there are other molecules that are as effective as fluoxetine. Such an extensive approach would increase the probability to discover therapies that are effective in humans too. Based on these premises, the overall goal of this project was to establish whether **neonatal treatment with "unexplored" molecules restores the major neurodevelopmental defects and cognitive performance in the Ts65Dn mouse model and whether their effect is retained after treatment cessation.** In this study, I have explored the effects of three different molecules administered to Ts65Dn mice during the neonatal period. 1) **ELND006**, a selective inhibitor of APP γ-secratase. ELND006 blocks the formation of a small APP-derived peptide, AICD, which inhibits the activity of the mitogenic SHH pathway, thereby reducing neurogenesis. 2) Epigallocatechin-3-gallate (**EGCG**), a natural inhibitor of the kinase DYRK1A, whose overactivity in the DS brain negatively affects neurogenesis. 3) 7,8-dihydroxyflavone (**7,8-DHF**), a natural mimetic of BDNF that by activating the TRKB receptor may compensate for the reduced levels of BDNF in the DS brain and, thus, the lack of the pro-neurogenic actions of BDNF. Neonatal treatment with ELND006 restored neurogenesis and neuron number in the dentate gyrus (DG) and synaptic development in the hippocampal formation of Ts65Dn mice. Most of these effects were retained at one month after treatment cessation and were accompanied by restoration of the synaptic function at the synapse between DG granule cells and field CA3 pyramidal neurons. However, ELND006 treatment caused some adverse effects. In Ts65Dn mice neonatally treated with EGCG, we found full restoration of hippocampal neurogenesis, neuron number and synapse development. At one month after treatment cessation, however, these effects had disappeared and there were no signs of behavioral improvement. 7,8-DHF, administered in neonate Ts65Dn mice, caused restoration of neurogenesis, DG granule cell number, and dendritic spine density. Mice that were treated with 7,8-DHF from postnatal day 3 to adolescence exhibited restoration of learning and memory, indicating that the recovery of the hippocampal anatomy translated into a functional rescue. No adverse effects were observed on the general health and growth of mice. A comparison of the three therapies used in this study indicates that although all are able to rescue neurogenesis, targeting the BDNF/TRKB pathway with 7,8-DHF may represent the treatment with the highest translational

impact for children with DS because it is effective and appears to have a high safety profile. Demonstration that it is possible to pharmacologically prevent brain developmental alterations in a mouse model of DS with a variety of agents may stimulate the design of clinical trials with the molecule/s with the highest efficacy and the safest profile. This is the challenge that faces the community of preclinical researchers interested in DS: to transform a dream into reality.

Abstract (italiano)

La sindrome di Down (SD) è una condizione genetica dovuta alla triplicazione del cromosoma 21. La SD ha una incidenza a livello mondiale di 1:700-1000 nati vivi. L'aspetto più invalidante della SD è la disabilità intellettiva (DI). La DI, che colpisce gli individui con la SD durante tutta la vita, è principalmente dovuta ad alterazioni del neurosviluppo, caratterizzate a loro volta da riduzioni dei processi di neurogenesi e maturazione neuronale. Questi difetti sono già presenti durante le prime fasi dello sviluppo fetale. Ad oggi, i meccanismi molecolari che sono alla base delle alterazioni fenotipiche della SD non sono stati compresi completamente, a causa dello sbilanciamento genico estremamente complesso della trisomia 21. Negli ultimi 10 anni, la comunità scientifica si è avvalsa di modelli murini di SD per comprendere più approfonditamente i meccanismi molecolari che portano al fenotipo cerebrale legato alla trisomia e, di conseguenza, sviluppare possibili strategie terapeutiche. Il modello murino di SD più studiato è il topo Ts65Dn, che mima in modo dettagliato la condizione umana. Nonostante gli intensi sforzi profusi dalla comunità scientifica, **al momento non esistono terapie per la SD**. Tenendo in considerazione l'andamento dello sviluppo cerebrale, un approccio farmacologico dovrebbe essere effettuato il prima possibile durante la vita degli individui. Ma è possibile ripristinare farmacologicamente i difetti del neurosviluppo tipici della SD? Il nostro gruppo ha recentemente effettuato un trattamento neonatale nel topo Ts65Dn con fluoxetina, un antidepressivo appartenente alla classe degli inibitori selettivi della ricaptazione della serotonina. Il trattamento è stato in grado di ripristinare la neurogenesi e le funzioni cognitive nei topi Ts65Dn. Questi risultati hanno mostrato, per la prima volta, che i difetti cerebrali legati alla trisomia sono reversibili, a patto che la terapia sia somministrata nelle fasi precoci della vita. Trials clinici saranno necessari per stabilire se la fluoxetina abbia nei bambini con SD lo stesso impatto positivo che ha avuto nei topi neonati. Non si può dare per scontato cha gli effetti positivi di una molecola osservati in un modello di topo siano riscontrabili anche nell'uomo; pertanto, è di estrema importanza stabilire se ci siano altre molecole efficaci quanto la fluoxetina. Sulla base di queste premesse, l'obiettivo generale di questo progetto è stato quello di stabilire se **un trattamento neonatale con molecole "inesplorate" fosse in grado di ripristinare i principali difetti del neurosviluppo e cognitivi nel topo Ts65Dn, e se gli effetti fossero mantenuti dopo la cessazione del trattamento.** In questo studio, ho valutato gli effetti di tre molecole differenti somministrate al topo Ts65Dn durante il periodo neonatale. 1) **ELND006**, un inibitore selettivo della γ-secratasi. ELND006 blocca la formazione di un piccolo peptide derivante da APP, AICD, che inibisce a sua volta l'attività mitogenica della via di segnalazione SHH, provocando quindi una riduzione del processo di neurogenesi. 2) Epigallocatechina-3-gallato (**EGCG**), un inibitore naturale della chinasi DYRK1A, la cui iper-attivazione nel cervello SD influenza negativamente il processo di neurogenesi. 3) 7,8-diidrossiflavone (**7,8-DHF**), una molecola naturale che mima l'attività del BDNF tramite l'attivazione del recettore TRKB. 7,8-DHF potrebbe compensare la scarsa produzione di BDNF (e quindi riduzione del processo di neurogenesis) nel cervello SD. Il trattamento neonatale con ELND006 ha ripristinato la neurogenesi nel giro dentato (DG) e lo sviluppo sinaptico nella formazione ippocampica del topo Ts65Dn. Molti di questi effetti si sono mantenuti un mese dopo cessazione del trattamento e sono stati accompagnati dal ripristino delle funzioni sinaptiche nel circuito "granuli del DG e neuroni piramidali del campo CA3". Il trattamento con ELND006 ha però causato qualche effetto collaterale. Nei topi Ts65Dn trattati neonatalmente con EGCG abbiamo osservato un completo ripristino della neurogenesi ippocampale e dello sviluppo sinaptico. Un mese dopo la cessazione del trattamento, però, questi effetti scomparivano e non vi erano segni di miglioramento comportamentale. 7,8-DHF, somministrato in topi Ts65Dn neonati, ha portato ad un ripristino della neurogenesi e della densità di spine dendritiche. I topi Ts65Dn trattati dal giorno post-natale 3 fino all'adolescenza hanno esibito un ripristino della memoria e dell'apprendimento,

suggerendo che il recupero dell'anatomia ippocampale si traduceva in un recupero funzionale. Non sono stati osservati affetti collaterali sulla salute generale e sulla crescita dei topi. Un confronto delle tre molecole utilizzate in questo studio indica che, sebbene tutte siano in grado di ripristinare il processo di neurogenesi, il 7,8-DHF potrebbe avere il più alto impatto traslazionale nei bambini con SD. Questo perché non solo è efficace, ma non causa alcun effetto collaterale. La dimostrazione che sia possibile prevenire farmcologicamente le alterazioni dello sviluppo cerebrale in un modello di topo di SD con diverse molecole potrebbe stimolare l'ideazione di trials clinici con la/le molecola/e con la più alta efficacia e sicurezza. Questa è la sfida con cui si confronta la comunità di ricercatori preclinici coinvolti nello studio della SD: trasformare il sogno in realtà.

INDEX OF CONTENTS

Abbreviations list

7,8-DHF = 7,8-dihydroxyflavone

Ach = Acetylcholine

AchE = Acetylcholine esterase

AD = Alzheimer's disease

AICD = Amiloyd intracellular domain

ANOVA = Analysis of variance

APP = Amyloid precursor protein

Aβ = Amyloid β

BACE1 = Beta-secretase 1

BDNF = Brain derived neurotropic factor

BFCN = Basal forebrain cholinergic neurons

BrdU = 5-Bromo-2'-deoxyuridine

BSA = Bovine serum albumin

CA1 = Cornus Ammoni 1

CA3 = Cornus Ammoni 3

CDKs = Cyclin-dependent kinases

CFC = Contextual fear conditioning

CGP = Cerebellar granule precursor

CNS = Central nervous system

CNTF = Ciliary neurotrophic factor

CP = Cortical plate

CR = Cognitive reserve

CREB = c-AMP response element-binding protein

CTFα/β = Carbossiterminal fragments α/β

Cy3 = Cyanine 3

DCX = Doublecortin

DFIHC = Double fluorescence immunohistochemistry

DG = Dentate gyrus

DREADDs = Designer receptors exclusively activated by designer drugs

DS = Down syndrome

DSCAM = Down syndrome cell adhesion molecule

DYRK1A = Dual-specific tyrosine-(Y)-phosphorylation regulated kinase 1A

E = Embryonic day

ECL = Enhanced chemiluminescence

EGCG = Epigallo-catechin-3-gallate

EGL = External granule layer

ELN = ELND006

ERK1/2 = Extracellular signal–regulated kinases 1/2

Eu = Euploid

F1 = First filial generation

FDA = Food and Drugs Administration

FLUM = Flumazenil

GABA = γ-Aminobutyric acid

GAPDH = Glyceraldehyde 3-phosphate dehydrogenase

GFAP = Glial fibrillary acidic protein

GIRK = G-protein coupled inward rectifying K^+ channel

Gli1/2 = Glioma-associated oncogene 1/2

GRIK1 = Glutamate ionotropic receptor kainate type subunit 1

GSK3β = Glycogen synthase kinase 3β

GW = Gestational week

HRP = Horse radish peroxydase

HSA21 = Human chromosome 21

ID = Intellectual disability

IFNs = Interleukins and interferons

IG = Immunoglobulin

IHC = Immunohistochemistry

IPSC = Inhibitory postsynaptic current

iPSC = Human pluripotent stem cell

IQ = Intelligence quotient

IZ = Inner zone

JAK = Janus kinase

KCNJ6 = Potassium voltage-gated channel subfamily j member 6.

L/M = Learning and memory

LC = Locus coeruleus

lncRNAs = Long-noncoding RNAs

LSD = Least significance difference

LTD = Long term depression

LTP = Long term potentiation

MAP2 = Microtubule associated protein 2

Mb = Megabases

mEPSC = Miniature excitatory postsynaptic current

MH = Muscle hypotonia

ML = Molecular layer of the DG

MMU = Mus musculus chromosome

MWM = Morris water maze

NA = Noradrenaline

NAP = NAPVSIPQ peptide

NCBI = National Center for Biotechnology Information

ncRNAs = Noncoding RNAs

NeuN = Feminizing locus on x-3 (neuronal marker)

NFATc = Nuclear Factor of Activated T-cells

NFTs = Neurofibtillary tangles

NGF = Nerve growth factor

NIH = National Institute of Health

NKCC1 = Na-K-Cl cotransporter

NMDA = N-methyl-D-aspartate

NOR = Novel object recognition

NPCs = Neural progenitor cells

OD = Optical density

OLIG1/2 = Oligodendrocyte transcription factor 1 and 2

P = Postnatal day

PBS = Phosphate buffer saline

PCNA = Proliferating cell nuclear antigen

PMSF = Phenylmethylsulfonyl fluoride

PSD-95 = Post-synaptic density protein 95

PTCH1 = Patched1

p-TRKB-FL = Phosphorylated tropomyosin receptor kinase B full-lenght

PTZ = Pentylentetrazole

RCAN1 = Regulator of calcineurin 1

ROS = Reactive oxygen species

S100β = S100 calcium binding protein **β**

SAL = SALLRSIPA peptide

sAPP = Soluble amyloid precursor protein

SE = Standard error

Ser = Serine

SGZ = Subgranular zone

SHH = Sonic hedgehog

shRNA = Short hairpin RNA

SIM2 = Single-minded homolog 2

SOD1 = Superoxide dismutase 1

SP = Subplate

SSRI = Selective serotonin reuptake inhibitor

STAT = Signal transducer and activator of transcription

SVZ = Subventricul zone

SYN = Synaptophysin

SYNJ1 = Synoptojanin 1

Thr = Threonine

TRKB = Tropomyosin receptor kinase B

TRKB-FL = Tropomyosin receptor kinase B full lenght

TRKB-T1 = Truncated form of Tropomyosin Receptor Kinase B

TSH = Thyroid-stimulating hormone

Veh = Vehicle

VGAT = Vesicular GABA transporter

VGLUT1 = Vesicular glutamate transporter 1

VZ = Ventricular zone

WB = Western blot

WHO = World Health Organization

WRAM = Water radial arm maze

YM = Y maze

α5IA = α5 inverse agonist

1. RATIONALE AND GOAL OF THE STUDY

Down syndrome (DS) is a relatively high-incidence (1:700-1000) genetic condition due to triplication of chromosome 21. Individuals with DS may have various medical problems but intellectual disability is the common hallmark of this pathology. Furthermore, individuals with DS are bound to develop Alzheimer's-like pathology after 40 years of age, with consequent development of dementia (Hartley et al., 2015). The intellectual disability that characterizes DS is mainly due to alteration of brain development that can be traced back to fetal life statges. In particular, the DS brain is characterized by a widespread **impairment in the processes of neurogenesis** that involves the ventricular and subventricular zones (the germinal niches of most of the brain neurons), the hippocampal dentate gyrus and the cerebellum (Contestabile et al., 2007, Guidi et al., 2008, Guidi et al., 2011a). The dendritic tree of the DS neurons exhibits a reduction both in total length and density of dendritic spines (Takashima et al., 1981, Becker et al., 1986, Vuksic et al., 2002), implying that the reduction of neurogenesis is worsend by **impairment in dendritic development**. The outcome of all these defects is a reduction in the complexity of brain wiring, which explains the impairment in several cognitive domains that characterizes DS.

Mouse models that accurately mirror human pathologies are essential tools in order to comprehend deeply the mechanisms that underlie a given pathology and to evaluate the outcome of targeted therapies. The most used and best-characterized model of DS is the **Ts65Dn** mouse, that recapitulates many aspects of the human condition, including reduced neurogenesis, defects in neuronal maturation, impaired long-term learning and memory, and the tendency to develop Alzheimer's-like pathology (Choong et al., 2015). Many molecular mechanisms have been proposed to underlie neurodevelopmental defects of DS. Indeed, numerous studies report that abnormal activity of the products of some triplicated genes, such as *APP*, *DYRK1A*, and *RCAN1*, may be implicated, directly or indirectly, in the alterations of neurogenesis, neuronal maturation**,** imbalance of excitation/inhibition, and the early onset of Alzheimer's-like pathology in DS. Due to the complexity

of the outcome of gene imbalance, the mechanisms whereby gene triplication impairs brain development in DS have not been fully clarified. Yet, knowledge gained during the past few years regarding perturbed pathways may provide a rational basis to attempt targeted therapies in DS mouse models. A variety of pharmacological approaches has been used so far in the Ts65Dn mouse model and some of them translated into an improvement in hippocampus-dependent learning (see (Stagni et al., 2015a)). However, when some of them (for instance, memantine, a drug prescribed for treatment of Alzheimer's disease, or folinic acid) were used for clinical trials in individuals with DS, they failed to replicate the good results obtained in mice. It must be enphasized that most of the brain neurons are born prenatally and their maturation takes place in the perinatal period. Therefore, it is not unexpected that clinical trials in individuals with DS at adult life stages may not translate into a behavioral benefit because the optimum time windows for the rescue of neurogenesis and dendritogenesis are are well over. **Thus, there are currently no therapies for DS.**

Since neurodevelopmental defects are present from early fetal life stages in DS, the better strategy to "heal" individuals with DS should be based on pharmacologycal interventions carried out as early as possible. This idea can be summarized in four words:"**The sooner, the better**". Indeed, recent work has shown that prenatal therapy with fluoxetine restores overall brain development and cognitive performance in the Ts65Dn mouse model (Guidi et al., 2014) and that neonatal therapy restores hippocampal development and hippocampus-dependent behavior (Bianchi et al., 2010b, Guidi et al., 2013, Stagni et al., 2013, Stagni et al., 2015b). These promising results show for the first time that the trisomy-linked brain defects are reversible, provided that therapy is administered very early during the life span. Clinical trials are necessary in order to establish whether fluoxetine has the same positive impact in children with DS as in neonate Ts65Dn mice. If so, this may prompt clinical trials during pregnancy. It must be noted that an unavoidable problem with clinical trials concerns the time that intervenes between proposal and acceptance of the protocol and, given that the protocol is approved, the actual execution of the clinical trial. It has been estimated that eight years represent the mean time neecessary for the whole process. This means that a very long time will elapse before knowing

whether a drug that is effective in the mouse model is equally effective in individuals with DS. This time will be wasted if the attempted therapy will prove to be ineffective. For this reason, it is important to "gain time" and expedite the discovery of several different treatments in mouse models. This will offer to the community of clinicians a panel of drugs that may be worthwhile testing in different clinical trials, which, of course, may increase the probability to discover treatments that are effective in humans too. Such an approach will meet the needs of the families of children with DS and open a breakthough for the "cure" of intellectual disability.

The overall goal of this project was to establish whether neonatal treatment with new "unexplored" molecules restores the major neurodevelopmental defects and cognitive performnce in the Ts65Dn mouse model and whether their effect is retained after treatment cessation. In this study, I have explored the effects of three different molecules in the Ts65Dn mouse model of DS, based on the rational basis described below.

ELND006, a selective inhibitor of the γ-secratase. ELND006 blocks the formation of AICD, a small peptide derived from the processing of APP, that triggers the transcription of PTCH1, the inhibitor of the SHH mitogenic pathway. Since *APP* is triplicated in DS and in Ts65Dn mice, we hypothesized that accumulation of AICD may cause overexpression of PTCH1, thereby reducing neurogenesis. If so, inhibition of AICD production in the early neonatal period may revert the trisomy-linked neurogenesis defects.

Epigallocatechin-3-gallate (**EGCG**), a flavonoid present in green tea extracts, is an inhibitor of DYRK1A. DYRK1A is a kinase that derives from a triplicated gene in individuals with DS and Ts65Dn mice. It has been proposed that *DYRK1A* is a candidate gene closely implicated in various DS phenotypes, including neurogenesis impairment. Thus, inhibition of DYRK1A with EGCG in the early neonatal phases may have a positive effect on neurogenesis.

7,8-dihydroxiflavone (**7,8-DHF**), a natural flavone present in several plants, is a mimetic of BDNF and activates the TRKB receptor. The BDNF/TRKB signaling pathway plays a key role in neurodevelopment by stimulating neuronal maturation and neurogenesis. There is evidence that the

BDNF/TRKB system is deregulated in DS, suggesting that this deregulation may contribute to neurogenesis impairment. Thus, restoration of BDNF/TRKB signaling through 7,8-DHF may have a positive impact on neurogenesis.

The results of this study are described in Section 3.1 (ELND006), Section 3.2 (EGCG) and Section 3.3 (7,8-DHF). The outcome of individual treatments is discussed in the corresponding section. A comparison of the advantages and disadvantages of these selected molecules is reported in the section "General Discussion".

2. INTRODUCTION

2.1 Down syndrome

Down syndrome (DS, OMIM 190685), also known as trisomy 21, is the most frequently survivable occurring chromosomal disorder due to aneuploidy in humans and is the most commonly known disorder of intellectual disability (Kazemi et al., 2016, Antonarakis, 2017). About 95% of affected individuals have the full/free trisomy of human chromosome 21 (HSA21) i.e. an extra copy of HSA21, and their chromosome count is 47. The leading cause of trisomy is attributed to meiotic non-disjunction, which occurs mainly in the ovum, although the reason for this phenomenon is not completely clear. Indeed, the maternal origin for trisomy of HSA21 is prevailing, the cases of paternal origin being less than 10%, and the maternal age is a major risk factor for the onset of DS [see (Vacca et al., 2016)]. The incidence of DS in the United States is ~1 per 700 live births, and the worldwide incidence is ~1 per 1000 live births. Disease prevalence varies among countries because of sociocultural and economic variables, including average maternal age at conception as well as prenatal screening and abortion opportunities (Coppede, 2016, Hefti and Blanco, 2017). Individuals with DS now live longer than they used to, thanks to improvements in health care and in care for people with disabilities. DS subjects have many physical and neurological problems such as congenital heart disease, Alzheimer's disease (AD), low IQ average (range 30–70) leukemia, hypotonia and motor disorders [see (Bartesaghi et al., 2011)].

2.2 History

In 1959, Jerome Lejeune, working with Gautier and Turpin at Necker Hospital in Paris, France, described DS, as we currently know it (**Fig. 2.1A**). Although they discovered the trisomy of HSA21, the path that brought to this finding started more than a century before. In a very interesting report for the 50th anniversary of the Lejeune's discovery, Giovanni Neri and John Opitz retraced all the

events that allowed Lejeune and colleagues to discover trisomy 21. Almost 100 years elapsed before the real cause of DS was correctly identified. The first description of what is now called DS was by Edouard Onesimus Seguin (1812–1880), a student of Jean Marc Gaspard Itard (the founding father of the special pedagogy), and founder, in France and the United States, of methods and systems for educating those with mental retardation. John H. Langdon Down in 1866 gave the next description of DS. In his paper, "Observations on an Ethnic Classification of Idiots", Down made a classification of patients with mental retardation based on ethnic characteristics (**Fig. 2.1B**). Down mixed visionary concepts, and old prejudice, such as that of parental degeneracy, and his language is all but politically correct in describing the different types of idiocy according to ethnic varieties. In 1923 T. Halbertsma of Haarlem, had a great intuition. He argued that DS was of germinal origin. He did so on the basis of twin data, 15 cases of dizygotic twins always being discordantly affected, and the two pairs of presumed monozygotic twins being concordantly affected. Then, in 1932, long before the discovery of the human karyotype, Waardenburg predicted that DS was probably caused by a chromosomal aberration. This thesis was sustained by two pediatricians, Adrien Bleyer of St. Louis, and Guido Fanconi of Zurich. A large and important work on DS was made by Penrose in 1939, who demonstrated that maternal age correlates with the occurrence of DS. Then came 1959, when Lejeune et al. discovered that a triplication of HSA21 is the cause of DS (Neri and Opitz, 2009).

2.3 Etiology

All the defective features that characterize DS are due to the triplication of HSA21. In Genetics, the presence of a normal set of chromosomes is called euploidy, while aneuploidy indicates the presence of an abnormal number of chromosomes. Among chromosomal aberration, DS is the most widespread aneuploid condition (Driscoll et al., 2009). It occurs during cell division when chromosomes do not

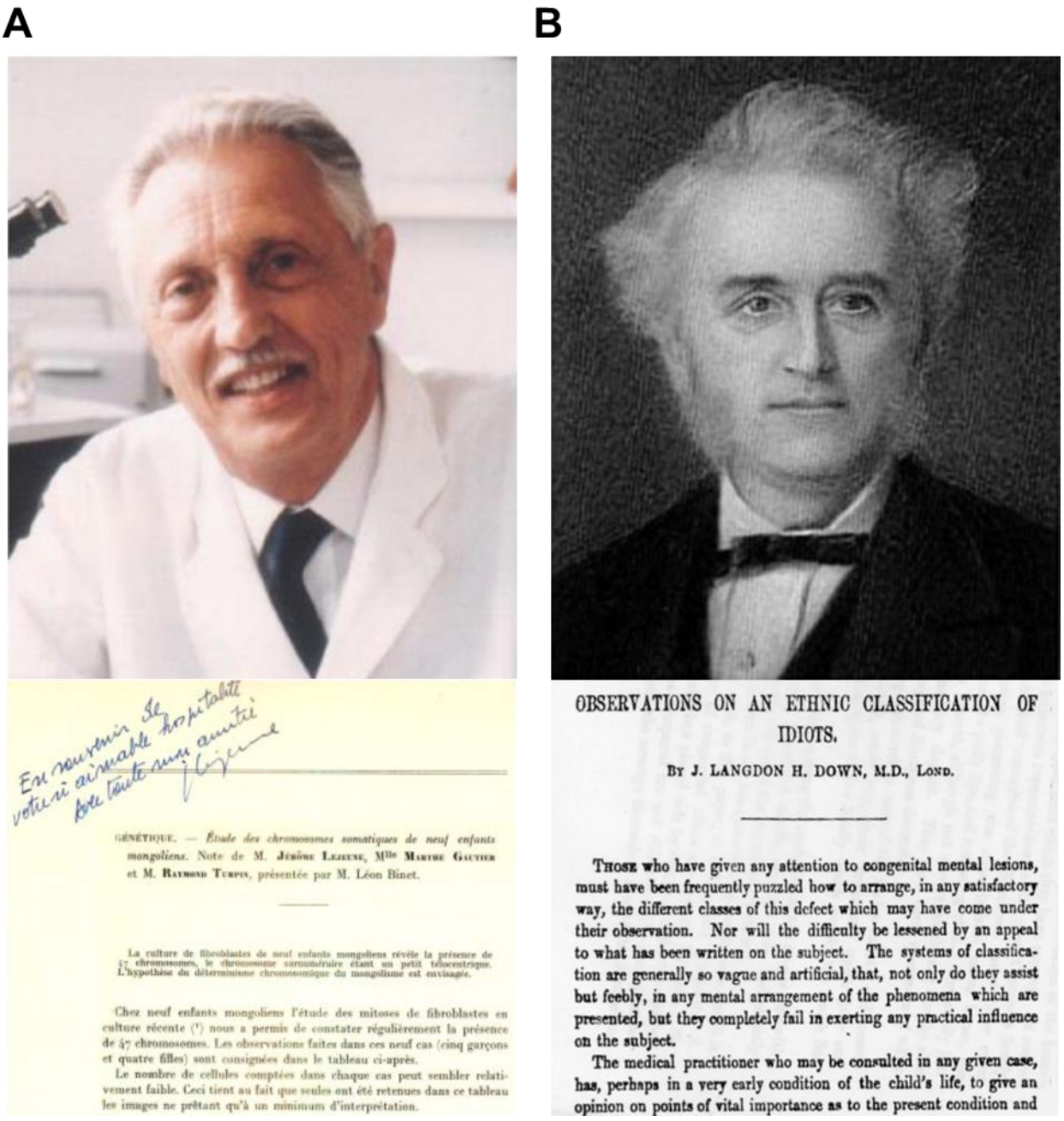

Figure 2.1. A bit of history. A: a picture of Jerome Lejeune (1926-1994) [top, image taken from (Neri and Opitz, 2009)] and the first page of the historic paper by Lejeune, Gautier, and Turpin [bottom, image taken from (Neri and Opitz, 2009)] published at the Rendering of the Academy of Sciences January 26 of 1959. B: a portrait of John Langdon Haydon Down, (1828-1896) (top, image taken from http://en.wikipedia.org/wiki/Image:JLHdown.jpg) and the first page (bottom, image taken from http://www.neonatology.org/classics/down.html) of the original paper "Observations on an Ethnic Classification of Idiots" by J. Langdon H. Down, M.D., London, London Hospital Reports, 3:259-262, 1866.

separate well between the two cells. In more than 90% of cases, DS occurs when maternal meiotic nondisjunction results in trisomy 21. Other chromosomal abnormalities that may result in DS include Robertsonian translocations (2–4 % of the cases), a structural chromosomal abnormality resulting from a trisomic dose of the long arm of HSA21 attached to chromosomes 14, 21, or 22 (also called isochromosomes); partial trisomy of HSA21 (mosaicism, 2–4 %), a condition in which individuals have both trisomic and euploid cell lines; and ring chromosomes (chromosomes whose arms have fused together to form a ring) (Papavassiliou et al., 2009).

2.4 Human Chromosome 21

HSA21 is the smallest human chromosome and represents about 1.5% of the total DNA of cells (**Fig. 2.2A**). Owing to its role in DS and its small size (~ 46 Mb), HSA21 is the most-studied human chromosome [see (Antonarakis, 2017)]. Sequencing of HSA21 was completed in 2000 within the Human Genome Project (Hattori et al., 2000). HSA21 was the second human chromosome to be fully sequenced after HSA22. So far, prediction of the number of genes set on HAS21 was estimated between 738-756 (data updated to January 2017; NCBI Map Viewer; Vega Genome Browser 54) and it has an average of 15 genes per Mb. Among these, 233 are protein coding genes (226 known proteins; 5 novel proteins, 2 putative proteins), 306 processed transcripts genes, i.e. long non-coding RNA (299 lncRNAs; 7 unclassified processed transcripts), 182 pseudogenes (141 processed pseudogenes; 32 unprocessed pseudogenes; 6 transcribed processed pseudogenes; 1 transcribed unprocessed pseudogenes), 1 IG (immunoglobulin) gene and 16 TEC (to be experimentally confirmed) genes (**Fig 2.2B**). All this genomic elements are spread on the entire length of the long arm of HSA21; the exact sequences of the short arm of HSA21 have not yet been completely elucidated. Looking at numbers reported above, it appears that HSA21 is among the poorest chromosomes in terms of functional DNA elements per Mb [see (Antonarakis, 2017)]; this could be the reason why triplication of this chromosome deals with life after birth. However, there are two rich regions of G-negative bands (thus, rich of structural genes) on the distal half of the HSA21q (21q22)

(Shapiro, 1997). Among the proteins known to be encoded by HSA21, 23 proteins are involved in signal transduction and 31 proteins are transcription factors that may influence the expression of other genes in the genome. Although proteins have a pivotal role in regulating gene activity, other central characters of the puzzle are ncRNA (non-coding RNA), which are likely to disturb several cellular functions and developmental processes. This further leads to a high phenotypic variability and heterogeneity in the DS population, highlighting the importance for understanding how over-expression of HSA21 proteins and RNA may influence the transcriptome of the entire genome. Summarizing, the phenotypic heterogeneity and variability in DS is primarily due to: i) the three copies of functional genomic elements on HSA21; ii) the genetic variation of HSA21; iii) the genetic variation on non-HSA21 loci.

Important advances have been made in understanding the phenotypic impact of the over-expression of some HSA21 genes. In particular, the molecular basis of the early onset AD, that is seen in DS, the molecular basis of the leukaemias that frequently occur in DS and the identification of genomic regions of HSA21 that harbor functional elements or causative genetic variation for certain phenotypes, such as congenital heart defects [see (Antonarakis, 2017)].

2.4.1 Most studied genes involved in DS phenotype

As deepened in the previous paragraph, many actors interact and bring to DS phenotype. Among them, in the last years some genes (and their products) were deeply studied because of either their overall influence on the genome or the role they hold in development of other pathologies (also present in DS), such as AD or leukaemia. As reported in EXaC database (http://exac.broadinstitute.org/), HSA21 genes may be divided based on haploinsufficiency (intolerability of loss-of-function variants). It has been argued that haploinsufficient genes are also

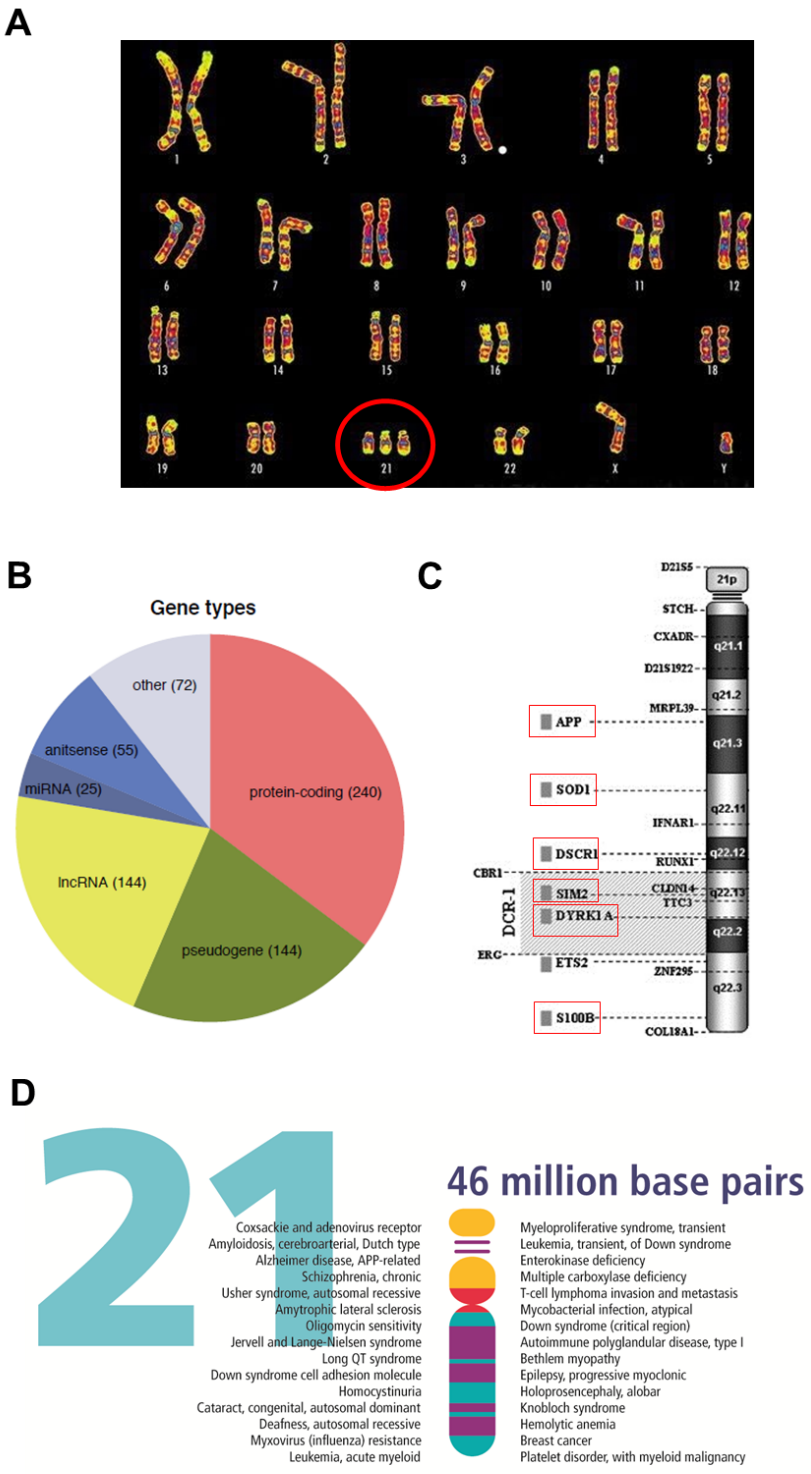

Figure 2.2. Chromosomic overview of Down syndrome. A: chromosomic pattern of an individual with trisomy 21 (image modified from https://www.huffingtonpost.com/lisa-pullen-kent/rockin-the-socks-for-worl_b_9513440.html). B: the pie chart indicates the gene content of HSA21 [see (Antonarakis, 2017)]. C: human chromosome 21 (HSA21). In the image are highlighted some genes that, when triplicated, play a key role in the phenotypic feature of DS [modified from (Rachidi and Lopes, 2008)]. D: some of heatlh problem due to the triplication of HSA21 that may affect individuals with Down syndrome (image taken from https://commons.wikimedia.org/wiki/File:Human_chromosome_21_from_Gene_Gateway_with_label.png).

sensitive to three copies and are thus good candidates for contributing to some of the phenotypes in full or partial trisomies. Genes with the highest haploinsufficiency index are most likely to contribute to a DS phenotype, whereas those with the lowest haploinsufficiency index are least likely to contribute to a DS phenotype [see (Antonarakis, 2017)]. Accordingly, some of the principal genes involved in DS phenotype that deserve a citation [see also (Rozier et al., 2003)] are *SIM2, DYRK1A, DSCAM, GRIK1, APP, S100β, SOD1, RCAN1, KCNJ6, OLIG1, SYNJ1* (**Fig. 2.2C**). Some characteristics of these gene products are briefly highlighted below.

***SIM2*.** Single-minded homolog 2. SIM2 is a transcription factor that is a master regulator of neurogenesis. It binds aryl hydrocarbon receptor nuclear translocator (ARNT) and together translocate into the nucleus stimulating gene expression (Chatterjee et al., 2013). It regulates many genes, thus resulting in some of the DS phenotypes [see (Antonarakis, 2017)].

***DYRK1A*.** Dual-specific tyrosine-(Y)-phosphorylation Regulated Kinase 1A. DYRK1A is a kinase that plays a significant role in a signalling pathway regulating cell proliferation and may be involved in brain development. *DYRK1A* was proposed to be one of the potent candidate genes closely implicated in various DS phenotypes. Down syndrome patient-derived fibroblasts exhibit impaired proliferation due to elongation of the G1 phase of the cell cycle and the extended G1 duration is restored by knocking down *DYRK1A* [see (Stagni et al., 2017)]. This evidence strongly suggests a key role of DYRK1A in the regulation of proliferation and differentiation of trisomic neural progenitor cells (Stagni et al., 2017).

***DSCAM*.** Down Syndrome Cell Adhesion Molecule. DSCAM, which acts as an adhesion molecule, is expressed in the developing nervous system, where it intervenes in various stages of neuronal development. For instance, it has important functions in early development (neuronal proliferation, maturation, and synaptogenesis) and in formation of neuronal networks (Perez-Nunez et al., 2016). Therefore, the over-expression of this protein in DS patients may be related to cellular dysfunctions that affect the development of the Central Nervous System (CNS), and/or favour AD-related dementia in adulthood (Perez-Nunez et al., 2016).

***GRIK1*.** Glutamate Ionotropic Receptor Kainate type subunit 1. GRIK1 is a subunit of the kainate family of glutamate receptors, which are composed of four subunits and function as ligand-activated ion channels. GRIK1 forms heteromeric ligand-activated ion channels with other kainate receptor subunits (GRIKs 2,3 and KA 1,2). Altering proportions of the subunits may alter overall channel composition and biochemical properties [see (Gardiner and Costa, 2006)]. This receptor is involved in pain sensitivity which may explain evidence that individuals with DS express pain or discomfort more slowly and less precisely than the general population [see (Gardiner and Costa, 2006)].

***APP*.** Amyloid beta (A4) Precursor Protein. APP is a transmembrane protein involved in the regulation of synapse formation, neural plasticity and iron export (Turner et al., 2003, Priller et al., 2006). APP is the precursor of the β-amyloid peptide, created by two successive proteolytic cut made by β- and *γ*-secretases. Accumulation of β-amyloid leads to the formation of amyloid plaques, one of the main actor involved in AD onset in the general population. Furthermore, it is one of the triplicated gene that is thought to play a key role in neurodevelopmental alterations in DS and to underlie development of Alzheimer's-like pathology in adults with DS [see (Stagni et al., 2017)].

***S100β*.** S100 calcium Binding protein beta. S100β is a cytoplasmic glial-specific protein and is expressed preferentially by astrocytes. It is involved in a number of cellular processes (cell cycle progression; differentiation) acting as a neurotropic and protective factor. Otherwise, it can contribute to neuroinflammation and cellular loss when its production and release increase in aging. So far, it seems to be involved in development of AD and it could be used as a prediction factor for the onset of the pathology [see (Lott, 2012)].

***SOD1*.** Superoxide Dismutase 1. SOD1 is one of the three copper-zinc superoxide dismutases expressed in humans and localizes on the outer mitochondrial membrane. SOD1 is a main element of the respiratory chain and its role is to convert superoxide anions into molecular oxygen and hydrogen peroxide (H_2O_2), having an antioxidant function. Dysfunctions of this enzyme provokes oxidative stress, in turn leading to inflammation and favouring some pathologies like amyotrophic lateral sclerosis or ischemic heart diseases. In DS, triplication of *SOD1* causes an accumulation of H_2O_2

(until 50% higher than normal in a variety of DS cells and tissues). This could imply a risk factor for subsequent neurodegeneration in aged DS patients [see (Perluigi and Butterfield, 2011)].

RCAN1. Regulator of Calcineurin 1. RCAN1 is a protein involved in numerous processes, included the regulation of neural proliferation and maturation. The protein encoded by this gene interacts with Calcineurin A and inhibits Calcineurin-dependent signalling pathways. Calcineurin is a calcium and calmodulin-dependent serine/threonine protein phosphatase. Calcineurin activates the nuclear factor of activated T cell cytoplasmic (NFATc; a transcription factor) by dephosphorylating it. The activated NFATc is then translocated into the nucleus, where it up-regulates the expression of interleukin 2 (IL-2), which, in turn, stimulates the growth and differentiation of T cell response [see (Stagni et al., 2017)]. RCAN1 was seen to be over-expressed in the DS fetal brain and in DS mouse models and this deregulation may contribute to neurodevelopmental alteration typical of DS.

***KCNJ6*.** Potassium voltage-gated Channel subfamily J member 6. *KCNJ6*, which encodes GIRK subunit 2 (GIRK2) of the G-protein coupled inward rectifying K^+ channel (GIRK), is located on human HSA21 (Hattori et al., 2000) and within triplicated segments of mouse chromosome 16 in mouse models of DS (Best et al., 2007). $GABA_B$ receptors are metabotropic G-protein coupled receptors that are thought to release Gβγ subunits that activate K^+ channels, causing neuron hyperpolarization (Chalifoux and Carter, 2011). This hyperpolarization decreases neuron excitability and enhances Mg^{2+} blockade of NMDA receptors to reduce their overall current and thus Ca^{2+} influx. This influx is fundamental for initiating the physiological changes that occur during synaptic plasticity. It has been shown that up-regulation of GIRK2 protein in the Ts65Dn mouse model of DS results in a larger slow inhibitory postsynaptic current (IPSC) mediated by $GABA_B$ receptors (Siarey et al., 1999). Moreover, evidence in Ts65Dn mice shows that GIRK2 is over-expressed in various brain regions, and that this leads to an exaggerated $GABA_B$ receptor-mediated inhibitory response in neurons from the hippocampus (Harashima et al., 2006).

***OLIG1/2*.** Oligodendrocyte transcription factor 1 and 2. OLIG1/2 are transcription factors that promote formation and maturation of oligodendrocytes, especially within the brain and that cooperate

during neural tube formation. *OLIG2* mis-expression impairs cortical progenitor proliferation, causes precocious cell cycle exit, massive neuronal cell death, downregulation of neuronal specification factors including NGN1, NGN2 and PAX6, and a defect in cortical neurogenesis [see (Stagni et al., 2017)]. It must be observed that during embryonic development neural precursors in the medial ganglionic eminence (MGE) of the Ts65Dn mouse exhibit a faster proliferation rate. This feature is abrogated by deletion of an allele of *Olig1* and *Olig2* (Chakrabarti et al., 2010). This suggests that *OLIG1* and *OLIG2* may play a differential role in the modulation of neurogenesis according to brain region and developmental time.

SYNJ1. Synoptojanin 1. This gene encodes a phosphoinositide phosphatase that regulates levels of membrane phosphatidylinositol-4,5-bisphosphate. The synaptojanin family comprises proteins that are key players in synaptic vesicle recovery at the synapse. As such, expression of this enzyme may affect synaptic transmission and membrane trafficking. There is evidence that over-expression of SYNJ1 in DS is functionally linked to the enlargement of early endosomes, that in turn provokes disruption of synaptic vesicle transportation (Cossec et al., 2012).

2.5 Typical features of individuals with DS

DS patients are characterized by numerous phenotypic defects and medical problems caused by the triplication of HSA21 (**Fig. 2.2D**). The most invalidating aspect of the DS condition is intellectual disability that is the unavoidable hallmark of DS and has a heavy impact on public health. In addition, DS is coupled with congenital heart defects, gastrointestinal anomalies, hypotonia, craniofacial abnormalities, audiovestibular and visual impairment and hematopoietic disorders. Furthermore, people with DS tend to develop leukemia, thyroid disorders, and AD like pathology with age [see (Kazemi et al., 2016)].

Congenital heart defects (CHD). The incidence of CHD in newborn babies with DS is up to 50% [see (Asim et al., 2015)]. The most common form of CHD in the DS population are atrioventricular canal/septal defects (AVSDs), which affects up to ~40% of the patients. Of all the heart defects,

AVSDs is the most serious and has an adverse impact on survival. Ventricular septal defects (VSD) are also present in DS and affect up to 35% of patients [see (Noble, 2008, Asim et al., 2015)]. AVSDs are characterized by the presence of a common atrioventricular junction with an ovoid shape, and defects of the muscular and membranous atrioventricular septum. There is disproportion of outlet and inlet dimensions of the left ventricle. These features possibly lead to a blood travelling from the left side (venous blood) of the heart to the right side of the heart (arteriosus blood), or the other way around. In case of VSD, the defect lies in ventricular septum of the heart due to which some of the blood from the left ventricle leaks into the right ventricle leading to pulmonary hypertension.

Although with minor incidence, abnormalities such as isolated secundum atrial septal defects (8%), isolated tetralogy of Fallot (4%) and isolated patent ductus arteriosus are present in DS patients (Freeman et al., 1998). Importantly, most of the anomalies in infants with DS are suitable for complete surgical correction, with single ventricle palliation recommended for children with complex cardiac anomalies [see (Arumugam et al., 2016)].

Gastrointestinal anomalies. DS patients present a large number of gastrointestinal defects. These defects, which could affect up to 7-12% of children with DS (Freeman et al., 2009, Bull and Committee on, 2011), are duodenal stenosis/atresia (3.9%), anal stenosis/atresia (1.0%), esophageal atresia with or without tracheoesophageal fistula (0.4%), pyloric stenosis (0.3%) and Hirschsprung disease (0.8%) [see (Arumugam et al., 2016)]. DS patients constitute ~12% of all cases of Hirschsprung disease (HD). HD is a form of low intestinal obstruction caused by the absence of normal myenteric ganglion cells in a segment of the colon (Amiel et al., 2008). In HD children, the absence of ganglion cells results in the failure of the distal intestine to relax normally, encouraging chronic constipation, poor weight gain, vomiting and swollen abdomen.

Hypotonia. Almost all children with DS suffer from muscle hypotonia (MH), a state of reduced muscle tone, usually related to the skeletal muscles. MH usually leads to numerous problems, as a delay in developmental milestones, mastication problems (due to poor neuromuscular control), muscular weakness and dental anomalies (Dey et al., 2013). MH in people with DS has been related

to a dysregulation of the expression of the α1 and α2 chains of type VI collagen (*COL6A1* and *COL6A2* respectively), that are located on the long arm of HSA21. Type VI collagen has a crucial role in the function and stability of skeletal and cardiac muscle (Dey et al., 2013).

2.5.1 Other medical problems associated with DS

Leukemia. Children with DS tend to develop leukemia, even though they develop solid tumors in lower rate in comparison with general population. The risk of developing acute megakaryoblastic leukemia (AMKL), a rare subtype of acute myeloid leukemia (AML), is increased 500-times in children with DS, and risk of acute lymphoblastic leukemia (ALL) is 20-fold greater in children with DS (Xavier and Taub, 2010). Although in childhood ALL is significantly more common than AML, for children with DS under 15 years of age the ratio of ALL to AML is 1.7. For the general population of non-DS children, the equivalent ratio is 6.5 (Xavier and Taub, 2010).

Thyroid disorders. Individuals with DS are at an increased risk of developing thyroid disease, with a lifetime prevalence ranging from 13% to 63% [see (Hardy et al., 2004)]. Furthermore, congenital hypothyroidism is about 28 times more common in infants with DS than in the general population with an incidence of 1%, detected by newborn screening (Forth 1984). Hypothyroidism in DS could contributes to intellectual disability. After the newborn period, TSH values in DS increase and they have been reported to be as high as 85% of euploid infants under the age of 12 months [see (Hardy et al., 2004)]. Thyroid dysfunction, expressed as a high TSH concentration, is associated with growth retardation in children with DS who are younger than 4 years. Unfortunately, there are very few studies systematically examining the frequency of thyroid disease in infants with DS.

Epilepsy. 5–13% of children with DS display seizures [see (Arya et al., 2011)]. The occurrence is bimodal with 40% having seizures before 1 year of age and with 40% developing seizures after thirty years, with generally tonic–clonic or myoclonic in manifestation [see (Lott, 2012)]. Infantile spasms are associated with electroencephalographic (EEG) characteristics. It appears that children with DS have better seizure control compared to other patients with symptomatic infantile spasms, and early

initiation of appropriate treatment may contribute to the prevention of late seizure development and better developmental outcome [see (Arya et al., 2011)].

2.6 Neurological defects in DS

The most common feature of DS is intellectual disability that affects almost 100% of people with this pathology. DS individuals typically display an average Intelligence Quotient (IQ) of 50 (30-70) and mental age is rarely over 8 years. Children with DS show a delay in cognitive development [see (Lott and Dierssen, 2010, Bartesaghi et al., 2011, Rueda et al., 2012)]. There is, however, a great inter-individual variability in the intensity of DS phenotype. Indeed, a few individuals with DS have been reported to have a normal IQ value. The IQ in DS is not constant over a lifetime, but it progressively decreases with age. The first deceleration occurs early, between the age of 6 months and 2 years, with a further decline in adolescents (Rachidi and Lopes, 2008). DS cognitive defects emerge in infancy and accumulates in early childhood, with impairment of speech, language, motor skills, cognition, adaptive behavior and a higher risk of psychopathology. Infants with DS are unable to roll until the sixth month and are unable to sit independently until between 8.5 and 11.7 months. The delay is greater for later developing motor skills: DS infants crawl on their hands and knees between 12.2 and 17.3 months of age and walk between 15 and 74 months (Vicari, 2006). During infancy, children with DS exhibit a slower transition from babbling to speech and a delay in expressive lexicon and syntax, although no difference in vocalization types are present. Adolescents and young adults with DS usually have very poor linguistic capacities and a longer period of phonological errors and poorer intelligibility, although language comprehension is relatively more advanced than syntax (Dykens et al., 1994, Chapman and Hesketh, 2000, Vicari, 2006). Individuals with DS perform visual-perceptual and imagery material processing in a significantly poorer way than mental age-matched individuals do. However, when the task involves the processing of spatial data, performance of DS individuals is similar to that of controls. Many individuals with DS exhibit impairment in verbal short-term and working memory [see (Vicari, 2006)]. Children with DS have normal learning ability for tasks

requiring implicit memory but exhibit selective impairment of explicit memory, with poor information encoding, impaired retrieval abilities and attention deficits (Carlesimo et al., 1997, Vicari et al., 2000). When tested for learning tasks that specifically assess the state of function of the hippocampal and prefrontal systems infants and adults with DS show severe impairment [see (Nadel, 2003)].

2.6.1 Alzheimer's-like pathology in DS

DS is characterized by a high incidence of early onset Alzheimer's disease (AD). Indeed, signs of AD-like pathology are found in the brains of virtually all people with DS by 35-40 years of age (**Fig. 2.3A**). The prevalence of dementia increases with age above 45 years, with the majority of people with DS developing dementia by the age of 65 [see (Lott, 2012, Ruparelia et al., 2013)]. Since AD develops only in some individuals of the general population but it is almost an invariable hallmark of DS (although not all individuals develop dementia, even by 70 years of age), this implies that trisomic genes play a paramount role in the development of the disease [see (Ruparelia et al., 2013, Choong et al., 2015)]. This condition makes DS an excellent natural genetic model for the study of AD-like biological mechanisms and identification of potential biomarkers. The progressive accumulation of AD pathology suggests that there is a preclinical phase in DS-AD with a delay of at least 10 years between the onset of AD pathology and dementia diagnosis, similar to what is described for AD in the general population, which provides a window for intervention [see (Hamlett et al., 2016)]. Biological mechanisms involved in DS-AD include extracellular amyloid β protein (Aβ) accumulation (**Fig. 2.3B**), intraneuronal neurofibrillary tangles (NFTs) deposition (**Fig. 2.3B**), BFCN (basal forebrain cholinergic neurons) loss, neuron loss in the locus coeruleus, hippocampal abnormalities, imbalance of neurotrophic factors, alterations in long-term potentiation, abnormal endosomal signaling, presence of neuroinflammation, and oxidative stress [see (Hartley et al., 2015, Hamlett et al., 2016)]. In DS there is an over-expression of the gene for APP from which the amyloid-β-protein is derived [see (Lott, 2012, Hartley et al., 2015)]. It has been suggested that an abnormal

APP metabolism initiates AD pathogenesis by triggering a set of events that result in Aβ aggregation, particularly of the Aβ42 peptide, in the extracellular plaques [see (Choong et al., 2015, Hartley et al., 2015)]. Evidence in favor of this hypothesis comes from rare families with early onset AD who have small internal duplications of HSA21 that include *APP*, and tends to be present with cerebral amyloid angiopathy [see (Ruparelia et al., 2013, Hamlett et al., 2016)]. Conversely, although very rare, partial trisomy 21 excluding *APP* (i.e., with two "doses" of APP) does not appear to lead to AD [see (Choong et al., 2015)]. According to recent evidence, in addition to over-expression of APP, other triplicated genes may be involved in the development of AD and contribute to excessive tau phosphorylation in DS. They are *DYRK1A, RCAN1, SOD1, ETS-2, BACE2,* and *S100β* [see (Lott, 2012, Hartley et al., 2015)]. The prevalence and time-course of AD in DS suggests that interventions may be attempted in young adults with DS in order to prevent the onset of AD. However, due to the difficulty in obtaining clinically and pathologically well-characterized human DS brain tissue, the need to develop and investigate animal models of this disorder is critical.

2.6.2 Cognitive reserve paradigm

The concept of "reserve" tries to explain how individual differences in susceptibility to age-related brain changes or Alzheimer's disease-related pathology originate. Cognitive reserve (CR) refers to individual differences in how tasks are performed that may allow some people to be more resilient than others. This theory considers two types of reserve: brain reserve, which refers to actual differences in the brain itself (for example more neurons or synapses to lose) that may increase tolerance for a given pathology, and CR. The idea of brain reserve is supported by studies that suggest

A

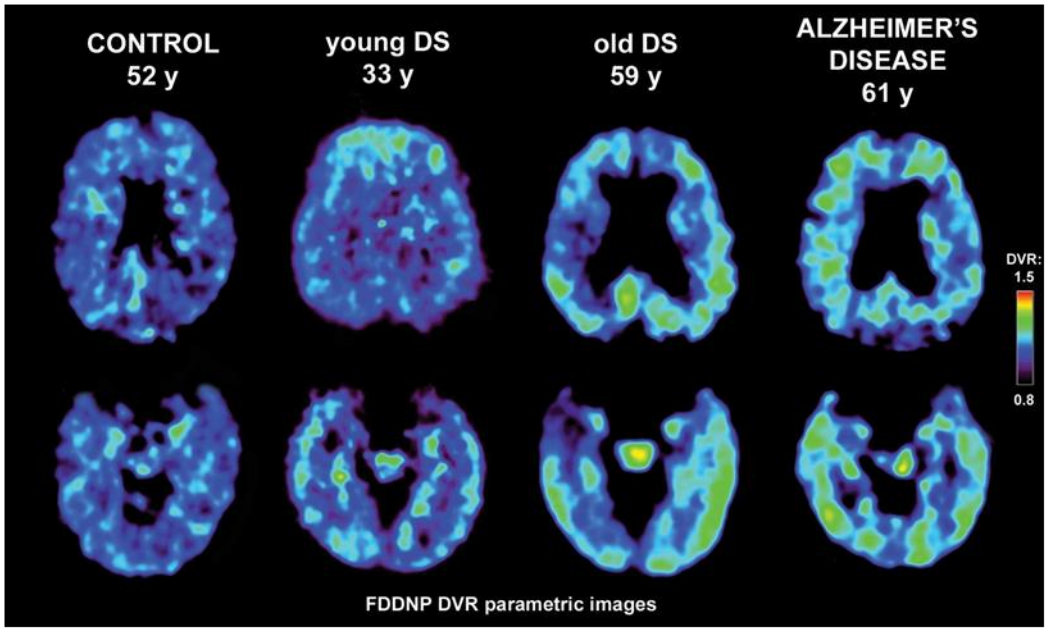

B

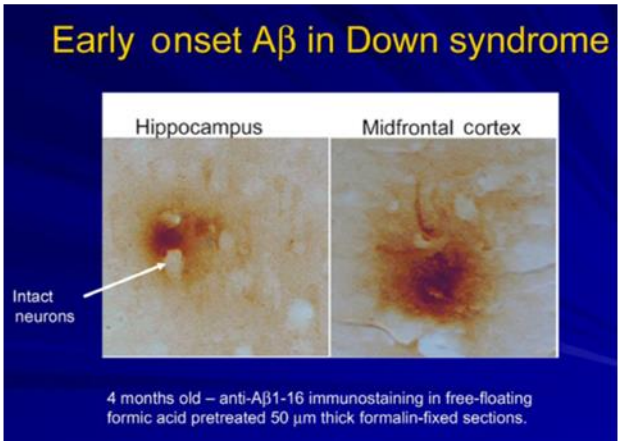

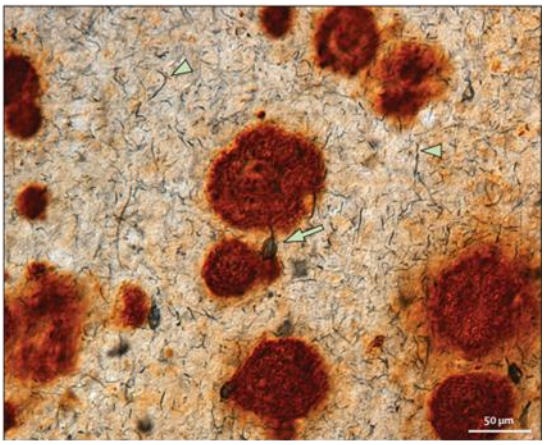

Figure 2.3. Alzheimer's disease in Down syndrome. A: A chemical marker that binds to plaques and tangles allows their detection in the brains of individuals with Down syndrome or Alzheimer's disease. The blue color corresponds to lower amounts of plaques and tangles, while yellow and green represent higher amounts (Lott, 2012). B: Aβ deposition in the brain of an infant with Down syndrome (Lott, 2012). C: Immunolabelling with anti-amyloid-β of the midfrontal cortex of a 46-year-old person with Down syndrome (Lott and Dierssen, 2010). Abbreviations: Aβ, β-amyloid; DS, Down syndrome; y, years.

.

that prevalence or incidence of dementia is lower in individuals with larger brains. In contrast, the concept of CR suggests that the brain actively attempts to cope with brain damage by using pre-existing cognitive processing approaches or by enlisting compensatory approaches. This would allow individuals with high CR to better counteract the brain damage than individuals with lower CR. Thus, the CR concept is an active form of reserve in that, the same amount of pathology will have different effects on different people, even when the brain size is held constant. There are recent suggestions that life experience may act to prevent or minimize pathology. For example stimulating environments upregulate BDNF expression that in turn fosters the growth of new neurons and stimulates neural plasticity. There are other suggestions that cognitively stimulating activities may slow the rate of hippocampal atrophy in normal aging, and perhaps even prevent accumulation of amyloid plaques. Although individuals with a higher CR can tolerate more pathology than those with a lower CR, it must be noted that there is common point in all people where the pathology is so severe that function cannot be maintained. Given these assumptions, individuals with higher CR will begin their cognitive decline when pathology is more advanced and thus have less time until they reach the point where pathology overwhelms function. This results in a more rapid rate of decline once it begins. Thus, it becomes extremely important to find a way to prevent this rapid decline, possibly by acting pharmacologically or by environmental stimuli very early (before the first symptoms of the pathology begin) in the life of an individual [all the information about cognitive reserve are based on the review by (Stern, 2012)].

Individuals with DS are bound to develop AD. Thus, the theory of cognitive reserve may also be valid for DS. In the last decade, many attempts have been made by the scientific community in order to find pharmacotherapies effective on brain development in DS. The discovery of pharmacological treatments that are able to foster neurogenesis and, thus, increase the cognitive reserve could be a useful tool for the “cure” of DS as well as prevention of AD in DS.

2.7 DS mouse models: tools for the understanding of DS pathology and therapy design

Mouse models that accurately mirror human pathologies are essential tools in order to comprehend deeply the mechanisms that underlie a given pathology and to evaluate the outcome of targeted therapies. So far, a number of DS mouse models carrying trisomy for different sets of HSA21 orthologous genes have been created with different methods [see (Bartesaghi et al., 2011)]. These models are briefly described hereafter. The difficulty for making a "perfect" model for DS lies in the fact that the ~160 HSA21 protein-coding genes are scattered among three mouse chromosomes: ~100 map to the telomeric segment of mouse chromosome 16 (MMU16); ~20 map of MMU17; ~40 to internal segments of MMU10 [see (Gardiner, 2015, Antonarakis, 2017)].

Model with triplication of the whole MMU16. The first mouse model of trisomy 21, generated by spontaneous Robertsonian translocations of MMU16, was labelled **Ts16** (**Fig.2.4A**) (Gropp et al., 1975). Ts16 and DS share a common genetic defect because the distal portion of mouse chromosome 16 is syntenic with most of the distal portion of human chromosome 21 (Holtzman et al., 1992). The value of this model, however, is limited because the Ts16 embryos die in utero.

Segmental trisomic mice. The most used and best-characterized model of DS is the **Ts65Dn** mouse that was created approximately 25 years ago (Davisson et al., 1993). The Ts65Dn mouse is trisomic for at least 55 % of HSA21 orthologous protein-coding genes, but it lacks the remaining ~45% (**Fig. 2.4A**). Moreover, it bears 50 protein-coding genes that are not orthologs for HSA21 genes, a segment that is an artefact of the method used in its construction (Duchon et al., 2011). These features may confound phenotypic consequences seen in this model. Although the Ts65Dn mouse shows genetic limitations, it is still the most popular choice among DS models because it recapitulates many aspects of the human condition, including, cytoarchitectural abnormalities in many brain regions and deficits in learning and memory [see (Bartesaghi et al., 2011, Rueda et al., 2012, Gardiner, 2015, Stagni et al., 2017)]. Ts65Dn mice have reduced dimension in comparison with euploid mice (**Fig.2.4B**).

Another characteristic of the Ts65Dn is to develop, like humans with DS, Alzheimer's-like pathology with age.

The **Ts1Cje** is trisomic for 81 genes located in the region of MMU16 that extend from *Sod1* to *Znf295* (**Fig. 2.4A**) (Sago et al., 1998). Ts1Cje mice show reduced cerebellar volume and abnormalities in craniofacial development similarly to Ts65Dn mice, but generally less severe. **Ts2Cje** model carries the same segment of MMU16 triplicated in the Ts65Dn mouse (**Fig. 2.4A**) but is translocated to chromosome 12 (Villar et al., 2005).

The **Ms1Ts65** mouse model has a partial trisomy that starts from *App* to *Sod1* and includes about 33 genes (**Fig. 2.4A**). The chromosomal region between *App-Sod1* is present in the Ts65Dn model and it lacks in the Ts1Cje model. This allows comparisons among the trisomies and permits to assess the contributions of the phenotype of Ts65Dn mice of genes proximal to *App* up to *Sod1* regarding the learning and behavioural phenotype (Sago et al., 2000).

The **Ts1Rhr** mouse model, which is trisomic for the *Cbr1-Orf9* genetic interval (DSCR) that includes 33 genes (**Fig. 2.4A**) (Olson et al., 2004), shows a reduction in the volume of the brain but not of the cerebellum and hippocampus (Aldridge et al., 2007). Moreover, the Ts1Rhr model displays derangement in the spatial organization of subcortical structures (Aldridge et al., 2007). This mouse became of particular interest because it demonstrated that trisomy of this region (the DSCR) was not sufficient to replicate all structural and functional abnormalities of DS.

The **Ms1Rhr** mouse model combines the deletion of the *Cbr1-Orf9* region with the Ts65Dn trisomy region (**Fig. 2.4A**). Ms1Rhr model shows a reduced volume, height, width, and length of the brain, reduced volume of the hippocampus at two and three months of age, but an increase in the volume of the cerebellum (Aldridge et al., 2007, Olson et al., 2007).

Models with triplication of MMU16, MMU17 and/or MMU10. Two models, which are trisomic for a segmental region of MMU17, have been recently created. The **Ts1Yah** mouse, which is trisomic for 12 genes in the MMU17 region, syntenic to the sub-telomeric region of HSA21, displays deficits in novel object recognition, similarly to other DS models, but no impairments in hippocampus-

dependent spatial memory. The **Ts(1617)43H(Ts43H)** mouse, which is trisomic for 30 Mb of proximal MMU17, exhibits spatial learning deficits analogous to those observed in Ts65Dn mice (Vacik et al., 2005). Differences between these models reveals the complexity of the genetic code that modulates different aspects of behaviour in DS patients.

The **Dp(16)Yey** mouse is a more recently created DS model (Li et al., 2007). It is trisomic for all MMU16 region orthologous to HSA21 and not for the non-HSA21 orthologs (**Fig. 2.4A**). Although the Dp(16) mouse still needs to be fully characterized, the few available studies indicate that it exhibits various brain dysmorphologies (Starbuck et al., 2014), is impaired in several tests of learning and memory (Goodliffe et al., 2016), and shows defects in long-term potentiation (Yu et al., 2010b). Other two models with a partial triplication of MMUs for the entire regions that are orthologous with HSA21 were developed. They are: the **Dp(10)Yey** mouse, with a partial triplication of MMU10 (**Fig. 2.4A**), that does not show cognitive impairment; the **Dp(17)Yey**, with a partial triplication of MMU17 (**Fig. 2.4A**), that shows abnormal hippocampal long-term potentiation (Yu et al., 2010b).

An attempt to create a "full-trisomic" mouse was made successfully by Yu et al (Yu et al., 2010a). They produced a triple transgenic mouse that carries triplications spanning the entire HSA21 syntenic regions on all MMU10, MMU16 and MMU17 mouse chromosomes (**Dp(10)1Yey/+;Dp(16)1Yey/+;Dp(17)1Yey/+**) (deriving from a consecutive breeding of models Dp(16)1Yey, Dp(17)1Yey and Dp(10)1Yey) (**Fig. 2.4A**). This model showed learning and memory deficits and LTP impairment. However, because of viability issues, time, and expense, this mouse has not been extensively studied yet [see (Gardiner, 2015)].

Models with insertion of HSA21. An alternative model is provided by "transchromosomic" (trans-species aneuploidy) mouse strains in which mice carry an extra human chromosome and are thus trisomic only for the genes on this chromosome. The **Tc1** mouse is unique in that it is a transchromosomic line that carries a freely segregating and almost complete copy of HSA21 (**Fig. 2.4A**) (Wiseman et al., 2009). Consistent with the impact of HSA21 trisomy in humans, Tc1 mice show reduced long-term potentiation (LTP) in the hippocampal dentate gyrus (DG) region (O'Doherty

et al., 2005) and impaired performance in tasks such as object recognition memory. However, the random loss of this human chromosomal fragment during mouse development resulted in variable levels of mosaicism of the extra chromosome in different tissues, confounding the analysis of the phenotypic consequences.

Transgenic mouse models. In order to evaluate the involvement of single triplicated genes in DS features, several transgenic mouse models with one orthologous HSA21 gene were created (**Tg*Sod1***, **Tg*App*, Tg*Ets2*, Tg*S100β*, Tg*Dyrk1a*, Tg*Dscr1*, Tg*Sim2*, Tg*Bace2*, Tg*Synj1*** and **Tg*Pfk1***). The transgenic mouse for *Sod1* gene for example, showed decreased cell number in several brain areas and decreased LTP in the hippocampal field Cornu Ammonis 1 (CA1) (Rachidi and Lopes, 2008). The transgenic mouse Tg*S100β* showed dendritic abnormalities similar to those in the fetal DS brain and astrocytosis, while transgenic mice Tg*App* exhibited over-expression of APP protein in the neocortex and hippocampus region and mimicked features of DS (Rachidi and Lopes, 2008). Recent work focused on the role of *Dyrk1a* triplication in the cognitive deficit of DS, showing that transgenic mice (Tg*Dyrk1a*) exhibit various but not all learning defects of Ts65Dn mice (Altafaj et al., 2001, Ortiz-Abalia et al., 2008).

2.8 Neurodevelopmental alterations in DS

Intellectual disability (ID) is the most invalidating feature of DS. ID, that lifelong affects DS individuals, is mainly due to brain hypotrophy. Several lines of evidence show that neurogenesis reduction and dendritic hypotrophy are the two major determinants of brain hypotrophy in DS. These defects starts at early fetal life stages and continues in the postnatal life.

This section provides comparative information on neuroanatomical defects and neurogenesis alterations in the fetal/neonatal DS brain and in mouse models of DS during early developmental stages and adulthood. In particular, evidence will be summarized regarding brain gross anatomy, cytoarchitecture, proliferation potency, phenotype acquisition, neuron maturation, and some molecular mechanism that could underlie neurodevelopmental defects in DS.

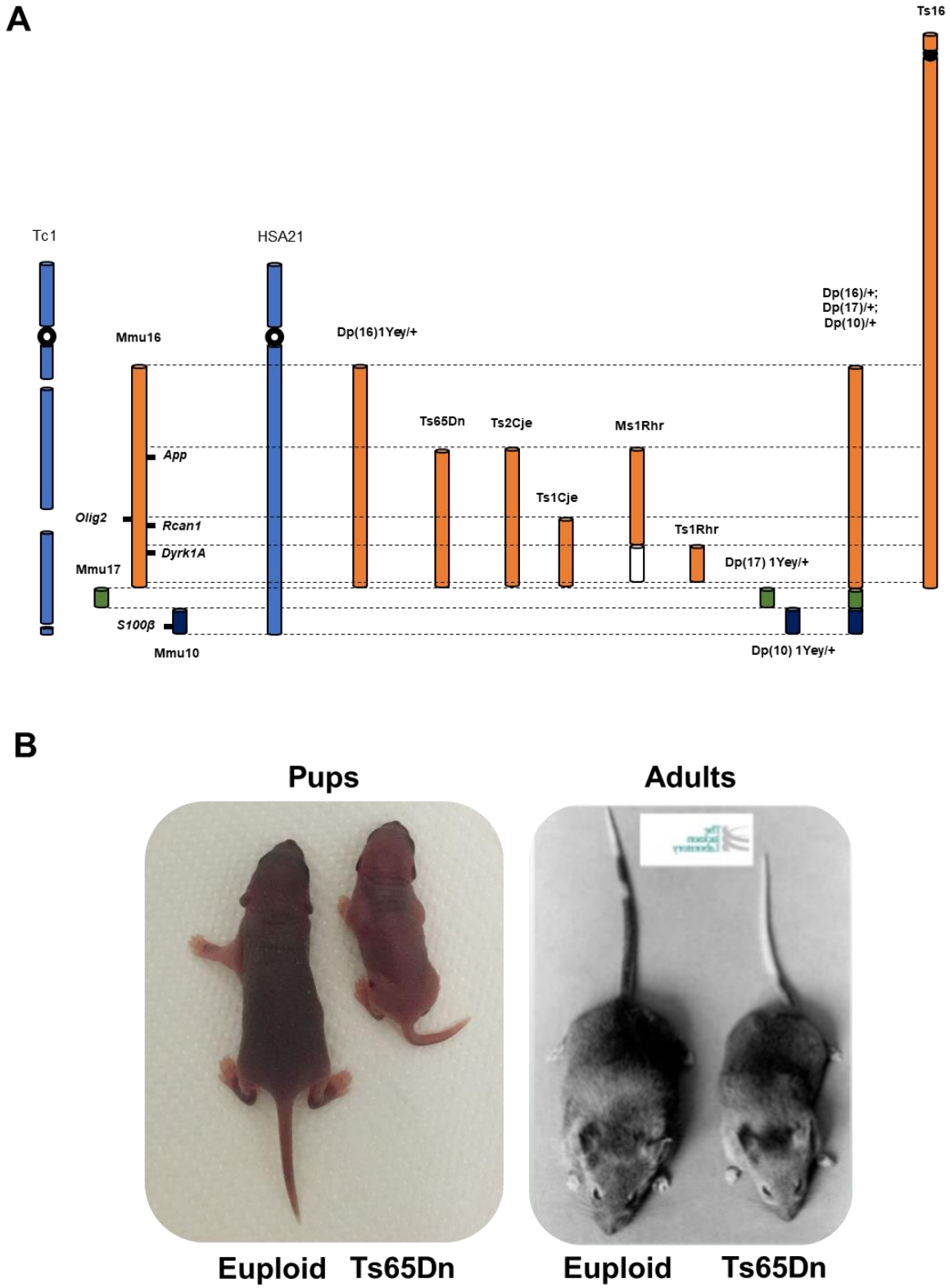

Figure 2.4. Mouse models of Down syndrome. A: Schematic representation of HSA21 and syntenic regions of MMU16, MMU17, and MMU10 and different mouse models trisomic for different sets of genes orthologous to those of HSA21. B: Ts65Dn mouse model of Down syndrome. The Ts65Dn mouse is the most popular choice among DS models because it recapitulates many aspects of the human condition, including, cytoarchitectural abnormalities in many brain regions and deficits in learning and memory. Image on the left is taken from (Kuehn, 2016); image on the right was modified from https://www.slideshare.net/plus15campaign/dsrtf-webinar-dr-h-craig-heller-stanford-university.
Abbreviations: HSA21, human chromosome 21; Mmu, mus musculus chromosome.

2.8.1 Anatomy of the DS brain: humans with DS

Individuals with DS have an overall reduced brain volume and numerous brain regions appear to be smaller in comparison with controls (Weis et al., 1991, Kesslak et al., 1994, Raz et al., 1995, Pinter et al., 2001b, Teipel and Hampel, 2006). Volume reduction is particularly prominent for the cerebellum and brainstem (Jernigan et al., 1993, Raz et al., 1995, Aylward et al., 1997), and for the hippocampus (Aylward et al., 1999). The brain hypotrophy that characterizes DS is already present in neonates and can be traced back to prenatal life stages (**Fig. 2.5**).

GROSS ANATOMY

Fetuses. A pioneering study in fetuses aged 15-22 weeks (Schmidt-Sidor et al., 1990) found no gross differences in brain shape, weight or fronto-occipital length. Neither were any differences in the cerebellum or hippocampus. This is in contrast with the hypotrophy found by other studies regarding the DS fetal brain. The absence of differences in Schmidt-Sidor's study may be attributable to the fact that fetuses were not stratified by age, which, may obscure differences between DS and non-DS fetuses. However, the evaluation of the brain of fetuses with DS during relatively restricted time windows of gestation shows that fetuses with DS exhibit reduced brain weight (Guihard-Costa et al., 2006) and volume reduction in various hippocampal structures (Guidi et al., 2008) and in the cerebellum (Guidi et al., 2011b). In addition to weight and volume differences, the fetal DS brain exhibits distinctive shape alterations. It is markedly brachycephalic due to a reduction in the length of the frontal lobe, with an increase in the transparietal length (Guihard-Costa et al., 2006). A pioneering study showed that the hippocampus of fetuses with DS is less well-formed in comparison with control fetuses (Sylvester, 1983). This evidence has been substantiated by a following study showing numerous neuroanatomical defects in the DG and hippocampus of DS fetuses (**Fig. 2.5**) (Guidi et al., 2008). A typical feature of DS fetuses is a notable reduction in the transcerebellar diameter (Rotmensch et al., 1997, Winter et al., 2000, Guihard-Costa et al., 2006). Moreover, the cerebellum has an abnormal shape, due to shorter lobes and shallower fissures (**Fig. 2.5**) (Guidi et al., 2011b).

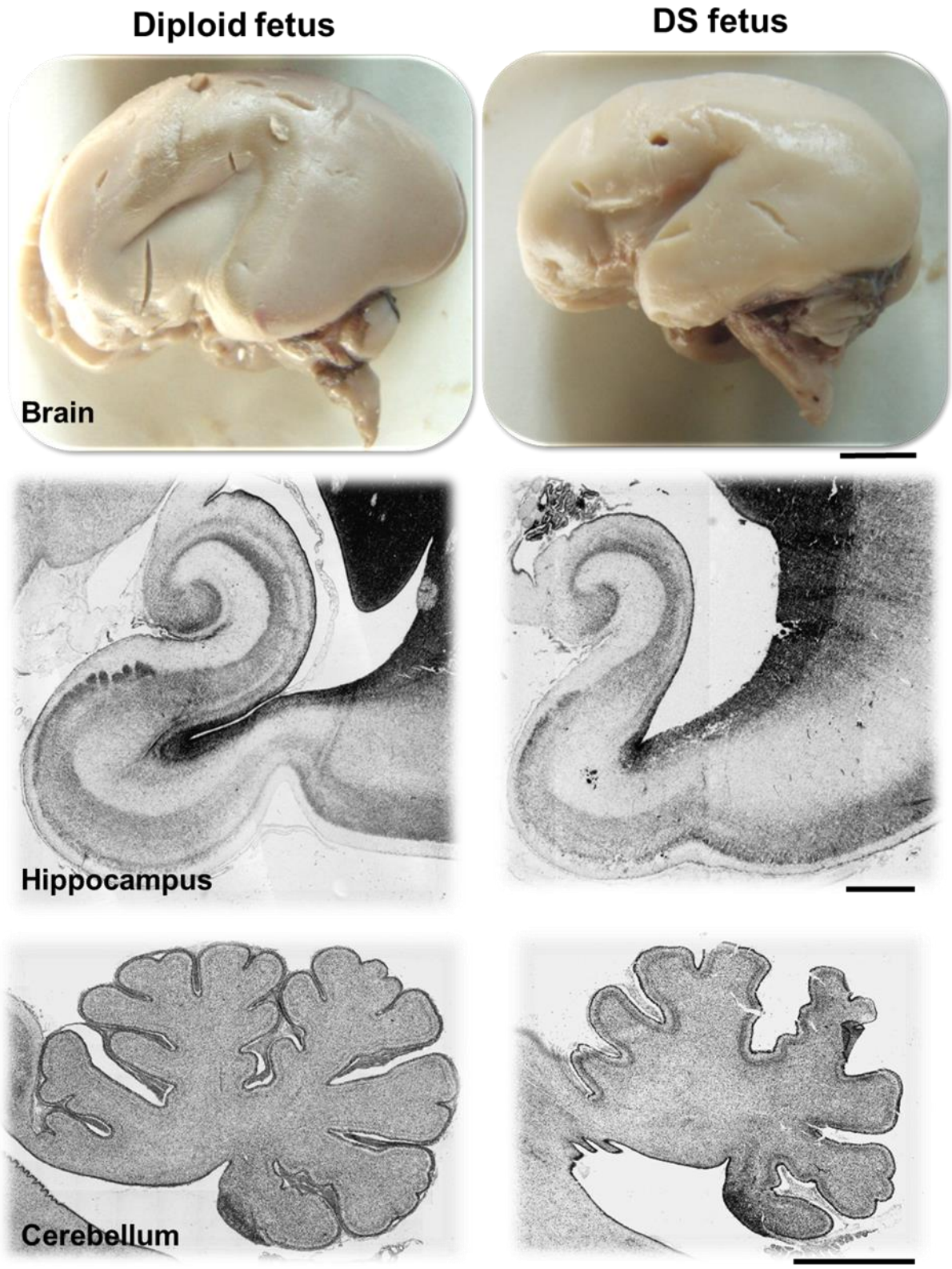

Figure 2.5. Brain hypotrophy in Down syndrome fetuses. Examples of the brain (scale bar 1 cm), hippocampus (scale bar 1 mm) and cerebellum (scale bar 2 mm) of a diploid (left) and a DS fetus (17–21 GW) (right). Images were taken from (Guidi et al., 2008, Guidi et al., 2011b, Stagni et al., 2017). Abbreviation: DS, Down syndrome.

Infants and children. The brains of infants and children with DS have a reduced volume in comparison with normal children due to a reduction in the volume of both the grey and white matter (Pinter et al., 2001b, Kates et al., 2002, Smigielska-Kuzia et al., 2011). In addition, save for the occipital lobes, all brain lobes have a reduced size (Pinter et al., 2001b, Kates et al., 2002, Smigielska-Kuzia et al., 2011). Volume reduction is also present in the hippocampus (Pinter et al., 2001b, Smigielska-Kuzia et al., 2011), cerebellum (Pinter et al., 2001b) and amygdala (Smigielska-Kuzia et al., 2011). Pinter et al. found no difference in the volume of the superior temporal gyrus (Pinter et al., 2001a) nor, at variance with the study by Smigielska-Kuzia et al., in the volume of the amygdala (Pinter et al., 2001a). The absence of differences in the volume of the amygdala may be related to the older age of children in Pinter's study (11.3 vs. 6.7 years). DS children exhibit a significant reduction in the volume of the gray matter in the posterior lobe of the cerebellum, cingulate gyri, parahippocampal gyri and hippocampi, and in the volume of the white matter in the left posterior/anterior lobes of the cerebellum, left brainstem and frontal and parietal lobes, and sub-lobar region (Carducci et al., 2013). In contrast, significant preservation in the volume of gray matter is present in the left middle temporal lobe, the right sub-lobar region (lentiform nucleus) and in the parietal lobes (Carducci et al., 2013). The shape alterations present at fetal life stages are retained in the brain of infants and children with DS. At 3-5 months, the fronto-occipital length is shortened (secondary to reduction of frontal lobe growth), the occipital poles are flattened, the superior temporal gyri are narrower and the brain stem and cerebellum are smaller (Schmidt-Sidor et al., 1990). A study in children with DS from birth to five years of age reports a reduction in the fronto-occipital circumferences (Wisniewski, 1990).

CYTOARCHITECTURE

Fetuses. By 40 weeks of gestation, the cellular distribution of the layers of the visual cortex appear to be scarcely defined in DS fetuses in comparison with control fetuses (Becker, 1991). Lamination of the temporal neocortex of fetuses with DS is both delayed and disorganized (Golden and Hyman, 1994). In the brain of fetuses with DS [Gestational Week (GW) 19.8±2.2] brain neuron density

appears normal (Weitzdoerfer et al., 2001), although stereological quantification of total cell number in the neocortex showed that fetuses with DS at GW 19 have notably fewer cells than control fetuses (Larsen et al., 2008). Moreover, fetuses with DS (GW 17-21) have fewer cells than controls in the hippocampus and parahippocampal gyrus (Guidi et al., 2008). In addition, the cellular layers of the cerebellum have a reduced thickness and a prominent hypocellularity (Guidi et al., 2011b).

***Infants and children*.** DS neonates have fewer cells in the primary visual cortex and this difference persists during infancy (Wisniewski, 1990). In the brain of children with DS, areas 3, 4, 17 and 41 are characterized by architectonic abnormalities and a significant poverty of granular cells. Likewise, extracortical structures, such as the ventral cochlear nucleus, exhibit a greatly reduced number of neurons and a low cell packing density (Gandolfi et al., 1981). The reduced granule cell density (Baxter et al., 2000) observed in the cerebellum of fetuses with DS is retained in children. In addition to brain hypocellularity, children with DS exhibit remarkable abnormalities in the size of cortical minicolums in the superior temporal gyrus (Buxhoeveden et al., 2002), indicating gross defects in the architecture of the functional units of the neocortex.

2.8.2 Anatomy of the DS brain: DS mouse models

GROSS ANATOMY

Embryonic period. There are relatively scarce data regarding brain development of DS mouse models at embryonic life stages. At embryonic day (E) 13.5, E14.5 and E16.5 the **Ts65Dn** mouse shows a smaller medial-lateral length of the telencephalon and a reduction in the wet brain weight at E13.5 and E18.5 in comparison with euploid mice. Surprisingly, at E18.5 the Ts65Dn mouse recovers both the brain weight and the telencephalon gross size, indicating a probable early delay during brain growth (Chakrabarti et al., 2007). In the embryonic period E13.5-18.5, the **Dp(16)** model does not show any defect in forebrain growth. Its brain hemispheres are comparable to the euploid littermates along both the medial–lateral and rostro-caudal axes (Goodliffe et al., 2016). Brain development has

also been shown to be disrupted in **Ts1Cje** and **Ts2Cje** mice and at E14.5 their brain are smaller when compared with their euploid counterparts (Ishihara et al., 2010).

Early postnatal period. Data about differences between euploid and **Ts65Dn** mice in brain weight in the early post-natal period are inconsistent. According to some studies the Ts65Dn mouse has a reduced brain weight at P2 (Guidi et al., 2014) and P15 (Stagni et al., 2016), but other studies do not reports differences at P8, P15 and P22 (Belichenko et al., 2004, Chakrabarti et al., 2007, Bianchi et al., 2010b). While some studies show that the Ts65Dn mouse has no volume defects in the DG of the hippocampus, cortex, striatum and cerebellum at P2, P6, P10 and P22 (Holtzman et al., 1996, Belichenko et al., 2004, Lorenzi and Reeves, 2006), other studies report differences in the volume of the DG at P2 and P15 (Contestabile et al., 2009) and in the size of cerebellum at P2, P6 and P14 (Roper and Reeves, 2006, Contestabile et al., 2007). **Ts1Cje** mice at P12 show no reduction in brain weight and no modifications of overall brain volume compared with euploid mice (Ishihara et al., 2010).

Adolescence/adulthood. At P45 **Ts65Dn** mice have a reduced brain weight when compared with controls (Bianchi et al., 2010b). Accordingly, also the volume of the neocortex, cerebellum and hippocampus (DG, CA1 and CA3) is compromised at this age (Bianchi et al., 2010b, Guidi et al., 2014). Three month-old Ts65Dn mice exhibit a reduction of the DG volume (Lorenzi and Reeves, 2006, Stagni et al., 2015b), of cerebellar volume (Aldridge et al., 2007, Necchi et al., 2008), but a normal brain weight (Holtzman et al., 1996, Belichenko and Kleschevnikov, 2011, Stagni et al., 2015b) and normal volume of the brain and of the hippocampus (Aldridge et al., 2007, Olson et al., 2007). Ts65Dn mice aged 20-28 weeks showed a volume reduction in the CA2 field, but a normal volume in the other regions of the hippocampus (Insausti et al., 1998). In **Ts1Rhr** mice aged 3 months the volume of the brain but not of the cerebellum and hippocampus is reduced in comparison with euploid mice (Aldridge et al., 2007). Moreover, the Ts1Rhr model displays derangement in the spatial organization of subcortical structures (Aldridge et al., 2007). While at three months of age Ts1Rhr mice have a reduced volume of the cerebrum and cerebellum, at 7.5 months they have a brain weight

and volume of the posterior hippocampus that are larger than euploid mice (Belichenko et al., 2009). The **Ms1Rhr** mouse has a reduced volume, height, width, and length of the brain, reduced volume of the hippocampus at two and three months of age, but an increase in the volume of the cerebellum when compared to their euploid counterparts (Aldridge et al., 2007, Olson et al., 2007). At 10-16 weeks, the **Ts1Cje** mouse exhibits a reduction in the cerebellar volume (Olson et al., 2004). Similarly to earlier life stages, at 3 month the Ts1Cje mouse has no difference in brain weight and volume (Hewitt et al., 2010, Ishihara et al., 2010). No differences in brain weight have been also found in Ts1Cje mice aged 6-6.5, 7-7.5 and 9-10 months (Belichenko et al., 2007). Likewise, the area of the hippocampus shows no difference between Ts1Cje mice aged 18 months and their euploid counterparts (Belichenko et al., 2007). **Dp(16)** mice aged 3 months show a reduction of cerebellum cross-sectional area in comparison with euploid mice (Starbuck et al., 2014). **The Dp(16)/Dp(17)/Dp(10)** mouse model at 3 months has hydrocephalus, with lateral ventricles of the brains abnormally dilated (Yu et al., 2010a).

CYTOARCHITECTURE

Embryonic period. In the period E13.5-E18.5, the **Ts65Dn** mouse shows a thickness reduction in the inner zone (IZ) and sub-plate/cortical plate (SP/CP), with no differences in the thicknesses of the ventricular zone (VZ) and subventricular zone (SVZ). By E18.5 to birth, all layers of the neocortical wall have the same dimension in Ts65Dn mice as in euploid mice (Chakrabarti et al., 2007). The Ts65Dn model during the embryonic period displays a reduction in the size of the pyramidal cell layer of the CA1 region (Chakrabarti et al., 2007). Both **Ts1Cje** and **Ts2Cje** mice exhibit a reduction in cortical thickness at E14.5 when compared with their euploid counterparts (Ishihara et al., 2010). The **Dp(16)** mouse, in contrast with the Ts65Dn and the Ts1Cje/Ts2Cje models, does not exhibit prenatal forebrain growth alterations. At E13.5–E18.5, Dp16 mice do not show differences in the thicknesses of the VZ/SVZ, IZ, CP, and overall thickness of neocortical and hippocampal layers (Goodliffe et al., 2016).

Early postnatal period. At P2, **Ts65Dn** mice exhibit a reduced cellularity in the neocortex, DG, hippocampus, striatum, thalamus, hypothalamus mesencephalon, and cerebellum (Contestabile et al., 2007, Guidi et al., 2014). Hypocellularity in the DG has also been documented at P6 (Lorenzi and Reeves, 2006) and P15 (Bianchi et al., 2010b). At P8 and P15, Ts65Dn mice exhibit a reduction in the number of glutamatergic neurons in the neocortex and a concomitant increase in the number of inhibitory interneurons both in the neocortex and field CA1 (Chakrabarti et al., 2010). While at P0 Ts65Dn mice exhibit a similar number of cerebellar granule cell precursors as euploid mice in the external granular layer of the cerebellum (Roper and Reeves, 2006), at P2 there is a reduction in cell density in the external granular layer, internal granular layer, and Purkinje cell layer (Roper et al., 2006, Roper and Reeves, 2006, Contestabile et al., 2008, Guidi et al., 2014). The reduced thickness of the internal granular layer lasts until adulthood (Roper and Reeves, 2006). At variance with other brain regions, no differences were reported in either the number or size of basal forebrain cholinergic neurons in P2, P10 and P22 Ts65Dn and age-matched euploid mice (Holtzman et al., 1996). **Dp(16)** mice, at P15, show a reduced number of both excitatory and inhibitory neurons in the somatosensory cortex (Goodliffe et al., 2016). **Tc1** and **Ts1Rhr** mice show neither abnormal distribution of neurons nor differences in neuron polarity and orientation over the cortex at P21 (Haas et al., 2013).

Adolescence/adulthood. The defects in cytoarchitecture displayed by **Ts65Dn** pups are retained in adolescent mice. At P45 the Ts65Dn mouse shows reduced cell density, fewer granule neurons in the DG and a reduced thickness of the terminal field of the mossy fibers in the CA3 field in comparison with euploid mice (Bianchi et al., 2010b, Stagni et al., 2013). Accordingly, at 3 months of age, there is a reduction in cell density and total granule cell number in the DG of Ts65Dn mice, but no significant differences in cell number in the CA1 and CA3 fields were detected (Lorenzi and Reeves, 2006, Stagni et al., 2015b). A reduction in total granule cell number has been also detected in Ts65Dn mice aged 20-28 weeks (Insausti et al., 1998). Recent evidence shows that that perhirinal cortex of P15 Ts65Dn mice exhibits a reduced cellularity. in comparison with age-matched euploid mice. The same defect was present in 1.5-4.5 months old Ts65Dn mice, that display a significant cellularity

reduction in layers V (-25%) and VI (-23%) (Roncace et al., 2017). The cerebellum exhibits a normal cortical layering, but a reduction in the thickness of the molecular layer and granule cell layer of the vermis and in the density of the granule cells and Purkinje cells (Olson et al., 2007, Necchi et al., 2008). At 8-10 weeks, the **Ts1Rhr** mouse does not have a cell density reduction in both the internal granule cell layer and Purkinje cell layer. Ts1Rhr mice aged 7.5 months shows a greater thickness of the motor cortex in comparison with euploid mice (Belichenko et al., 2009). The **Ms1Rhr** mouse exhibits a higher density and number of both granule cells and Purkinje cells in comparison with euploid mice (Olson et al., 2007). A reduction in granule cell and Purkinje cell density was observed at three months of age in the **Dp(16)** mouse (Starbuck et al., 2014). Finally, the **Ts1Cje** mouse differs from its euploid counterpart in granule cell density, but not in Purkinje cell density (Olson et al., 2004) and at 18 months it has a thickness of the granule cell layer and molecular layer of the DG that is similar to that of controls (Belichenko et al., 2007). Data focusing on subcortical structures are also available for adult Ts65Dn mice. It has been shown that Ts65Dn mice aged 3 months exhibit no differences in i) the number of cholinergic cells in the medial septum-diagonal band of Broca and distribution of AchE fibers in the hippocampus; ii) the shape and distribution of tyrosine hydroxylase positive neurons in the substantia nigra and locus coeruleus; iii) the distribution of serotonin-positive neurons along the midline of Raphe nuclei (Megias et al., 1997). In 5-8 month-old Ts65Dn mice there is a reduction in the number of BFCN in the medial septum, consistently with evidence at earlier life stages (Cooper et al., 2001, Contestabile et al., 2006, Ash et al., 2014, Kelley et al., 2014). Ts65Dn mice aged 6-8 months and 14-18 months exhibit a reduction in acetylcholine transferase immunoreactivity in the hippocampus in comparison with euploid mice, suggesting a reduction in the cholinergic innervation originated in the medial septum (Kelley et al., 2016).

2.8.3 Proliferation potency in DS

2.8.3.1 Humans with DS

Differentiation of the neural tube into an outer mantle layer and an inner proliferative zone has occurred by gestational week six and some neurons have already been born. At week 7 of gestation, the germinal matrix can be divided into a VZ and an overlying SVZ. Neurons migrate out of these germinal zones giving origin to the cortical plate (Chan et al., 2002). In the human forebrain, neocortical neurons are generated during a restricted period that begins at approximately GW 6 and is largely completed by GW 18 (Stiles and Jernigan, 2010). By week 24 of gestation, the size of the VZ and SVZ is considerably reduced and there is a marked decrease in proliferative activity (Chan et al., 2002). There is a more prolonged period of neurogenesis in the human DG and cerebellum in comparison with the other brain regions. In the DG, neurogenesis begins at approximately GW 12 and is almost accomplished within the first postnatal year (Seress et al., 2001, Rice and Barone, 2010). Production of cerebellar granule cells starts at GW 12 (Abraham et al., 2011) and continues in the first few postnatal months (ten Donkelaar et al., 2003). The reduced cellularity in the brain of fetuses with DS suggests a reduction in proliferation potency starting from the earliest periods of neurogenesis. Due to the obvious difficulties in obtaining fetal material, very little information is available concerning neurogenesis in the fetal DS brain. By exploiting immunostaining for Ki-67 (a protein expressed during all phases of the cell cycle) evidence was obtained that in fetuses with DS (GW 17-23) the number of proliferating cells was notably reduced in the hippocampal DG, germinal zones of the hippocampus proper and parahippocampal gyrus, and in the germinal matrix of the inferior horn of the lateral ventricle (Contestabile et al., 2007, Guidi et al., 2008). In addition, the number of proliferating cells was notably reduced in the external granular layer of the cerebellum, and in a region of the fifth cerebellar lobe that is the remnant of the cerebellar VZ (Guidi et al., 2011b). A notable reduction in cell proliferation, as assessed by the cell cycle marker Ki-67 and the M-phase marker phospho-histone H3 (PH3) immunostaining, was also found along the VZ and SVZ of the frontal cortex of DS fetuses (GW 18) (Lu et al., 2012). A corresponding decline in proliferation was

also discovered in vitro in neurospheres generated from the frontal cortex of DS fetuses (Lu et al., 2012). This evidence shows a widespread reduction in the number of actively dividing cells in numerous brain regions of fetuses with DS, clearly indicating that alterations in proliferation rate are present at the very beginning of the process of neurogenesis.

2.8.3.2 DS Mouse models

By exploiting DS mouse models it has been possible to better elucidate the spatio-temporal distribution of the proliferation defects in the trisomic brain. In mice, similarly to humans, the bulk of brain neurons derive from the VZ and SVZ and are generated before birth. In contrast, in the subgranular zone (SGZ) of the hippocampal DG, a neurogenic niche that produces neurons destined to the DG, the bulk of neurogenesis takes place during the first two postnatal weeks, continues in a relatively substantial manner until young adulthood, and thereafter decreases with age (Altman and Bayer, 1975, Altman and Bayer, 1990a, c). A second important postnatal neurogenic niche is the SVZ of the lateral ventricle that gives rise to cells (most likely astrocytes and oligodendrocites) destined for the neocortex in the first few postnatal days (Brazel et al., 2003) and, subsequently, gives origin to granule neurons destined for the olfactory bulb. In the mouse cerebellum, granule cell production begins at approximately E15 but continues up to the second postnatal week (Sillitoe and Joyner, 2007, Sudarov and Joyner, 2007). Table 4 summarizes data obtained from the literature regarding proliferation rate in DS mouse models at different life stages. Regarding the magnitude of the differences in comparison with their euploid counterparts, they are in the range from -4 to -64% (average 33.7) in the **Ts65Dn** model, -25 to -60% (average 31.8) in the **Ts1Cje** model, and -30 to -51% (average 41.8) in the **Ts2Cje** model.

Embryonic period. There might be different causes regarding brain development alteration during fetal stages, such as (i) a smaller progenitor cell population at the beginning of neuronogenesis, (ii) altered kinetics of neuroblast proliferation, or (iii) increased death of either progenitors or postmitotic neurons (discussed below). The **Ts65Dn** model shows an overall reduction of BrdU-positive cells in

the pallium during embryonic developmental stages due to delayed exit from the cell cycle (Chakrabarti et al., 2007). Another deficit regards a poor generation of neurons by the germinal zone and abnormal migration of newly generated neurons into the SP/CP (Chakrabarti et al., 2007). In agreement with no detectable differences in prenatal brain development, the **Dp(16)** model does not show any variations in the size of actively dividing cell population across genotypes from E13.5 to E18.5 in either the neocortex or the MGE (Goodliffe et al., 2016). Both **Ts1Cje** and **Ts2Cje** mice show an overall reduction in the number of BrdU-positive cells in the period E13.5-E14.5 throughout the dorsal pallium. In particular, there are fewer BrdU-positive cells in VZ, SVZ, IZ, SP and CP in comparison with their euploid counterparts (Ishihara et al., 2010). Furthermore, they exhibit a reduction in the number of Ki67-positive cells. Taken together, these findings indicate that the pool of neural progenitor cells is highly compromised in these models (Ishihara et al., 2010).

Early postnatal period. In mice, the SGZ of the DG and the SVZ continue to proliferate during the entire lifespan (as in human beings), while in the cerebellum the production of granule neurons lasts from birth to the second postnatal week (Altman, 1982). At P0, the **Ts65Dn** mouse shows a strong decrease in the mitotic potency of the cerebellar granule neuron precursors (CGP) of the cerebellum and, at P2, it has fewer BrdU-positive cells in the EGL in comparison with euploid mice (Roper and Reeves, 2006, Contestabile et al., 2009, Guidi et al., 2014). This defect does not ameliorate at P6 and it translates into a reduction of CGP population at P30 (Roper and Reeves, 2006, Contestabile et al., 2009). An explanation of these defects could be the elongation of the cell cycle, with the G1 and G2 phases being those mainly impaired (Contestabile et al., 2009). At P2, the Ts65Dn mouse also shows fewer BrdU-positive cells in the SVZ, DG, neocortex, striatum, thalamus, hypothalamus, mesencephalon and pons (Contestabile et al., 2009, Guidi et al., 2014). Proliferation deficits have been observed at P15 in the striatum, neocortex, SVZ and DG and at P6, P15 and P30 in the DG (Lorenzi and Reeves, 2006, Contestabile et al., 2007, Bianchi et al., 2010a).

Adolescence/adulthood. During pre- and early-postnatal developmental stages, the number of proliferating cells in the **Ts65Dn** model is strongly affected. This defect is retained at further life

stages. In particular, at P30 and P45 the Ts65Dn mouse has a reduced number of BrdU- and Ki-67-positive cells in both SGZ of the DG and SVZ (Bianchi et al., 2010b, Chakrabarti et al., 2011, Guidi et al., 2014). Defects in the number of granule cells of the DG are still present when Ts65Dn mice reach adulthood (Insausti et al., 1998). A region that does not have proliferation defects at P45 is the olfactory epithelium, were PCNA-positive cells are equal between genotypes (Bianchi et al., 2014). In Ts65Dn mice aged 2-3 months there is a significant decrease in the density of BrdU-positive cells and Ki-67-positive cells in the motor cortex, in the DG and in the SVZ, but not in the corpus callosum (Belichenko and Kleschevnikov, 2011, Stagni et al., 2015b). The proliferation potency and cellularity defects in the hippocampus and SVZ of Ts65Dn mice persist when they reach 5 months of age or later ages (Corrales et al., 2013, Martinez-Cue et al., 2013, Lopez-Hidalgo et al., 2016). Ts65Dn mice aged 14 months show a reduction in the number of BrdU-positive cells in the SVZ and rostral migratory stream, indicating that defects present in earlier life stages in these zones persist during the life span (Guidi et al., 2016). At 3 months both **Ts1Cje** and **Ts2Cje** mice show a reduction in the number of proliferating cells in the DG and SVZ (Ishihara et al., 2010).

2.8.4 Mechanisms underlying proliferation potency impairment

The reduced proliferation potency that characterizes DS is due to a complex interaction between different molecular mechanisms, in which both triplicated and non-triplicated genes are involved.

Progression through the cell cycle is regulated by cyclin-dependent kinases (**CDK**s), and their interactions with cyclins and CDK inhibitors (**CKIs**). CDKs bound to their cognate cyclins drive transition phases of the cell cycle. Regulation of G1 is crucial for the balance between maintenance of the progenitor pool and generation of differentiated neurons, and inhibition of positive regulators of cell cycle progression enhances differentiation and reduces the size of the pool of neural stem/progenitor cells (Hindley and Philpott, 2012). The activity of D-type cyclins is necessary for progression through the G1 phase of the cell cycle. In the Ts65Dn mouse model of DS neural progenitor cells of the embryonic VZ of the lateral ventricle and hippocampus exhibit an elongation

of the S-phase as well as total length of the cell cycle (Chakrabarti et al., 2007). In the cerebellum of neonate Ts65Dn mice, granule cell precursors exhibit cell cycle elongation due to an increase in the length of the G1 and G2 phases of the cell cycle (Contestabile et al., 2009). This evidence in a DS model suggests that a reduction in the proliferation rate may be one of the determinants of the reduced proliferation potency in DS. Data obtained in the hippocampal DG and ventricular germinal matrix of fetuses with DS, suggests that neural progenitors exhibit an elongation of the G2 phase of the cell cycle cell and, possibly, an overall cell cycle elongation (Contestabile et al., 2007). Altered proliferation dynamics has been shown in fibroblast from DS patients (Kimura et al., 2005). More recently, it has been shown that DS patient-derived fibroblasts have an extended G1 duration (Chen et al., 2013). Elongation of the G1 obviously implies an overall increase in the duration of the cell cycle and, thus, a reduction in proliferation rate. It is important to observe that the G1 phase of the cell cycle is considered to be the critical window during which cells decide to proliferate, assume a reversible arrest (G0), or begin a path towards terminal differentiation or senescence. The available evidence suggests that the reduction in the number of cycling cells in the trisomic brain may be accounted for by reduction in proliferation rate (increase in the cell cycle length) as well as by a precocious exit from the cell cycle. Although various triplicated genes are likely to be involved in cell cycle alteration, the evidence reported below strongly suggests that Dual specificity tyrosine-phosphorylation-regulated kinase 1A (***DYRK1A***) (**Fig. 2.6A**) and Amyloid precursor protein (***APP***) may play a particularly prominent role (**Fig. 2.6B**).

DYRK1A. *DYRK1A* was proposed to be one of key candidate genes closely implicated in various DS phenotypes. There is evidence that triplication of *DYRK1A* leads to over-expression of DYRK1A in the brain of fetuses and adults with DS (Lockstone et al., 2007, El Hajj et al., 2016) and in DS-human pluripotent stem cells (iPSC)-derived NPCs (Hibaoui et al., 2014). Knocking down *DYRK1A* in Down syndrome patient-derived fibroblasts restored the impaired proliferation (Chen et al., 2013). This effect has been attributed to restoration of the G1 phase. This evidence strongly suggests a key role of DYRK1A in the regulation of proliferation and differentiation of trisomic neural progenitor cells.

One of the targets of DYRK1A is **cyclin D1**, an important cell cycle protein that promotes G1-to-S phase transition and is required for cell proliferation (Hindley and Philpott, 2012, Chen et al., 2013). DYRK1A phosphorylates cyclin D1 at Thr286 (Chen et al., 2013), causing its nuclear export, followed by degradation by an ubiquitin-dependent mechanism (Soppa et al., 2014). There is evidence that DYRK1A increases G1 duration in a dose-dependent manner reducing cyclin D1 levels (Chen et al., 2013). Consistently with DYRK1A over-expression in DS, cyclin D1 levels are reduced in the frontal lobe of fetuses with DS (Bernert et al., 1996) and in fibroblasts of DS patients (Chen et al., 2013). This evidence suggests that DYRK1A/Cyclin D1 may be one of the mechanism underlying the reduced proliferation potency of the DS. Alteration of DYRK1A and cyclin D1 expression similar to those found in humans have also been observed in the Ts65Dn mouse. Embryonic cortical stem cells in the dorsal VZ of Ts65Dn embryos contains 1.5-fold more DYRK1A protein than euploid embryos and have reduced cyclin D1 levels with a consequent lengthening of the G1 cell cycle phase and a reduction in the number of divisions producing neurons (Najas et al., 2015). The resulting deficit in cortical neurons persists at postnatal life stages. Genetic normalization of *Dyrk1a* dosage in the Ts65Dn embryos restores cyclin D1 to normal levels and this effect is accompanied by a restoration of the number of cortical neurons at postnatal life stages (Najas et al., 2015). This evidence suggests that DYRK1A-mediated degradation of cyclin D1 may underlie the reduction of progenitor neurogenic potential. It has been shown that NPCs from Ts65Dn mice exhibit a premature neuronal differentiation that is prevented by normalization of DYRK1A activity with harmine (Mazur-Kolecka et al., 2012), suggesting that DYRK1A over-expression in DS leads to premature neuronal differentiation. In addition to reduce nuclear levels of Cyclin D1, over-expression of DYRK1A has been shown to increase the transcriptional levels of the antiproliferative cyclin-dependent kinase inhibitor **p27^{KIP1}** (CDKN1B) (Hammerle et al., 2011) and also its stability by phosphorylating it on Ser10 (Soppa et al., 2014). It is well-established that DYRK1A phosphorylates p53 and that DYRK1A-induced p53 phosphorylation leads to induction of p53 target genes and impaired G1/G0-S phase transition, resulting in attenuated proliferation. **p21^{CIP1}**, also known as cyclin-dependent

kinase inhibitor 1, represents a major target of p53 that promotes its transcription (Park et al., 2010). Accordingly, brains from embryonic *Dyrk1a* transgenic mice exhibit elevated levels of DYRK1A, phosphorylated p53, and $p21^{CIP1}$ as well as impaired neuronal proliferation (Park et al., 2010). Increased levels of DYRK1A, p53 and $p21^{CIP1}$ have been observed in the frontal cortex of fetuses and adults with DS (Park et al., 2010). Excessive $p21^{CIP1}$ levels have also been found in the hippocampus of young Ts65Dn mice (Stagni et al., 2015b). This evidence strongly suggests that DYRK1A may also hamper proliferation by increasing $p21^{CIP1}$ levels.

APP. *APP* is one of the triplicated gene that is thought to play a key role in neurodevelopmental alterations in DS and to underlie development of Alzheimer's-like pathology in adults with DS. Although in whole brain homogenates of fetuses with DS no significant differences in APP levels have been detected (Ferrando-Miguel et al., 2003), we found increased levels of APP protein in homogenates from the basal ganglia of fetuses with DS (Guidi et al., 2017). Moreover, increased APP levels have been detected in brains of fetuses with DS at the protein level (Tanzi et al., 1987). Consistently with increased APP expression, increased levels of APP carboxy-terminal fragments have been found in the brain of fetuses with DS (Russo et al., 2001). In addition, increased APP levels have been detected in cultures of cortical neurons from fetuses with DS (Busciglio et al., 2002). Consistently with evidence in DS brain tissue, increased levels of APP and of its derivatives were found in NPCs from SVZ of P2 Ts65Dn mice and cerebellar samples form P2 mice (Contestabile and Ciani, 2008, Trazzi et al., 2011, Trazzi et al., 2013). Over-expression of APP in HEK293 cells has been shown to inhibit cell proliferation. Consistently with this observation, gene expression profiling of HEK 293 cells overexpressing APP reveals an alteration of a set of genes involved in G1/S checkpoint regulation, cell proliferation and p53 signaling. This evidence, in conjunction with the higher expression levels of APP starting from the earliest phases of brain development, suggests that this gene may play a prominent role in neurogenesis alterations in DS. Processing of APP gives origin to various derivatives including **AICD** (amyloid precursor protein intracellular domain). Excessive

AICD levels appear to affect cell proliferation by interacting with glycogen synthase kinase 3-β (**GSK3β**) signaling and the Sonic Hedgehog (**SHH**) signaling pathway.

GSK3β is a constitutively active kinase that is inhibited by an increase in its phosphorylation (on ser9). Increased activity of its dephosphorylated form causes adverse effects, such as a reduction in neurogenesis and impairment of synapse development (Eldar-Finkelman and Martinez, 2011, Kim and Snider, 2011), and altered GSK3β activity appears to be involved in neurodegenerative and neurological disturbances (Eldar-Finkelman and Martinez, 2011). Reduced phosphorylation levels (on ser9) of GSK3β has been found in NPCs from Ts65Dn mice (Trazzi et al., 2014) and in the hippocampal DG and VZ of the hippocampus of fetuses with DS (Trazzi et al., 2014). More recently, a reduction in pSer9 of GSK3β have been observed in hippocampal homogenates of Ts65Dn mice aged 3 and 7 months (Kazim et al., 2017). The latter evidence suggests that early alterations in GSK3β activity may significantly contribute to impair proliferation of NPCs during brain development. Compelling evidence suggests that excessive levels of AICD prevent GSK3β phosphorylation (on ser9) thereby increasing its activity (Trazzi et al., 2014). Recent evidence shows that GSK3β phosphorylates cyclin D1 at Thr286 (Takahashi-Yanaga and Sasaguri, 2008). Therefore, the increased activity of GSK3β in trisomic cells may increase the phosphorylation of cyclin D1 and its nuclear export and degradation. GSK3β regulates the WNT/beta-catenin signaling pathway. Increased GSK3β activity increases beta-catenin phosphorylation and retains it in the cytoplasmic compartment, favoring ubiquitin-proteasome system beta-catenin degradation. On the contrary, non-phosphorylated beta-catenin escapes degradation, and translocates into the nucleus where it induces the expression of downstream target genes including cyclin Dl. In trisomic cells, increased activity of GSK3β reduces beta-catenin nuclear translocation and, consequently, the expression of cyclin D1 (Takahashi-Yanaga and Sasaguri, 2008). The fact that GSK3β regulates the levels of cyclin D1 in two different manners suggests that this kinase may play a prominent role in deregulation of cell proliferation in DS. AICD, in addition to interacting with GSK3β, increases the transcription of the Patched 1 (**PTCH1**) protein in trisomic NPCs (Trazzi et al., 2011). PTCH1 is an SHH receptor that

keeps the mitogenic SHH pathway repressed by inhibiting the 7-pass transmembrane protein Smoothened (SMO), thereby hampering proliferation. Consistently with the increased APP/AICD levels, PTCH1 is overexpressed in fetuses with DS and in the Ts65Dn mouse model (Trazzi et al., 2011), indicating that this deregulation is likely to play an important role in neurogenesis alterations in DS. Consistently with this idea, restoration of PTCH1 levels restores the proliferation defects of trisomic NPCs (Trazzi et al., 2011). There is evidence that activation of the SHH pathway induces sustained activity of the G1 cyclin-Rb axis by enhancing the expression of cyclin D1, cyclin D2, and cyclin E (Kenney and Rowitch, 2000). This suggests that increased PTCH1 levels in trisomic cells may hamper cell cycle progression by reducing the expression of cyclin D1 (and cyclin D2, cyclin E). Thus, increased AICD levels hamper the activity of the SHH pathway at two different levels: 1) because they increase PTCH1 expression and 2) because they increase GSK3β activity which, in turn, contributes to hamper translocation of the effectors of the SHH pathway to the nucleus.

GSK3β signaling activates the β-site APP cleaving enzyme 1 (BACE1) gene expression, resulting in enhanced β-secretase processing of APP and Aβ production (Ly et al., 2013). Since Aβ derives from the cleavage of the APP beta-carboxyterminal fragment that is composed by Aβ plus AICD, the observed increase in Aβ should be paralleled by an increase in AICD levels. This evidence suggests that overactivity of **GSK3β i**n DS may potentiate the production of **AICD** and the detrimental effects described above. It is of interest to observe that DYRK1A-mediated APP phosphorylation at the Thr668 residue enhances the formation of Aβ (Park et al., 2007) suggesting enhanced formation of AICD may also be mediated by DYRK1A over-expression.

Evidence in Ts65Dn mice showed reduction in **cyclin B1** and SKP2 levels and a larger number of dividing cells in the G2 phase and a prolonged G2 phase (Contestabile et al., 2009). Cyclin B1 is the regulatory subunit of CDK1, the key controller of mitosis entry (Takizawa and Morgan, 2000). Hence, downregulation of cyclin B1 is expected to induce a lengthening of the G2 phase. In addition, the cytoplasmic/nuclear subcellular localization of cyclin B1 has been shown to be regulated by the SHH pathway. Indeed, PTCH1 interacts with cyclin B1 and hampers its nuclear transfer

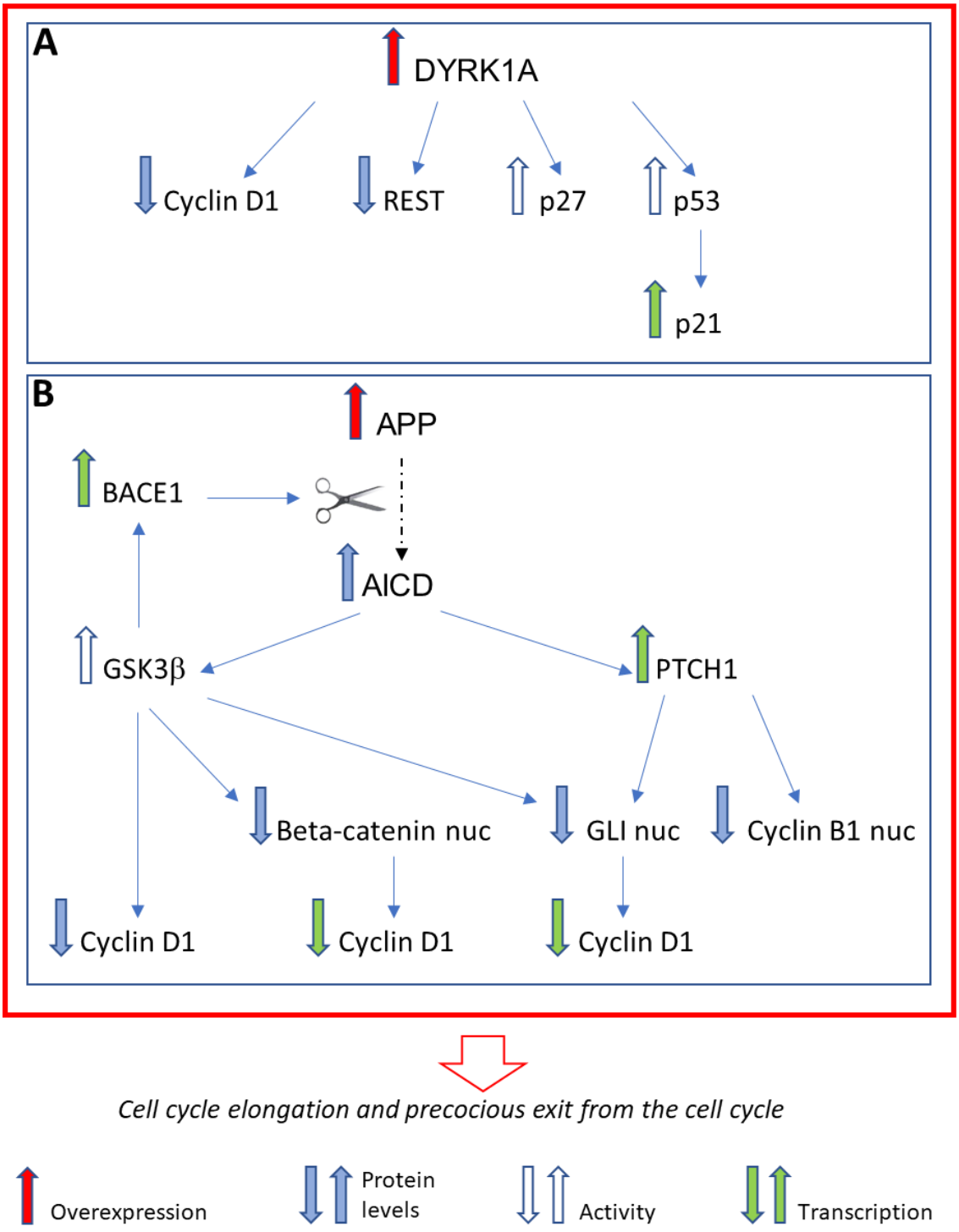

Figure 2.6. Mechanisms underlying impairment of proliferation potency in DS. The mechanisms whereby overexpression of the triplicated genes *DYRK1A* (A), *APP* (B) impair proliferation of NPCs in DS are schematically illustrated [modified from (Stagni et al., 2017)]. Abbreviation: nuc, nuclear.

(Barnes et al., 2001), indicating that PTCH1 also participates in the regulation of G2/M checkpoint (Adolphe et al., 2006).

2.8.5 Phenotype acquisition

2.8.5.1 Humans with DS

Various studies show that the reduced proliferation potency of the trisomic brain is worsened by reduction in the acquisition of a neuronal phenotype accompanied by an increase in the acquisition of an astrocytic phenotype. This defect is already present during the earliest phases of neurogenesis because quantification of the number of mature neurons (NeuN-positive cells) and astrocytes (GFAP-positive cells) in the hippocampal and parahippocampal region showed that in all these regions fetuses with DS have proportionally fewer neurons and a larger number of astrocytes compared with normal fetuses (Guidi et al., 2008). Consistently with this evidence, in neonates with DS the interlaminar glial palisade, composed by astroglial cells, appears to be altered by the first year of age (Colombo et al., 2005). Astrocytic hypertrophy and an increase in astrocyte number are present in the fetal DS brain and this defect is retained in adulthood (Mito and Becker, 1993, Griffin et al., 1998). Likewise, quantification of cells immunopositive for the astrocytic markers **S100β** and GFAP showed that children with DS have a notably larger number of astrocytes then controls in the hippocampus and frontal and occipital lobes (Becker, 1991). Results obtained in fetal tissue were confirmed in cortical neuronal cultures derived from fetuses with DS or from fibroblast-derived iPSCs from patients with DS. Human DS iPSC lines generated from second trimester amniotic fluid exhibit a reduction in the acquisition of a neuronal phenotype (Lu et al., 2013). Cell cultures derived from the cortex of fetuses with DS exhibit a reduced number of cells that differentiate into neurons (β III-Tubulin-positive cells; 7%) in comparison with control cultures (56%). Moreover, DS neurons exhibit a notable reduction in neurite length (Bahn et al., 2002). This study, however, did not show a difference between euploid and DS cultures in the number of cells differentiated into astrocytes (GFAP-positive cells) (Bahn et al., 2002). iPSC-derived NPCs from DS patients maintained under spontaneous differentiation

condition were shown to give rise to fewer neurons (β III-Tubulin-positive cells) and more astrocytes (S100β-positive cells) (19.7±0.9% and 78.2±0.7%, respectively) in comparison with control cultures (33.4±2.0% and 60.9±2.0%, respectively) (Chen et al., 2014). In addition, DS neurons generated under spontaneous differentiation conditions exhibited decreased neurite length compared with control neurons. iPSCs derived from monozygotic twins discordant for trisomy 21 show that DS iPSCs exhibit an abnormal neural differentiation. In particular, DS-cells exhibit decreased expression of neuronal markers (β III-Tubulin and MAP2) and an increase in astrocytic markers (GFAP, VIMENTIN, S100β, OLIG1 and OLIG2) consistent with a shift from neuronal to astroglial and oligodendroglial phenotypes (Hibaoui et al., 2014). Moreover, neurons derived from Twin-DS-iPSCs exhibited a reduced number and length of neuritis.

2.8.5.2 DS mouse models

DS mouse models show abnormalities in phenotype acquisition similar to those found in individuals with DS. A reduction in the number of cells differentiated into neurons and an increase in number of cells with an astrocytic phenotype has been found in cultures of NPCs from the SVZ of neonate Ts65Dn mice (Trazzi et al., 2011, Trazzi et al., 2013). Likewise, in the DG and cerebellum of young adult Ts65Dn mice the total number of new cells with a neuronal phenotype is significantly reduced and the number of new cells with an astrocytic phenotype is larger than in euploid mice (Contestabile et al., 2007, Contestabile et al., 2009, Bianchi et al., 2010b, Ishihara et al., 2010, Chakrabarti et al., 2011, Guidi et al., 2014). Although in absolute terms Ts65Dn mice may have a similar number of astrocytes as euploid mice, they have a higher ratio of astrocytes over total cell number due to their reduced number of new neurons (Guidi et al., 2014). Consistently with the enhancement in astrocytic phenotype acquisition, a higher number of astrocytes has been found in the hippocampus of Ts65Dn mice in comparison with euploid mice, although the difference did not reach significance (Holtzman et al., 1996, Guidi et al., 2014). In contrast to this evidence, a recent study shows that 4 month-old Ts65Dn mice have a lower percentage of BrdU/GFAP-positive cell in the DG in comparison with

euploid nice (Lopez-Hidalgo et al., 2016). Four- to five month-old Ts65Dn mice display higher density of total inhibitory neurons in the somatosensory cortex than in their euploid littermates, and, in particular of Calretinin-positive cells (Perez-Cremades et al., 2010). Cultures of NPCs from the SVZ of Ts1Cje mice exhibit a reduction in the number of cells differentiated into neurons and an increase in new astrocytes with no differences in the number of new oligodendrocytes (Moldrich et al., 2009, Hewitt et al., 2010, Kurabayashi et al., 2015). Impairment of neuronogenesis has been also found in the SVZ and DG of Ts1Cje mice aged 3 months (Ishihara et al., 2010). Much less information is available regarding the olygodendrocytic lineage in DS. Regarding the acquisition of an oligodendrocytic phenotype, the available evidence suggests no patent alterations in this process. Unlike NPCs, which are reduced in number in Ts65Dn mice, the number of oligodendrocyte precursor cells (OLIG2+NG2-positive cells) in P7-P60 Ts65Dn mice is similar to that of euploid mice (Olmos-Serrano et al., 2016). Moreover, an analysis of oligodendrocyte precursor cells isolated from the cortex of P7 mice showed no differences between euploid and trisomic cultures. However, cell culture experiments show that Ts65Dn oligodendrocytes exhibit cell-autonomous impairment in oligodendrocyte maturation and viability (Olmos-Serrano et al., 2016). This difference is consistent with the reduced myelination observed in fetuses and children with DS (Wisniewski and Schmidt-Sidor, 1989, Becker, 1991, Abraham et al., 2011) and in the Ts65Dn mouse model (Meraviglia et al., 2016, Olmos-Serrano et al., 2016).

2.8.6 Mechanisms underlying impairment of phenotype acquisition

As described above, acquisition of a neuronal phenotype is impaired in DS, and trisomic NPCs exhibit a shift towards the acquisition of an astrocytic phenotype. The Janus kinase-signal transducer and activator of transcription JAK-STAT pathway is one of the most crucial pathway for the astrogliogenic differentiation machinery in neural progenitor cells (Bonni et al., 1997). Ligands as interleukins and interferons (IFNs) family bind to their corresponding receptors. Binding to these receptors activates JAKs, which can activate the transcription factors STATs. STATs migrate from

the cytoplasm to the nucleus to bind the promoters of target genes and initiate transcription. Among STATs transcription factors, STAT3 specifies glial cell fate by transcriptional activation of astrocytic genes, such as *GFAP* and *S100β*. The increase in the acquisition of an astrocytic phenotype in the DS brain may be attributable to over-expression of ligands and receptors that activate the JAK-STAT signaling pathway. In this connection, it is important to note that on HSA21 there are several genes encoding receptors both for interferons (*IFNAR1*, *IFNAR2*, *IFNGR2*) and *IL10RB* and therefore responsible for activating JAK-STAT signaling cascades (**Fig. 2.7**). Consistently with triplication of these genes, a significant increase of IFNAR2 proteins has been found in the cerebral cortex of DS fetuses at 19–21 weeks of gestational age (Ferrando-Miguel et al., 2003). In addition, over-expression of the triplicated genes *Ifnar1*, *Ifnar2*, and *Il10rb* has been found at the RNA level in the brain of neonate Ts1Cje mice (Amano et al., 2004). The fact that *IFNR* genes are triplicated and upregulated in DS individuals and DS mouse models may predispose the DS brain to greater IFNs sensitivity. Interestingly, serum levels of IL-6 are increased in DS children (Corsi et al., 2006), which is consistent with the hypothesis of overactivation of the JAK-STAT signaling cascade in DS. Taken together, these data suggest that overstimulation of the JAK-STAT signaling pathway due to over-expression of IFNRs starting from early phases of brain development may promote neural progenitor cell fate toward astrogliogenic pathways in the DS brain. Overstimulation of JAK-STAT signaling pathway can also be linked to over-expression of two other triplicated genes, *APP* and *DYRK1A*. There is evidence that soluble secreted APP (sAPP) enhances the activity of the JAK-STAT signaling cascade, suggesting that increased levels of sAPP may enhance the process of astrogliognesis in DS (Trazzi et al., 2013). Indeed, NPCs from Ts65Dn mice exhibit enhanced expression of JAK1 and GFAP that is restored by treatment with an antibody that recognizes the N-terminal region of APP (sAPP). In line with data obtained in trisomic NPC cultures, upregulation of JAK1 and STAT3 has been detected in the hippocampus of neonate Ts65Dn mice. Taken together these results strongly suggest that in trisomic NPCs high levels of sAPP may activate the JAK/STAT signaling pathway, thus promoting the expression of GFAP (**Fig. 2.7**).

As mentioned above, increased levels of the APP-derived peptide AICD enhances *Ptch1* expression, which keeps the SHH pathway repressed. Consequently, in trisomic NPCs the levels of Gli1 and Gli2 transcription factors, the mediators of SHH signaling, are down regulated. Gli2 induces neuronogenesis in neuronal stem cells by positively regulating the expression of neurogenic basic helix-loop-helix genes, such as *Mash1*. Mash1 was found to be downregulated in trisomic NPCs and restoration of the activity of the SHH pathway restored its levels (Trazzi et al., 2013). Thus, the triplicated *APP* may account for enhancement of astrogliogenesis, through the JAK-STAT signaling cascade, and reduction of neurogenesis, through the APP/AICD system (**Fig. 2.7**).

Over-expression of DYRK1A in wild-type cortical progenitors increases STAT3 phosphorylation at Ser(727) (**Fig. 2.7**), a regulatory site that enhances the transcriptional activity of STAT3 (Kurabayashi et al., 2015), suggesting that the increased propensity of Ts1Cje neocortical progenitors to differentiate into astrocytes may be due to increased dosage of *DYRK1A*. Indeed, in Ts1Cje cortical progenitors STAT3 Ser(727) phosphorylation and STAT activity are elevated in a DYRK1A-dependent manner and reducing DYRK1A level attenuates deregulation of STAT (Kurabayashi et al., 2015). These findings strongly suggest that DYRK1A-dependent potentiation of STAT signaling pathway may contribute to the aberrant astrogliogenesis in DS. Consistently with this idea, targeting DYRK1A pharmacologically or by shRNA in iPSCs derived from monozygotic twins discordant for trisomy 21 resulted in a considerable correction in the acquisition of a neuronal phenotype in Twin-DS-iPSCs (Hibaoui et al., 2014).

2.8.7 Dendritic hypotrophy

Dendritic pathology is a typical feature of the DS brain and appears to correlate to some extent with the cognitive profile.

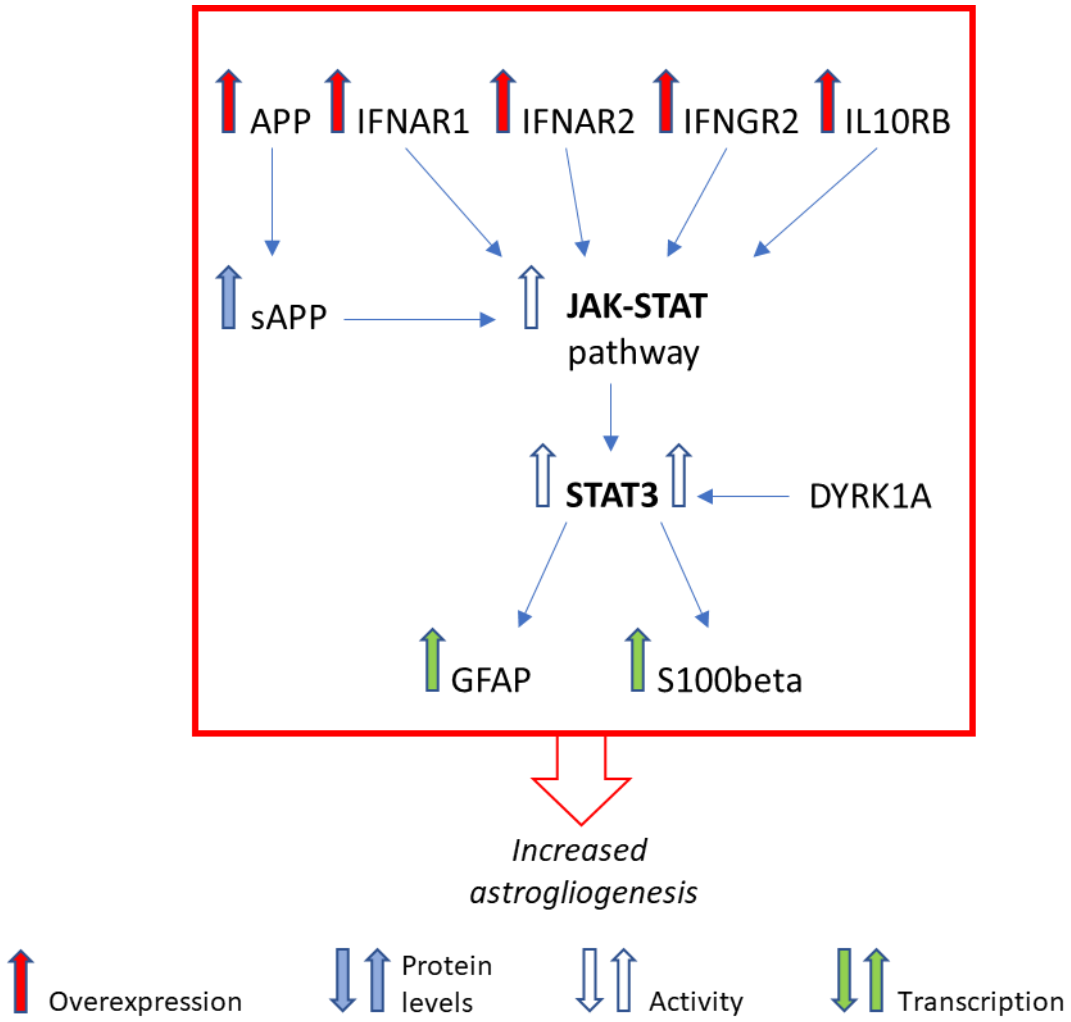

Figure 2.7. Mechanisms underlying impairment of phenotype acquisition in DS. Overexpression of the indicated triplicated genes enhances the activity of the JAK-STAT pathway which leads to increased expression of GFAP and S100β and, consequently, to the enhancement of astrogliogenesis [image modified from (Stagni et al., 2017)].

2.8.7.1 Humans with DS

Dendrites. It has been argued that DS persons start their lives with an apparently normal neuronal architecture that progressively degenerates. Thus, normal or even increased branching in the DS fetus and newborn contrasts with dendritic hypotrophy in older children with DS. Becker et al. showed that dendritic branching and length in both apical and basilar dendrites were greater in infants with DS younger than 6 months than in normal infants (Becker et al., 1986). During the peak period of dendritic growth and differentiation, quantitative analysis of dendrites showed no significant differences in dendritic differentiation of pyramidal neurons of prefrontal cortex of the brains of 2.5-month-old DS infants (Vuksic et al., 2002). In contrast, the pyramidal neurons of the visual cortex of newborns older than 4 months have shorter basilar dendrites (Takashima et al., 1981). Subsequent to 2.5-month of age, children with DS exhibit a steady decrease in dendritic length, especially in apical dendrites. Dendritic hypotrophy is also present in pyramidal neurons of the parietal cortex of children with DS (Schulz and Scholz, 1992). The dendritic hypotrophy seen in childhood continues into adulthood, with a marked decrease in dendritic branching and dendritic length in elderly adults with DS (Takashima et al., 1989). This evidence shows that in DS brains the dendritic tree begins to be atrophic in early infancy without a recovery at subsequent life stages. In agreement with the deteriorated dendritic development, down-regulation of various proteins forming neuron cytoscheleton or associated with the endoplasmic reticulum takes place in the DS brain. All these changes may be involved in the deteriorated neuritic outgrowth and arborization of DS neurons.

Spines. Spine counts (basilar dendrites) in the visual cortex of fetuses with DS are similar to those of control fetuses. After birth, infants with DS have a reduced number of spines, that show also an altered morphology (Takashima et al., 1981). While in normal subjects, spine density on the basal dendrites of cortical pyramidal neurons increases until 15 years of age and gradually decrease after 20 years, in subjects with DS spine density poorly increases in children and rapidly decreases in adults (Suetsugu and Mehraein, 1980, Takashima et al., 1989). A reduced spine density has been found in the apical dendrites of pyramidal neurons of the hippocampus and cingulate cortex and in both the apical and

basilar dendritic arbors of CA1 and CA2-3 pyramidal neurons in patients with DS when compared to age-matched controls (Suetsugu and Mehraein, 1980, Takashima et al., 1989). The dendritic spines of the DS brain exhibit also aberrant morphology. Indeed, starting from infancy, spines are small, have short stalks and are intermingled with unusually long spines (Marin-Padilla, 1976). Drebrin A, a neuron-specific F-actin binding proteins, regulates dendritic spine morphology, size and density, and is manifold decreased in brains of fetuses and adults with DS (Shim and Lubec, 2002). Over-expression of drebrin A favors excitation in mature hippocampal neurons (Ivanov et al., 2009). Since drebrin expression is reduced in DS individuals (Shim and Lubec, 2002), a reduced excitatory-inhibitory ratio is expected in DS individuals.

2.8.7.2 Mouse models of DS

Dendrites. Similarly to humans, mouse models of DS exhibit defects in their dendritic arborisation. In Ts65Dn mice aged 45 days, the granule cells of the DG show a reduction in total dendritic length, branch number and mean length of each branch (Guidi et al., 2013, Guidi et al., 2014). These defects are still present when mice become young adults (3 months of age) or aged adults (13-17 months of age) (Velazquez et al., 2013, Dang et al., 2014, Stagni et al., 2015b). Defects in the dendritic pattern were also found in neocortical pyramidal cells of **Ts65Dn** mice aged 10 weeks (Benavides-Piccione et al., 2004). In the brain of neonate Ts65Dn mice the levels of MAP2, an early marker of the dendrites, are significantly increased compared to littermate controls (Pollonini et al., 2008). The levels of MAP2 in hippocampal extracts of adult (4 months) Ts65Dn mice are similar to those of littermate controls, while in middle-aged (9-15 months old) Ts65Dn mice hippocampal MAP2 levels undergo a decrease vs. controls (Granholm et al., 2003), suggesting an age-related dendritic deterioration.

Spines. In Ts65Dn mice the basal dendrites of neocortical pyramidal cells exhibit a reduced spine density (Dierssen et al., 2003). A spine density reduction is also present in the granule cells of the DG, accompanied by a reorganization of inhibitory inputs, with a relative decrease in inputs to the

dendritic shafts and an increase in inputs to the necks of spines (Belichenko et al., 2004, Popov et al., 2011, Stagni et al., 2013). The thorny excrescences of CA3 pyramidal neurons (the site of termination of the axons of the granule cells) also exhibit a large decrease in the number of thorns (Popov et al., 2011, Stagni et al., 2013). The spines of Ts65Dn mice not only exhibit a density reduction, but also show an aberrant morphology. Indeed, the spines of young (21 days) and adult Ts65Dn mice have a larger volume in comparison with euploid mice in the DG, field CA1, motor, somatosensory and entorhinal cortices, and medial septum (Belichenko et al., 2004). Defects in spine density and spine shape, with a reorganization of inhibitory inputs were also detected in the granule cells of **Ts1Cje** and **Ts2Cje** mice, although these changes are less severe than in Ts65Dn mice (Villar et al., 2005, Belichenko et al., 2007). Similarly to other mouse models, the granule cells of Ts1Rhr mice exhibit a reduced spine density and a significant increase in the size of spine heads. In contrast, spine density is not reduced in pyramidal neurons of the motor cortex (Belichenko et al., 2009).

2.8.8 Synaptic density, excitatory vs. inhibitory synapses, and synaptic proteins

2.8.8.1 Humans with DS

The synapses of the DS brain exhibit various alterations in the expression of synaptic proteins. Synapsin I (a pre-synaptic protein which binds synaptic vesicles to the cytoskeleton and regulates synaptic vesicle release) is expressed at lower levels in neurospheres from human embryonic tissue (Bahn et al., 2002). Since this protein plays a role in the regulation of transmitter release, its down regulation may compromise synaptic function. Synaptojanin, a synaptic protein thought to be involved in clathrin mediated synaptic vesicle endocytosis, is mapped on HSA21q22.2. Consistent with HSA21 triplication, excessive expression of synaptojanin has been demonstrated in the cerebrum of individuals with DS from fetal life stages to adulthood (Arai et al., 2002). In addition to changes in the expression of synaptic proteins, synapses of individuals with DS show abnormalities in synaptic length and contact zones (Wisniewski, 1990).

2.8.8.2 Mouse models of DS

The synaptic density and the synapse-to-neuron ratio are reduced in the DG and hippocampal fields CA3 and CA1 of adult Ts65Dn mice (Kurt et al., 2004), with a reduced ratio that is specific for asymmetric synapses (presumably excitatory), while symmetric synapses (presumably inhibitory) are unchanged. In aged Ts65Dn mice, the temporal cortex has a lower number (30%) of asymmetric synapses while the number of symmetric synapses is not different vs. controls ((Kurt et al., 2000). The reduced number of excitatory synapses in Ts65Dn mice seems in agreement with the reduced levels of excitatory aminoacids found in the parahippocampal gyrus of patients with DS (Risser et al., 1997). The increase in the number of GABAergic interneurons found in the primary somatosensory cortex of 4-5 month old Ts65Dn mice (Perez-Cremades et al., 2010) suggests that in some brain regions excessive inhibition may be due to an absolute increase in the number of inhibitory synapses. In the brains of neonate Ts65Dn mice, the levels of synaptophysin, synapsin, spinophilin (a scaffold protein that is involved in spine morphology and density regulation) are similar to those of littermate controls (Pollonini et al., 2008). In the neocortex and hippocampal field CA1 of Ts65Dn mice a reduction in synaptic density has been detected as early as P8 (Chakrabarti et al., 2007). Ts65Dn mice aged 45 days or 3 months had fewer SYN and PSD-95 immunoreactive puncta in the DG, field CA3 and neocortex, suggesting a reduced number of presynaptic and postsynaptic terminals (Fernandez et al., 2009). Moreover, no differences were detected in the levels of other presynaptic proteins, such as synapsin, synaptotagmin (a putative calcium sensor in the presynaptic terminal) and synaptophysin (Fernandez et al., 2009). In the somatosensory cortex of 4-5 month-old Ts65Dn mice, there is an increment of synaptophysin vs. euploid littermates (Perez-Cremades et al., 2010). In the hippocampus of adult (4 months) Ts65Dn mice, whereas synapsin, spinophilin and gephyrin are expressed at levels similar to those of controls, the expression levels of synaptophysin are significantly decreased (Pollonini et al., 2008).

2.8.9 Trisomic genes and dendritic/synaptic alterations

The study of the mechanisms implicated in the regulation of neuronal morphology during development and maintenance of the adult CNS is object of intense research.

It has been reported that DYRK1A not only influences neurogenesis but also dendritic development (Yang et al., 2001, Hammerle et al., 2003). DYRK1A regulates development of the dendritic trees of neurons and modulates the activity of the c-AMP response element-binding protein (CREB), which participates in signal transduction pathways involved in synaptic plasticity and neuronal differentiation. Moreover, DYRK1A may modulate dendritic development by regulating vesicle trafficking that is dependent on dynamin1 (Hammerle et al., 2003), a GTPase putative substrate of DYRK1A that plays a fundamental role in neurite outgrowth (Chan et al., 2002). Interestingly, mice with one functional copy of *Dyrk1a* (*Dyrk1a*$^{+/-}$ mutants) display a brain size 30% smaller than that of wild-type mice, considerably smaller and less branched cortical pyramidal cells and behavioral defects (Benavides-Piccione et al., 2004). In humans, *DYRK1A* has been proposed to be associated with microcephaly and mental retardation, given its localization to the minimal overlapping region observed in patients with partial monosomy 21 (Moller et al., 2008). Transgenic mice over-expressing *Dyrk1a* exhibit altered synaptic plasticity associated to learning and memory defects (Ahn et al., 2006). The studies in humans and animal models that are monoallelic or triallelic for *DYRK1A/Dyrk1a*, indicate that this gene is important in neural plasticity and necessary for the normal size and development of the brain in a dosage-sensitive way.

Neurotrophins are a small family of soluble factors that include nerve growth factor (NGF), brain-derived neurotrophic factor (**BDNF**) and neurotrophin 3 and 4 (NT3 and NT4). There are two types of neurotrophin receptors, the tropomyosin-related kinase receptors (TRKs) and the p75 neurotrophin receptor (p75) [see (Gonzalez et al., 2016)]. By specifically binding to tropomyosin-related kinase receptor B (TRKB), BDNF plays a key role in brain plasticity (Haniu et al., 1997), such as axonal and dendritic growth, membrane trafficking and fusion, and synapse formation, function, and plasticity. BDNF and its receptor TRKB represent the most widely expressed and studied

neurotrophin signaling pathway in the brain, and their participation in learning and memory is well-established (Minichiello, 2009). Upon BDNF binding, the TRKB receptor dimerizes and undergoes autophosphorylation in specific tyrosines of the intracellular domain. Activation of TRKs leads to the activation of different molecular pathways, such as mitogen-activated protein kinases (MAPKs), phosphatidylinositol-3-kinase (PI3K)-AKT, phospholipase-C (PLC)-g-Ca^{2+}, cyclic AMP (cAMP)/PKA, and the small GTPases of the Rho family Cdc42/Rac/RhoA [see (Gonzalez et al., 2016)]. In the plasma membrane, activated TRKB can be translocated into lipid rafts after BDNF stimulation, a step that may be required to induce dendritic branching and spine formation in cortical neurons (Suzuki et al., 2004). These lipid domains are the sites where the Ca^{2+}/calmodulin-dependent protein kinase CLICK-III plays a critical role in BDNF-induced dendritogenesis [see (Gonzalez et al., 2016)]. As mentioned above, the signaling pathways that regulate dendritic branching and spine formation via BDNF/TRKB include the activation of the PI3K/AKT and ERK1/2 signaling pathways as well as the activation of local protein translation by the mTOR kinase and activation of the Rho GTPase family protein to regulate the actin cytoskeleton [see (Gonzalez et al., 2016)]. Several lines of evidence suggest that BDNF increases the local translation of a subset of mRNAs in dendrites, including proteins related to CNS plasticity. In addition, CREB is required for BDNF-induced dendritic branching and dendritic spines plasticity of hippocampal neurons (Kwon et al., 2011). Finsterwald and colleagues demonstrated that the BDNF-induced increase in dendritic length and branching of cultured cortical neurons depends on the activation of the ERK pathway and phosphorylation of CREB at serine-133 (Finsterwald et al., 2010). In the DS brain, BDNF levels are already reduced at fetal life stages (Guedj et al., 2009, Toiber et al., 2010) and reduced BDNF levels have been shown in various brain regions of the Ts65Dn mouse (Bimonte-Nelson et al., 2003, Bianchi et al., 2010a, Fukuda et al., 2010, Begenisic et al., 2015, Stagni et al., 2015b, Kazim et al., 2017, Villarroya et al., 2017). In view of the prominent role of the BDNF-TRKB system in dendritic morphogenesis, deregulation of this pathway is probably a key determinant of the alterations of dendritic development and spine formation in DS.

2.9 Behavior impairment in DS

2.9.1 Humans with DS

As summarized in the preceding sections, the DS brain is characterized by a constellation of neurodevelopmental defects. The functional consequence of these morphogenetic changes results in abnormal neuronal connectivity and limited processing of information. Although the precise effect of cyto-architectonic abnormalities on cognitive development in DS is not clear, it seems plausible that neuropsychological abnormalities in DS, such as impairment of attention, executive control, language learning, working memory, and emotional responses, may reflect dysfunction in the cerebellar–cortical–limbic circuitry (Lott, 2012, Karmiloff-Smith et al., 2016). Although most individuals with DS have mild-moderate cognitive impairment [see (Hart et al., 2017)], certain cognitive domains such as language and memory appear to be affected disproportionately in comparison to other types of intellectual disability, resulting in a characteristic neurocognitive phenotype. People with DS have relative strengths in visuospatial processing and implicit long-term memory but more difficulty in working memory, episodic long-term memory, expressive language, and executive function (Liogier d'Ardhuy et al., 2015). Children with DS have relative strengths in social motivation and engagement, but they may struggle with social problem solving or decision making and higher order social cognition tasks [see (Hart et al., 2017)].

2.9.2 Mouse models of DS

Behavioral analysis of different DS models may help to elucidate the contribution of different groups of triplicated genes to behavioral impairment. The Ts65Dn mouse, the best-characterized model for DS, shows significant hyperactivity in the dark and in other settings that provoke caution and lack of movement in normal animals, such as in open-field and plus-maze tests. In addition, the Ts65Dn model exhibits no deficits in sensory capabilities and coordinated behaviors such as olfactory sensitivity, visual abilities, orienting reactions, forelimb strength, postural skills, coordination, climbing, locomotion, and motor coordination and balance deficits (rotarod test). In contrast, Ts65Dn

mice display notably reduced levels of performance in tasks that require the integrity of the hippocampal system, such as spontaneous alternation (T-maze task), contextual memory (fear-conditioning test), spatial learning, long-term memory and cognitive flexibility (Morris water maze test; radial arm maze test), non-spatial short- and long-term declarative memory (novel object recognition). Ts65Dn mice also show deficits in learning an operant conditioning paradigm [see (Bartesaghi et al., 2011, Rueda et al., 2012)]. This evidence indicates that in Ts65Dn mice declarative memory which, in rodents is delineated along spatial and recognition memory domains, is impaired, similarly to individuals with DS. It is important to note that, similarly to humans with DS, the Ts65Dn mouse show a cognitive decline with age, indicating a strong correlation with the onset of AD-like pathology.

Ts1Cje mice do not show differences in spontaneous motility compared to controls. Similarly to Ts65Dn mice, they display poorer performance in the T-maze task and Morris water maze test (MWM). Ms1Ts65 mice do not show differences in spontaneous motility compared to controls. However, in the MWM test they exhibit impairment in learning but not memory, as assessed in the probe phase of the test. In a novel open field activity test, Ts1Rhr mice show no difference in comparison with controls. Ts1Rhr mice are significantly impaired in the T-maze task (TM) and in the long-term (but not short-term) memory in the NOR test but show no impairment in the MWM test [see (Bartesaghi et al., 2011, Rueda et al., 2012)]. Dp(16) mice show impaired performance in the Morris water maze and the contextual fear conditioning tests. Ts1Yah mice are impaired in the novel object recognition and Y-Maze (YM) test, but their performance in the MWM is enhanced. Dp(17) do not show alterations in the Morris water maze and in the contextual fear conditioning tests. The Dp(10)1Yey/+; Dp(16)1Yey/+; Dp(17)1Yey/+ mouse is impaired in the Morris water maze and in the contextual fear conditioning test. Finally, Tc1 mice show altered performance in the novel object recognition test but not in the TM [see (Bartesaghi et al., 2011, Rueda et al., 2012)].

Taken together, these data show that impairment of memory functions is a feature shared by various mouse models for DS. Different models may exhibit a different degree of impairment. In this regard,

it is noteworthy that the Ts65Dn mouse model is presently the one that best recapitulates the human condition.

2.10 Therapeutic approaches in DS

The HSA21 is the smallest human chromosome. Despite the reduced dimension, its triplication means that over 500 genes (protein coding genes plus non-coding RNAs) are expressed in an abnormal way. In addition to problems deriving from triplicated genes on HSA21 themselves, it should be taken into account that every gene can interact with a number of other genes scattered along the genome. This implies that the genetic imbalance in trisomy 21 is extremely complicated, and attempts to design a therapeutic strategy to counteract this genetic condition may represent a real challenge. However, in the 16 years since HSA21 genome was sequences (Hattori et al., 2000), there has been considerable progress in understanding the phenotypic impact of the over-expression of some HSA21 genes. In addition, the development of several different mouse models of DS and the improvement in techniques that use iPSCs have facilitated our understanding of DS. Important advances have been also made in understanding the molecular basis of the early onset AD in DS, the molecular basis of the leukaemias that frequently occur in DS and the identification of genomic regions of HSA21 that harbour functional elements or causative genetic variation for certain phenotypes, such as congenital heart defects. Importantly, the past decade of research in the field of DS has generated a cautious enthusiasm for attempting to treat individuals with DS using drugs that appeared to be effective in DS mouse models (Antonarakis, 2017).

2.10.1 Clinical trials in DS

Clinical trials in individuals with DS were based on condition-specific aspects of neurobiology, neurochemistry, and neuroplasticity or connectivity within the brain (Lott, 2012, Esbensen et al., 2017). Given the variability in the behavioral and cognitive phenotype associated with DS and the consequent difficulty to design a correct pharmacological approach, the National Institutes of Health

(NIH) has supported the development of clinical trials for DS through the Down Syndrome Research Plan (NICHD, 2014) and DS-Connect, a national registry to connect families with researchers conducting clinical trials and improve understanding of health in DS (DHHS, 2016). Between 1990 and 2000, pre-clinical research exploiting the Ts65Dn mouse model and other translational research made it possible to target molecular mechanisms in the brain to address the cognitive and functional deficits associated with DS (Hart et al., 2017).

2.10.1.1 Cholinergic system

Acethylcoline (Ach) is a key neurotransmitter in the peripheral and central nervous system. Ach is synthesized in cholinergic neurons by the enzyme choline acetyl-transferase and is converted in the inactive form by Acethylcoline esterase (AchE). DS has been associated with abnormalities in peripheral and central cholinergic functions [see (Hart et al., 2017)] and with reduction in the number of cholinergic neurons, which may affect cortical neuronal connectivity and maturation during early development (Becker, 1991). Cholinesterase inhibitors have been used to investigate potential effects of enhancing cholinergic function on cognition.

Donepezil, a reversible inhibitor of AchE approved for use in people with AD in the general population, was used in the earliest clinical trial of pharmaceutical interventions in DS (Kishnani et al., 1999). Several recently completed randomized double-blind, placebo-controlled trials showed that donepezil was generally safe and well-tolerated in children and adults with DS but gave no significant benefit as a cognitive enhancer (Kishnani et al., 2009, Kishnani et al., 2010). A recent review by the Cochrane Collaboration network (Livingstone et al., 2015) concluded that there was no difference in cognitive functioning or behavior between individuals with DS treated with donepezil and placebo, although the probability to undergo an adverse event was higher for individuals with DS on donepezil [see (Hart et al., 2017)].

Rivastigmine, an inhibitor of AchE and butyrylcholinesterase (BChE), is approved for the treatment of mild to moderate AD and has been shown to have benefit on the cognitive, functional and

behavioral problems commonly associated with dementia in AD (Finkel, 2004). A randomized double-blind, placebo-controlled trial in children and adolescents with DS suggested an improvement in a subset of participants for expressive language, but overall there were no with significant effects on adaptive function, executive function, language or memory measures (Spiridigliozzi et al., 2016). **Piracetam** is a member of the class of drugs known as nootropics, which are generally thought to enhance cognitive function by influencing vascular and neuronal functions in instances of brain dysfunction (Winblad, 2005). A Phase II placebo-controlled, 2-period crossover study was performed by Lobaugh et al. (2001) on children with DS (ages 6–13) in order to evaluate the effect of piracetam on cognitive functions, such a as attention, learning and memory. The trial showed that therapy with piracetam did not significantly improve cognitive functions and, in 7 of the 18 children who completed the study, was associated with side effects of the central nervous system (Lobaugh et al., 2001).

2.10.1.2 Glutamatergic system

Memantine, a low-affinity uncompetitive antagonist for glutamatergic NMDA receptors, is a drug approved for treatment of moderate-to-severe AD, and was tested in different clinical trials in individuals with DS (Boada et al., 2012, Hanney et al., 2012). Memantine has been shown to act indirectly on the cholinergic system (Aracava et al., 2005). In individuals aged 18-32 years, no differences were detected in the two primary measures, but a significant improvement was seen in hippocampus-dependent function (Boada et al., 2012). After 1-year treatment with memantine (at a dose of 10 mg/d) in adults with DS over age 40, no improvements were observed in primary or secondary measures of cognition or adaptive function (Hanney et al., 2012). An ongoing Phase II trial in young adults with DS aged 15–32 is trying to assess whether a 16-week treatment with memantine will have an effect on learning and memory (clinicaltrials.gov NCT02304302).

2.10.1.3 GABAergic system modulators

Excessive GABA-mediated neurotransmission has been proposed as one of the underlying causes of the cognitive deficits in Ts65Dn mice (Belichenko et al., 2004, Fernandez et al., 2007). Thanks to pre-clinical studies showing improvements in learning and memory with a $GABA_A$ antagonist (Fernandez et al., 2007) and selective $GABA_A$ α5 negative allosteric modulator (Martinez-Cue et al., 2013), recent clinical trials in DS have targeted the GABA system.

Pentylenetetrazole (PTZ) is a $GABA_A$ antagonist that was previously approved by the FDA for treatment of various cognitive impairments. PTZ is currently under investigation for cognitive enhancement in individuals with DS. A placebo-controlled study with PTZ up to 12 weeks in adolescents and young adults (ages 13–35) with DS has investigated the pro-cognitive effects in the domains of language, executive function, and adaptive behavior (Australian New Zealand Clinical Trials Registry ID ACTRN12612000652875). Although the study has completed enrollment and follow-up assessments, results have not been published yet.

Basmisanil (Hoffmann-La Roche Pharmaceuticals), a selective $GABA_A$ α5 negative allosteric modulator, has been used in two multi-centre, Phase II, randomized, double-blind, placebo-controlled studies in order to improve cognition in adolescents/adults (12–30 years old; CLEMATIS study, ClinicalTrials.gov identifier NCT02024789) and children (6-11 years old; ClinicalTrials.gov identifier NCT02484703) with DS in a 26-week treatment study. Unpublished results from the CLEMATIS study showed that Basmisanil was not associated with significant impacts on cognition or adaptive behavior in young adults and adolescents with DS, leading to early discontinuation of the study in the pediatric population [see (Hart et al., 2017)].

2.10.1.4 Natural compounds

Folinic acid is a vitamer of vitamin B9 (or folate). Several genes involved in folate metabolism are located on HSA21 and folate deficiency has been linked to intellectual disability. Thus, folinic acid has been investigated as a potential pharmacotherapy in DS in a randomized controlled trial of

antioxidants and folinic acid (0.1 mg/day). No effects of treatment on development or long-term communication abilities were found in infants with DS (Ellis et al., 2008). More recently, a double-blind, placebo-controlled, single-center study in DS infants (3–30 month-old) revealed an improvement in global developmental age for toddlers taking 1.0 mg/kg/day of folinic acid (Blehaut et al., 2010). The differences in the outcome of these two clinical trials may be due to the different dose used in DS infants. An ongoing 4-arm, placebo-controlled trial with folinic acid and thyroid hormone in combination is aimed at evaluating improvement of psychomotor development in 6–18 month-old DS toddlers (ClinicalTrials.gov identifier NCT01576705).

Epigallo-catechin-3-gallate (EGCG) is a flavonoid derived from green tea leaves and a well-known DYRK1A inhibitor. A randomized, placebo-controlled pilot study tested the effects of EGCG in combination with other green tea extracts on cognition in adolescents with DS (De la Torre et al., 2014). Three months of treatment with green tea extracts improved recognition and working memory. Another study by the same group (a Phase II clinical trial) revealed that in adolescents with DS, a combination of green tea extracts plus cognitive training for 12 months had positive effects on visual recognition memory, inhibitory control, and adaptive behavior (de la Torre et al., 2016). Phase III trials with a larger DS population will be needed to assess the long-term efficacy of green tea extracts and cognitive training. The specific contribution of EGCG and of the other constituents of green tea extracts on behavioural improvement remains to be established.

2.10.1.5 Molecules targeting AD

Interventions targeting AD pathogenesis are currently being explored in clinical trials for DS.

ACI-24, a recent developed vaccine targeting Aβ protein, has been designed to stimulate the immune system in order to prevent accumulation of amyloid plaques and trigger their clearance. It has been validated in a Phase I/II double-blind, randomised, placebo-controlled, adaptive design study of the safety, tolerability, immunogenicity and efficacy in patients with mild to moderate AD (WHO.int,

ICRT portal identifier EUCTR2008-006257-40-FI). A Phase I study in people with DS is currently investigating the effects of ACI-24 (ClinialTrials.gov identifier NCT02738450).

Intranasal glulisine, is a rapid-acting insulin. Due to the role of insulin signaling in Alzheimer's pathogenesis, the effects of glulisine have been investigated in AD (see (Hart et al., 2017)). The effects of intranasal glulisine are currently investigated in adults with DS to determine safety, feasibility, and cognitive effect on memory measures (ClinicalTrials.gov identifier NCT02432716).

The effects of transdermal **nicotine** are currently investigated as a treatment for cognitive decline in adults with DS with the aim to establish safety, tolerability and efficacy for cognitive performance (ClinicalTrials.gov identifier NCT01778946).

ELND005, an amyloid anti-aggregation agent, has been proposed to be used in individuals with DS because it may prevent the accumulation of plaques that might contribute to AD like dementia and may improve working memory by regulating brain myo-inositol levels. A clinical trial with ELND005 in the general population with AD did not show any effect on cognition or adaptive function [see (Hart et al., 2017)]. A recent phase II study, conducted in non-demented young adults with DS, showed that ELND005 was safe and well-tolerated, and that there were no side effects (Rafii et al., 2017). Results revealed improvements in the Neuropsychiatric Inventory score (examination of 10 behavioral sub-domains: delusions, hallucinations, agitation/aggression, dysphoria, anxiety, euphoria, apathy, disinhibition, irritability/lability, and aberrant motor activity, (Cummings et al., 1994) in 7 of 8 subjects receiving 250 mg twice daily of ELND005. There were, however, no significant overall treatment group-related trends on cognitive or behavioral measures.

2.10.2 Preclinical studies in DS mouse models

The idea of therapy for DS was unimaginable until few years ago. However, the initial knowledge of the HSA21 transcriptome, the continuous efforts to understand the signaling and other metabolic and developmental pathways that are dysregulated in DS, the availability of mouse models, the generation of T21 iPSCs and their differentiation to various cell types and tissues, and the understanding of the

numerous neurodevelopmental alterations, now provide some enthusiasm for potential therapeutic modalities. In the last 10 years, there has been an increase in research efforts focused on therapeutic interventions to rescue the brain phenotype and improve learning and memory in mouse models of DS. These therapies, which have been selected according to different rationales, have been mainly used in the Ts65Dn model. Most of the pharmacotherapies were conducted in adult Ts65Dn mice, while fewer therapies were explored at earlier life stages (neonatally or prenatally). This section summarizes what we know about the effects of pharmacotherapies during different life stages in DS mouse models. The attempted therapies may be grouped into five major classes. A) Therapies targeted to **transmitter systems**: (i) Therapies enhancing cholinergic transmission; (ii) Therapies antagonizing GABAergic transmission; (iii) Therapies enhancing noradrenergic transmission; (iv) Therapies targeted to the glutamate NMDA receptor; (v) Therapies targeted to the serotonergic system; (vi) Therapies targeted to the endocannabinoid system. B) Therapies employing **neuroprotective agents, antioxidants, and free radical scavengers**. C) Therapies targeted to **perturbed signaling pathways**. D) Therapies to normalize the **expression of proteins coded** by triplicated genes. E) Therapies that are known to have a **proneurogenic effect** [see (Stagni et al., 2015a)]. **Table 2.10.1** and **Table 2.10.2** summarize the outcomes of attempted therapies (divided by their classifications) in DS mouse models [see also (Stagni et al., 2015a)].

2.10.2.1 Therapies targeted to transmitter systems (Class A)

(i) Therapies enhancing cholinergic transmission

The rational basis for the use of AchE inhibitors in DS has been reported in the 2.10.1.1 section (Cholinergic system inhibitors). In the Ts65Dn models, AchE inhibitors were used mainly for the potential prevention or reversion of the loss of functional markers in the BFCN. Results obtained in Ts65Dn mice with AchE inhibitors or with choline supplementation are summarized below.

Donepezil, physostigmine and galantamine. These molecules are AchE inhibitors. Donepezil was administered for 8 weeks in 4 month-old Ts65Dn mice. Treatment did not improve sensorimotor

abilities, locomotor activity in the home cage and L/M, evaluated with the MWM test (Rueda et al., 2008a). Physostigmine, administered acutely to male Ts65Dn mice aged 4 months, rescued impairment in the four-arm spontaneous alternation task, but failed when administered to older mice (10 and 16 months) [see (Gardiner, 2015)]. Galantamine has been shown to be effective in 3-6 month-old Ts65Dn mice in an impaired olfactory test of learning and memory (L/M) when administered for 10 consecutively days [see (Gardiner, 2015)].

Choline supplementation. Choline, a vitamin-like nutrient, is a precursor of Ach. In a series of studies started in 2010, Strupp and colleagues analyzed the effects of choline supplementation in the diet of pregnant Ts65Dn dams (from E1 and continuing during lactation until the pups were weaned at P21). Their hypothesis was that treatment could improve BFCNs may thereby preventing the defects related to their degeneration (Moon et al., 2010, Velazquez et al., 2013, Ash et al., 2014, Kelley et al., 2014, Kelley et al., 2016). Ts65Dn progeny (6 months of age) of supplemented mothers showed improvement in the five-choice visual discrimination task (Moon et al., 2010). Choline supplementation plus environmental enrichment, restored hippocampal neurogenesis, reduced loss of BFCNs in the medial septum and restored hippocampus-dependent spatial cognition, tested with the Radial Arm Water Maze, in 13-17 month-old Ts65Dn mice (Velazquez et al., 2013, Ash et al., 2014, Kelley et al., 2014). These findings indicate that embryonic/early post-natal choline supplementation has effects that extend to very advanced life stages.

(ii) Therapies antagonizing GABAergic transmission

A number of studies have shown electrophysiological abnormalities in the hippocampal function of Ts65Dn mice, with repressed LTP and enhanced LTD. An imbalance between excitatory and inhibitory neurotransmission, probably due to increased generation of forebrain GABAergic interneurons, has been proposed to contribute to impair synaptic function and, consequently, L/M in the Ts65Dn model. Based on these premises, various $GABA_A$ receptor ($GABA_AR$) and some $GABA_B$

receptor ($GABA_BR$) antagonists were tested in the Ts65Dn mouse in order to equilibrate the excitation/inhibition ratio.

Pentylenetetrazole (PTZ). PTZ is a circulatory and respiratory stimulant and a $GABA_AR$ antagonist. Two weeks of treatment with PTZ in 3-4 month-old Ts65Dn mice rescued spontaneous alternation in the T-maze and performance in the NOR test. Importantly, at two months after treatment cessation treated Ts65Dn mice exhibited restoration of LTP in the DG and normalization of the NOR test and spontaneous alternation in the TM test (Fernandez et al., 2007). Seven weeks of treatment in 4 month-old Ts65Dn mice rescued performance in the MWM test, but caused some side effects (Rueda et al., 2008a). Recently, another study demonstrated that 2 weeks of PTZ treatment was effective in rescuing deficits in NOR in both younger (2–3 month-old) and older (12–15 month-old) male Ts65Dn mice (Colas et al., 2013).

Bilobalide and picrotoxin. They are two non-competitive $GABA_A$ receptor antagonists. Ts65Dn mice aged 3-4 months that had received bilobalide for four weeks underwent rescue of memory assessed with the NOR test. 2 weeks of treatment with picrotoxin in 3-4 month-old Ts65Dn mice was also able to rescue performance in the NOR test. Treated Ts65Dn with either bilobalide or picrotoxin retained their improved performance when evaluated 2 weeks later (Fernandez et al., 2007).

α5 inverse agonist (α5IA). $GABA_AR$ exhibit considerable heterogeneity in terms of their composition and functional properties because 19 different subunits are assembled as heteropentamers [see (Gardiner, 2015)]. The α5 subunit is mainly expressed in the DG of the hippocampus and is linked to long-term memory functions. In 3-month-old male Ts65Dn, a single injection of the α5 inverse agonist α5IA rescued performance in the NOR and in the learning phase of the MWM test, but not in the probe trial (Braudeau et al., 2011).

RO4938581. It is an α5 inverse agonist. RO4938581 was administered for 6 weeks to 3-4 month-old male Ts65Dn mice. This treatment restored LTP, hippocampal neurogenesis, and L/M in the MWM test (Martinez-Cue et al., 2013).

Bumetanide. In a recent study, Deidda et al. showed that $GABA_AR$ signaling was excitatory rather than inhibitory in Ts65Dn mice (Deidda et al., 2015). This excitatory activity was accompanied by (i) a shift in the reversal potential for $GABA_AR$-driven Cl^- currents (E_{Cl}) toward more positive potentials and (ii) increased hippocampal expression of the cation Cl^- cotransporter NKCC1 in both Ts65Dn mice and individuals with DS. Based on the evidence, Ts65Dn aged 10-16 weeks were treated with Bumetanide (a diuretic drug that inhibits NKCC1 cotransporter) for either one week or four weeks. Both treatment schedules rescued long-term hippocampus-dependent explicit memory, as assessed with CFC and NOR tests, in Ts65Dn mice. In contrast, one month of treatment with Bumetanide did not restore LTP in slices from Ts65Dn, indicating that effects of bumetanide on memory are independent of neuronal-circuit rearrangement. Finally, positive effects of Bumetanide on behavior disappeared after one week of drug withdrawal (Deidda et al., 2015).

Flumazenil. Flumazenil (FLUM) is a $GABA_AR$ antagonist that is in current clinical use as an antidote in the treatment of benzodiazepine overdoses. FLUM is of interest because, unlike PTZ that is a noncompetitive $GABA_AR$ antagonist, FLUM is a competitive antagonist acting at the benzodiazepine binding site. 2-3 month-old and 8-10 month-old Ts65Dn mice were treated with FLUM for two weeks and then tested with the NOR test one week after treatment cessation. FLUM restored NOR test performance in Ts65Dn mice (Colas et al., 2017). The positive effects of FLUM in the NOR test persisted one month after treatment cessation (Colas et al., 2017).

CGP55845. *KCNJ6*, encodes an inwardly-rectifying K^+ channel, G protein-coupled inwardly-rectifying potassium channel (GIRK) 2, that couples to $GABA_B$ receptors. Levels of GIRK2 are elevated in the hippocampus, frontal cortex, substantia nigra, and perhirinal cortex (Harashima et al., 2006, Roncace et al., 2017) of Ts65Dn mice and there is evidence that $GABA_B$-induced potassium currents are elevated in these brain regions, suggesting that they may contribute to the imbalance between excitatory and inhibitory neurotransmission (Best et al., 2007, Best et al., 2012). CGP55845, a $GABA_B$ receptor antagonist, was administered to 2-3 month-old Ts65Dn mice for 3 weeks or acutely (2-3 h before testing). CGP55845 rescued memory deficits assessed with the TM, NOR and

CFC behavioral tests and restored LTP in hippocampal slices from Ts65Dn mice (Kleschevnikov et al., 2012).

(iii) Therapies enhancing noradrenergic transmission

The noradrenergic input from the Locus Coeruleus (LC) exerts a modulatory role on hippocampal neurons via β-adrenergic receptors and is essential for contextual learning [see (Bartesaghi et al., 2011)]. Neurons of LC are affected in several neuropathologies, such as AD, Parkinson disease and Huntington disease. Middle-aged DS individuals show significant loss of cells from LC (Mann et al., 1985) and the same defect is present in the Ts65Dn mouse model starting from 6 months of age (Salehi et al., 2009). Ts65Dn mice also displays a reduction of the amount of noradrenaline (NA) in the hippocampus.

L-DOPS. It is a synthetic precursor of NA, metabolized into NA by cells. 6 month-old Ts65Dn male mice that were injected with L-DOPS during the CFC test underwent full restoration of performance (Salehi et al., 2009).

Xamoterol. It is a β1-adrenergic receptor partial agonist. 6 month-old Ts65Dn male mice that were injected with xamoterol with the same schedule used for L-DOPS underwent full restoration of freezing in the CFC test (Salehi et al., 2009). In a subsequent study, xamoterol was acutely administered to 9-12 month-old Ts65Dn male mice. Treatment rescued behavioral defects in NOR, CFC, and TM tests (Faizi et al., 2011).

Formoterol. Formoterol is a long-acting β2-adrenergic agonist that has been proposed as protective agent against cholinergic system degeneration (Antonarakis, 2017). In a recent study, formoterol was administered acutely (4 hours before behavior analyses) to 5-6 month-old Ts65Dn mice. Results showed that formoterol caused significant improvement in the cognitive function (CFC test) and was associated with a significant improvement in the density of synaptic terminals in the DG and increased the dendritic complexity of newly born granule neurons of the DG (Dang et al., 2014).

DREADDs. Designer receptors exclusively activated by designer drugs (DREADDs) are novel and powerful tools that can be used to enhance neuronal activity and investigate discrete neuronal populations in the brain (Vazey and Aston-Jones, 2014). 14 month-old Ts65Dn mice were treated acutely with a DREADD, hM3Dq, administered via adeno-associated virus into the LC under a synthetic promoter, PRSx8, to selectively stimulate LC neurons by exogenous administration of the inert DREADD ligand clozapine-N-oxide. This treatment enhanced performance in the NOR test and reduced hyperactivity in Ts65Dn mice (Fortress et al., 2015).

(iv) Therapies targeted to the glutamate NMDA receptor

Memantine. This molecule is an uncompetitive antagonist of the N-methyld-aspartate (NMDA) receptor that indirectly acts on the cholinergic system (see 2.10.1.1 paragraph). In a first study, Costa et al. showed that an acute treatment with memantine in both 4-6 and 10-14 month-old male Ts65Dn mice was able to rescue L/M deficits in the CFC test (Costa et al., 2008). In 9 month-old Ts65Dn mice, 9 weeks of memantine administration rescued impairments in the MWM test (Rueda et al., 2010). When administered from 4 to 9.5 months of age, memantine improved performance of Ts65Dn mice on the WRAM and NOR tests (although memantine had negative effects in euploid mice). Importantly, one week after treatment cessation, the positive effects seen on cognition disappeared. Finally, hippocampal slices from Ts65Dn mice preincubated with memantine exhibited normal levels of LTD after exposure to NMDA (Scott-McKean and Costa, 2011).

(v) Therapies targeted to the serotonergic system

Serotonin (5-HT), one of the major neurotransmitters of the CNS, is essential for neurodevelopment starting from the earliest fetal stages. The serotonergic system, which is altered in DS, has been linked to neurogenesis defect and reduced dendritic spine size in individuals with DS and Ts65Dn mice. Both individuals with DS and Ts65Dn mice displays a reduced expression of the serotonin 5-HT1A

receptor in the hippocampus, suggesting that a pharmacotherapy targeted to the serotonergic system may be a good strategy to ameliorate neurodevelopmental defects in DS.

Fluoxetine. Fluoxetine, also known by trade name Prozac, is an antidepressant belonging to the selective serotonin reuptake inhibitor (SSRI) class. Fluoxetine works by delaying the reuptake of 5-HT through the inhibition of serotonin transporter. This mechanism allows 5-HT to persist longer in the inter-synaptic cleft and, thus, to enhance its action on postsynaptic neurons. Based on evidence that antidepressants increase neurogenesis in the DG and SVZ of rodents, Clark et al tested the efficacy of fluoxetine administered for two weeks in Ts65Dn mice aged 2-5 months. The results of this study showed that treatment with fluoxetine rescued neurogenesis in the hippocampus of Ts65Dn mice (Clark et al., 2006). Based on these premises, our group investigated the effects of early treatment with fluoxetine on brain development and behavior in Ts65Dn mice (Bianchi et al., 2010b, Guidi et al., 2013, Stagni et al., 2013, Guidi et al., 2014, Stagni et al., 2015b). We administered fluoxetine neonatally (from P3 to P15) and we found that treatment restored hippocampal neurogenesis and total granule cell number (Bianchi et al., 2010b). Importantly, at one month after treatment cessation, treated Ts65Dn mice exhibited full restoration of granule cell number, granule cell dendritic pattern, hippocampal connectivity, signal transfer from the granule cells to CA3, and hippocampus-dependent memory (Bianchi et al., 2010b, Guidi et al., 2013, Stagni et al., 2013). In a subsequent study we examined the effects of neonatal treatment with fluoxetine when mice reached adulthood (3 months of age) and found that in neonatally-treated Ts65Dn mice hippocampal cellularity, dendritic architecture, spine density, and L/M functions were still fully rescued (Stagni et al., 2015b). Since serotonin is essential for neurogenesis and dendritic development from the earliest fetal life stages in humans (Faber and Haring, 1999, Whitaker-Azmitia, 2001), we hypothesized that treatment with fluoxetine during pregnancy could rescue most of the neurodevelopmental alterations that characterize the trisomic brain. Thus, we administered fluoxetine to pregnant Ts65Dn dams from E10 to birth, with the aim of restoring the bulk of neurogenesis in pups, and we analyzed the outcome of treatment when mice was P2. We found that fluoxetine restored neurogenesis and cell density

throughout the forebrain (SVZ, SGZ, neocortex, striatum, thalamus, hypothalamus), midbrain (mesencephalon) and hindbrain (cerebellum and pons). In addition, prenatal-treatment with fluoxetine had enduring effects on Ts65Dn mice aged 45 days. Indeed, neural precursor proliferation was still restored in SVZ and the DG of the hippocampus, the dendritic development of postnatally born granule neurons and pre- and post-synaptic terminals were normalized and there was restoration of cognitive performance (NOR and CFC tests). These results demonstrate, for the first time, that the neurodevelopmental defects that characterize DS are reversible. Heinen and colleagues treated Ts65Dn mice aged 5–7 months with fluoxetine for a total of 6 weeks and found no improvement in the MWM test and no change in the BFCN levels of ChAT (Heinen et al., 2012). In addition, they reported a very high rate of seizures and death in treated Ts65Dn mice. It must be noted that these adverse effects are very likely due to the dose used in this study (8-fold higher than that used by our group) and treatment duration (6 weeks vs 13 days) (Heinen et al., 2012). A study by Begenesic et al. (Begenisic et al., 2014) 2 month-old male and female Ts65Dn mice were treated for two weeks with fluoxetine. Treatment restored performances in olfactory learning and spontaneous alternation in a four arm maze and normalized levels of LTP and GABA release from synaptosomes (Begenisic et al., 2014).

The promising results obtained with fluoxetine in the Ts65Dn model have prompted the design of clinical trials for the DS population. In 2016 the University of Texas Southwestern Medical Center, proposed a pilot study to investigate the effects of prenatal treatment with fluoxetine in pregnant mothers with a fetal diagnosis of DS. Unfortunately, no official information about this clinical trial is reported in ClinicalTrials.gov. In the framework of a project entitled “Novel avenues for the rescue of intellectual disability in Down syndrome” and coordinated by our research group, the protocol for a Phase I clinical trial has been submitted to the Italian Authority regulating clinical trials (AIFA) by our collaborators at Federico II University (Naples, Italy). This is a prospective, single-center, not controlled, one-arm, open study aimed at evaluating the safety and tolerability of fluoxetine in a paediatric population with DS. We hope that this pilot study will start as soon as possible.

(vi) Therapies targeted to the endocannabinoid system

JZL184. The most abundant endocannabinoid in the brain is 2-arachidonoylglycerol (2-AG). The principal hydrolytic enzyme responsible for the degradation of 2-AG is monoacylglycerol lipase (MAGL). JZL184 is a selective inhibitor of monoacylglycerol lipase (MAGL). Ts65Dn mice aged 9.5-11.4 month were treated with JZL184 for 4 weeks, in order to evaluate its effects on behavior and synaptic function (Lysenko et al., 2014). Treatment with JZL184 appears to improve long-term memory (NOR test) and hippocampal LTP (in the CA1 field), but has no effects on short-term (NOR test) and working memory (YM test) (Lysenko et al., 2014).

2.10.2.2 Therapies employing neuroprotective agents, antioxidants, and free radical scavengers (Class B)

Neuroprotective agents

Neuropeptides are small proteinaceous substances produced and released by neurons through the regulated secretory route and acting on neural substrates. Neuropeptides are the most diverse class of signaling molecules in the brain and are engaged in many physiological functions (Burbach, 2011).

NAPVSIPQ (NAP) and SALLRSIPA (SAL). Glial cells release several survival-promoting factors, including the activity-dependent neuroprotective protein (ADNP) and the activity-dependent neurotrophic factor (ADNF) (Incerti et al., 2011). The active peptide fragments of these proteins, NAPVSIPQ (NAP) and SALLRSIPA (SAL), mimic the activity of their parent proteins, exerting a protective effect against oxidative stress, the severity of traumatic head injury, stroke, and toxicity associated with the Aβ peptide [see (Bartesaghi et al., 2011, Gardiner, 2015, Stagni et al., 2015a)]. Busciglio et al demonstrated that treatment of DS cultured cortical neurons with either NAP or SAL increased neuronal survival and reduced degenerative morphological changes (Busciglio et al., 2007). In a first study, Incerti et al. treated 10 month-old Ts65Dn mice with NAP/SAL for 9 days. During days 4-9 mice were subjected to the MWM test and showed rescued L/M functions (Incerti et al., 2011). However, after a further 10 days with no additional treatment, treated Ts65Dn mice no longer

remembered the platform location (Incerti et al., 2011). In another study, conducted by the same group, pregnant Ts65Dn dams were injected with NAP/SAL from E8 to E12. At 8-10 months of age the treated offspring were evaluated in the MWM test. Treated Ts65Dn offspring exhibited improved learning abilities. Unfortunately, data regarding probe test that assesses memory are lacking (Incerti et al., 2012).

Peptide 6. It is a derivative of the ciliary neurotrophic factor, which has been shown to enhance neurogenesis, dendritic and synaptic plasticity, and memory in rodents (Chohan et al., 2011). In a study by Blanchard et al. 11–15-month-old female Ts65Dn mice were treated for 1 month with peptide 6 (Blanchard et al., 2011). According to the authors, the performance in the MWM test was improved, although the reporetd data do not appear to completely support this conclusion [see (Gardiner, 2015)].

Peptide 021. Peptide 021 (P021) is a ciliary neurotrophic factor (CNTF) small-molecule mimetic. 2–3-month-old pregnant Ts65Dn dams were treated with compound P021 in the feed from E8 until weaning of the pups on P21 (Kazim et al., 2017). Evaluation of developmental milestones from P1 to P21 showed that treatment prevented the delay in neurobehavioral development in Ts65Dn pups. In addition, prenatally-neonatally treated 3 weeks-old Ts65Dn offspring displayed amelioration of a pre-synaptic protein (SYN) deficit, decrement of GSK3β activity, and an increment in the expression of synaptic plasticity markers (Kazim et al., 2017). Morever, authors demonstrated that this treatment schedule with P021 caused restoration of cognitive functions, assessed by MWM test, open field and one-trial object recognition/discrimination task when mice had 7 months of age (Kazim et al., 2017).

Estrogen. The fact that women with DS have premature menopause and early onset cognitive decline prompted some studies with estrogen. In a study by Granholm et al., 11-14 month-old female Ts65Dn mice were treated with estrogen for two months. Estrogen significantly improved initial learning in the discriminating water T-maze. Estrogen also reversed the age-related loss of ChAT and NGF, two BFCN functional markers (Granholm et al., 2002). Another study in male Ts65Dn mice aged 6

months showed that estrogen treatment for 3 weeks failed to rescue the learning deficit in the WRAM (Hunter et al., 2004b). These results suggest sex differences in estrogen responses.

Minocycline. Minocycline is an antibiotic (derivative of the tetracycline) that is of interest because it is considered to have neuroprotective effects. 3 months of treatment with minocycline in 10 month-old male Ts65Dn mice improved performance in the WRAM (not to euploid levels) and rescued age-related loss of ChAT in the BFCN (Hunter et al., 2004a).

Nerve Growth Factor (NGF). With aging, Ts65Dn mice exhibitd reductions in BFCN size and number and regressive changes in the hippocampal terminal fields of these neurons. These changes are associated with significantly impaired retrograde transport of NGF from the hippocampus to the basal forebrain [see (Bartesaghi et al., 2011)]. In a study by Cooper et al., Ts65Dn mice aged 18 months received NGF via a microosmotic pump implanted into the lateral ventricle for 12 weeks. Intracerebroventricular NGF infusion reversed abnormalities in BFCN size and number and restored the deficit in cholinergic innervation (Cooper et al., 2001).

Antioxidants and free radical scavengers

Oxidative stress and mitochondrial dysfunction are both considered hallmarks of DS tissues and contributors to neurological phenotypes across the DS lifespan. This oxidative stress, which damages mitochondrial membrane and lipids, occurs in DS during pre- and post-natal development and can modify critical processes of neurogenesis, differentiation, migration, and survival. Several HSA21 genes, among them *SOD1*, *BACH1*, *ETS2*, and *S100B*, are known to contribute to the regulation of oxidative stress when overexpressed [see (Gardiner, 2015, Stagni et al., 2015a)]. Consistent with these observations, it was shown that levels of oxidative stress are elevated in the brains of adult Ts65Dn (Lockrow et al., 2009).

α-tochopherol. This molecule is the most biologically active form of vitamin E. 4 month-old male Ts65Dn mice was fed with an α-tochopherol enriched diet for either 4 or 6 months. Treatment was found to reduce the levels of oxidative stress in Ts65Dn brains, to improve performance in the

WRAM at 8 and 10 months and prevent the loss of the TRKA receptor in the BFCN (Lockrow et al., 2009).

Vitamin E enriched diet was administered to pregnant Ts65Dn females from the day of conception throughout pregnancy and to their pups until 10 weeks of age. Supplementation of vitamin E was found to reduce lipid peroxidation products in the DG of adult Ts65Dn mice, to increase granule cell density, to ameliorate abnormal anxiety in the elevated plus maze test, and to improve spatial L/M in the MWM test (Shichiri et al., 2011).

SGS-111. SOD1 over-expression in DS individuals causes a three- to four-fold increase in intracellular reactive oxygen species (ROS) [see (Stagni et al., 2015a)]. SGS-111 is an analog of piracetam with neuroprotective and nootropic properties. It was administered to pregnant Ts65Dn dams from the day of conception, throughout pregnancy, and to their pups during the following 5 months. Treatment failed to improve L/M in the MWM test, although there was a reduced hyperactivity in Ts65Dn mice (Rueda et al., 2008b).

Melatonin. Melatonin is an indole amine mainly synthesized and secreted by the pineal gland. Its exogenous administration has been demonstrated to induce neuroprotective effects by regulating anti- and pro-oxidant enzymes, acting as a potent ROS scavenger, and repairing molecules damaged by ROS overgeneration. Due to these effects, melatonin has been proposed as a powerful tool in the treatment of neuropathologies in which oxidative stress is enhanced, such as DS (Parisotto et al., 2016). Melatonin, administered to 5 month-old male Ts65Dn mice in drinking water for 4 months plus another one-month (5 months in total) during behavioral testing was shown to rescue learning abilities tested with MWM test. In addition, melatonin increased the levels of ChAT in BFCNs (Corrales et al., 2013). In a subsequent study, administration of melatonin to 6 month-old Ts65Dn for 5-6 months was found to rescue neurogenesis and LTP (Corrales et al., 2014). In a recent work, the same group showed that melatonin also reduces oxidative stress and decreases hippocampal senescence in the Ts65Dn model (Parisotto et al., 2016).

2.10.2.3 Therapies targeted to perturbed signaling pathways (Class C)

Lithium. Lithium is largely used for the treatment of bipolar depression and was seen to have neuroprotective properties and to stimulate neurogenesis in the DG of rodents [see (Bartesaghi et al., 2011)]. Although the molecular mechanisms underlying responses to lithium are not known yet, it has been shown that it can inhibit GSK3β and inositol phosphatases, compete with Mg^{2+} in protein binding and modulate the Wnt/β-catenin pathway [see (Gardiner, 2015)]. 12 month-old Ts65Dn mice treated for one month with lithium exhibited restoration of cell proliferation in the SVZ, rostral migratory stream and olfactory bulb, restoration of the size of the proliferating pool of precursor cells in the SVZ, and olfactory functions. However, no neurogenesis enhancement was seen in the SGZ of the DG (Bianchi et al., 2010a, Guidi et al., 2016). In contrast, 5 month-old Ts65Dn mice treated for one month with lithium showed a complete rescue of DG neurogenesis, hippocampal LTP and performance in the CFC, NOR, and OL tests (Contestabile et al., 2013).

SAG 1.1. SHH signaling is extremely important for neuronal precursor proliferation. Roper et al. demonstrated that the reduced proliferation of cerebellar granule cell precursors from Ts65Dn mice is related to an attenuated response to SHH protein. SAG 1.1, a smoothened (SMO, the receptor of SHH) agonist, relieves the inhibitory effect of PTCH1 (the inhibitor of SHH pathway) on SMO. A single injection of SAG 1.1 in P0 Ts65Dn rescued at P6 the decreased cell number in the granule cell layer of the cerebellum (Roper and Reeves, 2006). Importantly, the positive effects of SAG1.1 on cerebellar cellularity lasted until 4 months of age. In addition, this treatment restored the MWM test performance and hippocampal LTP, but failed to improve cerebellar LTD and performance in the YM test (Das et al., 2013).

2.10.2.4 Therapies to normalize the expression of proteins coded by triplicated genes (Class D)

The role of DYRK1A in the neurodevelopmental alteration of DS has been highlighted in sections 2.8.4; 2.8.6; 2.8.9. Due to the involvement of DYRK1A in the DS neurological phenotype, in the last few years various therapies has been attempted in DS mouse models aimed at normalizing its activity.

Epigallo-catechin 3 gallate (EGCG). EGCG is a flavonoid present in green tea extracts. In addition to its antioxidant activity, it is a non-selective but highly specific inhibitor of DYRK1A. The first study on the effects of EGCG in DS demonstrated that incubation with EGCG of hippocampal slices from Ts65Dn mice restored LTP at the Schaffer collateral-CA1 synapse (Xie et al., 2008). A subsequent study on transgenic YACtg152F7 mice (that over-express *Dyrk1A*) showed that chronic administration with a polyphenol based diet (that includes EGCG) from gestation to adulthood was able to correct brain morphogenesis alterations, and long-term memory assessed using the NOR test (Guedj et al., 2009). In addition, *Dyrk1A* transgenic mice treated with EGCG for one month starting from P21 undergo restoration of hippocampal neurogenesis (Pons-Espinal et al., 2013). In adult *Dyrk1A* transgenic mice, a 4–6 week administration of green tea extracts rescues defective long-term potentiation in the prefrontal cortex (Thomazeau et al., 2014). Finally, treatment with extracts containing EGCG in adult mBACtg*Dyrk1a* mice restores components of GABAergic and glutamatergic pathways in the cortex and hippocampus, and improves behavioral deficits (Souchet et al., 2015). Recently, it has been reported that one month of treatment with EGCG in 3 month-old Ts65Dn male mice rescued their performance in the MWM test to the level of the euploid mice (De la Torre et al., 2014). In contrast, Stringer et al. demonstrated that pure EGCG administered to Ts65Dn mice from weaning for either three or 7 weeks (at a dose of 20.0 mg/kg/d), and 51 days (at a dose 100.0 mg/kg/d) did not improve performance in a battery of behavioral tasks (Stringer et al., 2015a, Stringer et al., 2015b). Green tea extracts containing EGCG (45%) were also administered in combination with environmental enrichment for 30 days in 1-2 month-old Ts65Dn female mice. Co-treatment restored cortico-hippocampal-dependent L/M (MWM, NOR tests), rescued dendritic spine density in field CA1 and normalized the proportion of excitatory and inhibitory synaptic markers in field CA1 and DG (Catuara-Solarz et al., 2016). There is evidence that incubation of NPCs isolated from the hippocampus of Ts65Dn mice with EGCG restores mitochondrial biogenesis and improves proliferation rate (Valenti et al., 2016).

ALGERNON (Altered generation of neurons). ALGERNON is a recenttly identified compound that inhibits DYRK1A and has been shown to rescue proliferative deficits in Ts65Dn-derived neurospheres and human neural stem cells derived from individuals with DS (Nakano-Kobayashi et al., 2017). ALGERNON was orally administered to pregnant Ts1Cje dams from E10 up to E15. Adult Ts1Cje mice that had been prenatally-treated with ALGERNON showed complete restoration of brain morphology, neurogenesis in the DG, and L/M functions (YM, Barnes Maze, CFC tests) (Nakano-Kobayashi et al., 2017).

DAPT (Class D). N-[N-(3,5-Difluorophenacetyl)-L-alanyl]-S-phenyl glycine t-butyl ester is a γ-secretase inhibitor developed in order to reduce Aβ deposition. Administration of DAPT to 4 month-old Ts65Dn mice for 4 days was found to normalize Aβ levels and to improve L/M (Netzer et al., 2010).

2.10.2.5 Therapies that are known to have a proneurogenic effect (Class E)

P7C3 (Class E). The aminopropyl carbazole P7C3 was discovered for its ability to enhance cell survival and decrease apoptosis, thereby preventing the neurogenic and cognitive decline seen in aged rats (Pieper et al., 2010) and rodent models of neurodegeneration (Tesla et al., 2012). In a recent study, 4-10 weeks-old Ts65Dn were chronically administered with P7C3 for 3 months. Evaluation of the brains at the end of treatment showed a complete restoration of neurogenesis (evaluated with immunohistochemistry for Ki-67, BrdU, DCX, and the apoptotic marker AC-3) in the DG (Latchney et al., 2015).

Table 2.10.1. Therapies administered at adult life stages in the Ts65Dn (and Ts1Cje) mouse model of DS.

Phenotype	Treatment	Mechanism	Age (M)	Treatment Duration	Outcome	Long-term effect	Reference
L/M (MWM)	Donepezil (Class A)	AChE inhibitor	4	7 w	Failed	NA	(Rueda et al., 2008a)
L/M (SA)	Physostigmine (Class A)	AChE inhibitor	4	Acute	Rescued	NA	(Chang and Gold, 2008)
			10	Acute	Failed	NA	
			16	Acute	Failed	NA	
Olfactory learning	Galantamine (Class A)	AChE inhibitor	3-6	Acute	Rescued	NA	(de Souza et al., 2011)
L/M (NOR, TM)	Pentylentetrazole (Class A)	Antagonist of $GABA_A$ R	3-4	17 d	Rescued	Yes (at 2 m)	(Fernandez et al., 2007)
L/M (MWM)	Pentylentetrazole (Class A)	Antagonist of $GABA_A$ R	4	7 w	Rescued	NA	(Rueda et al., 2008a)
L/M (NOR)	Pentylentetrazole (Class A)	Antagonist of $GABA_A$ R	2-3	2 w	Rescued	Yes (at 8 d)	(Colas et al., 2013)
L/M (NOR)	Pentylentetrazole (Class A)	Antagonist of $GABA_A$ R	12-15	2 w	Rescued	Yes (at 8 d)	(Colas et al., 2013)
L/M (NOR)	Flumazenil (Class A)	Antagonist of $GABA_A$ R	2-3	2 w	Rescued	Yes (at 1 w)	(Colas et al., 2017)
L/M (NOR)	Flumazenil (Class A)	Antagonist of $GABA_A$ R	2-3	2 w	Improved	Yes (at 4 w)	(Colas et al., 2017)
L/M (NOR)	Flumazenil (Class A)	Antagonist of $GABA_A$ R	8-10	2 w	Rescued	Yes (at 1 w)	(Colas et al., 2017)
L/M (MWM)	RO4938581 (Class A)	$GABA_A$ α5 negative allosteric modulator	3-4	6 w	Rescued	NA	(Martinez-Cue et al., 2013)

L/M (NOR, MWM)	α5IA (Class A)	$GABA_A$ α5 inverse agonist	3	Acute	Rescued Failed (Probe test)	NA	(Braudeau et al., 2011)
L/M (NOR, MWM, CFC)	CGP55845 (Class A)	Antagonist of $GABA_B$ R	2-3	3 w	Rescued	NA	(Kleschevnikov et al., 2012)
L/M (MWM, CFC)	Ethosuximide (Class A)	Inhibits KCNJ6/GIRK2 channel, a $GABA_B$–coupled ion channel	4.5-5	10 w	Failed	NA	(Vidal et al., 2012)
L/M (MWM, CFC)	Gabapentin (Class A)	Modulator of GABA synthesis	4.5-5	10 w	Failed	NA	(Vidal et al., 2012)
L/M (CFC; nesting behavior)	L-DOPS (Class A)	NA pro-drug	6	Acute	Rescued	No (at 2 w)	(Salehi et al., 2009)
L/M (NOR, CFC, TM)	Xamoterol (Class A)	β1 receptor agonist	9-12	Acute	Rescued	NA	(Faizi et al., 2011)
L/M (NOR, SA)	Clozapine-N-oxide (agonist of hM3Dq, administered via adeno virus into Locus Coeruleus) (Class A)	DREADD design in order to stimulate NA neurons of Locus Coeruleus	14	Acute	Rescued	NA	(Fortress et al., 2015)
L/M (SA)	L-DOPS (Class A)	NA pro-drug	11	2 w	Rescued	NA	(Fortress et al., 2015)
L/M (CFC)	Memantine (Class A)	Antagonist of NMDA R	4-7	Acute	Rescued	NA	(Costa et al., 2008, Ahmed et al., 2015)
L/M (WRAM, NOR)	Memantine (Class A)	Antagonist of NMDA R	4	6 m	Improved	No (at 1 w)	(Lockrow et al., 2011)

L/M (MWM)	Memantine (Class A)	Antagonist of NMDA R	9	8-9 w	Rescued	NA	(Rueda et al., 2010)
L/M (YM)	RO25-6981 (Class A)	Antagonist of NMDA R (GluN2B) /	3-6	Acute	Failed	NA	(Hanson et al., 2013)
L/M (YM, BM)	RO25-6981 (Class A)	Antagonist of NMDA R (GluN2B) /	3-6	2 w	Failed	NA	(Hanson et al., 2013)
L/M (NOR, YM)	Fluoxetine (Class A)	Inhibits serotonine reuptake	> 2 m	8 w	Rescued	NA	(Begenisic et al., 2014)
L/M (MWM)	Fluoxetine (Class A)	Inhibits serotonine reuptake	5-7	4 w	Failed	NA	(Heinen et al., 2012)
L/M (YM, NPR, NOR)	JZL184 (Class A)	Inhibitor of monoacylglycerol lipase that increases levels of 2-rachidonoylglycerol	11	4 w	Failed (YM, NPR) Rescued (NOR)	NA	(Lysenko et al., 2014)
L/M (MWM)	NAPVSIPQ+SALLRSIPA (fragments of ADNP and ADNF) (Class B)	Neuroprotection against oxidative stress	10	9 d	Rescued	No (at 10 d)	(Incerti et al., 2011)
L/M (MWM)	Peptide 6 (fragment of CNTF) (Class B)	Neurotrophic factor	11-15	30 d	Improved	NA	(Blanchard et al., 2011)
L/M (TM)	Estrogen (Class B)	Protects basal forebrain cholinergic neurons	11-15	2 m	Improved	NA	(Granholm et al., 2002)
L/M (MWM/NOR)	EGCG (Class B) + EE	Inhibits DYRK1A kinase	1-2	30 d	Improved	NA	(Catuara-Solarz et al., 2016)
L/M (MWM, PM)	Melatonin (Class B)	Free radical scavenger	5-6	5 m	Improved	NA	(Corrales et al., 2014)

L/M t (WRAM)	Vitamin E (Class B)	Antioxidant	4	4-6 m	Improved	NA	(Lockrow et al., 2009)
L/M (MWM)	Piracetam (Class B)	Nootropic	1.3	4 w	Failed	NA	(Moran et al., 2002)
L/M (MWM)	SGS-111 (Class B)	Analog of Piracetam; Nootropic	4-6	6 w	Failed	NA	(Rueda et al., 2008b)
L/M (WRAM)	Minocycline (Class B)	Anti-inflammatory	7	3 m	Improved	NA	(Hunter et al., 2004a)
L/M (MWM, NOR, CFC)	Lithium (Class C)	Mood stabilizer. Interferes with GSK3β signaling	5-6	4 w	Rescued	NA	(Contestabile et al., 2013)
L/M (MWM)	DAPT (Class D)	Γ-secretase inhibitor	4	Acute	Rescued	NA	(Netzer et al., 2010)
L/M (MWM, NOR)	Epigallocatechin-3-gallate (EGCG) (Class D)	Inhibitor of DYRK1A kinase	3	1 m	Rescued	NA	(De la Torre et al., 2014)
L/M (MWM, NOR)	Epigallocatechin-3-gallate (EGCG) (Class D)	Inhibitor of DYRK1A kinase	23 d	45 d	Failed	NA	(Stringer et al., 2017)
LTP	Pentylentetrazole (Class A)	$GABA_A$ R antagonist	3-4	17 d	Rescued	Yes (at 2 m)	(Fernandez et al., 2007)
LTP	RO4938581 (Class A)	$GABA_A$ α5 negative allosteric modulator	3-4	6 w	Rescued	NA	(Martinez-Cue et al., 2013)
LTP	CGP55845 (Class A)	Antagonist of $GABA_B$ R	2-3	3 w	Rescued	NA	(Kleschevnikov et al., 2012)
LTP	Picrotoxin (Class A)	Antagonist of $GABA_A$ R	3-4	Acute	Rescued	Acute (slices)	(Kleschevnikov et al., 2004)

LTP	Picrotoxin (Class A)	Antagonist of $GABA_A$ R	4-6	Acute	Rescued	Acute (slices)	(Costa and Grybko, 2005)
LTP	RO25-6981 (Class A)	Antagonist of NMDA R (GluN2B)	3-6	2 w	Rescued	Yes (at 2-4.5 w)	(Hanson et al., 2013)
LTP	Fluoxetine (Class A)	Inhibits serotonine reuptake	> 2	8 w	Rescued	NA	(Begenisic et al., 2014)
LTP	JZL184 (Class A)	Inhibitor of monoacylglycerol lipase / Endocann System	11	4 w	Improved	NA	(Lysenko et al., 2014)
LTP	Melatonin (Class B)	Free radical scavenger	6-6.5	5-5.5 m	Rescued	NA	(Corrales et al., 2014)
LTP	Lithium (Class C)	Mood stabilizer. Interferes with GSK3β signaling	5-6	4 w	Rescued	NA	(Contestabile et al., 2013)
LTP	Epigallocatechin-3-gallate (EGCG) (Class D)	Inhibitor of DYRK1A kinase	2-5	Acute	Rescued	Acute (slices)	(Xie et al., 2008)
Neurogenesis (DG)	RO4938581 (Class A)	$GABA_A$ α5 negative allosteric modulator	3-4	6 w	Rescued	NA	(Martinez-Cue et al., 2013)
Neurogenesis (DG)	Formoterol (Class A)	β2 Receptor agonist	5-6	15 d	Failed	NA	(Dang et al., 2014)
Neurogenesis (DG)	Fluoxetine (Class A)	Inhibits serotonin reuptake	2-5	24 d	Rescued	NA	(Clark et al., 2006)
Neurogenesis (DG)	Peptide 6 (fragment of CNTF) (Class B)	Neurotrophic factor	11-15	30 d	Rescued	NA	(Blanchard et al., 2011)
Neurogenesis (DG)	Melatonin (Class B)	Free radical scavenger	6-6.5	5-5.5 m	Rescued	NA	(Corrales et al., 2014)

Neurogenesis (DG)	Lithium (Class C)	Mood stabilizer. Interferes with GSK3β signaling	5-6	4 w	Rescued	NA	(Contestabile et al., 2013)
Neurogenesis (SVZ)	Lithium (Class C)	Mood stabilizer. Interferes with GSK3β signaling	12	1 m	Rescued	NA	(Bianchi et al., 2010a)
Neurogenesis (DG)	P7C3 (Class E)	Proneurogenic drug	1-2.5	3 m	Improved	NA	(Latchney et al., 2015)
Dendritic hypotrophy	Formoterol (Class A)	β2 Receptor agonist	5-6	15 d	Rescued	NA	(Dang et al., 2014)
Connectivity	Peptide 6 (fragment of CNTF) (Class B)	Neurotrophic factor	11-15	30 d	Rescued	NA	(Blanchard et al., 2011)
Neurodegeneration	Estrogen (Class B)	Protects basal forebrain cholinergic neurons	11-15	2 m	Rescued	NA	(Granholm et al., 2002)
Neurodegeneration	Estrogen (Class B)	Protects basal forebrain cholinergic neurons	9-15	2 m	Rescued	NA	(Granholm et al., 2003)
Neurodegeneration	Minocyclin (Class B)	Anti-inflammatory	7	3 m	Prevented	NA	(Hunter et al., 2004a)
Neurodegeneration	Vitamin E (Class B)	Antioxidant	4	4-6 m	Prevented	NA	(Lockrow et al., 2009)
Senescence (DG)	Melatonin (Class B)	Free radical scavenger	6	6 m	Prevented	NA	(Parisotto et al., 2016)
Ts1Cje mice Neurogenesis (DG)	ALGERNON (Class D)	Inhibits DYRK1A kinase	2.3	12 d	Rescued	NA	(Nakano-Kobayashi et al., 2017)
Ts1Cje mice Phenotype acquisition (DG)	ALGERNON (Class D)	Inhibits DYRK1A kinase	2.3	12 d	Rescued	NA	(Nakano-Kobayashi et al., 2017)

The classes reported in the column “Treatment” correspond to those summarized in the section **2.10.2**. The outcome “Rescued” means that in treated DS mouse models the examined phenotype became similar to that of untreated euploid mice. The outcome “Improved” means that in DS mouse models treatment ameliorated but did not rescue the examined phenotype. Abbreviations: ADNF, Activity Dependent Neurotrophic Factor; ADNP, Activity Dependent Neuroprotective Protein; BM, Barnes Maze; CFC, Contextual Fear Conditioning; CNTF, Ciliary Neurotrophic Factor; d, day; DG, dentate gyrus; m, month; MWM, Morris Water Maze; NA, not available; NOR, Novel Object Recognition; NPR, Novel Place Recognition; PM, Plus Maze; SA, Spontaneous Alternation Task; SVZ, subventricular zone; TM, T-Maze; w, week; WRAM, Water Radial Arm Maze; YM, Y-Maze.

Table 2.10.2. Therapies administered at neonatal and embryonic life stages in the Ts65Dn mouse model of DS.

Phenotype	Treatment	Mechanism	Age	Duration	Outcome	Long-term effect	Reference
NEONATAL TREATMENT							
L/M (CFC)	Fluoxetine (Class A)	Inhibits serotonine reuptake	P3	13 d	Rescued	Yes (at 1 m)	(Bianchi et al., 2010b)
L/M (MWM, NOR, PA)	Fluoxetine (Class A)	Inhibits serotonine reuptake	P3	13 d	Rescued	Yes (at 3 m)	(Stagni et al., 2015b)
L/M (YM)	SAG (Class C)	Synthetic activator of Sonic hedgehog pathway	P0	1 injection	Failed	Yes (at 4 m)	(Das et al., 2013)
L/M (MWM)	SAG (Class C)	Synthetic activator of Sonic hedgehog pathway	P0	1 injection	Rescued	Yes (at 4 m)	(Das et al., 2013)
LTP (CA1)	SAG (Class C)	Synthetic activator of Sonic hedgehog pathway	P0	1 injection	Rescued	Yes (at 4 m)	(Das et al., 2013)
Cerebellar-functional deficits	SAG (Class C)	Synthetic activator of Sonic hedgehog pathway	P0	1 injection	Failed	Yes (at 4 m)	Gutierrez-Castellanos et al. 2013
Neurogenesis (DG and SVZ)	Fluoxetine (Class A)	Inhibits serotonin reuptake	P3	13 d	Rescued	Yes (at 1 m)	(Bianchi et al., 2010b)
Neurogenesis (DG and SVZ)	Fluoxetine (Class A)	Inhibits serotonin reuptake	P3	13 d	Rescued	Yes (at 3 m)	(Stagni et al., 2015b)
Neurogenesis (DG)	SAG (Class C)	Synthetic activator of Sonic hedgehog pathway	P0	1 injection	Failed	Yes (at 6 days)	(Das et al., 2013)

Neurogenesis (Cerebellar granule cells)	SAG (Class C)	Synthetic activator of Sonic hedgehog pathway	P0	1 injection	Rescued	NA	(Roper and Reeves, 2006)
Neurogenesis (DG and SVZ)	Epigallocatechin-3-gallate (Class D)	Inhibits DYRK1A kinase	P3	13 d	Rescued	NA	(Stagni et al., 2014)
Cellularity (DG granule cells)	Fluoxetine (Class A)	Inhibits serotonin reuptake	P3	13 d	Rescued	Yes (at 1 m)	(Bianchi et al., 2010b)
Cellularity (DG granule cells)	Fluoxetine (Class A)	Inhibits serotonin reuptake	P3	13 d	Rescued	Yes (at 3 m)	(Stagni et al., 2015b)
Cellularity (Cerebellar granule cells)	SAG (Class C)	Synthetic activator of Sonic hedgehog pathway	P0	1 injection	Rescued	Yes (at 4 m)	(Das et al., 2013)
Cellularity (DG granule cells)	Epigallocatechin-3-gallate (Class D)	Inhibits DYRK1A kinase	P3	13 d	Rescued	NA	(Stagni et al., 2014)
Dendritic hypotrophy	Fluoxetine (Class A)	Inhibits serotonin reuptake	P3	13 d	Rescued	Yes (at 1 m)	(Guidi et al., 2013)
Dendritic hypotrophy	Fluoxetine (Class A)	Inhibits serotonin reuptake	P3	13 d	Rescued	Yes (at 3 m)	(Stagni et al., 2015b)
Connectivity	Fluoxetine (Class A)	Inhibits serotonin reuptake	P3	13 d	Rescued	Yes (at 1 m)	(Stagni et al., 2013)
Connectivity	Fluoxetine (Class A)	Inhibits serotonin reuptake	P3	13 d	Rescued	Yes (at 3 m)	(Stagni et al., 2015b)
PRENATAL TREATMENT							
L/M (RAWM)	Choline supplement (Class A)	Precursor of acetylcholine	Dams	E+21 d	Improved	Yes (at 13-17 m)	(Velazquez et al., 2013)

Visual attention tasks	Choline supplement (Class A)	Precursor of acetylcholine	Dams	E+21 d	Improved	Yes (at 6-12 m)	(Moon et al., 2010)
L/M (RAWM)	Choline supplement (Class A)	Precursor of acetylcholine	Dams	E+21 d	Improved	Yes (at 13-17 m)	(Ash et al., 2014)
L/M (RAWM)	Choline supplement (Class A)	Precursor of acetylcholine	Dams	E+21 d	Rescued	Yes (at 13-17 m)	(Kelley et al., 2016)
L/M (CFC)	Fluoxetine (Class A)	Inhibits serotonin reuptake	E10	Up to E20/21	Rescued	Yes (at 1.5 m)	(Guidi et al., 2014)
Neurobehavioral development	Peptide 021 (Class B)	Ciliary neurotrophic factor (CNTF) small-molecule peptide mimetic	E8	E+21 d	Rescued	NA	(Kazim et al., 2017)
L/M (MWM, One-trial object recognition discrimination task)	Peptide 021 (Class B)	Ciliary neurotrophic factor (CNTF) small-molecule peptide mimetic	E8	E+21 d	Rescued	Yes (at 7 m)	(Kazim et al., 2017)
Motor and sensory milestones	NAPVSIPQ+SALL RSIPA (Class B)	Active fragments of ADNP and ADNF	E8	Up to E12	Rescued	Yes (at P5-P20)	(Toso et al., 2008)
L/M (MWM)	NAPVSIPQ+SALL RSIPA (Class B)	Active fragments of ADNP and ADNF	E8	Up to E12	Rescued	Yes (at 8-10 m)	Incerti et al. 2012
L/M (MWM)	Vitamin E (Class B)	Antioxidant	Dams	E+12 w	Improved	NA	(Shichiri et al., 2011)
Motor and sensory milestones L/M (MWM, PA)	SGS-111 (Class B)	Analog of Piracetam; Nootropic	Dams	E+5 m	Failed	NA	(Rueda et al., 2008b)
Neurogenesis (DG)	Choline supplement (Class A)	Precursor of acetylcholine	Dams	E+21 d	Improved	Yes (at 13-17 m)	(Velazquez et al., 2013)

Neurogenesis (all brain regions)	Fluoxetine (Class A)	Inhibits serotonin reuptake	E10	Up to E20/21	Rescued	Yes (at 1.5 m)	(Guidi et al., 2014)
Cellularity (all brain regions)	Fluoxetine (Class A)	Inhibits serotonin reuptake	E10	Up to E20/21	Rescued	Yes (at 1.5 m)	(Guidi et al., 2014)
Cellularity (DG granule cells)	A-tochopherol (Class B)	Antioxidant	Dams	E+12 w	Rescued	NA	(Shichiri et al., 2011)
Dendritic hypotrophy	Fluoxetine (Class A)	Inhibits serotonin reuptake	E10	Up to E20/21	Rescued	Yes (at 1.5 m)	(Guidi et al., 2014)
Connectivity	Fluoxetine (Class A)	Inhibits serotonin reuptake	E10	Up to E20/21	Rescued	Yes (at 1.5 m)	(Guidi et al., 2014)
Neurodegeneration	Choline supplement (Class A)	Precursor of acetylcholine	Dams	E+21 d	Improved	Yes (at 13-17 m)	(Ash et al., 2014)
Neurodegeneration	Choline supplement (Class A)	Precursor of acetylcholine	Dams	E+21 d	Improved	Yes (at 4.3-7.5 m)	(Kelley et al., 2014)
Ts1Cje mice Cortical formation (IZ/CP)	ALGERNON (Class D)	Inhibits DYRK1A kinase	E10	Up to E15	Rescued	No (the age was not reported)	(Nakano-Kobayashi et al., 2017)
Ts1Cje mice L/M (YM, Barnes Maze, CFC)	ALGERNON (Class D)	Inhibits DYRK1A kinase	E10	Up to E15	Rescued	Yes (the age was not reported)	(Nakano-Kobayashi et al., 2017)

The classes reported in the column “Treatment” correspond to those summarized in the section **2.10.2.** The outcome “Rescued” means that in treated Ts65Dn mice the examined phenotype became similar to that of untreated euploid mice. The outcome “Improved” means that in Ts65Dn mice treatment ameliorated but did not rescue the examined phenotype. Abbreviations: CFC, Contextual Fear Conditioning; d, day; DG, dentate gyrus; E, embryonic; m, month; MWM, Morris Water Maze; NA, Not Available; NOR, Novel Object Recognition; PM, Plus Maze; TM, T-Maze; RAWM, Radial Arm Water Maze; SVZ, subventricular zone; w, week; YM, Y-Maze.

3. Results Sections

3.1 Section 1

”Short- and long-term effects of the γ-secretase inhibitor ELND006 in the Ts65Dn mouse model of Down syndrome”

Information reported in this section refers to:

1) **“**Inhibition of APP γ-secretase restores Sonic Hedgehog signaling and neurogenesis in the Ts65Dn mouse model of Down syndrome”. **Giacomini A**, Stagni F, Trazzi S, Guidi S, Emili M, Brigham E, Ciani E, Bartesaghi R. *Neurobiology of Disease* 82 (2015) 385–396.
2) “Long-term effect of neonatal inhibition of APP γ-secretase on hippocampal development in the Ts65Dn mouse model of Down syndrome”. Stagni F, Raspanti R, **Giacomini A**, Guidi S, Emili M, Ciani E, Giuliani A, Bighinati A, Calzà L, Magistretti J, Bartesaghi R. Stagni, Raspanti and Giacomini contributed equally to the article. *Neurobiology of Disease* 103 (2017) 11–23.

3.1.1 Abstract

Neurogenesis impairment is considered a major determinant of the intellectual disability that characterizes Down syndrome (DS). Excessive levels of AICD, a cleavage product of the trisomic gene *APP*, increase the transcription of *PTCH1*, a Sonic Hedgehog (SHH) receptor that keeps the mitogenic SHH pathway repressed. This suggests that excessive inhibition of the SHH pathway may concur to impair neurogenesis in DS. Since AICD results from APP cleavage by γ-secretase, the goal of the current study was to establish whether treatment with a γ-secretase inhibitor normalizes AICD levels and restores neurogenesis by restoring the functionality of the SHH pathway. To this purpose we exploited the Ts65Dn mouse, a widely used model of DS. We found that treatment with a selective γ-secretase inhibitor (ELND006) in Ts65Dn pups (postnatal period P3-P15) restored neurogenesis in the subventricular zone and hippocampus, hippocampal granule cell number and synapse development, indicating a positive impact of treatment on brain development. In the hippocampus of treated Ts65Dn mice there was a reduction in the expression levels of PTCH1, which is consistent with reduction of AICD formation due to ELND006-mediated inhibition of γ-secretase. In the framework of potential therapies for DS, it is extremely important to establish whether the positive effects of early intervention are retained after treatment cessation. A second goal of the study was to establish whether early treatment with ELND006 leaves an enduring trace in the brain of Ts65Dn mice. We found that in neonatally treated (postnatal period P3-P15) Ts65Dn mice the pool of proliferating cells in the hippocampal dentate gyrus and total number of granule neurons were still restored as was the number of pre- and postsynaptic terminals in the stratum lucidum of CA3 when mice reached 45-days of age. Accordingly, patch-clamp recording from field CA3 showed functional normalization of the input to CA3. Unlike in field CA3, the number of pre-and postsynaptic terminals in the dentate gyrus of treated Ts65Dn mice was no longer fully restored. The finding that many of the positive effects of neonatal treatment were retained after treatment cessation provides proof of principle demonstration of the efficacy of early inhibition of γ-secretase for the improvement of brain development in DS.

3.1.2 Introduction

Generalized neurogenesis impairment during critical developmental stages and impaired dendritic maturation are the major determinants of intellectual disability in individuals with DS. Alterations of various signaling pathways due to gene triplication are likely to be involved in these neurodevelopmental alterations. Accumulating evidence in the Ts65Dn mouse model of DS suggests that alteration of the Sonic Hedgehog (SHH) pathway may be one important factor involved in neurogenesis impairment in DS (Roper and Reeves, 2006, Trazzi et al., 2011, Trazzi et al., 2013). In particular, defective functioning of the SHH pathway appears to cause reduced proliferation of neural precursor cells (NPCs) of the cerebellum, the subventricular zone (SVZ) of the lateral ventricle and the subgranular zone (SGZ) of the hippocampal dentate gyrus. Regarding the causes of SHH signaling impairment in DS, recent data suggest that the triplicated gene *APP* (amyloid precursor protein), a gene that is important for cell cycle progression and neuron migration (Nalivaeva and Turner, 2013), may be a key candidate underlying trisomy-linked alteration of SHH signaling (Trazzi et al., 2013).
APP undergoes complex proteolytic processing, giving rise to several fragments. Cleavage of APP by α- and β-secretases gives origin to the carboxy-terminal fragments (CTFs) αCTF and βCTF, respectively. Cleavage of βCTF by the enzyme γ-secretase gives origin to the amyloid precursor protein intracellular domain (AICD) and p3, and cleavage of βCTF gives origin to β-amyloid (Aβ) and AICD. Previous evidence showed that excessive AICD levels in trisomic NPCs caused over-expression of Patched 1 (PTCH1), the inhibitor of the SHH pathway (Trazzi et al., 2011, Trazzi et al., 2013). The outcome of this over-inhibition was impairment of neurogenesis and neurite development. Treatments that restored SHH signaling reverted both these defects. In agreement with a key role played by AICD in neurogenesis alterations in the Ts65Dn model, it has been shown that AICD transgenic mice exhibit impaired neurogenesis, similarly to trisomic mice (Ghosal et al., 2010). The evidence reported above suggests that impairment of the SHH pathway due to AICD-dependent PTCH1 over-expression may be a key mechanism that underlies reduced proliferation and impaired

maturation of neuronal precursors in the trisomic brain. Since PTCH1 over-expression keeps the pathway under repression, therapies have been attempted with SAG, a drug that activates the SHH pathway by acting downstream of PTCH1 (Roper et al., 2009, Das et al., 2013). Although this strategy is effective, the use of activators of the SHH pathway may pose some caveats because the SHH pathway is implicated in the development of cancers (Katoh and Katoh, 2009). Since PTCH1 over-expression in the DS brain is due to excessive AICD levels, an ideal approach to restore PTCH1 levels and, hence, SHH signaling, would be to reduce AICD formation through inhibitors of γ-secretase. During the last few years, various selective APP γ-secretase inhibitors have been developed by ELAN Inc (Fleisher et al., 2008, Basi et al., 2010) as strategic tools to reduce Aβ levels in Alzheimer's disease. So far, no study has explored the possibility to exploit γ-secretase inhibitors as a pharmacological tool to reduce the excessive levels of AICD that characterize the DS brain. Based on this rationale, the goal of the current study was to establish whether early treatment with a selective γ-secretase inhibitor, ELND006, positively impacts neurogenesis in the Ts65Dn model, and, if so, whether this effect is followed by a long-lasting improvement in the organization of the hippocampal circuits.

3.1.3 Materials and methods

Colony

Female Ts65Dn mice carrying a partial trisomy of chromosome 16 (Reeves, 1995) were obtained from Jackson Laboratories (Bar Harbour, ME, USA) and the original genetic background was maintained by mating them with C57BL/6JEi x C3SnHeSnJ (B6EiC3) F1 males. Animals were genotyped as previously described (Reinholdt et al., 2011). The day of birth was designated postnatal day zero (P0). A total of 98 mice were used. The animals' health and comfort were controlled by the veterinary service. The animals had access to water and food ad libitum and lived in a room with a 12:12 h dark/light cycle. Experiments were performed in accordance with the Italian and European

Community law for the use of experimental animals and were approved by Bologna University Bioethical Committee. In this study, all efforts were made to minimize animal suffering and to keep the number of animals used to a minimum.

Experimental protocol.

During the last few years, various selective APP γ-secretase inhibitors have been developed by ELAN Inc (Basi et al., 2010), as strategic tools to reduce Aβ levels in Alzheimer's disease. Among these, ELND006 is a γ-secretase inhibitor which retains selectivity and incorporates improved drug-like properties (Basi et al., 2010). In order to test the efficacy of ELND006 in DS, euploid and Ts65Dn mice received a daily subcutaneous injection of ELND006 (ELN; gift by ELAN Inc, USA) dissolved in 25% PEG300, 25% ethylen glycol, 25% cremophor, 15% ethanol, 10% propanol from postnatal day 3 (P3) to postnatal day 15 (P15). We evaluated the outcome of the treatment immediately after its cessation (Experiment 1, P15 mice) and one month later (Experiment 2, P45 mice).

Experiment 1. Based on previous evidence, Euploid (n=11) and Ts65Dn (n=11) mice were daily treated with ELN at a dose of 30.0 mg/kg (**Fig. 3.1.1A**) (Basi et al., 2010). Age-matched euploid (n=8) and Ts65Dn (n=8) mice were injected with the vehicle. These mice will be called here untreated mice. Each treatment group had approximately the same composition of males and females. Animals (4-7 animals for each condition) received a subcutaneous injection (150 μg/g body weight) of BrdU (5-bromo-2-deoxyuridine; Sigma), a marker of proliferating cells (Nowakowski et al., 1989) in Tris HCl 50 mM (at 11-12am) 2 h before being killed. The brain of the other animals (4 animals for each condition) was quickly removed, the hippocampal formation was dissected, kept at –80°C and used for western blot experiments.

Experiment 2. We found that the dose (30.0 mg/kg) of ELN used in the first part of the study (Experiment 1) had no acute effect on mice viability. However, euploid and Ts65Dn mice treated with this dose exhibited a higher mortality rate (death rate=30-40%) after weaning. For this reason, we decided to reduce the dose of ELN. In a pilot experiment we found that a 20.0 mg/kg dose did not

increase the mortality rate and was able to reinstate cell proliferation in the DG of Ts65Dn mice (n=4-5 mice for each experimental group; data not shown), similarly to the dose of 30.0 mg/kg. Therefore, in this part of the study (Experiment 2) we treated mice with a dose of 20.0 mg/kg. Euploid (n=20) and Ts65Dn (n=11) mice received a daily subcutaneous injection of ELN (dose 20.0 mg/kg) dissolved in the vehicle from P3 to P15 (**Fig.3.1.1B**). Age-matched euploid (n=19) and Ts65Dn (n=10) mice were injected with the vehicle. Each treatment group had approximately the same composition of males and females. On P45-P50 mice were weighed, sacrificed, the brain was quickly removed and weighed. These mice will be called here P45 mice (**Fig. 3.1.1B**). The left hemisphere was fixed by immersion in PFA 4%, frozen and used for immunohistochemistry. The right hemisphere was kept at –80°C and used for western blotting. The number of animals used for each of the experimental procedures described below is specified in the figure legends. Other groups of mice were treated from P3 to P15 with either ELN (20.0 mg/kg) (euploid: n=8; Ts65Dn: n=4) or vehicle (euploid: n=9; Ts65Dn: n=7) and at 30-45 days of age were used for electrophysiological recordings from field CA3.

Histological procedures

P15 mice. Mice that had received BrdU were deeply anesthetized, the brain was removed cut along the midline. The left hemisphere was fixed by immersion in Glyo-Fixx as previously described (Bianchi et al., 2010b) and the right hemisphere was fixed in 4% PFA and frozen. The left hemisphere was embedded in paraffin and cut in series of 8-µm-thick coronal sections that were attached to poly-lysine coated slides and used for BrdU, Ki-67, and cleaved caspase-3 immunohistochemistry and for hematoxylin staning. The right hemisphere was cut with a freezing microtome in 30-µm-thick coronal sections that were serially collected in PBS and used for synaptophysin (SYN) and postsynaptic density protein-95 (PSD-95) immunohistochemistry.

P45 mice. The left hemisphere was cut with a freezing microtome in 30-µm-thick coronal sections that were serially collected in anti-freezing solution (30% glycerol; 30% ethylen-glycol; 10% PBS10X; 0.02% sodium azide; MilliQ to volume) and used for immunohistochemistry for Ki-67,

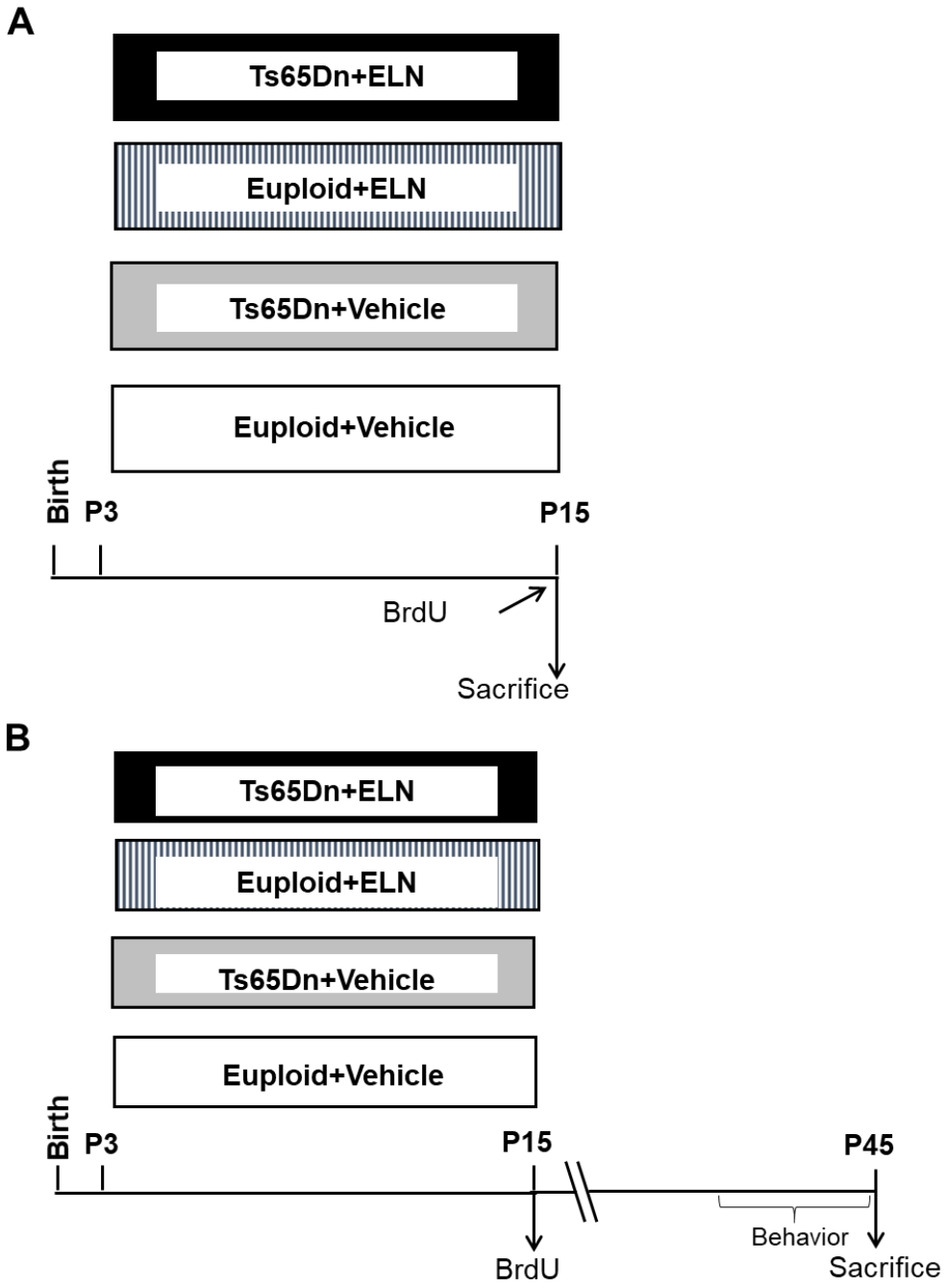

Figure 3.1.1. Experimental protocols. A: Euploid and Ts65Dn mice received a daily injection of either vehicle (Euploid + Vehicle; Ts65Dn + Vehicle) or ELND006 (30.0 mg/kg; Euploid + ELN; Ts65Dn + ELN) from postnatal (P) day 3 to P15. At P15, mice received one injection of BrdU, and were killed after 2 h in order to evaluate the number of cells in the S-phase of the cell cycle. The brains of these mice were used for immunohistochemistry and western blotting. B: Euploid and Ts65Dn mice received a daily injection of either vehicle (Euploid + Vehicle; Ts65Dn + Vehicle) or ELND006 (20.0 mg/kg; Euploid + ELN; Ts65Dn + ELN) from P3 to P15. Mice were killed on P45-P50. The brains of these mice were used for immunohistochemistry and western blotting. Abbreviations: BrdU, bromodeoxyuridine; ELN, ELND006; P, postnatal.

SYN and PSD-95.

BrdU immunohistochemistry in P15 mice. One out of 20 sections was taken from the beginning of the lateral ventricle to the end of the hippocampal formation (n=16-20 sections). After inactivation of endogenous peroxidases, sections were blocked for 1 h in PBS containing 1% bovine serum albumin and 0.1% Triton X-100. Sections were treated prior to blocking with 2 N HCl for 45 min at 37°C, washed in borate buffer 0.1 M pH 8.5 and then incubated overnight at 4°C in blocking buffer containing the primary antibody anti-BrdU (mouse monoclonal 1:100, Roche Applied Science, Mannheim, Germany). Detection was performed with an HRP-conjugated anti-mouse secondary antibody (dilution 1:200; Jackson Immunoresearch, West Grove, PE, USA) and DAB kit (Vector Laboratories, Burlingame, CA, USA).

Ki-67 immunohistochemistry in P15 mice. One out of 20 sections were taken starting from the beginning of the lateral ventricle up to the end of the hippocampal formation. Sections were incubated overnight at 4°C with a rabbit monoclonal anti-Ki67 antibody (1:100; Thermo Scientific). Detection was performed with a HRP-conjugated anti-rabbit secondary antibody (1:200; Jackson Immunoresearch) and DAB kit (Vector Laboratories).

Ki-67 immunohistochemistry in P45 mice. One out of 6 sections were taken starting from the beginning to the end of the hippocampal formation (n=16-20 sections). Sections were incubated overnight at 4°C with rabbit monoclonal anti-Ki67 antibody (1:100; Thermo Scientific). Section were then incubated for 2 h with a Cy3 conjugated anti-rabbit IgG (1:200; Jackson Immunoresearch). Sections were counterstained with Hoechst 33342 in order to label cell nuclei.

Cleaved caspase–3 immunohistochemistry in P15 mice. One out of 20 sections from the beginning of the lateral ventricle to the end of the hippocampal formation (n=16-20 sections) were processed for cleaved caspase-3 immunohistochemistry, as previously described. Deparaffinized sections were permeabilized with 0.1% Triton X-100 in PBS for 30 min, blocked for 1 h in 3% BSA in 0.1% Triton X-100 and PBS, incubated overnight at 4°C with a primary antibody [rabbit cleaved caspase-3 (Asp 175) antibody (Cell Signaling Technology)], and diluted 1:200 in 3% BSA in 0.1% Triton X-100 and

PBS. Sections were washed in 0.1% Triton X-100 in PBS for 40 min and incubated for 2 h with a secondary antibody, Cy3-conjugated anti-rabbit IgG (1:200; Jackson Immunoresearch) diluted in 0.1% Triton X-100 in PBS and 3% BSA, and rinsed in 0.1% Triton X-100 in PBS for 30 min. Fluorescent images were taken with an Eclipse TE 2000-S microscope.

SYN and PSD-95 immunohistochemistry in P15 and P45 mice. Free-floating sections (n=4-6 per animal) taken at the level of the hippocampal formation were submitted to fluorescence immunohistochemistry for SYN and PSD-95. Sections were counterstained with Hoechst dye in order to label cell nuclei. Sections were incubated for 48 h at 4°C with a mouse monoclonal anti-SYN (SY38) antibody (Millipore-Biomanufacturing and Life Science Research, Billerica, MA, USA) and rabbit polyclonal anti-PSD-95 antibody (Abcam) both diluted 1:1000. Sections were then incubated overnight at 4°C with a FITC-conjugated goat anti-mouse antibody or with a CY3-conjugated anti-rabbit (Jackson Laboratory) antibody both diluted 1: 200.

Hematoxylin-staining in P15 mice. One out of 20 sections, taken from the beginning to the end of the hippocampal formation (n=9-12) were stained with hematoxylin.

Measurements

Image acquisition. A light microscope (Leitz) equipped with a motorized stage and focus control system and a color digital camera (Coolsnap-Pro; Media Cybernetics, Silver Spring, MD, USA) were used to take bright field images of section processed for BrdU (P15) and Ki67 (P15) immunohistochemisty. Immunofluorescence images of sections processed for cleaved caspase-3 (P15) and Ki-67 (P45) were taken with a Nikon Eclipse TE 2000-S inverted microscope (Nikon Corp., Kawasaki, Japan), equipped with a Nikon digital camera DS 2MBWc. Immunofluorescence images of sections processed for SYN and PSD-95 immunohistochemistry were taken with a LEICA TCS SL confocal microscope. Measurements were carried out using Image Pro Plus software (Media Cybernetics, Silver Spring, MD 20910, USA).

Number of BrdU-positive cells. Cells were sampled from the dentate gyrus (DG) and the rostral

subventricular zone (SVZ). BrdU-positive cells in the DG and SVZ of P15 mice were detected using a light microscope (Eclipse; objective: x 40, 0.75 NA; final magnification: x 400). Quantification of BrdU-labeled nuclei was conducted in every 20th section using a modified unbiased stereology protocol that has previously been reported as successfully quantifying BrdU labeling (Malberg et al., 2000, Kempermann and Gage, 2002, Tozuka et al., 2005). All BrdU labeled cells located in the granule cell and subgranular layers were counted in their entire z axis (1 µm steps) in each section. To avoid oversampling errors, nuclei intersecting the uppermost focal plane were excluded. The total number of BrdU labeled cells per animal was determined and multiplied by 20 to obtain the total estimated number of cells per DG.

Number of Ki-67-positive cells. In P15 mice, cells were sampled from the rostral SVZ. The total number of positive cells in the DG and SVZ was estimated by multiplying the total number counted in the series of sampled sections by the inverse of the section sampling fraction (ssf = 1/20). Quantification of Ki-67-labeled nuclei in the DG of P45 mice was conducted in every 6th section throughout the whole extent of the DG using a Nikon Eclipse TE 2000-S microscope (objective x 40, NA 0.75; final magnification x 400). A modified unbiased stereology protocol for quantification of proliferating cells (Malberg et al., 2000, Kempermann and Gage, 2002, Tozuka et al., 2005) was used. All Ki-67-labeled cells located in the granule cell and subgranular layers were counted along the entire z axis (1 µm steps) of each section. To avoid oversampling errors, the nuclei intersecting the uppermost focal plane were excluded. The total number of Ki-67-labeled cells per animal was determined and multiplied by six to obtain the total estimated number of cells per DG. We additionally evaluated, in P45 mice, the mean number of Ki-67-positive cells per section by dividing the number of counted cells by the number of sampled sections.

Number of cleaved caspase-3 positive cells. In the series of sections processed for cleaved caspase-3 IHC, cleaved caspase-3-positive cells were counted in the SVZ and DG of P15 mice. Images were taken using a fluorescence microscope (Eclipse; objective x 40, 0.75 NA; final magnification: x 400).

Total cell count was obtained from the sum of counts across all sections counted.

Synaptic terminals. The intensity of SYN and PSD-95 immunoreactivity in the molecular layer of the DG and in the stratum lucidum of field CA3 of P15 mice was determined by the optical densitometry of immunohistochemically-stained sections. Fluorescence images were captured using a Nikon Eclipse E600 microscope equipped with a Nikon Digital Camera DXM1200 (ATI system). Densitometric analysis of SYN and PSD95 was carried out using the Nis-Elements Software 3.21.03 (Nikon, Melville, NY, USA). A box of 490 μm^2 was placed in the inner, middle and outer third of the molecular layer of the upper blade of the DG. Six measurements were taken for each region. For each image, the intensity threshold was estimated by analyzing the distribution of pixel intensities in the image areas that did not contain IR. This value was then subtracted to calculate IR of each sampled area.

Images of sections immunoprocessed for SYN or PSD-95 of P15 and P45 mice were acquired with a confocal microscope (Nikon Ti-E fluorescence microscope coupled with an A1R confocal system, Nikon). In each section three images from the molecular layer of the DG and the stratum lucidum of field CA3 were captured and the density of individual puncta exhibiting SYN or PSD-95 immunoreactivity was evaluated as previously described (Guidi et al., 2013).

Stereology of the DG. Unbiased stereology was performed on Hoechst-stained sections. The optical disector method was used to obtain cell density, and the Cavalieri principle was used to estimate volume of the granule cell layer of the DG (West and Gundersen, 1990). In P45 mice, one DG is represented in 90-110 30-μm-thick sections. To include 16-18 sections, every 6th section was selected, beginning at a random position within the first 6 sections. For determination of the granule cell number, granule cell nuclei were counted with an x 63 oil objective (NA 1.32). In order to obtain granule cell numerical density, cells were counted in 30 x 30 counting frames spaced in a 100 μm square grid superimposed over each section. Cells that intersected the uppermost focal (exclusion) plane and those that intersected the exclusion boundaries of the unbiased sampling frame were excluded from counting. Cells that met the counting criteria through a 30 μm axial distance were

counted according to the optical disector principle.

The neuron density (Nv) is given by

$N_V = (\Sigma Q/\Sigma dis)/Vdis$

where Q is the number of particles counted in the disectors, dis is the number of disectors and Vdis is the volume of the disector. For volume (Vref) estimation with the Cavalieri principle, in each sampled section, the area of the granule cell layer was measured by tracing its contours. The volume of the granule cell layer (Vref) was estimated (West and Gundersen, 1990) by multiplying the sum of the cross sectional areas by the spacing T between sampled sections (180 μm). The total number (N) of granule cells was estimated as the product of V_{ref} and the numerical density (Nv).

$N= N_V \times V_{ref}$

Western blotting

Total proteins were obtained from hippocampi of P15 and P45 mice. Briefly, hippocampi were homogenized in ice-cold RIPA buffer (1% Triton-X100, 150 mM NaCl, 1 mM EDTA and 20 mM Tris pH 8) supplemented with 1mM phenyl-methanesulphonylfluoride (PMSF) and 1% proteases and phosphatases inhibitors cocktail (Sigma). Samples were then incubated in ice for 30 minutes, sonicated for 15 minutes and clarified by centrifugation at 14 000 ¥ g for 20 minutes at 4°C. Protein concentration was determined by the Lowry method. Proteins (50 μg) extracted from P15 mice were subjected to electrophoresis on a 4-12% Mini-PROTEAN® TGX™Gel (Bio-Rad) and transferred to a Hybond ECL nitrocellulose membrane (Amersham Life Science). The following primary antibodies were used: anti-Amyloid Precursor Protein, C-Terminal (anti-APP; 1:5000; Sigma-Aldrich); anti-PTCH1 (1:50; R&D systems), anti-GSK3β (anti-GSK3β; 1:1000; Cell Signaling Technology); anti-Phospho-GSK3β (Ser9) XP® (anti-pGSK3β Cell Signaling Technology); anti-GAPDH (anti-GAPDH; 1:10000; Sigma-Aldrich). Proteins (50-80 μg) extracted from P45 mice were subjected to electrophoresis on a 4-12% NuPAGE Bis-Tris Precast Gel (Novex, Life Technologies, Ltd, Paisley, UK) and transferred to a Hybond ECL nitrocellulose membrane (Amersham Life Science). The

following primary antibodies were used: anti-PTCH1 (1:1000; Abcam), anti-p21 (1:500; Santa Cruz Biotechnology), anti-APP C-Terminal (1:2000; Sigma-Aldrich) and anti-GAPDH (1:5000; Sigma-Aldrich). Densitometric analysis of images digitized with ChemiDoc XRS+ was performed with Image Lab software (Bio-Rad Laboratories, Hercules, CA, USA) and intensity for each band was normalized to the intensity of the corresponding GAPDH band.

Patch-clamp experiments

Preparation of slices. Mice (P30-P45) were anesthetised by inhalation of isoflurane (Merial Italia, Milan, Italy) and transcardially perfused with a cutting solution. The brain was quickly extracted under hypothermic conditions and submerged in ice-cold cutting solution. For the preparation of slices for the voltage-clamp recordings. Two coronal cuts were made, in order to remove the anterior half and the occipital pole of the brain, and the piece thus obtained was laid on the posterior section plane. The tissue was blocked on the stage of a Microslicer DTK-1000 vibratome (Dosaka, Kyoto, Japan) using cyanoacrilate glue. Coronal slices of the hippocampus, 350-μm thick, were cut maintaining the tissue submerged in an ice-cold solution composed of (in mmol/l): 130 K gluconate, 15 KCl, 20 HEPES, 0.2 EGTA, 11 glucose. The use of this high-K^+ solution was found to improve neuron viability (Stephane Dieudonné, unpublished results). The slices were then transferred to a recovery chamber filled with a maintaining solution continuously bubbled with 95% O_2, 5% CO_2, at room temperature (21-22°C) for at least one hour before starting the recording.

Voltage-clamp recordings, drugs, and data analysis. Whole-cell, patch-clamp recordings from CA3 pyramidal neurons were carried out on acute slices of the dorsal hippocampus obtained as described above. The experimental set-up employed and the basic procedures followed were the same as described elsewhere. Briefly, cells were visualized by means of an upright microscope (Axioskop 2 FS; Zeiss, Oberkochen, FRG) equipped with a x 60 water-immersion objective lens, differential-contrast optics, and a near-infrared charge-coupled device (CCD) camera. Slices were perfused with ACSF (continuously bubbled with 95% O_2, 5% CO_2) at a rate of about 1.5 ml/min. Patch pipettes

were fabricated from thick-wall borosilicate glass capillaries (CEI GC 150-7.5; Harvard Apparatus, Edenbridge, UK) by means of a Sutter P-87 horizontal puller (Sutter Instruments, Novato, CA, USA). The pipette solution contained (in mmol/l): 150 CsF, 4 CsCl, 2 $MgCl_2$, 10 N-2-hydroxyethyl piperazine-N-2-ethanesulphonic acid (HEPES), 10 ethylene glycol-bis (β-aminoethyl ether) N,N,N´,N´-tetraacetic acid (EGTA), 2 adenosine 5′-triphosphate (ATP)-Na_2, 0.2 guanosine 5′-triphosphate (GTP)-Na, 2.5 lidocaine N-ethyl bromide (QX-314) (pH adjusted to 7.2 with CsOH). The patch pipettes had a resistance of 3-5 MΩ when filled with the above solution. Tight seals (> 5 GΩ) and the whole-cell configuration were obtained by suction according to the standard technique (Hamill et al., 1981). Excitatory postsynaptic currents (EPSCs) were recorded at room temperature (21-22 °C) by means of an Axopatch 200B patch-clamp amplifier (Axon Instruments, Foster City, CA, USA). Series resistance (R_s) was evaluated on line by canceling the whole-cell capacitive transients evoked by –5-mV voltage square pulses with the amplifier built-in compensation section, and reading out the corresponding values. R_s was normally 5-12 MΩ and always < 20 MΩ, and was compensated by ~90%. Current signals were acquired in gap-free modality with a personal computer interfaced to a Digidata 1322A interface (Axon Instr.) using the Clampex program of the pClamp 8.2 software package (Axon Instr.). Current signals were low-pass filtered at 5 kHz and digitized at 20 kHz. Miniature synaptic currents were recorded in the presence of tetrodotoxin (used to block voltage-gated Na+ channels, and therefore the discharge of Na+-dependent action potentials) in the perfusing solution, so as to prevent spontaneous synaptic events due to presynaptic action potential firing. Tetrodotoxin (TTx) was purchased from Alomone Labs (Jerusalem, Israel). D-(-)-2-amino-5-phosphonopentanoic acid (APV; NMDA-receptor antagonist) and (2,3-dihydroxy-6-nitro-7-sulfamoyl-benzo[f]quinoxaline-2,3-dione) (NBQX; AMPA receptor antagonist) were purchased from Tocris (Bristol, UK). Drugs were preliminarily dissolved in H_2O and stored in concentrated aliquots at -20 °C. At the time of recording, the small aliquots were dissolved to the final concentrations (TTx: 1μM; APV 50 μM; NBQX: 10 μM).

Data analysis. Results were off-line detected using an automated threshold routine in the LabView

environment. All detected events were also visually inspected one-by-one for confirmation or rejection. To be considered a synaptic event the amplitude of the EPSC was required to be at least twice the noise amplitude: the events that showed a lower amplitude were ignored. Accepted events were then used to construct frequency distribution diagrams of mEPSC amplitude. The EPSCs amplitude from whole-cell recordings were analyzed by means of the program Clampfit of pClamp 8.2 (Axon Instr.). Peak amplitude values of postsynaptic currents were analyzed with Origin 6.0 (MicroCal Software, Northampton, MA, USA) in order to build up frequency-distribution diagrams of the current recorded.

Statistical analysis

Data from single animals represented the unity of analysis. Results are presented as mean ± standard error of the mean (SE). Distribution of data and the homogeneity of variances were evaluated with Shapiro-Wilk test and Levene's test respectively. Statistical analysis of all examined variables was carried out using a two-way ANOVA with genotype (euploid and Ts65Dn) and treatment (vehicle and ELN) as factors. *Post hoc* multiple comparisons were carried out using the Fisher least significant difference (LSD) test. Data were analyzed with IBM SPSS 22.0 software. For the overall mEPSC frequency, a linear mixed model was used. The model has been fit using the Restricted or Residual Maximum Likelihood (REML). It calculated the average frequency keeping memory of the number of cells recorded in each animal of the same experimental group (95% confidence interval). Data were analysed with the software R (The R Project for Statistical Computing; version 3.2.3). For the analysis of the decay time constant (τdec) of mEPSC as a function of mEPSCs amplitude a linear regression analysis was used ($y=A+B*X$). The relative weight of each data point in the fitting procedure was made proportional to the number of events from which the corresponding average current had been obtained. Data were analysed with the software Origin 6.0 using the Fit Linear function. For all analyses, a probability level of $p < 0.05$ was considered to be statistically significant.

3.1.4 Results

Short-term effect of neonatal treatment with ELN on neurogenesis in the SVZ and SGZ of Ts65Dn mice

We treated euploid and Ts65Dn mice with ELN from P3 to P15, in order to establish whether treatment was able to restore neurogenesis in this model. At P15 mice were injected with BrdU and were killed after 2h. Evaluation of the number of proliferating cells in SGZ of the dentate gyrus (DG) and in the subventricular zone (SVZ) of the lateral ventricle showed that Ts65Dn mice had fewer BrdU-positive cells in comparison with euploid mice (**Fig. 3.1.2A-D**). Treatment with ELN increased the number of BrdU-positive cells in Ts65Dn mice, so that treated mice had a similar number of BrdU-positive cells as untreated euploid mice both in the DG (**Fig. 3.1.2C**) and SVZ (**Fig. 3.1.2D**). Treatment had no effects in euploid mice when compared with their untreated counterparts (**Fig. 3.1.2C,D**). To establish whether treatment with ELN restores the overall size of the population of neural precursors in the DG and SVZ of Ts65Dn mice, we evaluated the number of cells immunopositive for Ki-67, an endogenous marker expressed during all the phases of the cell cycle (Scholzen and Gerdes, 2000). We found that in the DG of untreated Ts65Dn mice there were fewer Ki-67-positive cells in comparison with euploid mice (**Fig. 3.1.2E**). In treated Ts65Dn mice the number of cycling cells underwent a large increase and became similar to that of euploid mice (**Fig. 3.1.2E**). Similar findings were obtained in the SVZ (**Fig. 3.1.2F**). The protein cleaved caspase-3 is one of the hallmarks of apoptotic death (Blomgren et al., 2007). The number of apoptotic cells was not different between untreated euploid and Ts65Dn mice in both DG and SVZ and treatment did not alter cleaved caspase-3- positive cells (**Fig. 3.1.2G,H**). Taken together, these results indicate that treatment with ELN during the first two postnatal weeks restores the number of neural precursor cells in the DG and SVZ of Ts65Dn mice and suggest that this effect is due to an increase in

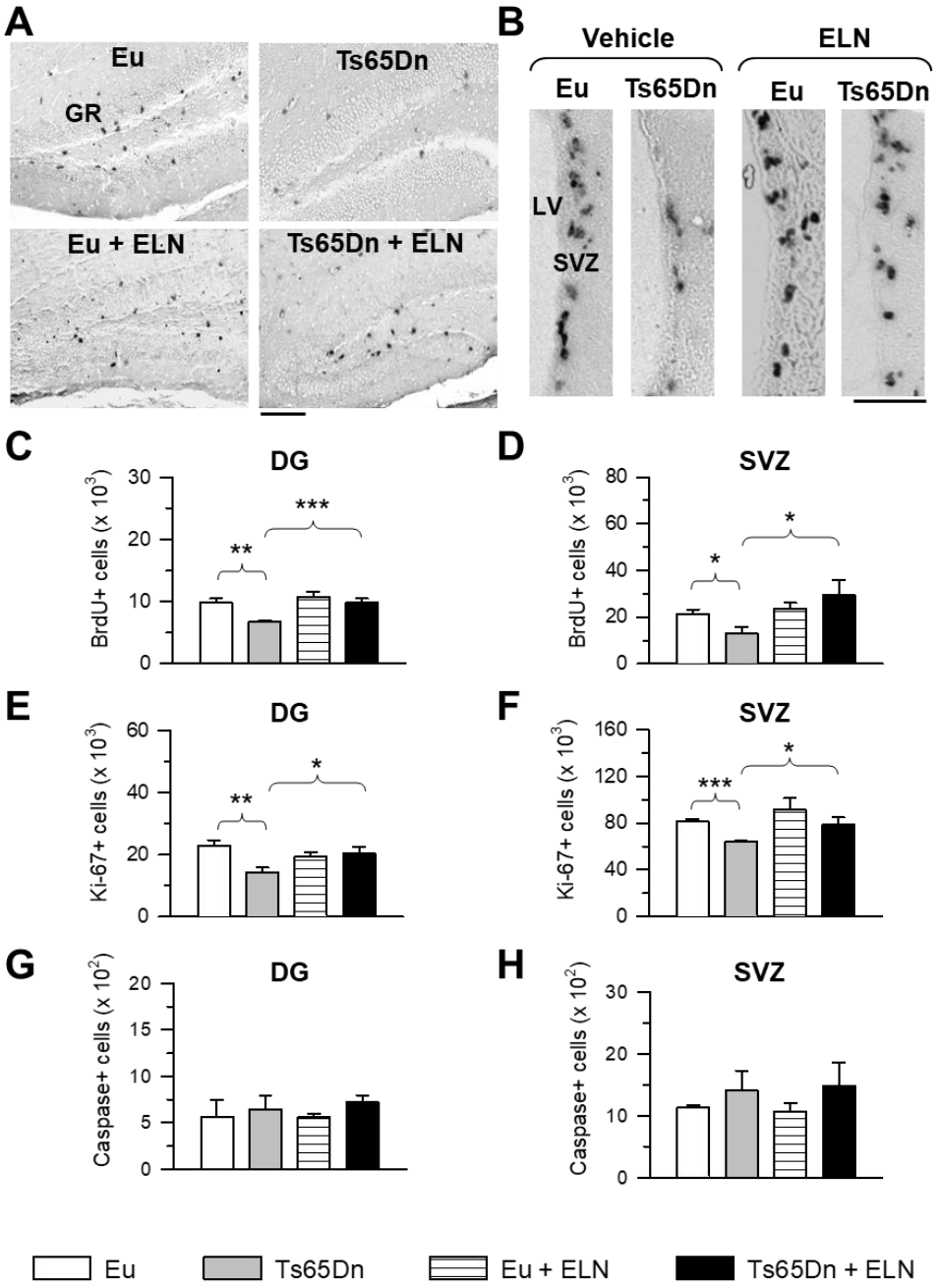

Figure 3.1.2. Effect of APP γ-secretase inhibition on proliferation potency in the dentate gyrus and subventricular zone of Ts65Dn and euploid mice aged 15 days. Animals received a daily injection of ELND006 or vehicle in the period P3-P15. On P15 they received one injection of BrdU and were sacrificed after 2 h. A-B: Sections immunostained for BrdU from the DG (A) and SVZ (B) of untreated and treated euploid and Ts65Dn mice. Scale bar: 100 µm (A); 50 µm (B). C, D: Total number of BrdU-positive cells in the DG (C) and SVZ (D) of untreated euploid (n= 5) and Ts65Dn (n=4) mice and euploid (n=4) and Ts65Dn (n=5) mice treated with ELN. E, F: Number of Ki-67-positive cells in the dentate gyrus (E) and SVZ (F) of untreated euploid (n= 5) and Ts65Dn (n=4) mice and euploid (n=4) and Ts65Dn (n=5) mice treated with ELN. G,H: Number of cleaved caspase-3-positive cells in the DG (G) and SVZ (H) of untreated euploid (n= 5) and Ts65Dn (n=4) mice and euploid (n=4) and Ts65Dn (n=5) mice treated with ELN. Values (mean ± SE) in (C-H) represent totals for one hemisphere. * $p < 0.05$; ** $p < 0.01$; *** $p < 0.001$. Abbreviations: DG, dentate gyrus; ELN, ELND006; Eu, euploid; LV, lateral ventricle; SVZ, subventricular zone.

proliferation potency and not to a decrease in cell death.

In mice, the SGZ produces most of the granule cells that populate the granule cell layer of the DG in the first two postnatal weeks (Altman and Bayer, 1975). In order to establish whether the increase in the number of neural cell precursors in the DG of treated Ts65Dn mice translated into restoration of total granule cell number we evaluated the number of granule cells. In euploid mice, treatment did not change the volume of the granule cell layer, granule cell density and total granule cell number (**Fig. 3.1.3**). In contrast, in Ts65Dn mice, treatment significantly increased the volume of the granule cell layer, granule cell density and total granule cell number (**Fig. 3.1.3**). Treated Ts65Dn and untreated euploid mice had the same volume of the granule cell layer, granule cell density and total granule cell number (**Fig. 3.1.3**), indicating a treatment-induced rescue in the morphogenesis of the granule cell layer.

Short-term effect of neonatal treatment with ELN on hippocampal synapse development

Since treatment with ELN restored total granule cell number in Ts65Dn mice we wondered whether there were also positive effects on synapse development, a process that is impaired in the trisomic brain (Kurt et al., 2004, Belichenko et al., 2007, Chakrabarti et al., 2007, Guidi et al., 2013). To answer this question, we evaluated the immunoreactivity for synaptophysin (SYN), a marker of presynaptic terminals, and the postsynaptic density protein-95 (PSD-95), a marker of postsynaptic terminals, in hippocampal sections from treated and untreated euploid and Ts65Dn mice. We focused on two regions of the hippocampal formation, the molecular layer of the DG because this layer receives inputs from the perforant pathway (the major input to the hippocampus), and the stratum lucidum of field CA3, the site of termination of the axons of the granule cells (Amaral and Witter, 1995).

Results showed that the levels of SYN immunoreactivity in untreated Ts65Dn mice was significantly lower than in untreated euploid mice in the inner (-21%), middle (-16%) and outer (-15%) molecular layer of the DG (**Fig. 3.1.4B**) and in the stratum lucidum (-13%) of CA3 (**Fig. 3.1.4C**). In parallel

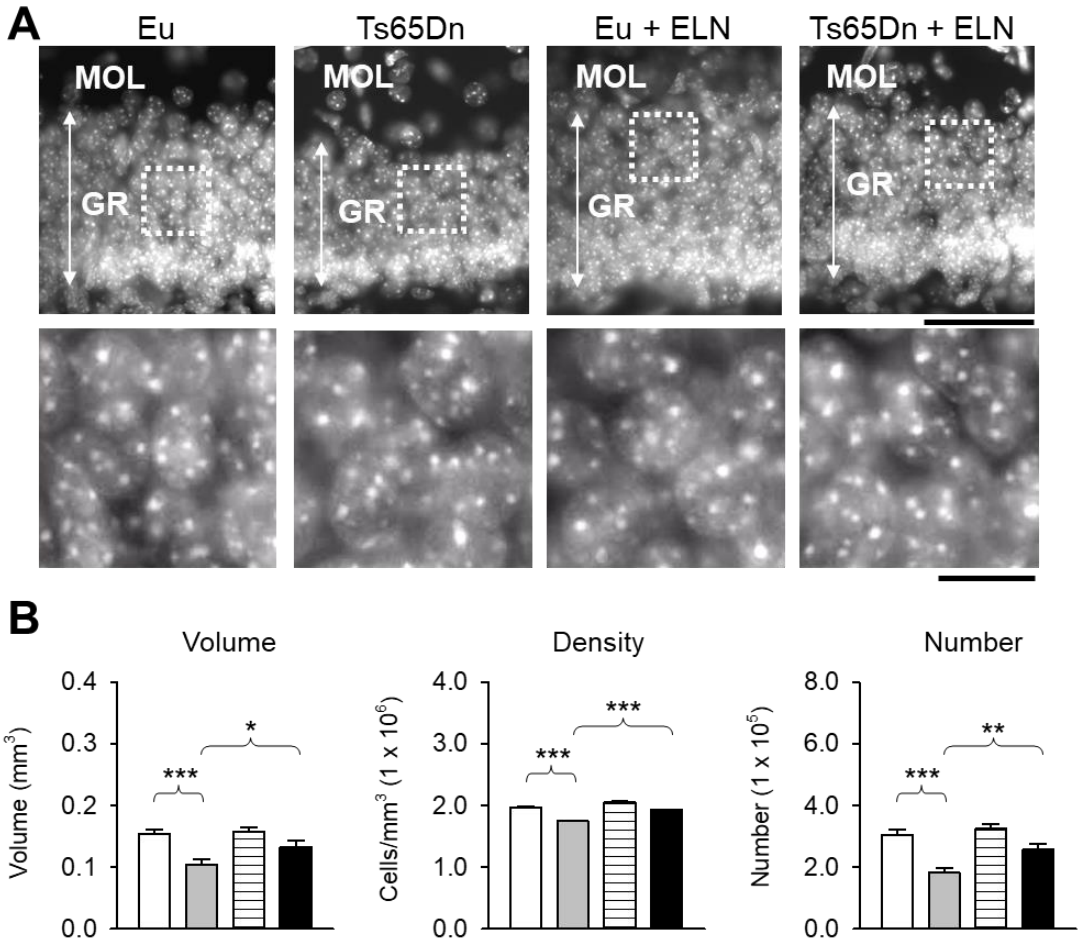

Figure 3.1.3. Effect of APP γ-secretase inhibition on total granule cell number in the dentate gyrus of P15 mice. A: Hoechst-stained coronal section across the dentate gyrus of an animal of each experimental group. The higher magnification images in the lower row correspond to the region enclosed in the dotted box in the upper row. Scale bar = 50 µm (upper row); 10 µm (lower row). B: Volume of the granule cell layer, density of granule cells (number per mm^3) and total number of granule cells of the DG. Values are mean ± SE. Volume and granule cell number refer to one hemisphere. * $p < 0.05$; ** $p < 0.01$; *** $p < 0.001$. Abbreviations: ELN, ELND006; Eu, euploid; GR, granule cell layer; MOL, molecular layer.

with the low levels of SYN immunoreactivity, in Ts65Dn mice there was fewer immunoreactivity for PSD-95 in the inner (-10%), middle (-15%) and outer (-8%) molecular layer of the DG (**Fig. 3.1.4E**) and in the stratum lucidum (-10%) of CA3 (**Fig. 3.1.4F**). Treatment with ELN increased the immunoreactivity for SYN (**Fig. 3.1.4B,C**) and PSD-95 (**Fig. 3.1.4E,F**) in all zones of the molecular layer and in the stratum lucidum of CA3 in Ts65Dn mice, that became similar to that of untreated euploid mice. In euploid mice, treatment did not affect the immunoreactivity for SYN (**Fig. 3.1.4B,C**) and PSD-95 (**Fig. 3.1.4E,F**) both in the DG and CA3. In order to establish whether the effects of genotype and treatment on protein levels were attributable to different levels of synaptic proteins per synapse or to differences in the number of synapses, we evaluated the density of individual puncta exhibiting either SYN or PSD-95 immunoreactivity. While untreated Ts65Dn mice had fewer SYN- (**Fig. 3.1.5B,C**) and PSD-95- (**Fig. 3.1.5E,F**) positive puncta both in the DG and CA3, neonatal treatment with ELN increased the number of SYN (**Fig. 3.1.5B,C**) and PSD-95- positive puncta (**Fig. 3.1.5E,F**) in Ts65Dn mice, that became similar to that of euploid mice in both regions. Together, these evidence suggests that treatment had restored hippocampal synapse development.

Short-term effect of treatment with ELN on AICD levels

An important issue regards the effects of ELN on the activity of γ-secretase and hence, AICD levels after treatment cessation. Unfortunately, unlike in cultures of NPCs, it was extremely difficult to detect AICD in brain samples processed for western blotting (we detected AICD band in 3% of all examined cases only). This small peptide has a very short half-life (about 5 min) (Cupers et al., 2001). Thus, its degradation in the phase of brain excision may render it undetectable. Since AICD derives from the cleavage of the CTFs, inhibition of the activity of *γ*-secretase should reduce the levels of AICD and, consequently, increase the levels of CTFs. This suggests that an estimate of AICD levels can be obtained indirectly by quantifying the levels of the CTFs. Thus, in order to obtain information regarding the short-term effect of treatment on AICD levels we evaluated the levels of the CTFs in

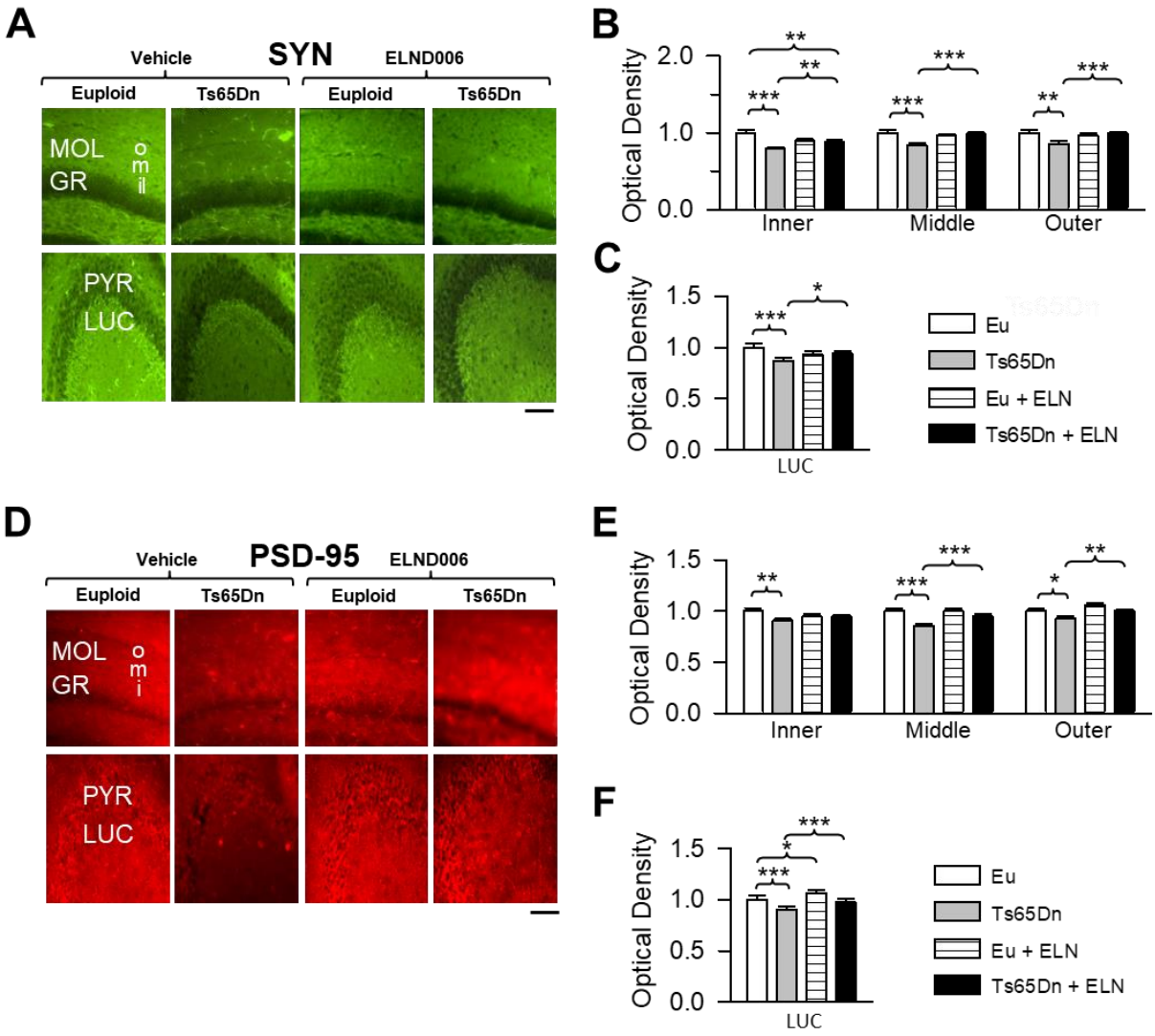

Figure 3.1.4. Effect of APP γ-secretase inhibition on synapse development in the hippocampal formation. A, D: Sections processed for SYN (A) and PSD-95 (D) immunofluorescence from the DG (upper row) and CA3 (lower row) of an animal from each experimental group. Scale bar = 100 μm. B, C, E, F: Optical density of SYN (B, C) and PSD-95 (E, F) immunoreactivity in the inner, middle and outer third of the molecular layer of the DG (B, E) and the stratum lucidum of CA3 (C, F) of untreated euploid (n= 6) and Ts65Dn (n=5) mice and euploid (n=6) and Ts65Dn (n=5) mice treated with ELN. For each region, data of SYN and PSD-95 immunoreactivity are given as fold difference vs. untreated euploid mice. Values in B, C, E, F represent mean ± SE. * $p < 0.05$; ** $p < 0.01$; *** $p < 0.001$. Abbreviations: ELN, ELND006; Eu, euploid; GR, granule cell layer; i, inner; LUC, stratum lucidum; m, middle; MOL, molecular layer; o, outer; PYR, pyramidal layer.

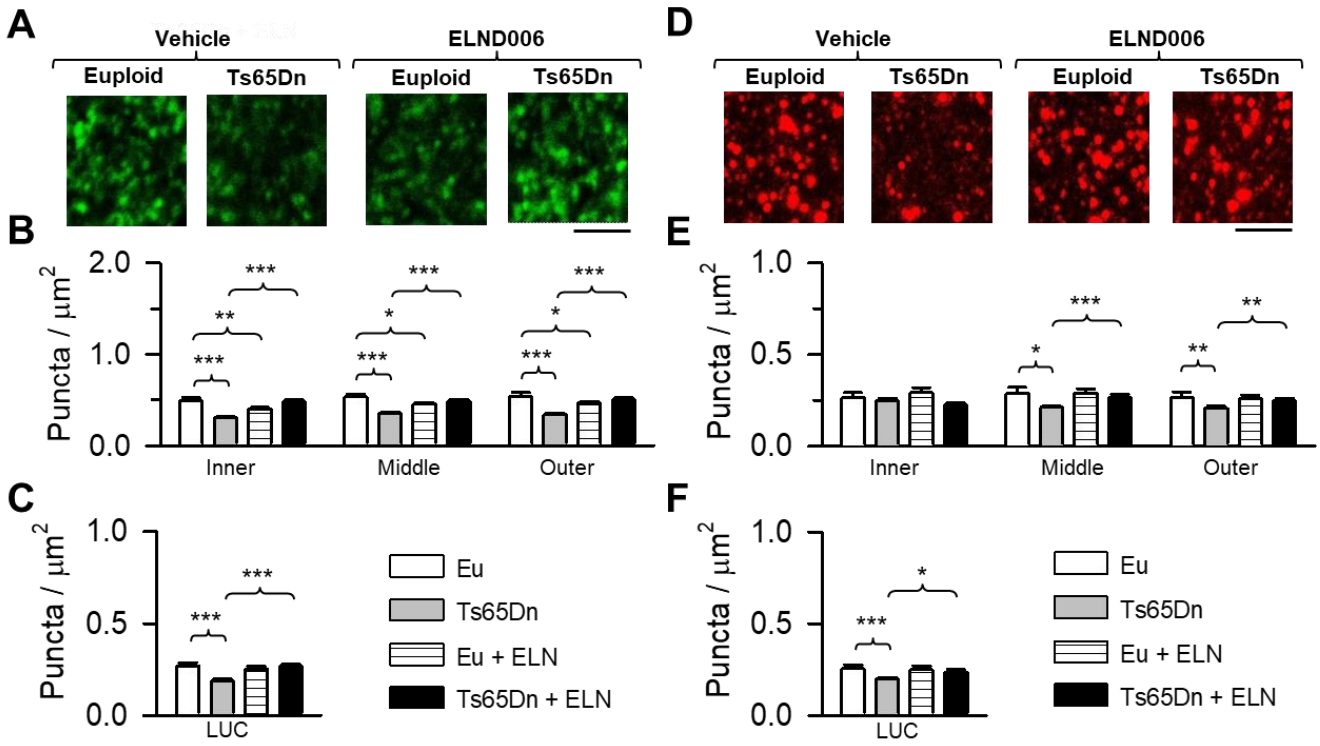

Figure 3.1.5. Effect of APP γ-secretase inhibition on the number of puncta in the hippocampal formation. A,D: Images, taken with the confocal microscope, of sections processed for SYN (A) and PSD-95 (D) immunofluorescence from the DG of an animal of each experimental group. Scale bar = 3 µm. B, C, E, F: Number of puncta per μm^2 exhibiting SYN (B, C) and PSD-95 (E, F) immunoreactivity in the inner, middle and outer third of the molecular layer of the DG (B, E) and the stratum lucidum of CA3 (C, F) of untreated euploid (n=6), untreated Ts65Dn (n=5), and euploid (n=6) and Ts65Dn (n=5) mice treated with ELND006. Values in B, C, E, F represent mean ± SE. * $p < 0.05$; ** $p < 0.01$; *** $p < 0.001$. Abbreviations: ELN, ELND006; Eu, euploid; LUC, stratum lucidum.

P15 euploid and Ts65Dn mice.Results showed that in the hippocampus of untreated Ts65Dn mice there were higher levels of CTFs in comparison to euploid mice (**Fig. 3.1.6A,B**). Treatment with ELN in Ts65Dn mice provoked an increase in the levels of CTFs in comparison with their untreated counterparts (**Fig. 3.1.6A,B**), which is consistent with the inhibitory action exerted by ELN on the activity of γ-secretase. This indicates that probably levels of AICD underwent a reduction after treatment with ELN.

Short-term effect of treatment with ELN on AICD targets

AICD is a transcription factor that up-regulates various genes, including *PTCH1, BACE1, APP* and *GSK3β* (Cao and Sudhof, 2001, von Rotz et al., 2004, Nalivaeva and Turner, 2013). In light of this, we decided to examine the expression levels of these genes in the hippocampus of treated and untreated euploid and Ts65Dn mice. Untreated Ts65Dn mice had higher Ptch1 levels in comparison with euploid mice, and treatment with ELN decreased the levels of this protein. As in Ts65Dn mice, a reduction in PTCH1 levels also took place in treated euploid mice (**Fig. 3.1.7A**). BACE1 is an enzyme of the beta amyloidogenic pathway that cleaves APP, producing βCTF. Ts65Dn mice had higher BACE1 levels in comparison with euploid mice. Treatment with ELN reduced treated BACE1 levels in Ts65Dn mice, that became similar to those of untreated euploid mice, and in euploid mice (**Fig. 3.1.7B**). Untreated Ts65Dn mice had notably higher levels of APP in comparison with euploid mice (**Fig. 3.1.7C**). In Ts65Dn mice APP levels largely decreased after neonatal treatment with ELN in comparison with their untreated counterparts, though they remained larger in comparison with untreated euploid mice (**Fig. 3.1.7C**). In euploid mice treatment had no effect on APP levels (**Fig. 3.1.7C**). Another protein presents at high levels in Ts65Dn mice in comparison with euploid mice is GSK3β, a kinase involved in neurogenesis and neuron maturation (Kim and Snider, 2011). Treated Ts65Dn mice showed a large reduction in GSK3β levels (**Fig. 3.1.7D**). A reduction in GSK3β levels also took place in treated in comparison with untreated euploid mice (**Fig. 3.1.7D**). In addition to regulate GSK3β transcription, AICD has been shown to reduce GSK3β phosphorylation at ser9

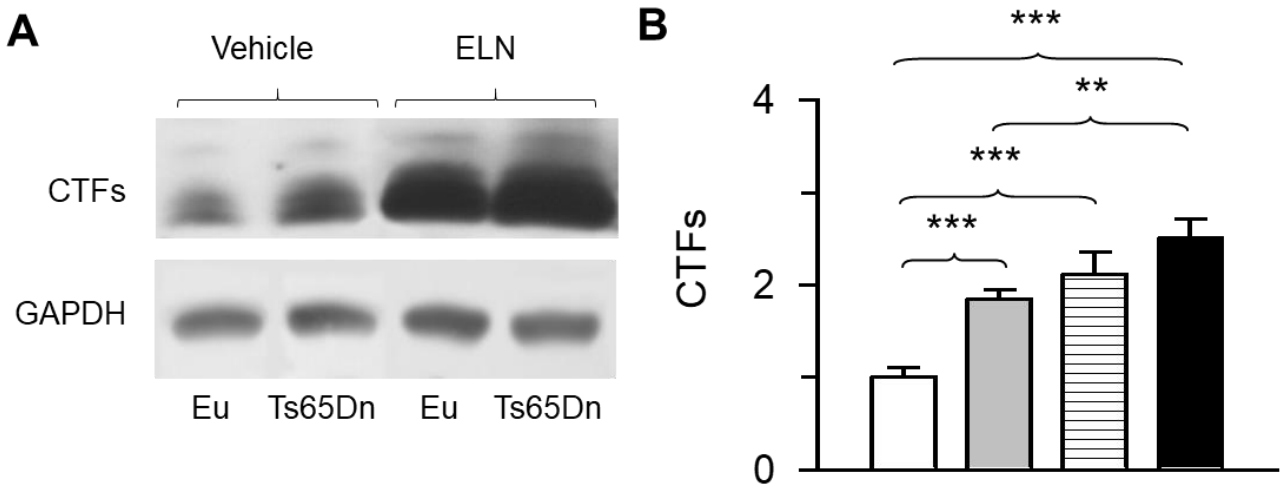

Figure 3.1.6. Short-term effect of treatment with ELN on CTFs levels. Western blot analysis of CTFs in the hippocampus of treated and untreated Ts65Dn and euploid mice (n=8 for each experimental group). Mice were treated with ELN in the period P3-P15 and sacrificed at P15. A: Examples of western blot images. B: Quantification of CTFs levels in untreated euploid (n = 4) and Ts65Dn (n = 4) and treated euploid (n = 4) and Ts65Dn (n = 5) mice normalized to GAPDH. Values (mean ± SE) are expressed as fold difference in comparison with untreated euploid mice. ** $p < 0.01$; *** $p < 0.001$ (Fisher LSD test after two-way ANOVA). Abbreviations: ELN, ELND006; Eu, Euploid.

(Zhou et al., 2012).This kinase becomes active when dephosphorylated at ser9, thereby negatively influencing proliferation and differentiation of neural precursor cells. Evaluation of the hippocampal levels of the phosphorylated form of GSK3β showed that in untreated Ts65Dn mice the levels of the phosphorylated form were reduced in comparison with euploid mice (**Fig. 3.1.7E**), while after treatment there was an increase in the levels of p-GSK3β in Ts65Dn mice, becoming higher than those of untreated euploid mice. An increase in p-GSK3β levels also took place in treated in comparison with untreated euploid mice (**Fig. 3.1.7E**).

Long-term effect of treatment with ELN on body and brain weight

We examined the effects of treatment on the body and brain weight in order to obtain information on the general effect of neonatal treatment with ELN when mice reached 45 days of age. A two-way ANOVA on body weight showed no genotype x treatment interaction; an effect of genotype [$F(1,56) = 25.704$, $p \leq 0.001$] was shown, but no effect of treatment emerged. A *post hoc* Fisher LSD test showed that, as previously described, untreated Ts65Dn mice had a reduced body weight in comparison with their euploid counterparts (**Fig. 3.1.8A**). Treatment with ELN did not affect the body weight of either Ts65Dn or euploid mice (**Fig. 3.1.8A**).

A two-way ANOVA on brain weight revealed no genotype x treatment interaction; a significant effect of genotype [$F(1,56) = 33.463$, $p \leq 0.001$] but no effect of treatment. A *post hoc* Fisher LSD test showed that the brain of untreated Ts65Dn mice had a reduced weight in comparison with their euploid counterparts (**Fig. 3.1.8B**). As for the body weight, treatment did not influence the brain weight on either Ts65Dn or euploid mice (**Fig. 3.1.8B**). These results suggest that neonatal treatment with ELN has no patent long-term adverse effects on animals' general conditions.

Long-term effect of treatment with ELN on cell proliferation and cellularity in the dentate gyrus

We had demonstrated that immediately after neonatal treatment with ELN there was a restoration of

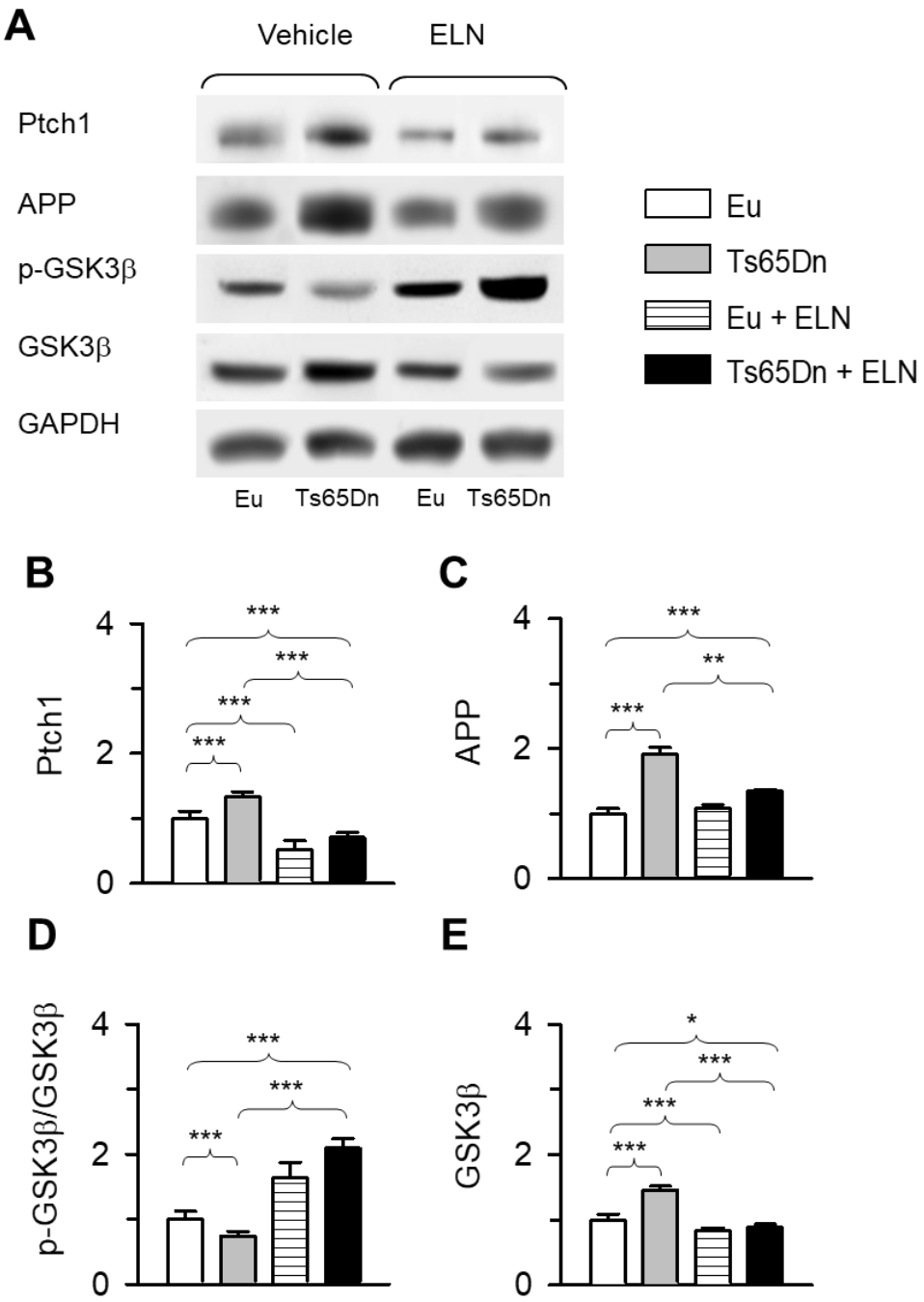

Figure 3.1.7. Effect of APP γ-secretase inhibition on AICD targets in P15 mice. A: Western blot analysis of PTCH1, APP, phosphorylated GSK3β and total GSK3β in the hippocampus of untreated Ts65Dn (n = 4) and euploid (n = 4) mice and treated Ts65Dn (n = 5) and euploid (n = 4) mice. B-E: PTCH1 (B), APP (C), p-GSK3β (D) and total GSK3β (E) levels. Data in (B, C and E) were normalized to GAPDH and data in (D) were normalized to total GSK3β. Values in (B-E) (mean ± SE) are expressed as fold difference in comparison with untreated euploid mice. All western blot images are explicative reconstructions. * $p < 0.05$; ** $p < 0.01$; *** $p < 0.001$. Abbreviations: ELN, ELND006; Eu, euploid.

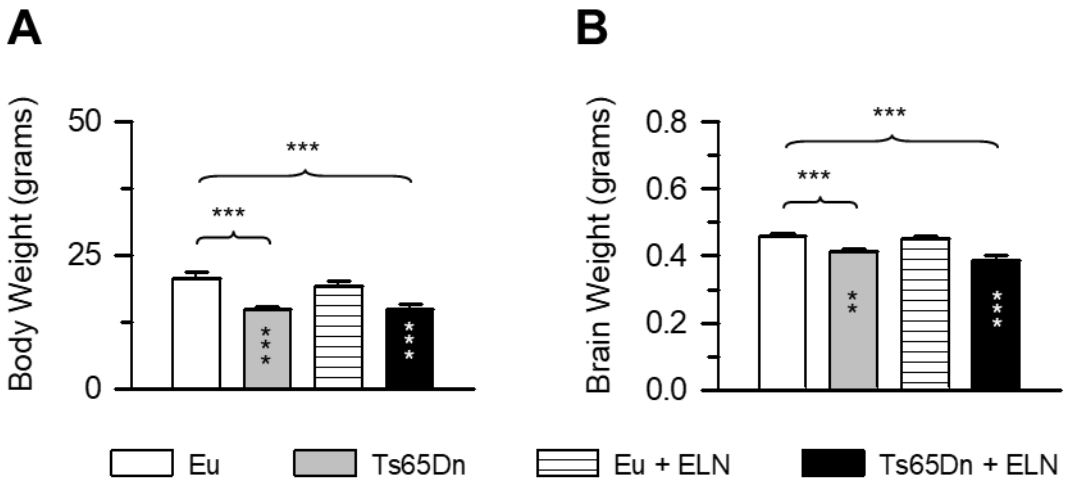

Figure 3.1.8. Body and brain weight of P45 euploid and Ts65Dn mice treated with either vehicle or ELND006. Untreated euploid mice: n=19; untreated Ts65Dn mice: n=10; treated euploid mice: n=20; treated Ts65Dn mice: n=11. ** p < 0,01; *** p < 0.001 (Fisher LSD test after two-way ANOVA). Black asterisks in the gray bar indicate a difference between untreated Ts65Dn mice and treated euploid mice; white asterisks in the black bar indicate a difference between treated Ts65Dn mice and treated euploid mice. Abbreviations: ELN, ELND006; Eu, Euploid.

the pool size of actively dividing granule cell precursors. Thus, we wondered whether this positive effect was retained after treatment cessation. To this purpose, we evaluated the number of Ki-67-positive cells in the DG of P45 mice. A two-way ANOVA showed a genotype x treatment interaction [$F(1,20) = 23.164$, $p \leq 0.001$] on total Ki-67-positive cells counted and a genotype x treatment interaction [$F(1,20) = 16.652$, $p = 0.001$] on Ki-67-positive cells per section. Fisher LSD test showed that untreated Ts65Dn mice had fewer number of Ki-67-positive cells per section (**Fig. 3.1.9B**) and fewer total number of Ki-67-positive cells (**Fig. 3.1.9C**) than untreated euploid mice. In contrast, Ts65Dn mice that had been neonatally-treated with ELN had a similar number of Ki-67-positive cells per section (**Fig. 3.1.9B**) and a similar total cell number (**Fig. 3.1.9C**) as untreated euploid mice, indicating that the positive effect of treatment on precursor proliferation was retained with time. In euploid mice treated with ELN there was a reduction in the number of Ki-67-positive cells per section (**Fig**. **3.1.9B**) and total number of Ki-67-positive cells (**Fig. 3.1.9C**) in comparison with untreated euploid mice.

Then we asked whether the positive impact of treatment on the cellularity of the DG observed in neonates in Ts65Dn mice was retained after treatment cessation. To investigate this, we stereologically examined the granule cell layer of the DG.

A two-way ANOVA on total number of granule cells showed a genotype x treatment interaction [$F(1.20) = 16.070$, $p \leq 0.001$] but not significant effect of genotype or treatment. As in P15 mice, a *post hoc* Fisher LSD test showed that untreated Ts65Dn mice had fewer granule cells than untreated euploid mice (**Fig. 3.1.10B**), while ELN neonatally-treated Ts65Dn mice had a similar number of granule cells as untreated euploid mice (**Fig. 3.1.10B**), indicating that the positive effect of treatment on total granule cell number was retained with time. Unlike in Ts65Dn mice, in euploid mice neonatally-treated with ELN there was a reduction in the total number of granule cells in comparison with untreated euploid mice (**Fig. 3.1.10B**).

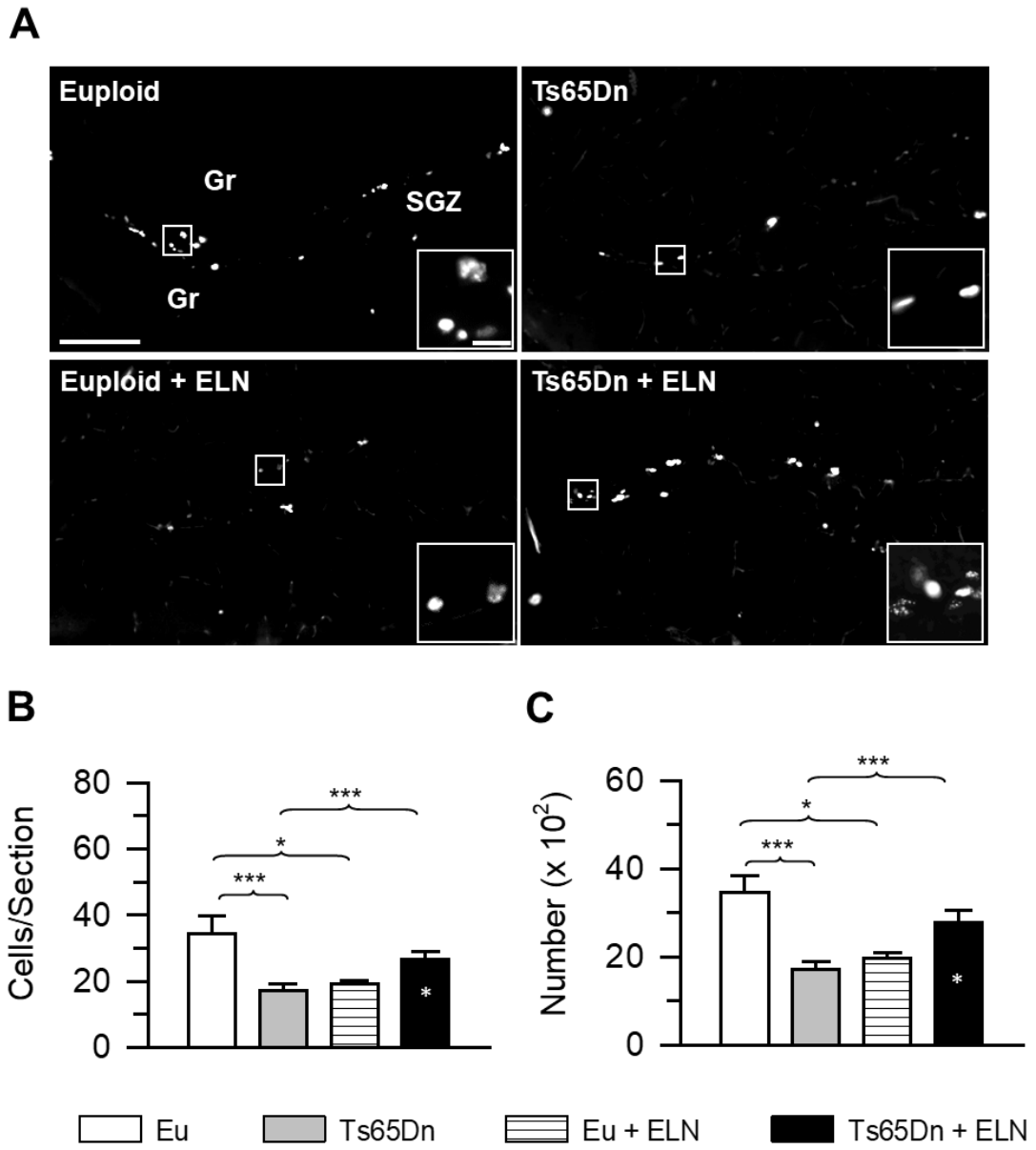

Figure 3.1.9. Long-term effect of treatment with ELN on the size of the population of neural precursor cells in the dentate gyrus. A: Examples of sections processed for fluorescence immunostaining for Ki-67 from the dentate gyrus of untreated euploid and Ts65Dn mice and euploid and Ts65Dn mice treated with ELN. Examples of Ki-67-positive cells are indicated in the enlarged boxed area. Calibrations = 200 μm (lower magnification) and 40 μm (higher magnification). B, C: Mean number of Ki-67-positive cells per section (B) and total number of Ki-67-positive cells (C) in the DG of treated and untreated Ts65Dn and euploid mice (n=6 for each experimental group). Values represent mean ± SE. * $p < 0.05$; *** $p < 0.001$ (Fisher LSD test after two-way ANOVA). White asterisks in the black bar indicate a difference between treated Ts65Dn mice and treated euploid mice. Abbreviations: ELN, ELND006; Eu, Euploid; Gr, granule cell layer; SGZ, subgranular zone.

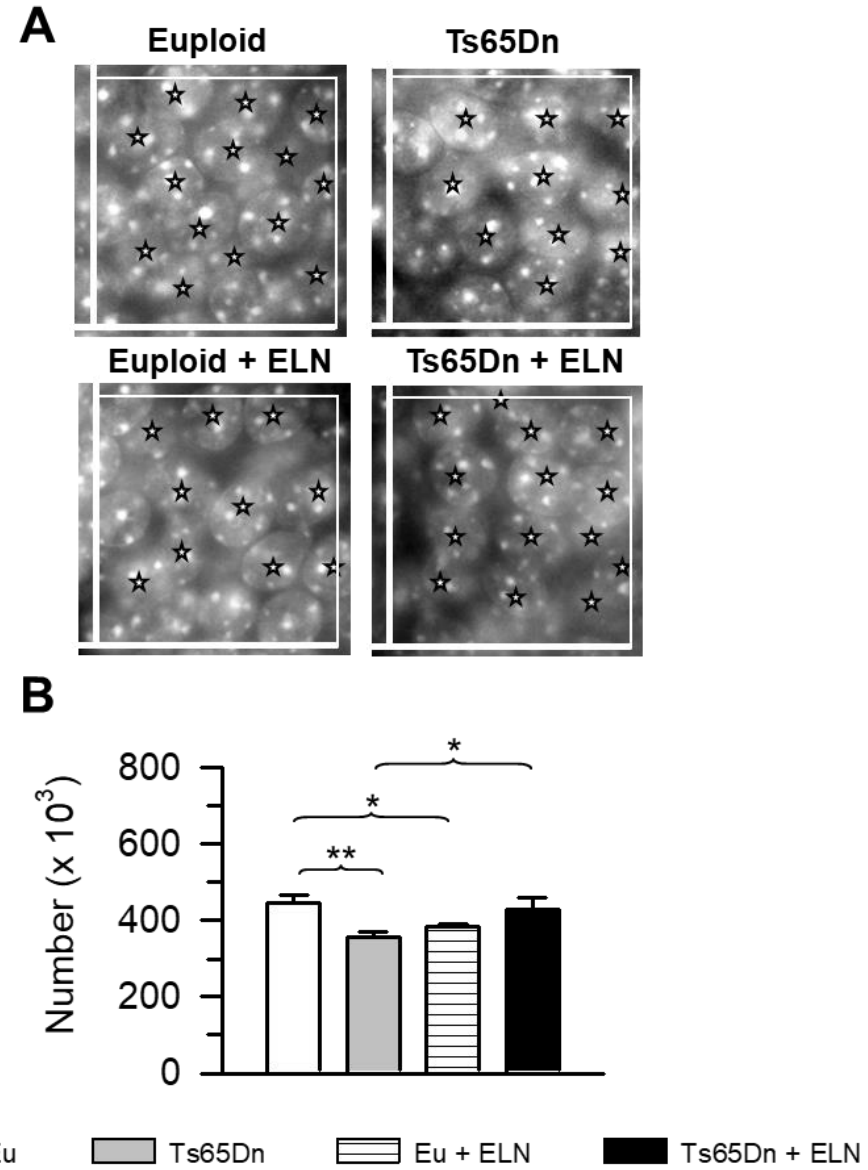

Figure 3.1.10. Long-term effect of treatment with ELN on the number of granule neurons of the dentate gyrus. A: Representative images of Hoechst-stained sections of the granule cell layer of an animal from each experimental group. The sides of the superimposed optical disector are 30 μm in length. The stars indicate individual nuclei. Note that nuclei intersecting the exclusion sides (thick lines) were not counted. B: Total number of granule cells in untreated and treated euploid and Ts65Dn mice (n=6 for each experimental group). Values (mean ± SE) refer to one hemisphere. * $p < 0.05$; ** $p < 0.01$ (Fisher LSD test after two-way ANOVA). Abbreviations: ELN, ELND006; Eu, Euploid.

Long-term effects of neonatal treatment with ELN on CTFs levels

The increased levels of CTFs in P15 mice provided indirect evidence that treatment with ELN had caused a reduction in AICD levels. In order to establish whether this effect was retained after treatment cessation, we evaluated hippocampal CTFs levels in P45 mice. A two-way ANOVA did not reveal a genotype x treatment interaction, no significant effect of treatment but a main effect of genotype [$F(1,28) = 30.081$, $p \leq 0.001$]. A *post hoc* Fisher LSD test showed that CTFs levels in the hippocampus of untreated Ts65Dn mice were higher in comparison with euploid mice (**Fig. 3.1.11B**). P45 Ts65Dn mice treated with ELN, however, had similar levels of CTFs as their untreated counterparts (**Fig. 3.1.11B**), indicating that the inhibition exerted by ELN on the activity of γ-secretase did not outlast treatment cessation.

Long-term effects of neonatal treatment with ELN on PTCH1 levels

As reported above, P15 Ts65Dn mice show high levels of PTCH1 in the hippocampus, supporting our idea that neurogenesis impairment may be attributable to over-inhibition of the Shh pathway. In order to establish whether neonatal treatment with ELN caused an enduring effect on PTCH1 levels in Ts65Dn mice, we evaluated the expression of this protein in hippocampal homogenates of P45 mice, i.e. one month after treatment cessation. A two-way ANOVA on hippocampal PTCH1 levels did not highlight a genotype x treatment interaction and no significant effects of both genotype and treatment were emerged. A *post hoc* Fisher LSD test showed no statistical differences among the four experimental groups (**Fig. 3.1.12A,B**). These results indicate an age-related normalization of PTCH1 expression and suggest that the neurogenesis impairment still present in P45 Ts65Dn mice (**Fig. 3.1.9**) cannot be attributed to over-inhibition of the Shh pathway. Unlike in P15 mice, in P45 mice ELN did not cause a reduction in PTCH1 hippocampal levels neither in euploid nor in Ts65Dn (**Fig. 3.1.12A**). These findings suggest that neurogenesis defects in P45 Ts65Dn cannot be attributable the alterations of the SHH pathway. p21 is a cyclin-dependent kinase inhibitor that inhibits cell cycle progression and is expressed at high levels in embryos and infants with Down syndrome and in Ts65Dn mice.

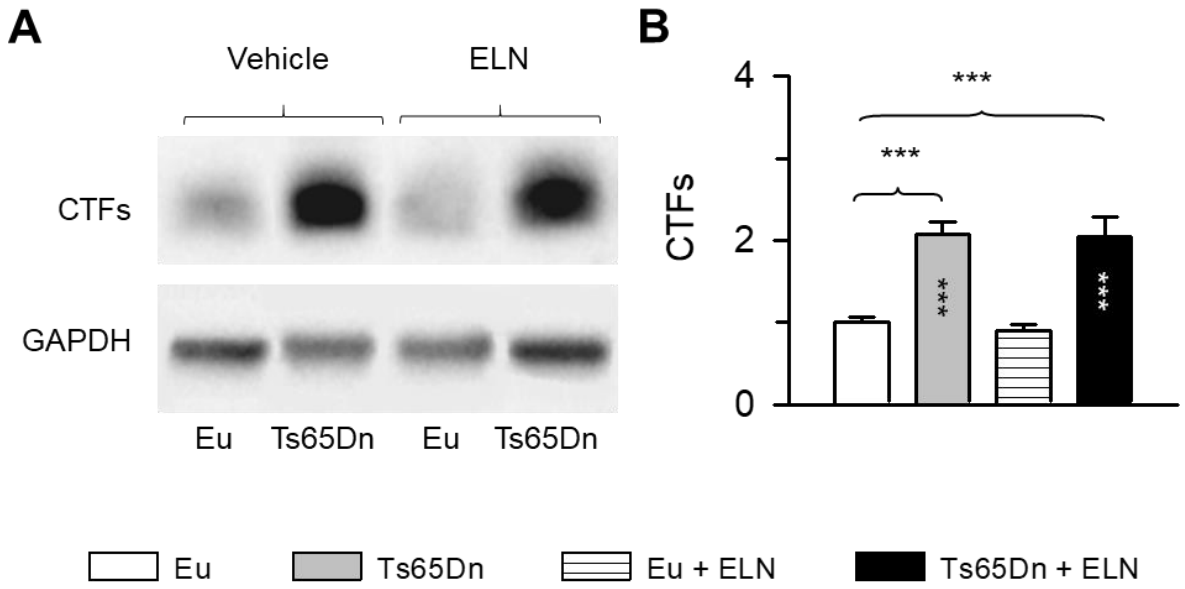

Figure 3.1.11. Long-term effect of treatment with ELN on CTFs levels. Western blot analysis of CTFs in the hippocampus of treated and untreated Ts65Dn and euploid mice (n=8 for each experimental group). Mice were treated with ELN in the period P3-P15 and were sacrificed at P45. A: Examples of western blot images of CTFs. B: Quantification of CTFs levels normalized to GAPDH. Values (mean ± SE) are expressed as fold difference in comparison with untreated euploid mice. *** $p < 0.001$ (Fisher LSD test after two-way ANOVA). Black asterisks in the gray bar indicate a difference between untreated Ts65Dn mice and treated euploid mice. White asterisks in the black bar indicate a difference between treated Ts65Dn mice and treated euploid mice. Abbreviations: ELN, ELND006; Eu, Euploid.

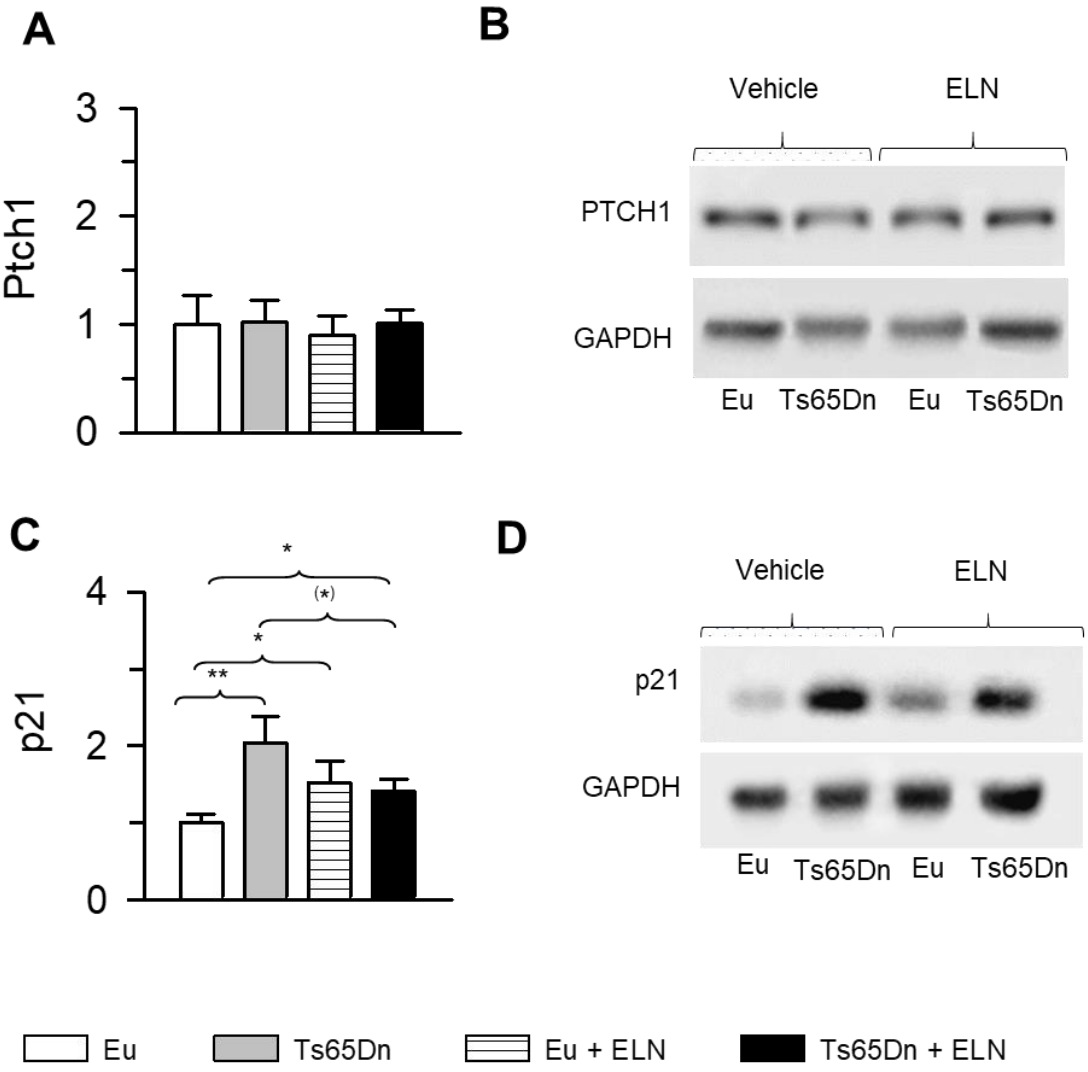

Figure 3.1.12. Long-term effect of treatment with ELN on protein levels. Western blot analysis of PTCH1 and p21 in the hippocampus of treated and untreated Ts65Dn and euploid mice (n=8 for each experimental group). Mice were treated with ELN in the period P3-P15 and were sacrificed at P45. A-D: Examples of western blot images of PTCH1 (B) and p21 (D) and quantification of PTCH1 (A) and p21 (C) levels normalized to GAPDH. Values (mean ± SE) are expressed as fold difference in comparison with untreated euploid mice. (*) $p < 0.06$; * $p < 0.05$; ** $p < 0.01$ (Fisher LSD test after two-way ANOVA). Abbreviations: ELN, ELND006; Eu, Euploid.

Thus, p21 may be one of the factors that contribute to neurogenesis impairment in DS. For this reason, we examined p21 protein levels in the hippocampus of P45 euploid and Ts65Dn mice. A two-way ANOVA on p21 levels showed a genotype x treatment interaction [$F(1, 28) = 8.354$, $p = 0.007$], but no effects of genotype or treatment were revealed. A *post hoc* Fisher LSD showed that untreated Ts65Dn mice had higher levels of p21 than euploid mice. Treatment caused a reduction in p21 levels in Ts65Dn mice although this effect was only marginally significant (**Fig. 3.1.12C**). In contrast, in treated euploid mice p21 levels underwent an increase in comparison with untreated euploid mice (**Fig. 3.1.12C**). This evidence provides a mechanistic link between the long-term restoration of precursor proliferation found in P45 treated Ts65Dn mice and the reduction in the number of neural precursors in treated euploid mice (**Fig. 3.1.9**).

Long-term effects of neonatal treatment with ELN on hippocampal synapses

We counted the number of SYN and PSD-95 immunoreactive puncta in the middle molecular layer of the DG and the stratum lucidum of field CA3, in order to establish whether neonatal treatment with ELN has a long-term effect on hippocampal synapses.

A two-way ANOVA on the number of SYN puncta in the molecular layer of the DG showed no genotype x treatment interaction; a main effect of genotype [$F(1,20) = 14.330$ $p \leq 0.001$] emerged, but there was no effect of treatment. A two-way ANOVA on the number of PSD-95 puncta in the molecular layer of the DG showed no genotype x treatment interaction; there was an effect of genotype [$F(1,20) = 46.893$, $p \leq 0.001$], but no effect of treatment. A *post hoc* Fisher LSD test showed that in the molecular layer of the DG, untreated Ts65Dn mice had fewer SYN (**Fig. 3.1.13A**) and PSD-95 (**Fig. 3.1.13B**) immunoreactive puncta in comparison with untreated euploid mice. Even though in treated Ts65Dn mice the number of puncta was slightly larger in comparison with their untreated counterparts, this difference was not statistically significant. In the DG of treated Ts65Dn mice SYN and PSD-95 immunoreactive puncta were lower in comparison with untreated euploid

mice.

A two-way ANOVA on the number of SYN puncta in the stratum lucidum of field CA3 showed no genotype x treatment interaction but did show a significant effect of both genotype [$F(1,20) = 13.046$, $p \leq 0.002$] and treatment [$F(1,20) = 60.003$, $p \leq 0.001$]. A two-way ANOVA on the number of PSD-95 puncta in field CA3 showed a genotype x treatment interaction [$F(1,20) = 8.181$, $p \leq 0.010$] and a main effect of both genotype [$F(1,20) = 22.792$, $p \leq 0.001$] and treatment [$F(1,20) = 9.432$, $p \leq 0.006$]. A *post hoc* Fisher LSD test showed that in the field CA3 untreated Ts65Dn mice had fewer SYN (**Fig. 3.1.13C**) and PSD-95 (**Fig. 3.1.13D**) immunoractive puncta in comparison with untreated euploid mice. However, treated Ts65Dn mice showed a larger number of SYN and PSD-95 immunoreactive puncta in comparison with their untreated counterparts and their number of puncta became than that of untreated euploid mice (**Fig. 3.1.13C,D**), indicating a long-term positive effect on the DG-CA3 connections.

Long-term effect of ELN on basal synaptic input to CA3 neurons

"Miniature" synaptic events reflect the spontaneous release of neurotransmitters from all presynaptic terminals converging on the recorded neuron. The frequency of these events is related to the total number of presynaptic terminals and the probability of release at each terminal. In order to functionally evaluate the basal excitatory synaptic input to CA3 pyramidal neurons, we recorded spontaneous miniature excitatory postsynaptic currents (mEPSCs) from individual CA3 pyramidal neurons by performing whole-cell, patch-clamp experiments in the voltage-clamp mode. Miniature events were recorded in the presence of tetrodotoxin (TTx, 1 μM) in the perfusing solution, in order to prevent spontaneous synaptic events due to presynaptic action-potential firing.

Fig. 3.1.14C shows examples of mEPSCs recorded, under the above conditions, in representative cells from untreated and ELN-treated euploid and Ts65Dn mice. No spontaneous synaptic events were observable any longer after application of the glutamatergic inhibitors NBQX (10 μM) + APV (50 μM) (n=4 cells; not shown). Due to baseline noise levels normally observed at –70 mV, events

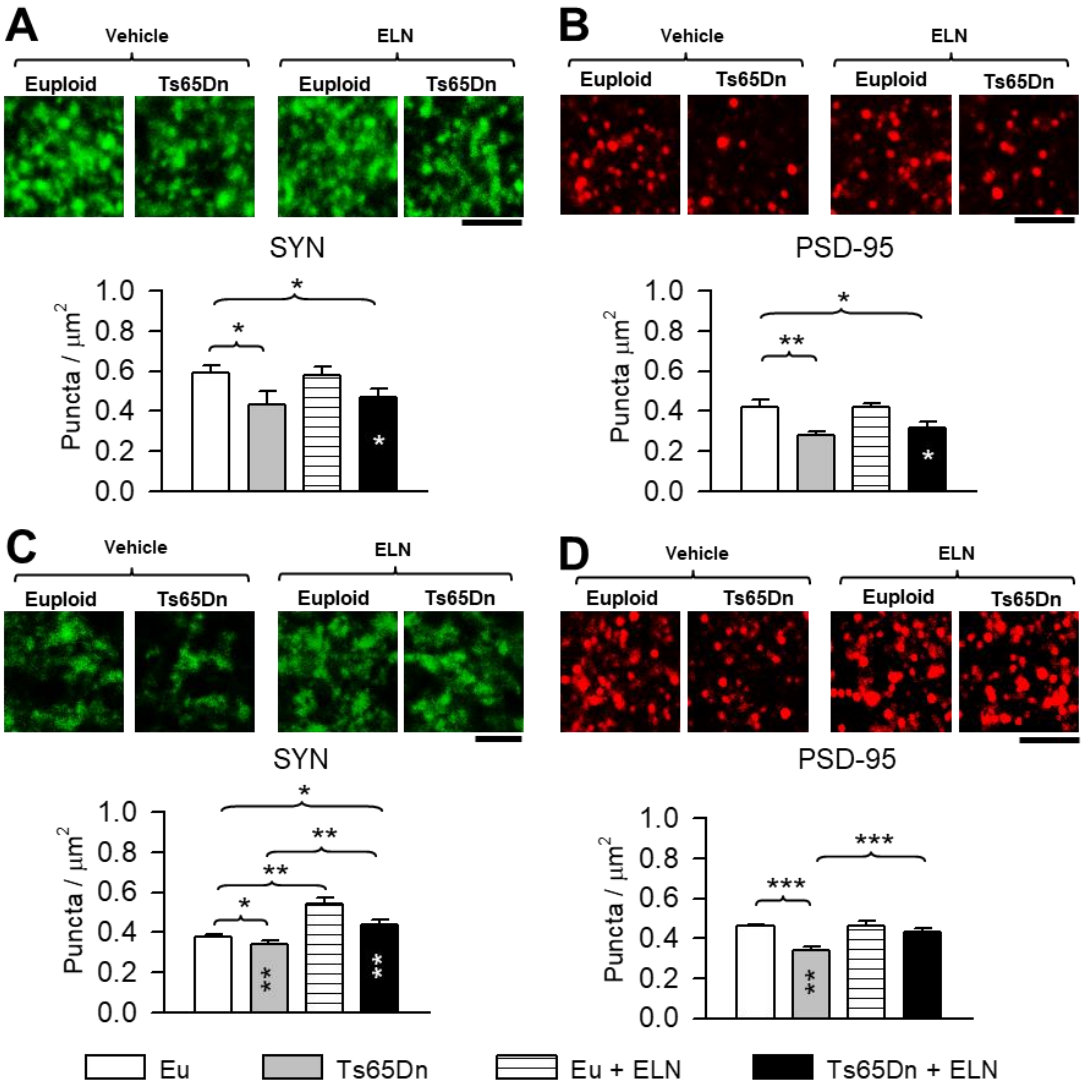

Figure 3.1.13. Long-term effect of treatment with ELN on hippocampal synapses in Ts65Dn and euploid mice. A-D: Images in the panels at the top represent confocal microscope images of sections processed for SYN (A, C) and PSD-95 (B,D) immunofluorescence from the molecular layer of the DG (A, B) and the stratum lucidum of field CA3 (C, D) of an animal from each experimental group. Calibration=5 µm. The histograms represent the number of puncta per µm^2 exhibiting SYN (A, C) and PSD-95 (B, D) immunoreactivity in the molecular layer of the DG (A, B) and the stratum lucidum of CA3 (C, D) of treated and untreated Ts65Dn and euploid mice (n=6 for each experimental group). Values represent mean ± SE. * $p < 0.05$; ** $p < 0.01$; *** $p < 0.001$ (Fisher LSD test after two-way ANOVA). Black asterisks in the gray bar indicate a difference between untreated Ts65Dn mice and treated euploid mice; white asterisks in the black bar indicate a difference between treated Ts65Dn mice and treated euploid mice. Abbreviations: ELN, ELND006; Eu, Euploid.

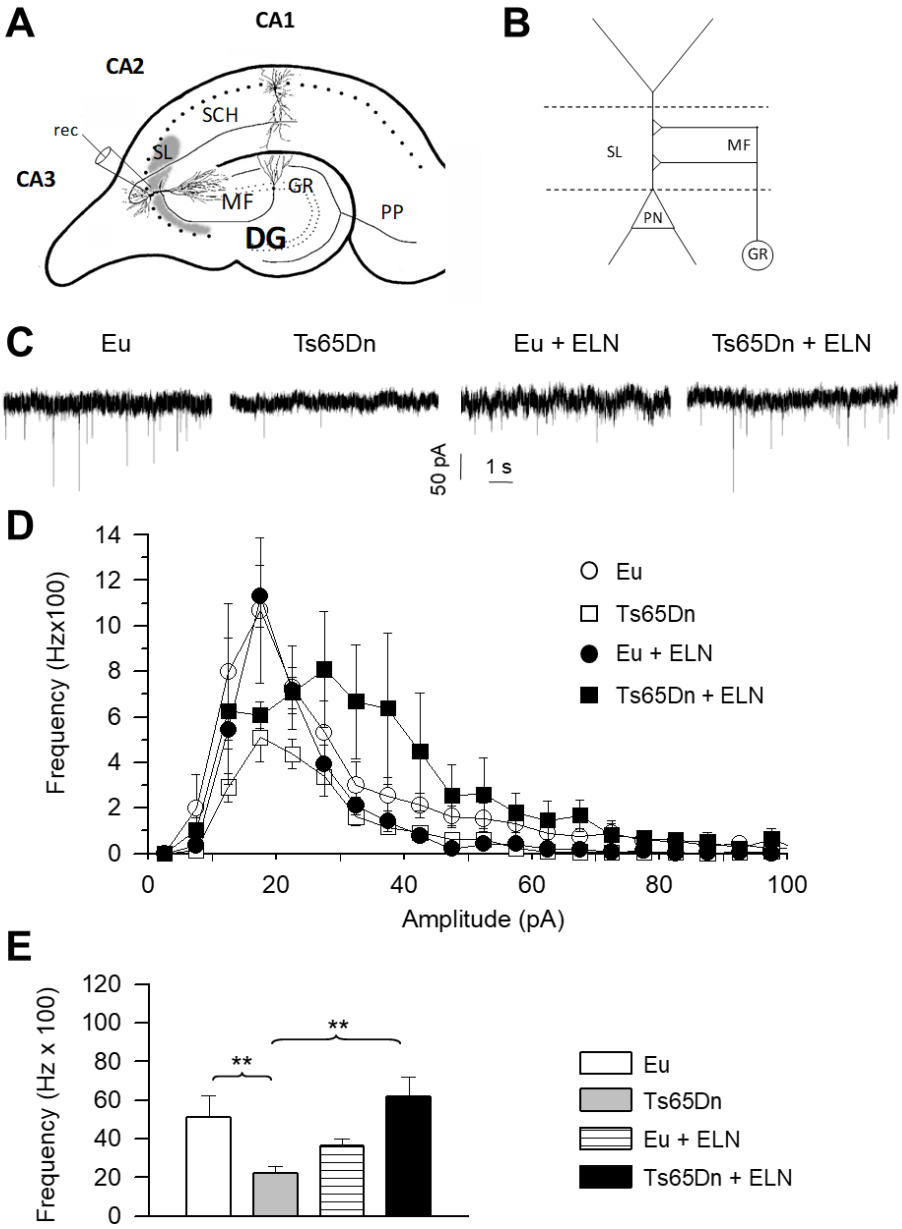

Figure 3.1.14. Long-term effect of treatment with ELN on mEPSC frequency in CA3 pyramidal neurons. A: Schematic drawing of a section across the hippocampal formation showing the major intrinsic connections. Patch clamp recording (rec) of miniature synaptic potentials were carried out from pyramidal neurons of field CA3. The area occupied by the mossy fiber terminals in the stratum lucidum of field CA3 is indicated in gray. B: Mossy fiber circuitry in CA3. Mossy fibers establish excitatory synapses (+) with pyramidal neurons in the stratum lucidum of CA3. C: Exemplary current tracings recorded in the gap-free mode in four representative cells from untreated euploid and Ts65Dn mice and euploid and Ts65Dn mice treated with ELN, showing mEPSC activity. Holding potential was –70 mV. Recordings were made in the presence of 1-µM TTx in the superfusing solution. D: Average frequency-distribution diagrams of mEPSC amplitude for untreated euploid and Ts65Dn mice and euploid and Ts65Dn mice treated with ELN. E: Average, overall mEPSC frequency in the four animal groups. Data derive from 9 untreated euploid mice (13 cells), 7 untreated Ts65Dn mice (18 cells), 8 ELN-treated euploid, mice (15 cells), and 4 ELN-treated Ts65Dn mice (12 cells). Values in D-E represent mean ± SE. ** $p < 0.01$ (Linear mixed model analysis). Abbreviations: CA1-3, hippocampal fields; DG, dentate gyrus; ELN, ELND006; Eu, Euploid; GR, granule cell layer; MF, mossy fivers; PN, pyramidal neuron; PP, perforant pathway; PYR, pyramidal layer; SCH, Shaffer collaterals; SL, stratum lucidum.

of less than 10 pA in peak amplitude were ignored. Accepted events were then used to construct frequency-distribution diagrams of mEPSC amplitude. Data were averaged among the cells (*n*=2 to 4), from each animal and then among the animals pertaining to the same experimental group. The plots obtained are reported in **Fig. 3.1.14D**. As previously shown (Stagni et al., 2013), in untreated Ts65Dn mice there was a reduction in mEPSC frequency for all amplitude classes, with a prominent reduction for amplitudes higher than 35 pA (**Fig. 3.1.14D**). An evaluation of the overall mEPSC frequency showed that in untreated Ts65Dn mice it was reduced by ~53% in comparison with untreated euploid mice (DF=29; WALD t=-2.670283; p = 0.0123) (**Fig. 3.1.14E**). In Ts65Dn mice treated with ELN there was a global increase in mEPSC frequency. This increase was particularly prominent for synaptic events of amplitude greater than 35 pA (**Fig. 3.1.14E**). The overall mEPSC frequency in treated Ts65Dn mice it was increased by ~156% in comparison with untreated Ts65Dn mice (DF=28; WALD t=-3.186090; p = 0.0035) and became similar to that of untreated euploid mice (**Fig. 3.1.14E**). In treated euploid mice there was little reduction in the mEPSC frequency in comparison with untreated euploid mice (**Fig. 3.1.14E**).

Results reported in **Fig. 3.1.14D** show that genotype and treatment had differential effects on the frequency of mEPSCs of different magnitude. According to the theory of electrotonic decay of locally generated electric signals, it can be predicted that postsynaptic currents of low magnitude recorded from the soma correspond to the activation of synapses with a distal dendritic location, while mEPSCs with larger magnitude should mainly correspond to synaptic activation of synapses with a location proximal to the soma. Thus, assuming that mEPSCs kinetics are similar among different synaptic contacts, the mEPSCs of smaller magnitude should display a slower onset and decay kinetics in comparison with mEPSCs of larger amplitude. In order to clarify this issue, we carried out a systematic analysis aimed at correlating mEPSC amplitude and decay kinetics. To this purpose, mEPSCs recorded in each cell and belonging to the same class of amplitude were used to create a single average mEPSC. The decay phase of this average mEPSC was fitted with a single exponential function of the first order, which allowed us to obtain a single value for the decay time constant

(τdec). The τdec values obtained for each mEPSCs amplitude class were plotted as a function of the corresponding average amplitude. In all experimental groups, save for the group of untreated Ts65Dn mice, there was a significant inverse relationship between amplitude of the mEPSCs and their τdec (untreated euploid mice: R=-0.54975, SD=1.6319, n=24, p = 0.00539; treated euploid mice: R=-0.40739, SD=0.50525, n=65, p = 7.56715×10^{-4}; treated Ts65Dn mice: R=-0.25085, SD=0.77471, n=148, p = 0.0021). The finding that this was not the case for untreated Ts65Dn mice (R=0.03051, SD=3.3066, n=51, p=0.83168) suggests that the amplitude heterogeneity of their mEPSCs may be due to additional factors, independent from the distance from the soma. For instance, the shape and size of the dendritic spines may affect the number of postsynaptic receptors and, thus, the magnitude of the mEPSCs.

3.1.5 Discussion

Neonatal treatment with a γ-secretase inhibitor restores neurogenesis in the major postnatal neurogenic niches

Since the hippocampal DG mainly develops in the first two postnatal weeks in mice, we decided to treat neonate mice with ELN in this period in order to impact on hippocampal development. We found that the reduced number of NPCs in the DG of Ts65Dn mice was fully normalized after 13 days of treatment. Similar results were observed in the SVZ, indicating that ELN has a positive impact on neurogenic niches throughout the brain. Treatment had no effect on cell death, suggesting that there was no effect on cell survival. In agreement with the treatment-induced restoration of neurogenesis in Ts65Dn mice, the volume of the granule cell layer and total granule cell number became similar to those of euploid mice. In euploid mice, although treatment reduced the levels of PTCH1, there was no increase in the proliferation rate either in the SVZ or the SGZ (**see Fig. 3.1.8A,B**). This suggests that in the euploid brain the SHH pathway is normally regulated and that a strong disinhibition does

not influence its efficacy.

Neonatal treatment with a γ-secretase inhibitor has long-term positive effects on neurogenesis in Ts65Dn mice

We found here that inhibition of the activity of the APP γ-secretase by ELN in the neonatal period restores PTCH1 levels, the number of hippocampal granule cell precursors and total number of granule neurons in P15 mice(Giacomini et al., 2015)(Giacomini et al., 2015)(Giacomini et al., 2015). Since it seemed of relevance to establish the duration of these effects, we examined the long-term effects of treatment on the pool of neural precursor cells in the DG. We found that at one month after treatment cessation the pool of neural precursor cells was still normalized. Consistently with the long-term restoration of neurogenesis, in treated Ts65Dn mice total number of granule cells was also normalized.

In contrast with P15 Ts65Dn mice, P45 untreated Ts65Dn mice had normal levels of PTCH1. Since *Ptch1* transcription in addition of being enhanced by AICD is positively and negatively modulated by other factors (He et al., 2011, Huang et al., 2012, Memmi et al., 2015), the normalization of its expression in P45 Ts65Dn mice suggests age-related changes in the mechanisms that regulate its transcription. The finding that untreated P45 Ts65Dn mice still had a reduced pool of neural precursor cells in the DG in spite of normal PTCH1 levels suggests that other perturbed mechanisms, such as enhanced levels of p21 (**Fig. 3.1.12D**) may contribute to neurogenesis impairment. This idea is strengthened by the observation that in treated P45 Ts65Dn mice there was a reduction in p21 levels and a parallel increase of neurogenesis and that in treated euploid mice there was an increase in p21 levels with a reduction of neurogenesis. These findings suggest that inhibition of γ-secretase in the neonatal period leads to changes in p21 levels that outlast the period of treatment. Further studies are needed to elucidate the mechanism of p21 regulation mediated by ELN. Taken together, results in P15 and P45 mice suggest that the proliferation impairment of trisomic NPCs is due to alteration of various pathways and that deregulation of the SHH pathway plays a prominent role during early life

stages. The finding that in treated euploid mice there was a reduction in the number of NPCs in the DG and in total granule cell number indicates that inhibition of γ-secretase activity in the normal brain negatively affects the process of neurogenesis.

Neonatal treatment with a γ-secretase inhibitor reduces the production of AICD, disinhibits the SHH pathway and reduces the levels of AICD targets.

Among the triplicated genes, some located inside and outside the Down syndrome critical region have been reported as likely candidates involved in the neurogenesis impairment that characterizes this genetic condition (Dierssen, 2012, Costa and Scott-McKean, 2013). Previous (Trazzi et al., 2011, Trazzi et al., 2013) and current results highlight the contribution of the triplicated gene *APP* in neurogenesis impairment in DS. *App* triplication causes excessive formation of AICD which, in turn, causes excessive transcription of various genes, including *Ptch1*, the SHH receptor that inhibits the SHH pathway. This pathway is strongly involved in neural precursor cell proliferation, migration and differentiation (Machold et al., 2003, Angot et al., 2008). We found that treatment with ELN largely increase CTFs levels both in euploid and Ts65Dn mice when compared with their untreated counterparts, suggesting a reduction of the AICD levels. Accordingly, we observed a reduction of the levels of some AICD target as PTCH1. PTCH1 downregulation and, consequently, SHH pathway disinhibition, explains the effects of treatment with ELN on hippocampal proliferation rate restoration in the Ts65Dn hippocampus.

Reduction of AICD levels is probably the cause of the reduction of APP and GSK3β (two AICD targets) levels in mice treated with ELN and inhibition of GSK3β activity. Since these proteins may affect proliferation potency, their reduction/inhibition could concur to the positive effects of treatment in Ts65Dn mice.

The reduction of PTCH1 levels seen in P15 mice was no longer present in P45 mice, indicating that treatment with ELN had no long-term effects on the SHH pathway. This evidence is consistent with the observation that CTFs levels in P45 treated Ts65Dn mice were similar to those of untreated

Ts65Dn mice, indicating that the inhibitory effect on γ-secretase mediated by ELN disappears with time. This implies that ELN should be administered continuously in order to maintain the inhibition of γ-secretase.

Neonatal treatment with a γ-secretase inhibitor restores connectivity the molecular layer of the DG and in the CA3 field of the hippocampus.

A reduced number of synaptic terminals in the Ts65Dn mice has been evidenced in various brain regions, including the molecular layer of the DG (Kurt et al., 2004, Belichenko et al., 2007, Chakrabarti et al., 2007, Guidi et al., 2013). Therefore, the trisomy-dependent defective functioning of hippocampal circuits appears to be also due to input-output alterations. The major hippocampal input derives from the entorhinal cortex; then, these signals progress to the DG and are transferred by the latter to fields CA3 and then CA1. These signals are essential for hippocampus-dependent long-term memory functions. We observed that ELN restored the number of pre- and postsynaptic terminals in the molecular layer of the DG, suggesting restoration of the major input to the DG. In view of the increase in total granule cell number and the number of pre- and postsynaptic terminals in the molecular layer of the DG, we wondered whether the counterpart of this effect was an increase in the number of terminals in the stratum lucidum of CA3, where the axons of the granule cells end. Treated Ts65Dn mice exhibited full restoration of pre- and postsynaptic terminals, suggesting restoration of signal transfer to CA3. Neuron maturation is finely regulated by various molecular mechanisms, among which the kinase GSK3β appears to play a key role. Activation (de-phosphorylation) of GSK3β leads to marked shrinkage of dendrites, whereas its inhibition (phosphorylation) enhances dendritic growth. Furthermore, there are evidence that GSK3β inhibition is required for proper synapse development (Kim and Snider, 2011, Jin et al., 2012, Rui et al., 2013). Treatment with ELN increased GSK3β phosphorylation at ser9 in Ts65Dn mice and this could explain the observed restoration of synapse development.

Neonatal treatment with a γ-secretase inhibitor has long-term positive effects on connectivity in field CA3 of Ts65Dn mice

As we have discussed above, immediately after treatment cessation Ts65Dn mice had a significantly larger number of both SYN and PSD-95 immunoreactive puncta in the hippocampus. Evaluation of the pre- and postsynaptic terminals in the molecular layer of the DG in P45 mice showed that one month after treatment cessation Ts65Dn mice had still a slight larger number of SYN and PSD-95 immunoreactive puncta in comparison with their untreated counterparts but this difference was not statistically significant. These results show that the restoration of connectivity observed in the DG of P15 mice at the end of treatment is not maintained one month after treatment cessation, suggesting that continuous treatment may be necessary in order to maintain this effect. Unlike in the molecular layer of the DG, in the stratum lucidum of field CA3 of treated Ts65Dn mice there was still a larger number of pre- and postsynaptic terminals in comparison with their untreated counterparts. The persistence of the effects of treatment on the connectivity in field CA3 can be accounted for by the fact that treatment induces long-term restoration of total granule cell number and, hence, of the axons sent by the granule neurons to CA3. The number of puncta in CA3 field in the different experimental groups is in agreement with patch-clamp recordings from the pyramidal neurons of CA3. In untreated Ts65Dn mice there was an overall reduction in the mEPSCs, indicating impairment in the functional connectivity of field CA3. The prominent reduction in the frequency of mEPSCs of large amplitude in untreated Ts65Dn mice (**Fig. 3.1.14D**) is thus consistent with loss of synapses proximal to the soma. These synapses derive from the mossy fibers, the axons of the granule cells. This conclusion is in agreement with the reduction of PSD-95 immunoreactive puncta observed here. The finding that in Ts65Dn mice treated with ELN there was a global increase in mEPSC frequency and that this increase was particularly prominent for synaptic events of large amplitude (**Fig. 3.1.14D**) suggests that treatment had a positive impact on the mossy fiber input to the proximal dendrites of CA3 pyramidal neurons. This is fully in agreement with the restoration of the number of SYN and PSD-

95 immunoreactive puncta in the stratum lucidum of field CA3 and indicates that the restored connections are functionally effective.

Side effects of ELND006

ELND006 is a drug that was created in order to reduce Aβ formation in AD (Basi et al., 2010). Our results suggest that inhibitors of APP γ-secretase may be exploited in order to improve neurogenesis defects in DS through a reduction in AICD formation. Indeed, we found that early treatment with ELN in Ts65Dn mice restored neurogenesis in the two major neurogenic niches of the postnatal brain and development of the hippocampal dentate gyrus. Furthermore, we observed that ELN had positive long-lasting effects on hippocampal circuitry. Studies have shown that ELN has no toxic effects on wild-type mice and primates (Basi et al., 2010), but a clinical trial with ELN for the cure of AD was interrupted due to adverse side effects (Hopkins, 2011). In this short article, Hopkins reported that ELN, although it is more selective than other γ-secretase inhibitors [such as Semagacestat, Eli Lilly, (Hopkins, 2010)], had liver side effects that are thought to be unrelated to ELN mechanism of action. In our studies, we observed that a dose of 30.0 mg/kg of ELN from postnatal day 3 (P3) to postnatal day 15 (P15) had no acute effect on mice viability, but mice treated with this dose exhibited a higher mortality rate (death rate=30-40%) after weaning. For this reason, we decided to reduce the dose of ELN to 20.0 mg/kg and we observed that this those was safe for our mice. Yet, though ELN by itself may not be a suitable drug for DS (or AD), our studies provides novel demonstration that inhibitors of γ-secretase can completely reinstate neurogenesis in the trisomic brain, and that some of the positive effects observed in pups were retained with time. Intense research is being carried out in order to devise safe inhibitors of γ-secretase for the cure of AD. Moreover, a direct inhibitor of AICD activity has recently been developed (Branca et al., 2014). All this evidence prospects that there will soon be the possibility to exploit safe drugs in order to reduce AICD levels/activity and correct the

neurogenesis defects of DS.

3.2 Section 2

”Short- and long-term effects of the green tea extract epigallo-catechin-3-gallate in the Ts65Dn mouse model of Down syndrome”

Information reported in this section refers to:

“Short- and long-term effects of neonatal pharmacotherapy with epigallocatechin-3-gallate on hippocampal development in the Ts65Dn mouse model of Down syndrome”. Stagni F, **Giacomini A**, Emili M, Trazzi S, Guidi S, Sassi M, Ciani E, Rimondini R, Bartesaghi R. Stagni, Giacomini and Emili contributed equally to the article. *Neuroscience* 333 (2016) 277–301.

3.2.1 Abstract

Down syndrome (DS) is associated with alterations of neurogenesis, neuron maturation and connectivity that are already present at prenatal life stages. Many triplicated genes may be involved in the neurodevelopmental alterations that characterize DS. Recent evidence suggests that DYRK1A, a kinase that is over-expressed in the DS brain starting from early developmental stages, may play a prominent role in the brain phenotype of DS. Epigallocatechin-3-gallate (EGCG), the major polyphenol of green tea, performs many actions in the brain, including inhibition of DYRK1A activity. A pilot study in young adults with DS has shown that treatment with green tea extracts exerts some behavioral benefit, although these effects disappear after treatment cessation. Considering that the bulk of neurogenesis takes place very early during development, we deemed it extremely important to establish whether treatment with EGCG at the initial stages of brain development leads to plastic changes that outlast treatment cessation. In the current study, we treated the Ts65Dn mouse model of DS with EGCG from postnatal day 3 (P3) to P15, i.e. during the peak of neurogenesis in the hippocampal dentate gyrus and examined the short- and long-term term effects of treatment in P15 and P45 mice, respectively. We found that at P15, treated Ts65Dn pups exhibited restoration of neurogenesis, total hippocampal granule cell number and levels of pre- and postsynaptic proteins in the dentate gyrus, hippocampus and neocortex. However, at P45 none of these effects were still present, nor did treated Ts65Dn mice exhibit any improvement in hippocampus-dependent tasks. These findings show that treatment with EGCG carried out in the neonatal period rescues numerous trisomy-linked brain alterations. However, even during this, the most critical time window for hippocampal development, EGCG does not elicit enduring effects on the hippocampal physiology.

3.2.2 Introduction

DYRK1A is located on HSA 21 and its ortholog, *Dyrk1A*, is ttriplicated in the Ts65Dn model of DS (Gardiner, 2015). DYRK1A over-expression has been linked to neurogenesis deficits (Garcia-Cerro et al., 2014, Najas et al., 2015) and connectivity alterations (Benavides-Piccione et al., 2005, Murakami et al., 2009). In mice that over-express DYRK1A there are brain and behavioral alterations resembling those seen in DS (Dierssen, 2012).

Epigallocatechin-3-Gallate (EGCG) is a phytochemical found in green tea. Green tea consumption appears to be inversely correlated with dementia, Alzheimer's disease and Parkinson's disease (Hu et al., 2007, Mandel et al., 2008). EGCG appears to have many actions on the brain, including inhibition of DYRK1A (Schroeter et al., 2007, Spencer, 2009, Kelsey et al., 2010, Wang et al., 2012, Kim et al., 2014), and treatment with green tea extracts has been demonstrated to correct brain developmental alterations in transgenic mice that over-express DYRK1A (Guedj et al., 2009, De la Torre et al., 2014). There is evidence that after one month of treatment with green tea extracts there is an improvement in learning deficits in adult Ts65Dn mice (Guedj et al., 2009, De la Torre et al., 2014). A pilot study in young adult with DS showed that treatment with green tea extractcs exerts some behavioral benefits but that the effects decline after treatment cessation (De la Torre et al., 2014). It must be observed that neurogenesis, and the overall organization of the brain circuits, is determined at early life stages (Stiles and Jernigan, 2010), with the exception of the hippocampal dentate gyrus (DG), where neurogenesis continues during the whole life span (Seress et al., 2001, Rice and Barone, 2010, Stiles and Jernigan, 2010). In mice, most of the granule cells of the hippocampal DG are generated during the first two postnatal weeks (Altman and Bayer, 1975, Altman and Bayer, 1990a, b, Workman et al., 2013). Therefore, it is conceivable that treatment with EGCG during the most important neurodevelopmental period of the hippocampus may restore neurogenesis and neuron maturation and, possibly, engender permanent effects on behavior. Based on these premises, the current study was aimed at establishing whether neonatal therapy with EGCG restores

development of the hippocampal DG in the Ts65Dn mouse model and, if so, whether this effect is followed by an improvement in cognitive performance.

3.2.3 Materials and Methods

Colony

In order to obtain Ts65Dn mice, B6EiC3Sn a/ATs(17<16>)65Dn females were mated with C57BL/6JEiJ x C3H/HeSnJ (B6EiC3Sn) F1 hybrid males provided by Jackson Laboratories (Bar Harbor, ME, USA). We used the first generation of this breeding. The genotyping of the animals was carried out as previously described (Reinholdt et al., 2011). The day of birth was designated postnatal day zero (P0). A total of 143 mice were used. The mice were kept in a room with a 12:12 h light/dark cycle and had free access to water and food. Experiments were performed in accordance with the European Communities Council Directive of 24 November 1986 (86/609/EEC) for the use of experimental animals and were approved by Bologna University Bioethical Committee (Prot. N.28-IX/9). All efforts were made to minimize animal suffering and to keep the number of animals used to a minimum.

Experimental protocol

Euploid (n=40) and Ts65Dn (n=25) mice received a daily subcutaneous injection (at 9-10 am) of EGCG (Sigma-Aldrich) in 0.9% NaCl solution from postnatal day 3 (P3) to P15 (25.0 mg/kg) (**Fig. 3.2.1A,B**). Age-matched euploid (n=53) and Ts65Dn (n=25) mice were injected with the vehicle (hereafter referred to as "untreated mice"). Each group was composed of approximately the same number of males and females.

Experiment 1. A group of mice (euploid mice: n=15 untreated; n=15 treated; Ts65Dn mice: n=15 untreated; and n=15 treated) was killed at the age of 15 days (P15 mice). Before being killed, six mice from each of these groups were i.p. injected with BrdU (5-bromo-2-deoxyuridine; Sigma; 150 μg/g

body weight) in TrisHCl 50 mM 2h, in order to label proliferating cells (**Fig. 3.2.1A**) (Nowakowski et al., 1989). The brains of some P15 mice were fixed by immersion in Glyo-Fixx (as previously described (Bianchi et al., 2010b) and embedded in paraffin and the brains of the other P15 mice were fixed by immersion in PFA 4% and frozen (left hemisphere) or kept at –80°C for western blotting (right hemisphere). Mice were weighed before being sacrificed. After sacrifice, the brain was excised and weighed. The body and brain weights of the mice used are reported in **Table 3.2.2**. The number of animals used for each experimental procedure is specified in the figure legends.

Experiment 2. A second group of mice (euploid mice: n=38 untreated; n= 25 treated; Ts65Dn mice: n=10 untreated; and n=10 treated), was treated with EGCG from P3 to P15 h. On P15, mice received an i.p. injection (150 μg/g body weight) of BrdU in TrisHCl 50 mM and were killed after 30-35 days, i.e. at the age of 45-50 days (**Fig. 3.2.1B**). These mice will be called hereafter P45 mice. Because C3H/HeSnJ mice carry a recessive mutation that leads to retinal degeneration, animals were genotyped by standard PCR to screen out mice carrying this gene. Mice that did not carry a recessive mutation that leads to retinal degeneration entered the behavioral study. Behavioral testing started 9 days before mice reached 45-50 days of age. The brains of P45 mice were fixed by immersion in PFA 4% and frozen (left hemisphere) or kept at –80°C for western blotting (right hemisphere). Mice were weighed before being sacrificed. After sacrifice, the brain was excised and weighed. The body and brain weights of the mice used are reported in **Table 3.2.2**. The number of animals used for each experimental procedure is specified in the figure legends.

Histological procedures

P15 mice. The brains of P15 mice embedded in paraffin were cut into 8-μm-thick coronal sections. Slices were processed for Ki-67 and cleaved caspase-3 immunohistochemistry. The frozen brains of P15 mice were cut with a freezing microtome into 30-μm-thick coronal sections that were serially collected in anti-freezing solution (30% glycerol; 30% ethylen-glycol; 10% PBS10X; sodium azide 0.02%; MilliQ to volume) (free-floating sections). Slices were used for BrdU and SYN/PSD95 double

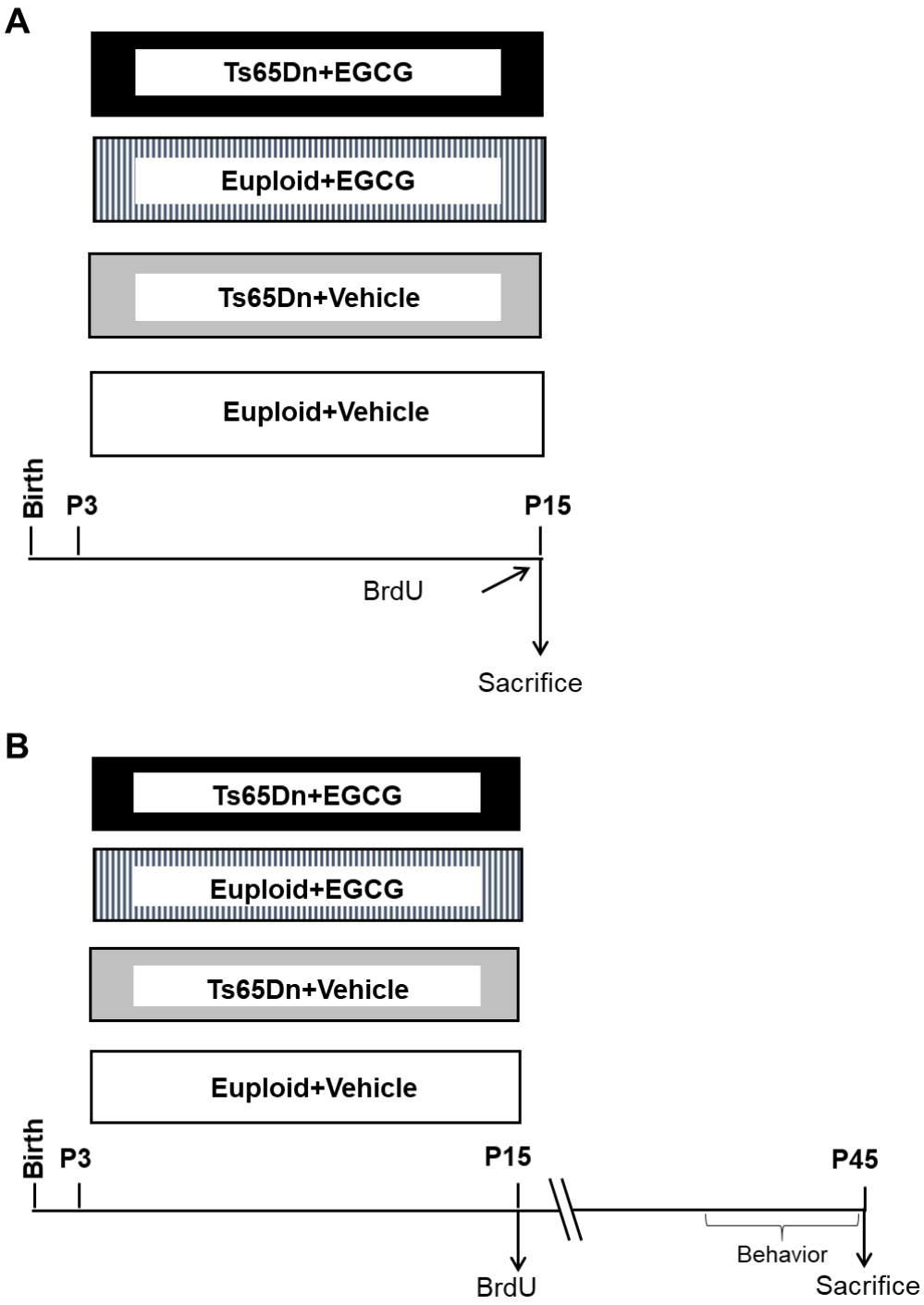

Figure 3.2.1. Experimental protocols. A: Euploid and Ts65Dn mice received a daily injection of either vehicle (Euploid + Vehicle; Ts65Dn + Vehicle) or EGCG (25.0 mg/kg; Euploid + EGCG; Ts65Dn + EGCG) from postnatal (P) day 3 to P15. At P15, mice received one injection of BrdU, and were killed after 2 h in order to evaluate the number of cells in the S-phase of the cell cycle. The brains of these mice were used for immunohistochemistry and western blotting. B: Euploid and Ts65Dn mice received a daily injection of either vehicle (Euploid + Vehicle; Ts65Dn + Vehicle) or EGCG (25.0 mg/kg; Euploid + EGCG; Ts65Dn + EGCG) from P3 to P15. Mice were killed on P45-P50 after 9 days of behavioral tests. The brains of these mice were used for immunohistochemistry and western blotting. Abbreviations: BrdU, bromodeoxyuridine; P, postannatal.

immunofluorescence.

P45 mice. The frozen brains of P45 mice were cut with a freezing microtome into 30-μm-thick coronal sections that were serially collected in anti-freezing solution (free-floating sections). Slices were used for BrdU/NeuN, BrdU/GFAP, and SYN/PSD-95 double immunofluorescence.

Immunohistochemistry

The antibodies for immunohistochemistry, with their dilution and purpose are summarized in **Table 3.2.1**.

Ki-67 immunohistochemistry in P15 and P45 mice. One out of 20 sections (n=14-18 sections) of paraffin-embedded brains taken from the rostral pole of the lateral ventricle to the end of the hippocampal formation of P15 mice, and one out of six free-floating sections (n=14-17 sections) from the hippocampal formation of P45 mice, was processed for Ki-67 immunohistochemistry. The secondary antibodies used for detection are reported in **Table 3.2.1**.

Cleaved caspase-3 immunohistochemistry in P15 and P45 mice. One out of 20 sections (n=14-18 sections) of paraffin-embedded brains taken from the rostral pole of the lateral ventricle to the end of the hippocampal formation of P15 mice, and one out of six free-floating sections (n=14-17 sections) from the hippocampal formation of P45 mice, was processed for cleaved caspase-3 immunohistochemistry. The secondary antibodies used for detection are reported in **Table 3.2.1**.

BrdU immunohistochemistry in P15. One out of six free-floating sections (n=13-16 sections) from the hippocampal formation of P15 mice was processed for BrdU immunohistochemistry as described in **Section 3.1**. Slices were incubated with a rat anti-BrdU antibody (mouse monoclonal 1:100, Roche Applied Science, Mannheim, Germany). Detection was performed with a CY3-conjugated anti rat-secondary antibody as indicated in **Table 3.2.1**.

Double-fluorescence IHC for BrdU/NeuN and BrdU/GFAP in P45 mice. One out of six free-floating sections (n=14-17 sections) from the hippocampal formation of P45 mice was incubated with a primary anti-BrdU antibody and either a NeuN or GFAP primary antibody as indicated in

Table 3.2.1 Antibodies used for immunohistochemistry and western blotting.

Antigen	Application	Antibody – Dilution- Manufactures	Purpose
5-bromo-2-deoxyuridine (BrdU)	**FIH DFIHC**	**Primary:** rat monoclonal 1:200 (Roche Applied Science) **Secondary:** Cy3-conjugated anti-rat IgG 1:200 (Jackson Immunoresearch)	To detect BrdU positive cells (surviving cells)
Cleaved caspase-3	**IHC**	**Primary:** rabbit monoclonal 1:100 (Cell Signaling Technology **Secondary:** Cy3-conjugated anti-rabbit IgG 1:200 (Jackson Immunoresearch)	To label apoptotic cells
GAPDH	**WB**	**Primary:** rabbit polyclonal 1:5000 (Sigma-Aldrich) **Secondary:** HRP-conjugated anti-rabbit 1:10000 (Jackson Immunoresearch)	To examine the levels of the housekeeping protein GAPDH
Glial fibrillary acidic protein (GFAP)	**DFIHC**	**Primary:** rabbit polyclonal 1:400 (Abcam) **Secondary:** FITC-conjugated anti-rabbit IgG 1:200 (Jackson Immunoresearch)	To detect surviving cells differentiated into astrocytes
GSK3β	**WB**	**Primary:** mouse monoclonal 1:1000 (Cell Signaling Technology) **Secondary:** HRP-conjugated anti-mouse 1:10000 (Jackson Immunoresearch)	To examine the expression of the dephosphorylated form (active) of the kinase GSK3β
Phospho-GSK3β (Ser9)	**WB**	**Primary:** rabbit monoclonal 1:1000 (Cell Signaling Technology) **Secondary:** HRP-conjugated anti-rabbit 1:10000 (Jackson Immunoresearch)	To examine the expression of the phosphorylated form (inactive) of the kinase GSK3β
Ki-67	**IHC**	**Primary:** rabbit monoclonal 1:100 (Thermo Scientific) **Secondary:** HRP-conjugated anti-rabbit dilution 1:200 (Jackson Immunoresearch) and DAB kit (Vector Laboratories)	To label cycling cells (Ki-67 is expressed in all phases of the cell cycle except early G1)
Neuronal-specific nuclear protein (NeuN)	**DFIHC**	**Primary:** mouse monoclonal 1:400 (Millipore) **Secondary:** FITC-conjugated anti-mouse IgG 1:200 (Jackson Immunoresearch)	To detect surviving cells that have differentiated into neurons
p21	**WB**	**Primary:** mouse monoclonal 1:500 (Santa Cruz Biotechnology) **Secondary:** HRP-conjugated anti-mouse 1:10000 (Jackson Immunoresearch)	To examine the expression p21, an inhibitor of cell cycle progression
Postsynaptic density protein-95 (PSD-95)	**IHC**	**Primary:** rabbit polyclonal 1:1000 (Abcam) **Secondary:** CY3-conjugated anti-rabbit 1:200 (Jackson Immunoresearch)	To label postsynaptic regions
Synaptophysin (SYN)	**IHC**	**Primary:** mouse monoclonal 1:1000 (Millipore-Biomanufacturing and Life Science Research) **Secondary:** FITC-conjugated anti-mouse 1:200 (Jackson Immunoresearch)	To label presynaptic terminals

IHC, immunohistochemistry; DFIHC, Double-fluorescence immunohistochemistry; FIH, fluorescence immunohistochemistry; WB, Western blotting.

Table 3.2.1. The secondary antibodies used for detection are reported in **Table 3.2.1**.

Double-fluorescence IHC for SYN and PSD-95 in P15 and P45 mice. One out of six free-floating sections from the rostral two-thirds of the hippocampal formation of P15 and P45 mice (n=4-6 sections) was incubated with the antibodies indicated in **Table 3.2.1**.

Nissl-staining

One out of six free-floating sections taken from the beginning to the end of the hippocampal formation of P15 (n=13-16 sections) and P45 (n=14-17 sections) mice was stained with toluidine blue according to the Nissl method.

Measurements

Image acquisition. A light microscope (Leitz) equipped with a motorized stage and focus control system and a color digital camera (Coolsnap-Pro; Media Cybernetics, Silver Spring, MD, USA) were used to take bright field images. Immunofluorescence images were taken with a Nikon Eclipse TE 2000-S inverted microscope (Nikon Corp., Kawasaki, Japan), equipped with a Nikon digital camera DS 2MBWc. Immunofluorescence images of sections processed for i) SYN and PSD-95 immunohistochemistry of P15 and P45 animals, and ii) BrdU/NeuN or BrdU/GFAP of P45 animals were taken with a LEICA TCS SL confocal microscope. Measurements were carried out using Image Pro Plus software (Media Cybernetics, Silver Spring, MD 20910, USA) or ImageJ v1.51a.

Ki-67 positive cells in P15 and P45 mice. Images of the series of sections processed for Ki-67 IHC from the subventricular zone (SVZ) and dentate gyrus (DG) of P15 mice and from the DG of P45 mice were taken using a light microscope (Leitz; objective: x 40, 0.70 NA; final magnification: x 500). Images were taken at the focal plane at which the largest number of cells was recognizable. In this study, the SVZ corresponds to the region comprised between the beginning of the lateral ventricle and the beginning of the hippocampal formation. In the SVZ, an area enclosing the dorso-lateral and medial wall of the lateral ventricle was manually traced and all Ki-67-positive cells within this area

were counted. In the DG, an area enclosing the granule cell layer + subgranular zone + hilus was manually traced and all Ki-67-positive cells within this area were counted. Cells were counted in the series of sections processed for Ki-67 immunohistochemistry from the SVZ and DG. The counted cells are expressed here as "total cell count", obtained from the sum of counts across all sections counted, and as "cells per unit area", obtained by dividing the number of counted cells by the traced area and expressed as cells/mm^2. The number of cells per unit area in individual sections was averaged in order to obtain the mean number of cells per unit area in each mouse.

Cleaved caspase-3 positive cells in P15 and P45 mice. In the series of sections processed for cleaved caspase-3 immunohistochemistry, cleaved caspase-3-positive cells were counted in the SVZ and DG of P15 mice and in the DG of P45 mice. Images were taken using a fluorescence microscope (Eclipse; objective x 40, 0.75 NA; final magnification: x 400). Total cell count was obtained from the sum of counts across all sections counted.

BrdU-positive cells in P15 mice. Images of the series of sections processed for BrdU immunohistochemistry from the DG were taken using a fluorescence microscope (Eclipse; objective: x 40, 0.75 NA; final magnification: x 400). Images were taken at the focal plane at which the largest number of cells was recognizable. Cells were counted in the series of sections processed for BrdU immunohistochemistry from the DG, within a manually-traced area enclosing the granule cell layer + subgranular zone + hilus. Total cell count and the number of cells per unit area were obtained as indicated above for Ki-67-positive cells.

Number of BrdU-positive cells and cell phenotypes in the DG of P45 mice. Quantification of BrdU-labeled nuclei in the DG was conducted in every 6th section using a confocal microscope (objective x 40, NA 0.75; final magnification x 400). In order to quantify BrdU labeling, we used a modified unbiased stereology protocol (Malberg et al., 2000, Kempermann and Gage, 2002, Tozuka et al., 2005). All BrdU-labeled cells located in the granule cell and subgranular layers were counted along the entire z axis (1 µm steps) of each section. To avoid oversampling errors, the nuclei intersecting the uppermost focal plane were excluded. The total number of BrdU-labeled cells per animal was

determined and multiplied by six to obtain the total estimated number of cells per DG. For double-labeling, we randomly selected 100 BrdU-labeled nuclei across the DG and counted the number of BrdU-positive nuclei that co-expressed either NeuN or GFAP. BrdU-positive nuclei were analyzed (oil objective x 63, NA 1.32) along the entire z-axis (0.5 µm steps) and were rotated onto orthogonal planes (x–y) to verify double-labeling and to exclude false double-labeling caused by the overlay of signals from different cells. The percentage of BrdU-labeled nuclei that co-expressed either NeuN or GFAP, or neither of these two markers, was calculated. The total number of cells with a neuronal (BrdU+/NeuN+ cells) phenotype, an astrocytic (BrdU+/GFAP+ cells) phenotype, or an undetermined phenotype (i.e. BrdU+ cells that did not express either of the two markers) was estimated by multiplying the absolute numbers of BrdU-positive cells by the percentage of co-localisation for each of those two markers, or by no co-localization for either marker.

Synaptic terminals in P15 and P45 mice. Optical densitometry was used to evaluate the intensity of SYN and PSD-95 immunoreactivity in the DG, hippocampal fields CA3 and CA1, and neocortex overlying the hippocampus in fluorescence images captured with an Eclipse microscope (objective x 20, 0.50 NA; final magnification x 200). Densitometric analysis was carried out using Image Pro Plus software, as described in **Section 3.1**. For evaluation of puncta exhibiting SYN or PSD-95 immunoreactivity in the DG, hippocampal fields CA3 and CA1, and neocortex overlying the hippocampus, images were acquired using a confocal microscope (objective x 63, NA 1.32; zoom factor=8). Three images from the regions of interest were captured in each section and the density of SYN or PSD-95 immunoreactive puncta was evaluated as previously described (Guidi et al., 2013).

Stereology of the DG. Unbiased stereology was performed on Nissl-stained sections of the brain of P15 and P45 mice, as previously described (Severi et al., 2005, Bianchi et al., 2010b). The protocol used for the stereology of the DG is the same as the one used in **Section 3.1.**

Western blotting

Total proteins were obtained from hippocampal homogenates of P15 and P45 as described in **Section**

3.1. Equivalent amount of proteins (50 μg) were subjected to electrophoresis on a 4-12% NuPAGE Bis-Tris Precast Gel (Novex, Life Technologies, Ltd, Paisley, UK) and transferred to a Hybond ECL nitrocellulose membrane (Amersham Life Science). The levels of p21, ser9 phosphorylated GSK3β, and total GSK3β were examined using the antibodies reported in **Table 3.2.2**. Images were digitized with ChemiDoc XRS+ and densitometric analysis was carried out with Image Lab software (Bio-Rad Laboratories, Hercules, CA, USA). Intensity of each band was normalized to the intensity of the corresponding GAPDH band.

Behavioral testing

Ts65Dn (untreated n=10, treated n=10) and euploid (untreated n=38, treated n=25) mice were behaviorally tested using the Y-maze (YM) tests and the Morris Water Maze (MWM). All behavioural tests were conducted on P45 mice, i.e. 30-35 days after treatment cessation.

YM. YM testing was performed using an apparatus with three equal arms (35 cm long, 5 cm wide, 10 cm high) made of gray solid plastic and set at angles of 120°. Each mouse was placed at the center of the maze and allowed to move freely for a 10-min session. Data were collected during the first 6-min period of each session. Mice with fewer than 10 arm entries during the 6-min observation period were not included in the analysis. All four limbs were required to enter an arm for the entry to be considered valid. A series of three entries into three different arms is defined as a triad. The percentage of alternations was calculated as 100 x (number of correct alternations)/(total number of arm entries - 2).

MWM. Mice were trained in the MWM task to locate a hidden escape platform in a circular pool, using a previously a protocol based on a published protocol (Vorhees and Williams, 2006). The apparatus consisted of a large circular water tank (1.00 m diameter, 50 cm height) with a transparent round escape platform (10 cm^2). The pool was virtually divided into four equal quadrants identified as northeast, northwest, southeast, and southwest. The tank was filled with tap water at a temperature of 22±1.0ºC. The tank was filled with water up to 0.5 cm above the top of the platform and the water

was made opaque with milk. The platform was placed in the tank in a fixed position (in the middle of the south-west quadrant). The pool was placed in a large room with various intra- (squares, triangles, circles and stars) and extra-maze visual cues. Each mouse was tested in one session of 4 trial on the first day and in two sessions of 4 trials in the following 4 days with an inter-session interval of 45 min. A video camera was placed above the center of the pool and connected to a videotracking system (Ethovision 3.1; Noldus Information Technology B.V., Wageningen, Netherlands). Mice were randomely released facing the wall of the pool from one of the following starting points: North, East, South, or West and allowed to search for up to 60 s for the platform. If a mouse did not find the platform, it was gently guided to it and allowed to remain there for 15 s. During the inter-trail time (10 s) mice were placed in an empty cage. For the learning phase, we evaluated the latency to find the hidden platform. Retention of memory was assessed with one trial (probe trial), on the sixth day, 24 h after the last acquisition trial, using the same starting point for all mice. The platform was removed from the tank and mice were allowed to search for up to 60 s for the platform. For the probe trial, the latency of the first entrance in the trained platform zone, the frequency of entrances in the platform quadrant, and the percentage of time spent in the trained platform quadrant were employed as measures of retention of acquired spatial preference. All experimental sessions were carried out between 9.00am and 5.00pm.

Statistical analysis

Data from single animals represented the unity of analysis. Results are presented as mean ± standard error of the mean (SE). Data were analyzed with IBM SPSS 22.0 software. Distribution of data and the homogeneity of variances were evaluated with Shapiro-Wilk test and Levene's test respectively. Statistical analysis was carried out using a two-way ANOVA with genotype (euploid and Ts65Dn) and treatment (vehicle, EGCG) as factors. *Post hoc* multiple comparisons were carried out using the Fisher least significant difference (LSD) test. For the learning phase of MWM, statistical analyses was performed using a three-way mixed ANOVA, with genotype and treatment as grouping factors

and days as a repeated measure. For the probe test of MWM and for the YM, we used a two-way ANOVA with genotype and treatment as factors followed by the Fisher LSD *post hoc* test. A probability level of $p \leq 0.05$ was considered to be statistically significant.

3.2.4 Results

General results of P15 mice

The Ts65Dn strain is characterized by a high mortality rate during gestation and before weaning (Roper and Reeves, 2006). In the current study, treatment with either EGCG or vehicle began on postnatal day 3 (P3). All mice of the litters used in this study that survived in the P0 to P3 period entered the study, with no specific selection criteria. Six vehicle-treated (7%) and five EGCG-treated (7%) mice died before weaning, in the P6-P22 period. The similarity in the mortality rate across groups suggests that treatment has no adverse effects on the health of mice. We evaluated the body and brain weight of P15 mice in order to establish the short-term effect of treatment. A two-way ANOVA on the body weight of P15 mice showed no genotype x treatment interaction, a main effect of genotype in males [$F(1,26) = 12.81$, $p \leq 0.001$] and females [$F(1,26) = 6.29$, $p \leq 0.05$] and no effects of treatment. Two-way ANOVA on brain weight did not show genotype x treatment interaction and no significant effects of both genotype and treatment. *Post hoc* Fisher LSD test showed no statistical differences among the four experimental groups. The finding that the body and brain weight were not reduced by treatment (**Table 3.2.2**) suggests that treatment has no adverse effects.

Short-term effects of neonatal treatment with EGCG on the proliferation potency of neural precursor cells

The subventricular zone (SVZ) and the hippocampal dentate gyrus (DG) represent the major neurogenic regions of the postnatal brain. We made Ki-67 immunohistohemistry in P15 mice in order

Table 3.2.2. Body and brain weights of treated and untreated mice.

		Vehicle			EGCG			
		Mean	**SE**	**n**	**Mean**	**SE**	**n**	***p***
P15								
Body								
Males	Euploid	7.67	± 0.60	(7)	7.53	± 0.36	(8)	n.s.
	Ts65Dn	5.68	± 0.41	(8)	6.60	± 0.44	(7)	n.s.
	p	0.01			n.s.			
Females	Euploid	6.40	± 0.57	(8)	7.71	± 0.48	(7)	n.s
	Ts65Dn	5.77	± 0.45	(7)	5.64	± 0.58	(8)	n.s
	p	n.s.			0.01			
Brain								
Males	Euploid	0.396	± 0.003	(7)	0.399	± 0.008	(8)	n.s.
	Ts65Dn	0.389	± 0.009	(8)	0.386	± 0.010	(7)	n.s.
	p	n.s			n.s			
Females	Euploid	0.390	± 0.007	(8)	0.405	± 0.007	(7)	n.s
	Ts65Dn	0.397	± 0.008	(7)	0.396	± 0.011	(8)	n.s
	p	n.s			n.s.			
P45								
Body								
Males	Euploid	21.62	± 0.60	(17)	21.10	± 0.72	(12)	n.s.
	Ts65Dn	17.86	± 1.16	(5)	17.74	± 1.46	(5)	n.s.
	p	0.05			n.s.			
Females	Euploid	17.58	± 0.40	(21)	20.61	± 1.69	(13)	0.05
	Ts65Dn	16.23	± 1.43	(5)	15.34	± 1.08	(5)	n.s.
	p	n.s			n.s.			
Brain								
Males	Euploid	0.474	± 0.006	(17)	0.460	± 0.006	(12)	n.s.
	Ts65Dn	0.437	± 0.017	(5)	0.443	± 0.010	(5)	n.s.
	p	0.01			n.s.			
Females	Euploid	0.456	± 0.009	(21)	0.452	± 0.004	(13)	n.s.
	Ts65Dn	0.428	± 0.015	(5)	0.442	± 0.013	(5)	n.s.
	p	0.05			n.s.			

Body and brain weight (mean ± SE) in grams of P15 and P45 euploid and Ts65Dn mice that received either vehicle or EGCG in the period P3-P15, measured on postnatal days 15 (P15) or P45. The number of mice of each group is reported in the n column. The p values in the row below the body and brain weight refer to the comparison between euploid and Ts65Dn mice. The *p* values in the column on the right refer to the comparison between untreated and treated mice of the same genotype. n.s. not significant (Fisher LSD test after two-way ANOVA with genotype and treatment as factors).

to evaluate the number of NPCs in both these regions.

We evaluated the total number of Ki-67-positive cells counted in the series of sampled sections and their number per unit area.

A two-way ANOVA on total Ki-67-positive cells counted in the SVZ showed a genotype x treatment interaction [$F(1,20) = 5.93$, $p \leq 0.05$] and a significant effect of treatment [$F(1,20) = 24.49$, $p \leq 0.001$], but no effect of genotype. A *post hoc* Fisher LSD test showed that the number of Ki-67-positive cells in untreated Ts65Dn mice was reduced in comparison with untreated euploid mice. This difference disappeared in neonatally-treated Ts65Dn mice (**Fig. 3.2.2B**). A two-way ANOVA on the density of Ki-67-positive cells in the SVZ showed no genotype x treatment interaction, but there was a significant effect of both genotype [$F(1,20) = 6.35$, $p \leq 0.05$] and treatment [$F(1,20) = 29.67$, $p \leq 0.001$]. A *post hoc* Fisher LSD test showed that in untreated Ts65Dn mice the density of Ki-67-positive cells was reduced in comparison with untreated euploid mice. This difference disappeared in neonatally-treated Ts65Dn mice (**Fig. 3.2.2C**).

A two-way ANOVA on total Ki-67-positive cells counted in the DG showed a genotype x treatment interaction [$F(1,20) = 25.42$, $p \leq 0.001$] and a significant effect of both genotype [$F(1,20) = 21.11$, $p \leq 0.001$] and treatment [$F(1,20) = 26.68$, $p \leq 0.001$]. A *post hoc* Fisher LSD test showed that the total number of Ki-67-positive cells in untreated Ts65Dn mice was lower than that found in untreated euploid mice. Ts65Dn mice neonatally-treated with EGCG showed a similar number of Ki-67-positive cells in comparison with untreated euploid mice (**Fig. 3.2.3B**). A two-way ANOVA on the density of Ki-67-positive cells in the DG showed a genotype x treatment interaction [$F(1,20) = 5.51$, $p \leq 0.05$], with no effect of genotype, but a significant effect of treatment [$F(1,20) = 38.62$, $p \leq 0.001$]. A *post hoc* Fisher LSD test showed that in untreated Ts65Dn mice the density of Ki-67-positive cells was reduced in comparison with untreated euploid mice and that treatment with EGCG restored this defect (**Fig. 3.2.3C**).

In order to establish whether treatment affects apoptotic cell death, brain sections comprising the SVZ and the DG were subjected to immunohistochemistry for cleaved caspase-3. No genotype x treatment

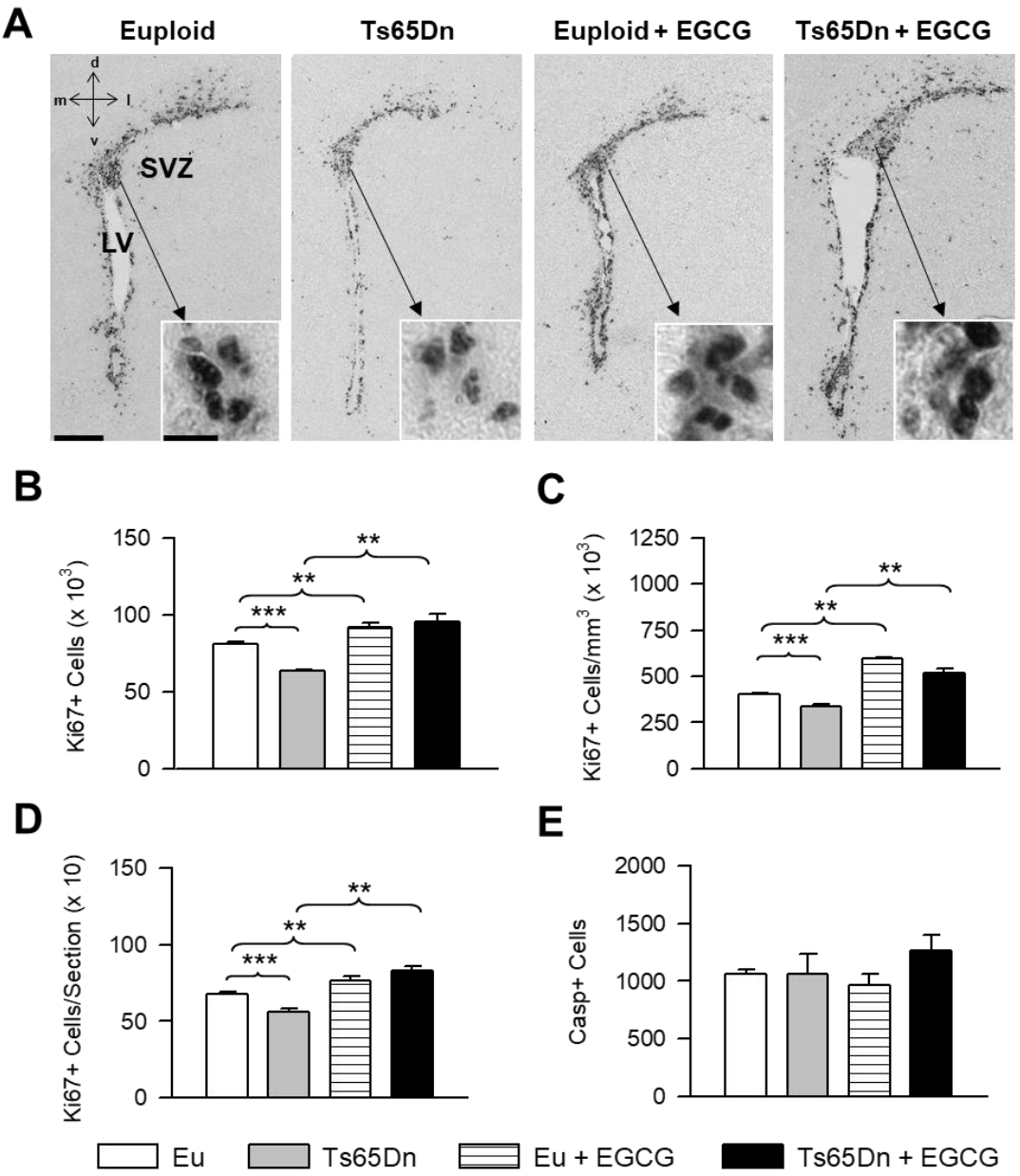

Figure 3.2.2. Effects of neonatal treatment with EGCG on neural precursor number in the subventricular zone of P15 mice. A: Examples of sections immunostained for Ki-67 from the subventricular zone of an animal from each experimental group. Calibration bar=200 μm. The insets show zoomed images with examples of individual Ki-67-positive cells. Calibration bar=10 μm. B-E: Ki-67 positive cells expressed as total cell count (B), as cells/mm^3 (C), as cells per section (D) and number of cleaved caspase-3-positive cells expressed as total cell count (E) in the SVZ of untreated and treated euploid and Ts65Dn mice (n=6: 3 males and 3 females for each of the four experimental groups). Values (mean ± SE) refer to one hemisphere. * $p < 0.05$; ** $p < 0.01$; *** $p < 0.001$ (Fisher LSD test after two-way ANOVA). Asterisks over the brackets indicate a difference between the two indicated groups. Abbreviations: Casp, Caspase-3; d, dorsal; l, lateral; LV, lateral ventricle; m, medial; SVZ, subventricular zone; v, ventral.

interaction was found; nor there were any main effects of genotype or treatment for the total number of cleaved caspase-3-positive cells counted in the SVZ and DG. A *post hoc* Fisher LSD test showed no differences between untreated euploid and Ts65Dn mice in the number of cleaved caspase-3-positive cells and that treatment did not affect this parameter in both the SVZ (**Fig. 3.2.2E**) and DG (**Fig. 3.2.3D**).

In view of its role on cell cycle progression, we analyzed the levels p21 (cip1/WAF1), a cyclin-dependent kinase that inhibits cell cycle progression and is overexpressed in brains of DS people. A two-way ANOVA on p21 protein levels in hippocampal homogenates of mice aged 15 days showed a genotype x treatment interaction [$F(1,20) = 6.86$, $p \leq 0.05$], no main effect of genotype, but a main effect of treatment [$F(1,20) = 17.07$, $p \leq 0.001$]. A *post hoc* Fisher LSD test showed that untreated mice had higher levels of p21 in comparison with untreated euploid mice (**Fig. 3.2.3E**) and that treatment with EGCG normalized p21 levels (**Fig. 3.2.3E**). No effect of treatment on p21 levels was found in euploid mice (**Fig. 3.2.3E**).

We then evaluated the effect of treatment on the population of cells in the S-phase of the cell cycle. To this purpose, we administered to Ts65Dn and euploid mice BrdU on P15 and the number of BrdU-positive cells in the DG was evaluated 2h after the injection. A two-way ANOVA on the total number of BrdU-positive cells showed no genotype x treatment interaction, but a main effects of both genotype [$F(1,20) = 16.74$, $p \leq 0.001$] and treatment [$F(1,20) = 5.00$, $p \leq 0.05$] emerged. A *post hoc* analysis with Fisher LSD test showed that in untreated Ts65Dn mice there were fewer BrdU-positive cells than that of untreated euploid mice; this difference disappeared in treated Ts65Dn mice (**Fig. 3.2.4B**). A two-way ANOVA on the density of BrdU-positive cells showed a genotype x treatment interaction [$F(1,20) = 6.19$, $p \leq 0.05$], no effect of genotype, but a main effect of treatment [$F(1,20) = 4.48$, $p \leq 0.05$]. A *post hoc* Fisher LSD test showed that untreated Ts65Dn mice had a number of BrdU positive cells/mm^2 lower than that of untreated euploid mice and that treatment restored this defect (**Fig. 3.2.4C**).

Taken together these results show that neonatal treatment with EGCG restores the population of the

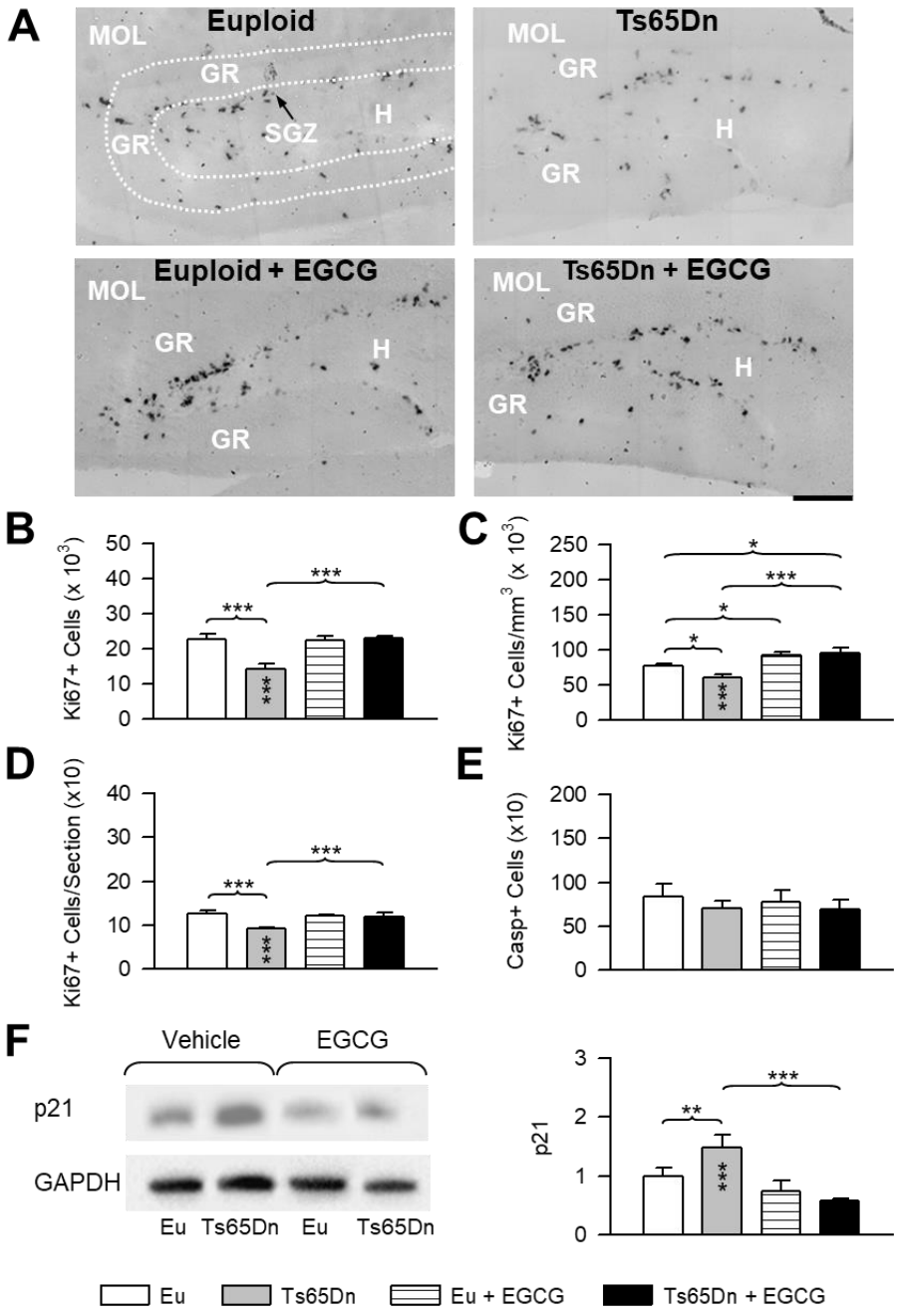

Figure 3.2.3. Effects of neonatal treatment with EGCG on neural precursor number in the dentate gyrus of P15 mice. A: Examples of sections immunostained for Ki-67 from the dentate gyrus of an animal from each experimental group. Calibration bar=100 μm. Calibration bar=10 μm. B-E: Ki-67-positive cells expressed as total cell count (B), as cells/mm^3 (C), as cells per section (D) and number of cleaved caspase-3-positive cells expressed as total cell count (E) in the dentate gyrus of untreated and treated euploid and Ts65Dn mice (n=6: 3 males and 3 females for each of the four experimental groups). Values (mean ± SE) refer to one hemisphere. F: Western blot analysis of p21 levels in the hippocampal formation of untreated and treated euploid and Ts65Dn mice. Western immunoblots (left panel) are examples from animals of each experimental group. The histograms on the right show p21 levels normalized to GAPDH and expressed as a fold difference in comparison with untreated euploid mice (n=6: 3 males and 3 females for each experimental group). Values in (B-E) are mean ± SE. * $p < 0.05$; ** $p < 0.01$; *** $p < 0.001$ (Fisher LSD test after two-way ANOVA). Black asterisks in the gray bar indicate a difference between untreated Ts65Dn mice and treated euploid mice. Abbreviations: Casp, caspase-3; Eu, euploid; GR, granule cell layer; H, hilum; MOL, molecular layer.

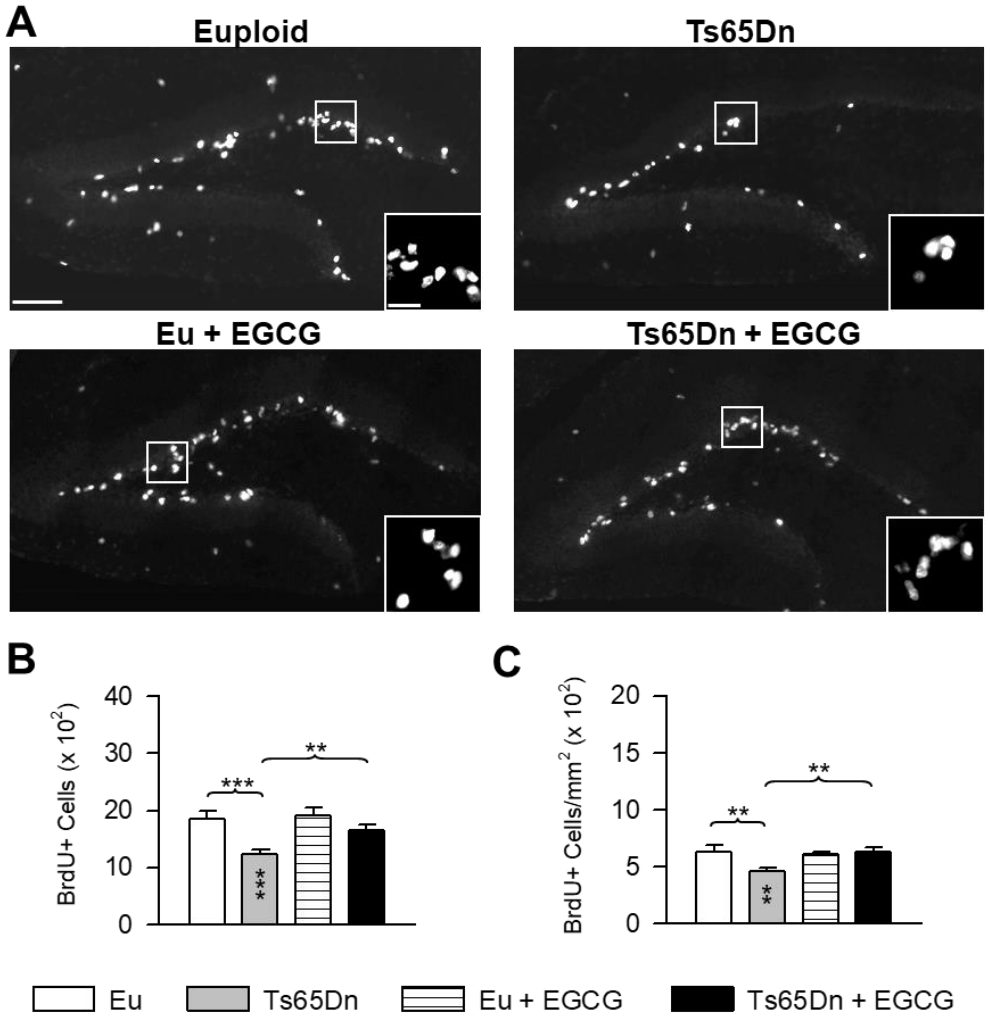

Figure 3.2.4. Effects of neonatal treatment with EGCG on the size of the population of cells in the S-phase of the cell cycle of P15 mice. A: Representative images of sections immunostained for BrdU from the dentate gyrus of an animal for each experimental group. Calibration bar=100 μm. The insets show zoomed images of the boxed area with examples of individual BrdU-positive cells. Calibration bar=20 μm. B, C: BrdU-positive cells, expressed as total cell count (B) and cells/mm^2 (C), in the dentate gyrus of untreated and treated euploid and Ts65Dn mice (n=6: 3 males and 3 females for each of the four experimental groups). Values (mean ± SE) refer to one hemisphere. ** $p < 0.01$; *** $p < 0.001$ (Fisher LSD test after two-way ANOVA). Black asterisks in the gray bar indicate a difference between untreated Ts65Dn mice and treated euploid mice. Abbreviations: BrdU, bromodeoxyuridine; Eu, euploid.

actively dividing cells in both the DG and SVZ and suggest that this effect is linked to a restoration of the proliferation potency and not to a decrease in apoptotic cell death.

Short-term effects of neonatal treatment with EGCG on total number of hippocampal granule cells

Neurogenesis in the hippocampal DG starts embryonically in both humans and mice, but in mice most of the granule cells are born in the first two postnatal weeks (Altman and Bayer, 1975, Altman and Bayer, 1990a, c, Seress et al., 2001, Rice and Barone, 2010, Stiles and Jernigan, 2010). In order to establish whether treatment restores the defective cellularity that characterizes the DG of Ts65Dn mice, we stereologically analyzed the volume of the granule cell layer, the density of the granule cells and the total number of granule cells. A two-way ANOVA on the volume of the granule cell layer showed a genotype x treatment interaction [$F(1,20) = 8.37$, $p \leq 0.01$], a main effect of genotype [$F(1,20) = 17.88$, $p \leq 0.001$], but no effect of treatment. A *post hoc* Fisher LSD test showed that the volume of the granule cell layer was reduced in untreated Ts65Dn mice in comparison with untreated euploid mice (**Fig. 3.2.5B**), which is in agreement with previous evidence (Bianchi et al., 2010b) and that its size was normalized by treatment. A two-way ANOVA on granule cell density showed a genotype x treatment interaction [$F(1,20) = 9.05$, $p \leq 0.01$] and a main effect of both genotype [$F(1,20) = 10.32$, $p \leq 0.001$] and treatment [$F(1,20) = 18.69$, $p \leq 0.001$]. A *post hoc* Fisher LSD test revealed that untreated Ts65Dn mice had a reduced granule cell density in comparison with untreated euploid. Treated Ts65Dn mice underwent a restoration of this defect (**Fig. 3.2.5B**). A two-way ANOVA on total number of granule cells showed a genotype x treatment interaction [$F(1,20) = 11.10$, $p \leq 0.005$] and a main effect of both genotype [$F(1,20) = 17.02$, $p \leq 0.001$] and treatment [$F(1,20) = 6.99$, $p \leq 0.05$]. A *post hoc* Fisher LSD test showed that untreated Ts65Dn mice had fewer granule neurons in comparison with euploid mice and that this defect was restored by treatment (**Fig. 3.2.4B**).

Short-term effects of neonatal treatment with EGCG on cortical and hippocampal synapses

The altered functionality of the trisomic brain is mainly due to neurogenesis defects (Chakrabarti et

al., 2007, Contestabile et al., 2007, Guidi et al., 2008, Bianchi et al., 2010a, Bianchi et al., 2010b, Guidi et al., 2011a, Trazzi et al., 2011) and to altered synaptic connectivity (Takashima et al., 1989, Becker, 1991, Belichenko et al., 2004, Benavides-Piccione et al., 2004, Guidi et al., 2013). Circuit formation critically takes place in the early postnatal period when the newborn neurons establish synaptic contacts with other neurons. To establish whether treatment with EGCG had an effect on brain circuitry, in P15 mice we examined the levels of immunoractivity for (optical density; OD) SYN (synaptophysin) PSD-95 (postsynaptic density protein-95). We took into account the superficial (II-III) and deep (IV-VI) layers of the somatosensory cortex, the molecular layer of the DG, the stratum lucidum of field CA3, and the stratum radiatum of field CA1. Additionally, we also evaluated the number of SYN and PSD-95 immunoreactive puncta using confocal microscopy, in order to establish whether possible differences in SYN and PSD-95 OD reflected differences in the number of pre- and post-synaptic terminals.

A two-way ANOVA on the OD of SYN and PSD-95 and on the number of SYN- and PSD-95-immunoreactive puncta revealed numerous interactive effects and main effects of genotype and treatment (summarized in **Table 3.2.3**). A *post hoc* Fisher LSD test showed that in untreated Ts65Dn mice the OD of SYN and PSD-95 was significantly lower than in untreated euploid mice in all regions analyzed (**Fig. 3.2.6C-F**). Furthermore, an evaluation of the number of puncta revealed that untreated Ts65Dn mice had fewer SYN- and PSD-95 immunoreactive puncta in all the examined regions. This suggests that Ts65Dn mice have a reduced number of pre- and postsynaptic terminals. Importantly, in Ts65Dn mice that had been neonatally-treated with EGCG there was a total restoration of the OD of SYN and PSD-95 and the number of SYN- and PSD-95-immunoreactive puncta (**Fig. 3.2.7C-F**) in comparison with untreated euploid mice. Treatment also had an effect on SYN and PSD-95 OD and number of puncta in some of the examined regions of euploid mice (**Fig. 3.2.7C-F**).

General results of P45 mice

We evaluated the body and brain weight of P45 mice in order to establish the long-term effect of

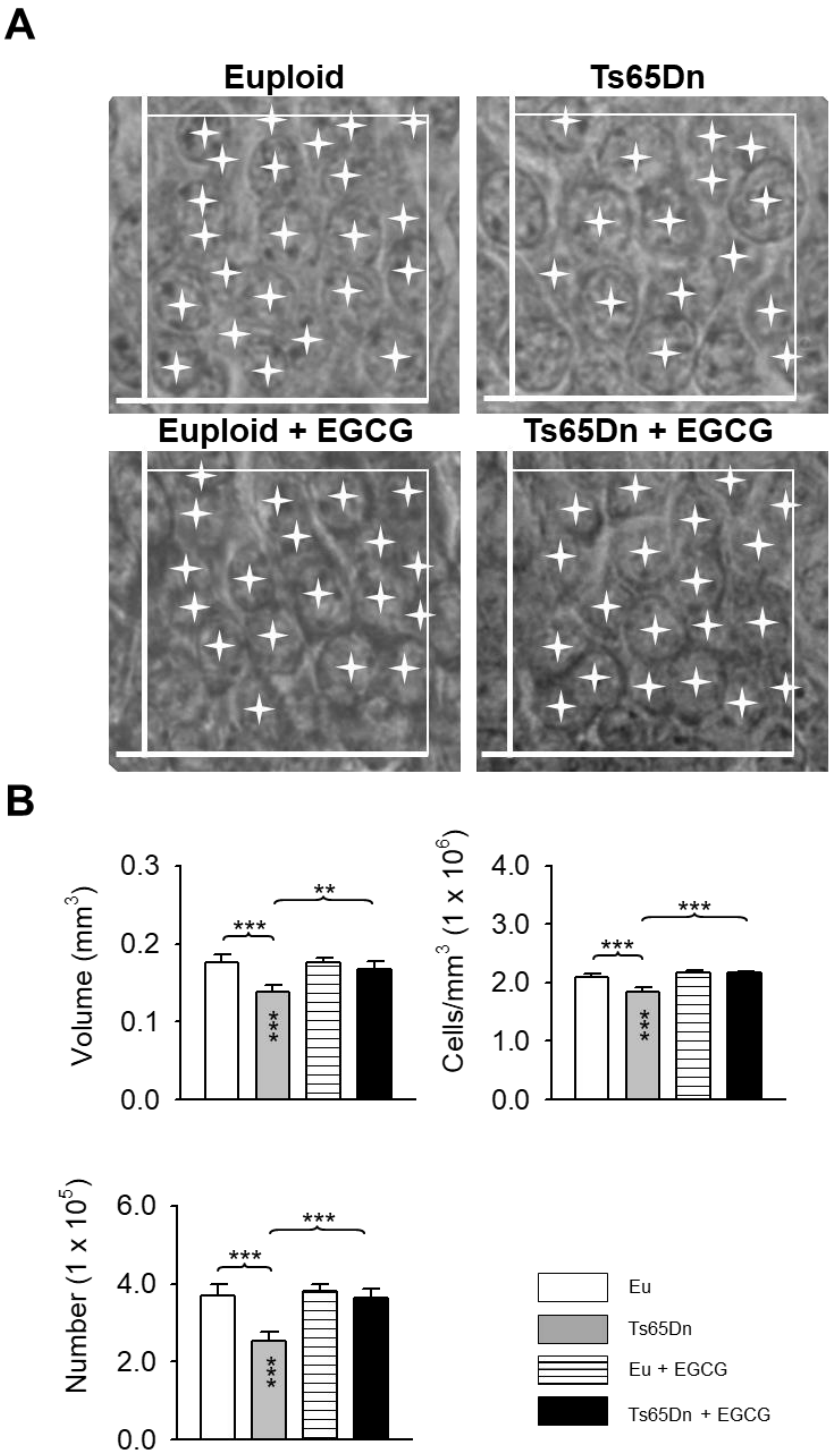

Figure 3.2.5. Effects of neonatal treatment with EGCG on granule cell number in the dentate gyrus of P15 mice. A: Representative images of Nissl-stained sections in the granule cell layer of an animal from each experimental group. The sides of the superimposed optical disector are 30 μm in length. The stars indicate individual nuclei. Note that nuclei intersecting the exclusion sides (thick lines) were not counted. B: Volume of the granule cell layer, density of granule cells (cells/mm^3) and total number of granule cells of untreated and treated euploid and Ts65Dn mice (n=6: 3 males and 3 females for each of the four experimental groups). Values (mean ± SE) refer to one dentate gyrus. ** $p < 0.01$; *** $p < 0.001$ (Fisher LSD test after two-way ANOVA). Black asterisks in the gray bar indicate a difference between untreated Ts65Dn mice and treated euploid mice. Abbreviation: Eu, euploid.

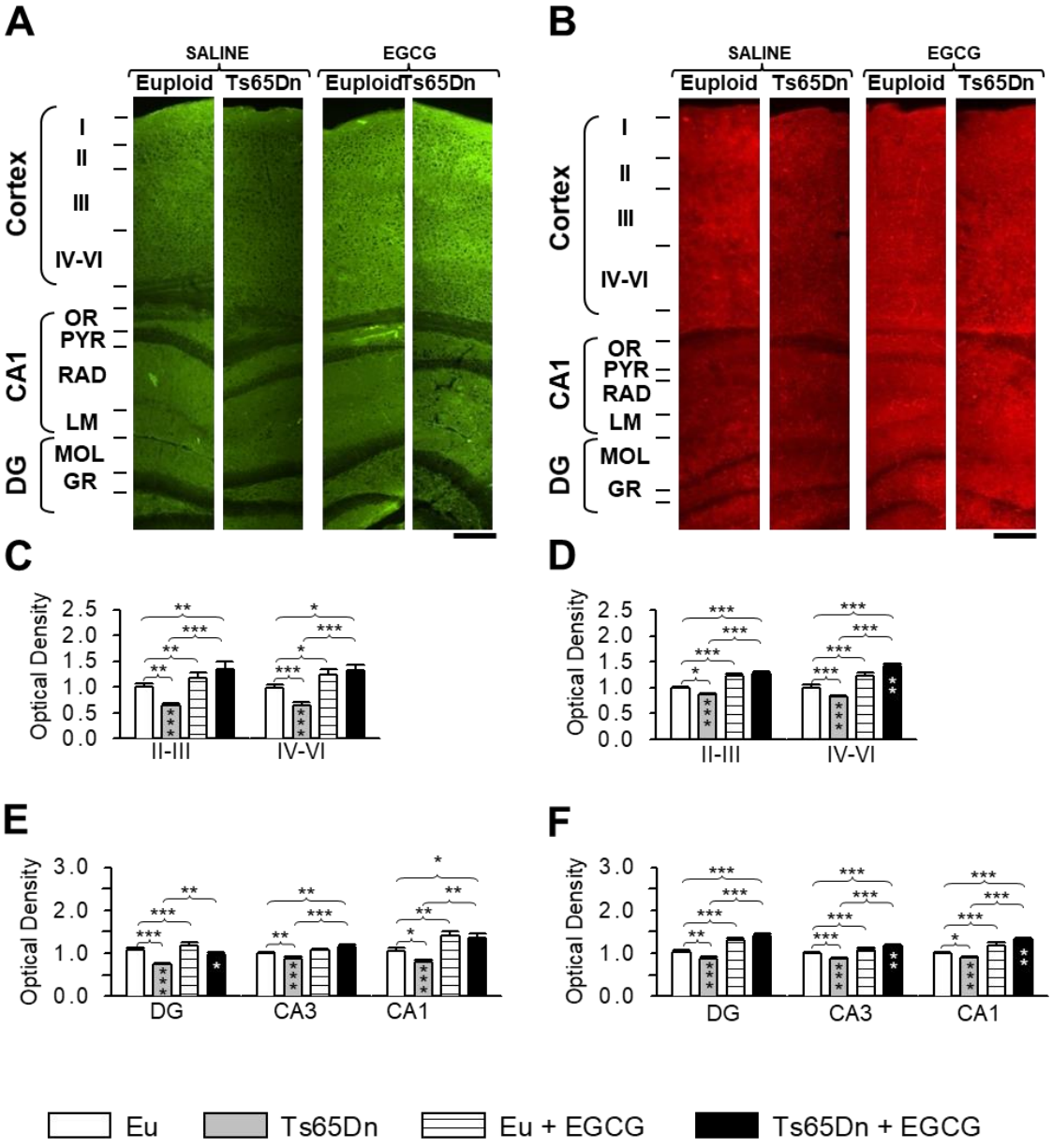

Figure 3.2.6. Effects of neonatal treatment with EGCG on synapse development in P15 mice. A, B: Sections processed for SYN (A) and PSD-95 (B) immunofluorescence from the neocortex overlying the hippocampus, hippocampal field CA1 and DG of an animal from each experimental group. Calibration bar=200 μm. C-F: Optical density of SYN and PSD-95 immunoreactivity in layers II-III and IV-VI of the neocortex (C: SYN; D: PSD-95), molecular layer of the dentate gyrus, stratum radiatum of field CA1 and stratum lucidum of field CA3 (E: SYN; F: PSD-95) of untreated and treated euploid and Ts65Dn mice (n=6: 3 males and 3 females for each of the four experimental groups). For each region, data of SYN and PSD-95 optical density are given as fold difference in comparison with untreated euploid mice. Values in (C-F) represent mean ± SE. * $p < 0.05$; ** $p < 0.01$; *** $p < 0.001$ (Fisher LSD after two-way ANOVA). Black asterisks in the gray bar indicate a difference between untreated Ts65Dn mice and treated euploid mice; white asterisks in the black bar indicate a difference between treated Ts65Dn mice and treated euploid mice. Abbreviations: CA1 and CA3, hippocampal fields; DG, dentate gyrus; GR, granule cell layer; LM, stratum lacunosum-moleculare; LUC, stratum lucidum; MOL, molecular layer; OR, stratum oriens; PYR, pyramidal layer; RAD, stratum radiatum.

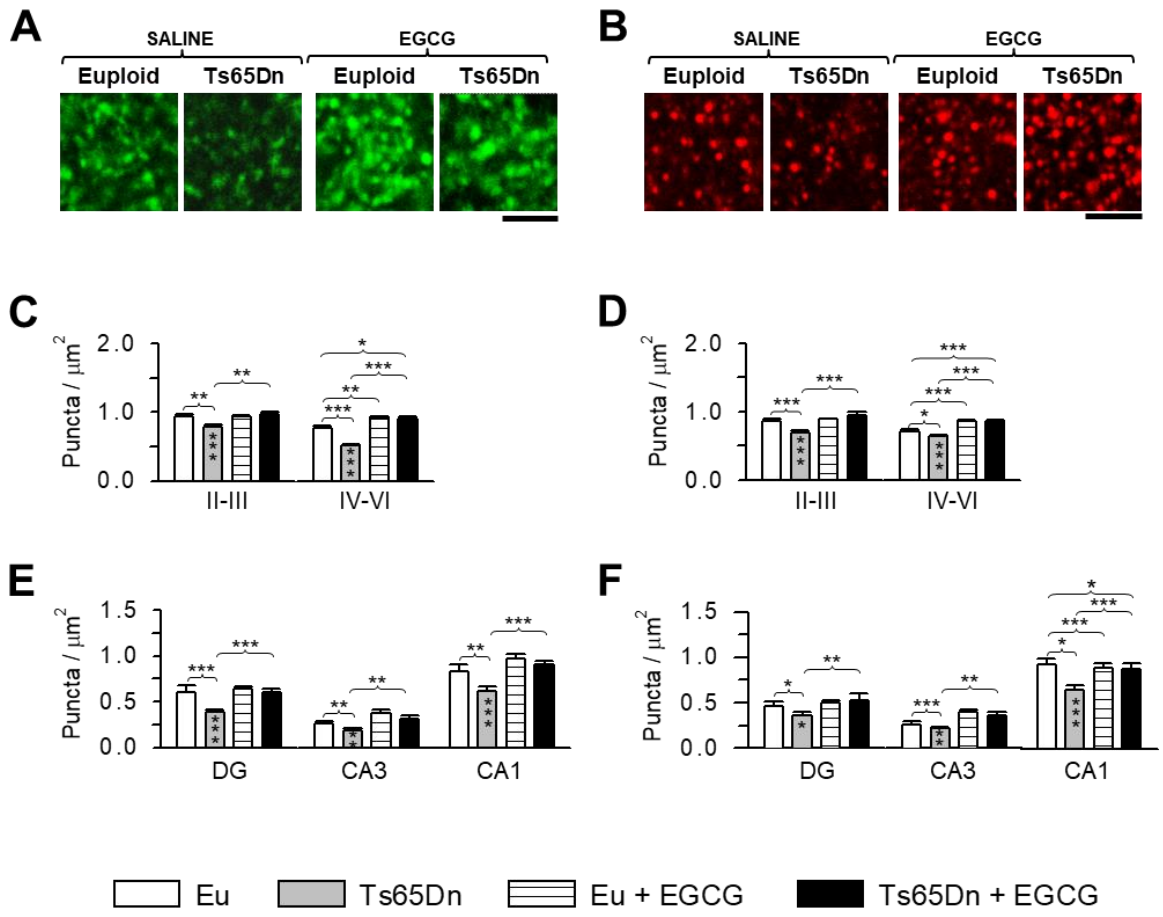

Figure 3.2.7. Effects of neonatal treatment with EGCG on number of synaptic puncta in P15 mice. A, B: Representative confocal microscope images of sections processed for SYN (A) and PSD95 (B) immunofluorescence from the neocortex of an animal of each experimental group. Calibration bar=3 µm. C-F: Number of puncta per µm^2 exhibiting SYN and PSD-95 immunoreactivity in layers II-III and IV-VI of the neocortex (C: SYN; D: PSD-95), molecular layer of the dentate gyrus, stratum lucidum of field CA3, and stratum radiatum of field CA1 (E: SYN; F: PSD-95) of untreated and treated euploid and Ts65Dn mice (n=6: 3 males and 3 females for each of the four experimental groups). Values in C-F represent mean ± SE. * $p < 0.05$; ** $p < 0.01$; *** $p < 0.001$ (Fisher LSD after two-way ANOVA). Black asterisks in the gray bar indicate a difference between untreated Ts65Dn mice and treated euploid mice; white asterisks in the black bar indicate a difference between treated Ts65Dn mice and treated euploid mice. Abbreviations: Eu, euploid; DG, dentate gyrus; CA1 and CA3, hippocampal fields.

treatment. A two-way ANOVA (genotype x treatment) showed a main effect of genotype on body weight [$F(1,35) = 8.67$, $p \leq 0.01$] and brain weight [$F(1,35) = 4.98$, $p \leq 0.05$] in males with nointeraction between genotype x treatment. A main effect of treatment on body weight [$F(1,40) = 4.09$, $p \leq 0.05$] was found in females with no interaction between genotype x treatment (and no effect of treatment). These results suggest that neonatal treatment has no long-term adverse effects on body and brain weight in P45 mice (**Table 3.2.1**).

Long-term effects of neonatal treatment with EGCG on cell survival, cell phenotype and proliferation potency

We evaluated the number and phenotype of BrdU-positive cells present in the DG of P45 mice that had been injected with BrdU at P15 (i.e. at the end of treatment). A two-way ANOVA on the total number of BrdU-positive cells showed no genotype x treatment interaction, a main effect of genotype [$F(1,20) = 24.88$, $p \leq 0.001$], but no effect of treatment. A *post hoc* Fisher LSD test showed that the total number of BrdU-positive cells in untreated Ts65Dn mice was reduced in comparison with euploid mice (**Fig. 3.2.8C**). Unexpectedly, even though neonatal treatment with EGCG had restored the number of BrdU-positive cells in Ts65Dn mice at P15 (**Fig. 3.2.4B**), one month after treatment cessation these positive effects disappeared and the number of their BrdU-positive cells was againreduced in comparison with that of euploid mice (**Fig. 3.2.8C**).

One peculiar characteristic of a trisomic brain is the higher astrocyte/neuron ratio (Guidi et al., 2008, Lu et al., 2012). In order to establish whether neonatal treatment with EGCG had an effect on phenotype acquisition, we evaluated the percentage and number of BrdU/NeuN (a marker of mature neurons), BrdU/GFAP (a marker of astrocytes) double-labeled cells. Additionally, we evaluated the percentage and number of not double-labeled cells (i.e. only marked with BrdU).

A two-way ANOVA on the percentage of BrdU/NeuN cells showed no genotype x treatment interaction, a main effect of genotype [$F(1,20) = 21.62$, $p \leq 0.001$], and no effect of treatment. A *post hoc* Fisher LSD test showed that untreated Ts65Dn mice had a reduced percentage of new neurons in comparison with untreated euploid mice and that treatment did not affect this condition (**Fig. 3.2.8D:**

upper panel). A two-way ANOVA on the number of BrdU/NeuN-positive cells showed no genotype x treatment interaction, a main effect of genotype [$F(1,20) = 37.13$, $p \leq 0.001$], but no effect of treatment. A *post hoc* Fisher LSD test showed that untreated Ts65Dn mice had a reduced number of new neurons in comparison with untreated euploid mice and that this defect was not rescued by treatment (**Fig. 3.2.8D: lower panel**). In euploid mice, no effect of treatment was found on both the percentage and total number of BrdU/NeuN positive cells (**Fig. 3.2.8D**).

A two-way ANOVA on the percentage of BrdU/GFAP-positive cells revealed no genotype x treatment interaction, a main effect of genotype [$F(1,20) = 21.63$, $p \leq 0.001$] and no effect of treatment. A *post hoc* Fisher LSD test showed that untreated Ts65Dn mice had an increased percentage of new astrocytes in comparison with untreated euploid mice and that this defect was not corrected after neonatal treatment with EGCG (**Fig. 3.2.8E: upper panel**). In agreement with results obtained for the percentage of BrdU/GFAP-positive cells, two-way ANOVA analysis on the number of cells with an astrocytic phenotype showed no genotype x treatment interaction and no significant effect of either genotype or treatment. A *post hoc* Fisher LSD test showed no differences between groups (**Fig. 3.2.8E: lower panel**). In euploid mice, no effect of treatment was found either in the percentage or number of new astrocytes (**Fig. 3.2.8E**).

From these results it emerges that early treatment with EGCG has no long-term effect on the abnormal phenotype acquisition that characterizes the trisomic brain.

Long-term effects of neonatal treatment with EGCG on hippocampal proliferation potency and total number of granule cells

We evaluated the number of Ki67-positive cells in the DG of P45 mice in order to evaluate the long-term effects of neonatal treatment with EGCG on the size of the population of NPCs one month after treatment cessation. A two-way ANOVA on the total number of Ki-67-positive cells counted showed no genotype x treatment interaction, a main effect of genotype [$F(1,20) = 26.13$, $p \leq 0.001$], but there was no effect of treatment. A *post hoc* Fisher LSD test showed that treatment was ineffective in P45

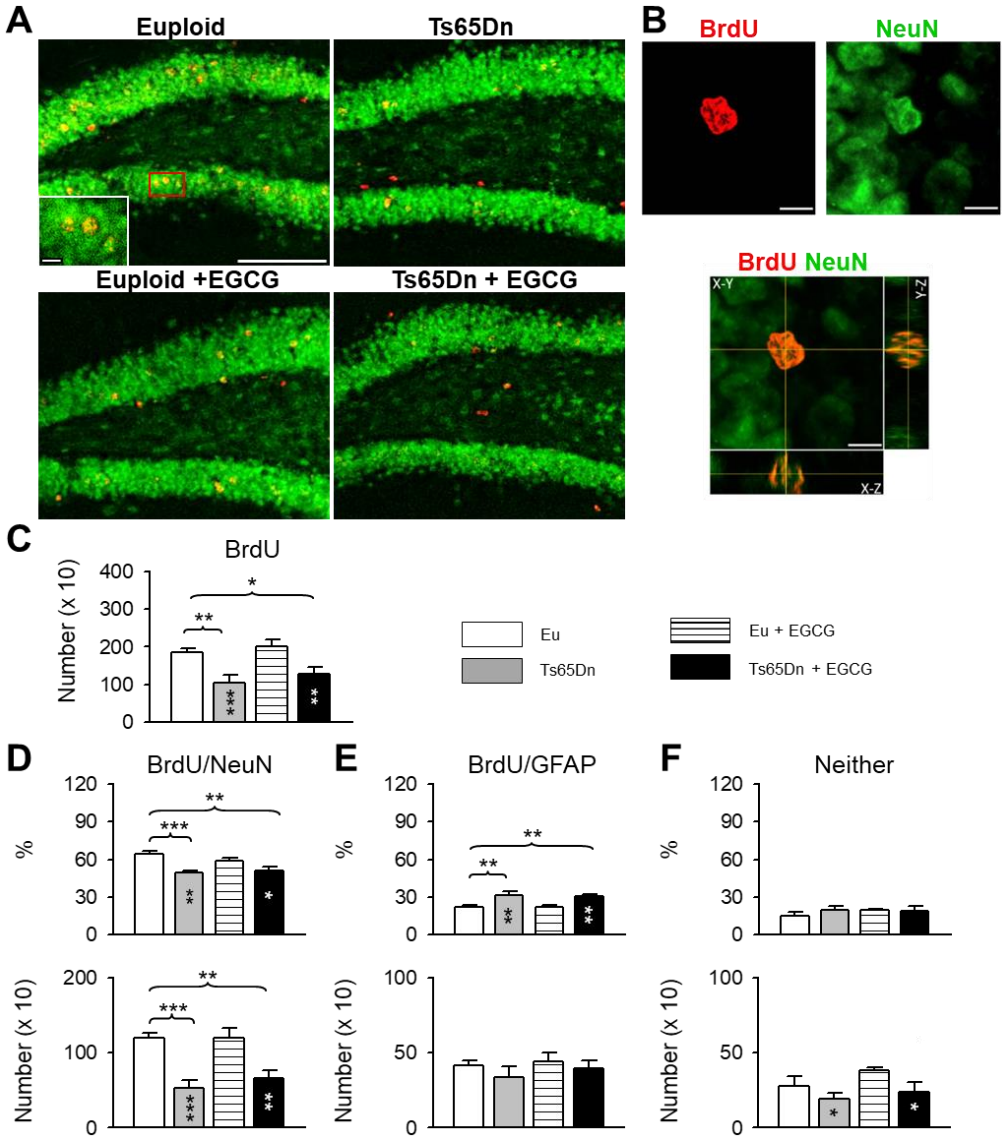

Figure 3.2.8. Long-term effects of neonatal treatment with EGCG on the fate of neural precursor cells of P45 euploid and Ts65Dn mice. A: Representative confocal images of sections processed for fluorescence immunostaining for BrdU/NeuN from the dentate gyrus of an animal from each experimental group. Calibration bar=100 mm. The inset shows a zoomed image of the boxed area with examples of individual BrdU/NeuN-positive cells. Calibration bar=10 mm. B: Confocal laser scanning microscope stack image at higher magnification showing a cell double-labeled for BrdU (red) and NeuN (green) in the dentate gyrus. The BrdU/NeuN-double-labeled cell is shown in x–y orthogonal planes and z-sectioning at 0.5 mm intervals to confirm overlap of the two immunoreactions. Calibration bar=5 µm. C: Total number of BrdU-positive cells in the dentate gyrus of untreated and treated euploid and Ts65Dn mice (n=6: 3 males and 3 females for each of the four experimental groups). Values refer to one hemisphere. These animals were injected with BrdU at P15 and killed at P45. D: Percentage (upper panel) and number (lower panel) of surviving cells with a neuronal phenotype (BrdU/NeuN). E: Percentage (upper panel) and number (lower panel) of surviving cells with an astrocytic phenotype (BrdU/GFAP). F: percentage (upper panel) and number (lower panel) of surviving cells with an undetermined phenotype (Neither) in the DG of untreated and treated euploid and Ts65Dn mice. Same animals as in (C). Values in (C-F) are mean ± SE. * $p < 0.05$; ** $p < 0.01$; *** $p < 0.001$ (Fisher LSD test after two-way ANOVA). Black asterisks in the gray bar indicate a difference between untreated Ts65Dn mice and treated euploid mice; white asterisks in the black bar indicate a difference between treated Ts65Dn mice and treated euploid mice. Abbreviations: BrdU, bromodeoxyuridine; Eu, euploid.

Ts65Dn mice since the number of Ki-67-positive cells was not increased (**Fig. 3.2.9A**). Neither was there any effect of treatment in euploid mice (**Fig. 3.2.9A**). A two-way ANOVA on the density of Ki-67-positive cells showed no genotype x treatment interaction, a main effect of genotype [$F(1,20) = 21.33$, $p \leq 0.001$], but no effect of treatment. A *post hoc* Fisher LSD test showed that in P45 Ts65Dn and euploid mice the density of Ki-67-positive was not increased by treatment (**Fig. 3.2.9B**). In P45 mice, similarly to P15 mice, a two-way ANOVA analysis on the number of caspase-3-positive cells in the DG showed that there were no genotype x treatment interactions and no effects of either genotype or treatment (**Fig. 3.2.9C**). A two-way ANOVA on p21 protein levels in in the hippocampus of P45 mice showed no genotype x treatment interaction; a main effect of genotype [$F(1,20) = 7.00$, $p \leq 0.05$], but no effect of treatment. A *post hoc* Fisher LSD test showed that in P45 treated Ts65Dn mice p21 levels did not undergo a reduction and were still higher in comparison with euploid mice (**Fig. 3.2.9D**). In treated P45 euploid mice, p21 levels were unaffected by treatment (**Fig 3.2.9D**).

We then stereologically examined the DG of P45 mice in order to establish whether the restoration of cellularity observed in P15 mice was retained with time. A two-way ANOVA on the volume of the granule cell layer showed no genotype x treatment interaction; a main effect of genotype [$F(1,20) = 17.80$, $p \leq 0.001$], but no effect of treatment. A *post hoc* Fisher LSD test showed that in Ts65Dn mice the volume of the granule cell layer was not increased by treatment and remained reduced in comparison with that of euploid mice (**Fig. 3.2.9E**), indicating no retention of short-term effects. A two-way ANOVA on granule cell density showed a genotype x treatment interaction [$F(1,20) = 4.39$, $p \leq 0.05$] and a main effect of both genotype [$F(1,20) = 26.76$, $p \leq 0.001$] and treatment [$F(1,20) = 5.85$, $p \leq 0.05$]. A *post hoc* Fisher LSD test showed that treated Ts65Dn mice had no improvement when compared with untreated euploid mice. Surprisingly, in euploid mice treatment caused a small but significant reduction in granule cell density (**Fig. 3.2.9F**). A two-way ANOVA on total granule cell number showed no genotype x treatment interaction, a main effect of genotype [$F(1,20) = 32.15$, $p \leq 0.001$], but no effect of treatment. A *post hoc* Fisher LSD test showed that untreated Ts65Dn mice had a reduced number of granule neurons in comparison with euploid mice and that this defect was

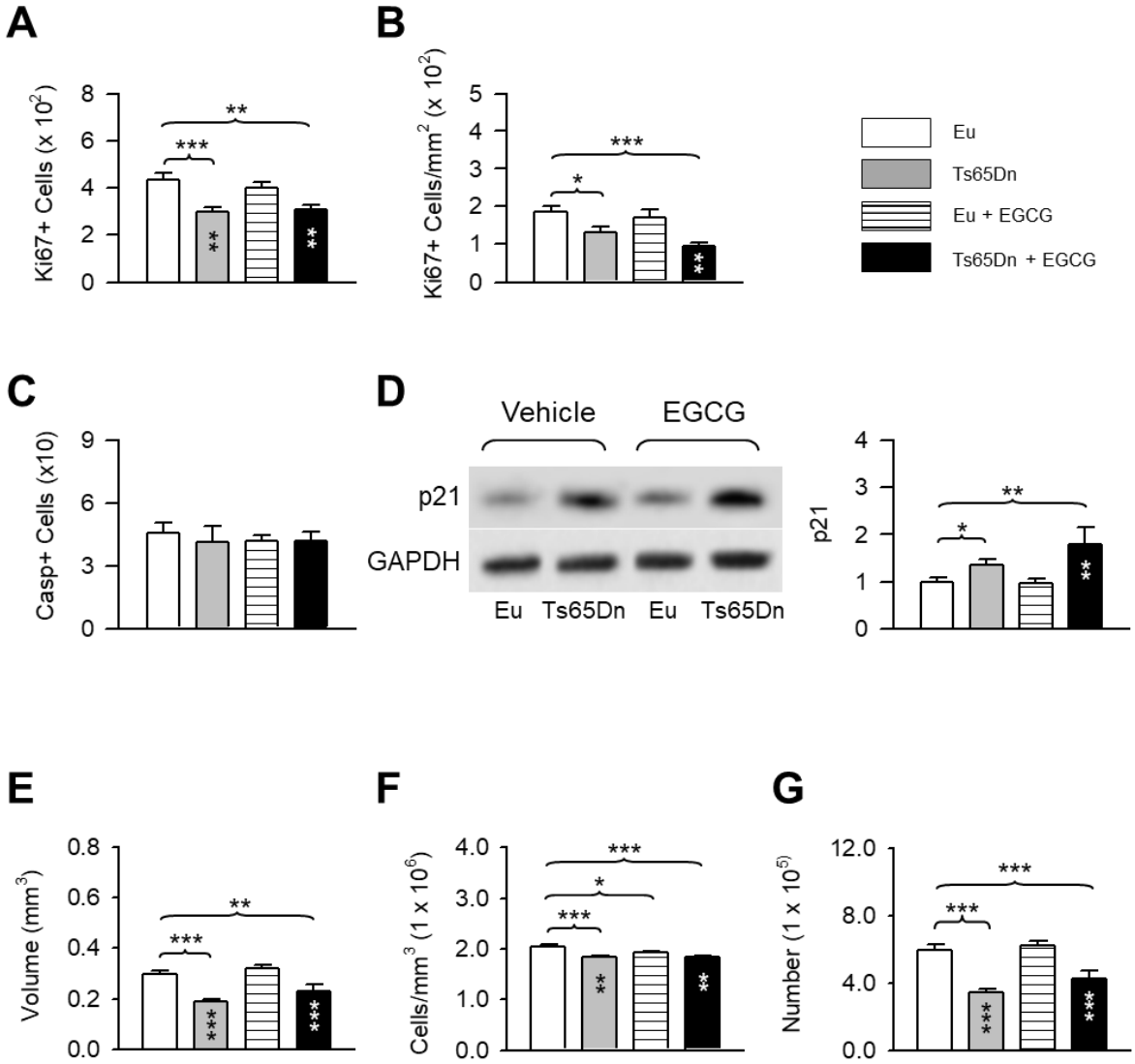

Figure 3.2.9. Long-term effects of neonatal treatment with EGCG on neural precursor cell number and granule cell number in the dentate gyrus of P45 Ts65Dn and euploid mice. A-C: Ki-67 positive cells, expressed as total cell count (A) and cells/mm^2 (B), and cleaved caspase-3 positive cells, expressed as total cell count (C), in the dentate gyrus of untreated and treated euploid and Ts65Dn mice (n=6: 3 males and 3 females for each of the four experimental groups). D: Western blot analysis of p21 levels in the hippocampal formation of untreated and treated euploid and Ts65Dn mice (n=6: 3 males and 3 females for each of the four experimental groups). Western blots (left) are examples taken from one animal from each experimental group. Histograms (right) show p21 levels normalized to GAPDH and expressed as a fold difference in comparison with untreated euploid mice. E-G: Volume of the granule cell layer (E), density of granule cells (F) and total number of granule cells (G) in untreated and treated euploid and Ts65Dn mice (n=6: 3 males and 3 females for each of the four experimental groups). Values (mean ± SE) in (A-G) refer to one hemisphere. * $p < 0.05$; ** $p < 0.01$; *** $p < 0.001$ (Fisher LSD test after two-way ANOVA). Black asterisks in the gray bar indicate a difference between untreated Ts65Dn mice and treated euploid mice; white asterisks in the black bar indicate a difference between treated Ts65Dn mice and treated euploid mice. Abbreviations: Casp, caspase-3; Eu, euploid.

not rescued by treatment (**Fig. 3.2.9G**).

Long-term effects of neonatal treatment with EGCG on cortical and hippocampal synapses

In P45 mice, we evaluated the long-term effects of neonatal EGCG treatment on the expression of SYN and PSD-95 in the same regions examined in P15 mice, in order to compare the outcomes. A two-way ANOVA on the OD of SYN and PSD-95 and revealed no genotype x treatment interactions, a main effect of genotype in most of the examined regions and a main effect of treatment in a few regions (summarized in **Table 3.2.3**). Similar results were obtained after two-way ANOVA on the number of SYN and PSD-95 immunoreactive puncta (**Table 3.2.3**). A *post hoc* Fisher LSD test showed that untreated Ts65Dn mice had OD levels of SYN and PSD-95 and a number of puncta smaller than in untreated euploid mice in the neocortex, DG, field CA3 and field CA1 (**Fig. 3.2.10C,D; Fig. 3.2.11C,D**). This evidence indicates that trisomy-linked defects in synapse development do not ameliorate in mice aged P45. In addition, similarly to the other morphological parameters analyzed in this study, the positive effects of neonatal treatment with EGCG on synaptic proteins seen in Ts65Dn mice did not outlast treatment cessation. Rather, in the DG and field CA1 the immunoreactivity for SYN was reduced in comparison with untreated Ts65Dn mice (**Fig. 3.2.10E**). Some negative effects of treatment took place in the hippocampal region of treated euploid mice, in which a reduction in the OD of both SYN and PSD-95 was observed (**Fig. 3.2.10D,F**).

Effects of treatment with EGCG on GSK3β protein levels and phosphorylation

The main activity of EGCG is to inhibit DYRK1A, but there is evidence that this catechin has also antioxidant properties (Kim et al., 2014), acts on the Shh pathway (Wang et al., 2012), activates a pro-survival PKC pathway (Kelsey et al., 2010), activates the MEK-ERK pathway (Spencer, 2009), and stimulates the activity of ERK-dependent cyclic AMP response element (Schroeter et al., 2007). Thus, various mechanisms may take part in the positive effects induced by treatment with EGCG. Recent evidence shows that EGCG is able to increase the phosphorylation levels of GSK3β at ser9

Table 3.2.3. Two-way ANOVA of SYN and PSD-95 measurements in P15 and P45 mice.

Measurement	Region	Variable	Main effect				Two-way interaction	
			GEN		TREAT		GEN x TREAT	
			F(1,20)	p	F(1,20)	p	F(1,20)	p
P15 mice								
SYN	Cx (II-III)	OD	1.09	n.s.	24.40	0.0005	9.02	0.01
		Puncta	4.93	0.05	10.45	0.005	4.27	0.05
	Cx (IV-VI)	OD	2.48	n.s.	31.22	0.0005	6.27	0.05
		Puncta	14.14	0.001	47.44	0.0005	7.58	0.01
	DG (Mol)	OD	24.35	0.0005	7.84	0.01	2.29	n.s.
		Puncta	12.26	0.01	12.09	0.005	6.47	0.05
	CA3 (Luc)	OD	0.39	n.s.	31.16	0.0005	12.48	0.005
		Puncta	8.37	0.01	24.64	0.0005	0.07	n.s.
	CA1 (Rad)	OD	3.28	n.s.	28.87	0.0005	1.68	n.s.
		Puncta	8.09	0.01	20.57	0.0005	2.71	n.s.
PSD-95	Cx (II-III)	OD	0.71	n.s.	31.43	0.0005	2.28	n.s.
		Puncta	5.68	0.05	13.87	0.001	14.19	0.001
	Cx (IV-VI)	OD	0.00	n.s.	26.22	0.0005	5.77	0.05
		Puncta	0.43	n.s.	28.79	0.0005	1.17	n.s.
	DG (Mol)	OD	0.31	n.s.	28.74	0.0005	3.38	n.s.
		Puncta	1.35	n.s.	7.65	0.05	3.25	n.s.
	CA3 (Luc)	OD	0.70	n.s.	29.07	0.0005	11.71	0.005
		Puncta	10.02	0.005	5.14	0.05	9.41	0.01
	CA1 (Rad)	OD	0.08	n.s.	30.14	0.0005	4.83	0.05
		Puncta	6.90	0.05	32.17	0.0005	0.23	n.s.
P45 mice								
SYN	Cx (II-III)	OD	14.50	0.001	1.21	n.s.	0.79	n.s.
		Puncta	10.60	0.01	0.02	n.s.	0.07	n.s.
	Cx (IV-VI)	OD	21.83	0.0005	0.30	n.s.	3.23	n.s.
		Puncta	8.20	0.01	0.00	n.s.	0.14	n.s.
	DG (Mol)	OD	20.07	0.0005	7.72	0.05	0.38	n.s.
		Puncta	11.19	0.005	0.61	n.s.	0.05	n.s.
	CA3 (Luc)	OD	3.37	n.s.	15.58	0.001	3.93	n.s.
		Puncta	21.01	0.0005	2.06	n.s.	0.87	n.s.
	CA1 (Rad)	OD	17.08	0.001	11.86	0.005	0.78	n.s.
		Puncta	20.64	0.0005	0.55	n.s.	0.01	n.s.
PSD-95	Cx (II-III)	OD	26.11	0.0005	0.01	n.s.	2.18	n.s.
		Puncta	12.96	0.005	2.99	n.s.	0.11	n.s.
	Cx (IV-VI)	OD	17.23	0.0005	1.84	n.s.	0.90	n.s.
		Puncta	14.98	0.001	0.04	n.s.	0.03	n.s.
	DG (Mol)	OD	25.27	0.0005	2.90	n.s.	0.42	n.s.
		Puncta	22.70	0.0005	0.36	n.s.	0.00	n.s.
	CA3 (Luc)	OD	6.15	0.01	1.60	n.s.	4.26	0.05
		Puncta	18.18	0.0005	0.01	n.s.	0.43	n.s.
	CA1 (Rad)	OD	13.92	0.001	7.18	0.05	4.01	n.s.
		Puncta	14.63	0.001	1.99	n.s	0.01	n.s.

The F and p values of two-way ANOVA with genotype (euploid, Ts65Dn) and treatment (vehicle, EGCG) as factors are reported for the optical density of SYN and PSD-95, and number of SYN and PSD-95 immunoreactive puncta. The p values are reported as: $p < 0.05$, 0.01, 0.005, 0.001, 0.0005. n.s.: not significant. Abbreviations: Cx, cortex; DG, dentate gyrus; GEN, genotype; Luc, stratum lucidum; Mol stratum moleculare; OD, optical density, PSD-95, postsynaptic density protein-95; Rad, stratum radiatum; SYN, synaptophysin; TREAT, treatment.

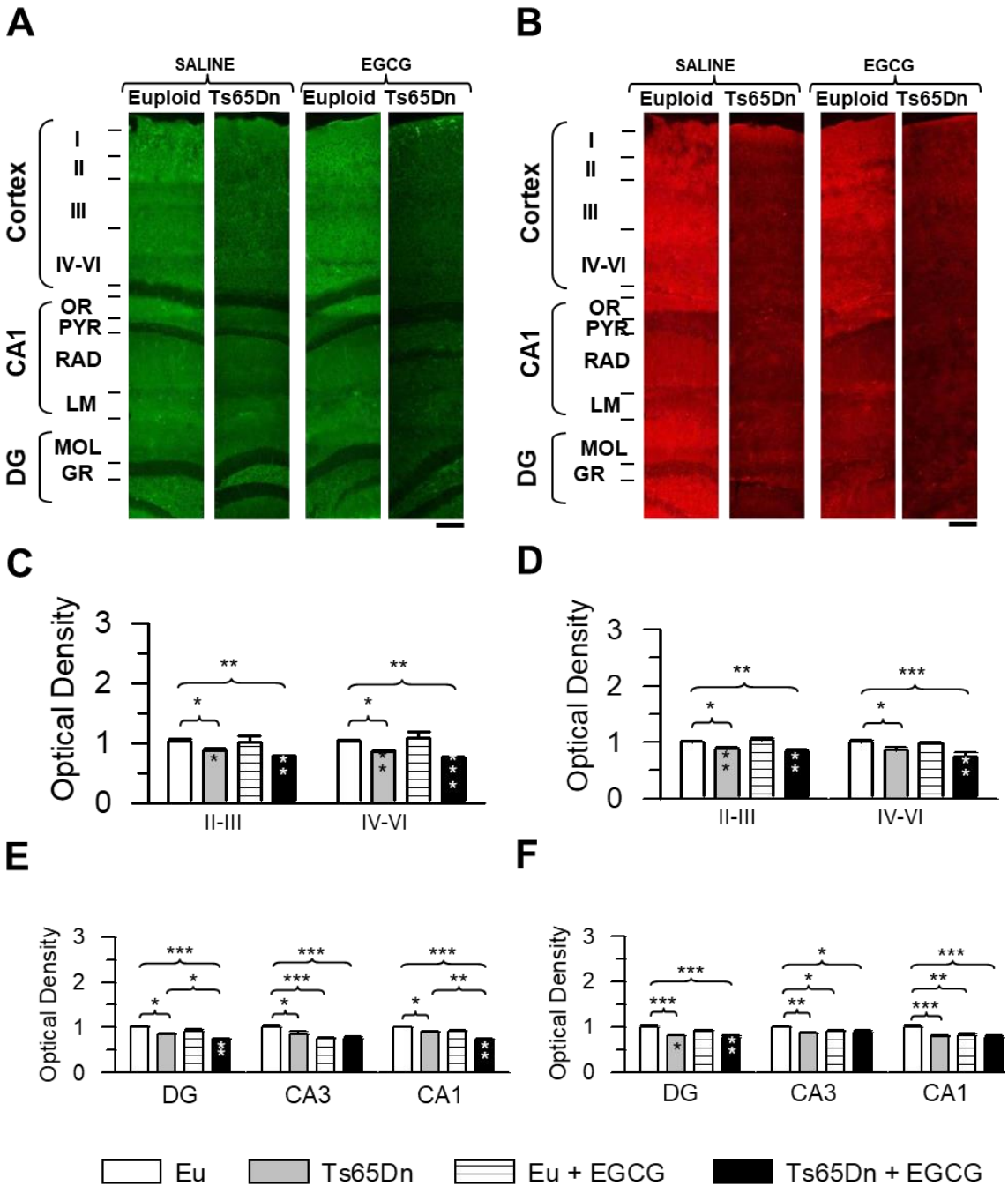

Figure 3.2.10. Long-term effects of neonatal treatment with EGCG on synapse development in P45 Ts65Dn and euploid mice. A, B: Sections processed for SYN (A) and PSD-95 (B) immunofluorescence from the neocortex overlying the hippocampus, hippocampal field CA1, and DG of an animal from each experimental group. Calibration bar=200 μm. C-F: Optical density of SYN and PSD-95 immunoreactivity in layers II-III and IV-VI of the neocortex (C: SYN; D: PSD-95), molecular layer of the dentate gyrus, stratum lucidum of field CA3, and stratum radiatum of field CA1 (E: SYN; F: PSD-95) of untreated and treated euploid and Ts65Dn mice (n=6: 3 males and 3 females for each of the four experimental groups). For each region, data of SYN and PSD-95 optical density are given as a fold difference compared to untreated euploid mice. Values in C-F represent mean ± SE. * $p < 0.05$; ** $p < 0.01$; *** $p < 0.001$ (Fisher LSD test after two-way ANOVA). Black asterisks in the gray bar indicate a difference between untreated Ts65Dn mice and treated euploid mice; white asterisks in the black bar indicate a difference between treated Ts65Dn mice and treated euploid mice. Abbreviations: CA1 and CA3, hippocampal fields; DG, dentate gyrus; Eu, euploid; GR, granule cell layer; LM, stratum lacunosum-moleculare; LUC, stratum lucidum; MOL, molecular layer; OR, stratum oriens; PYR, pyramidal layer; RAD, stratum radiatum.

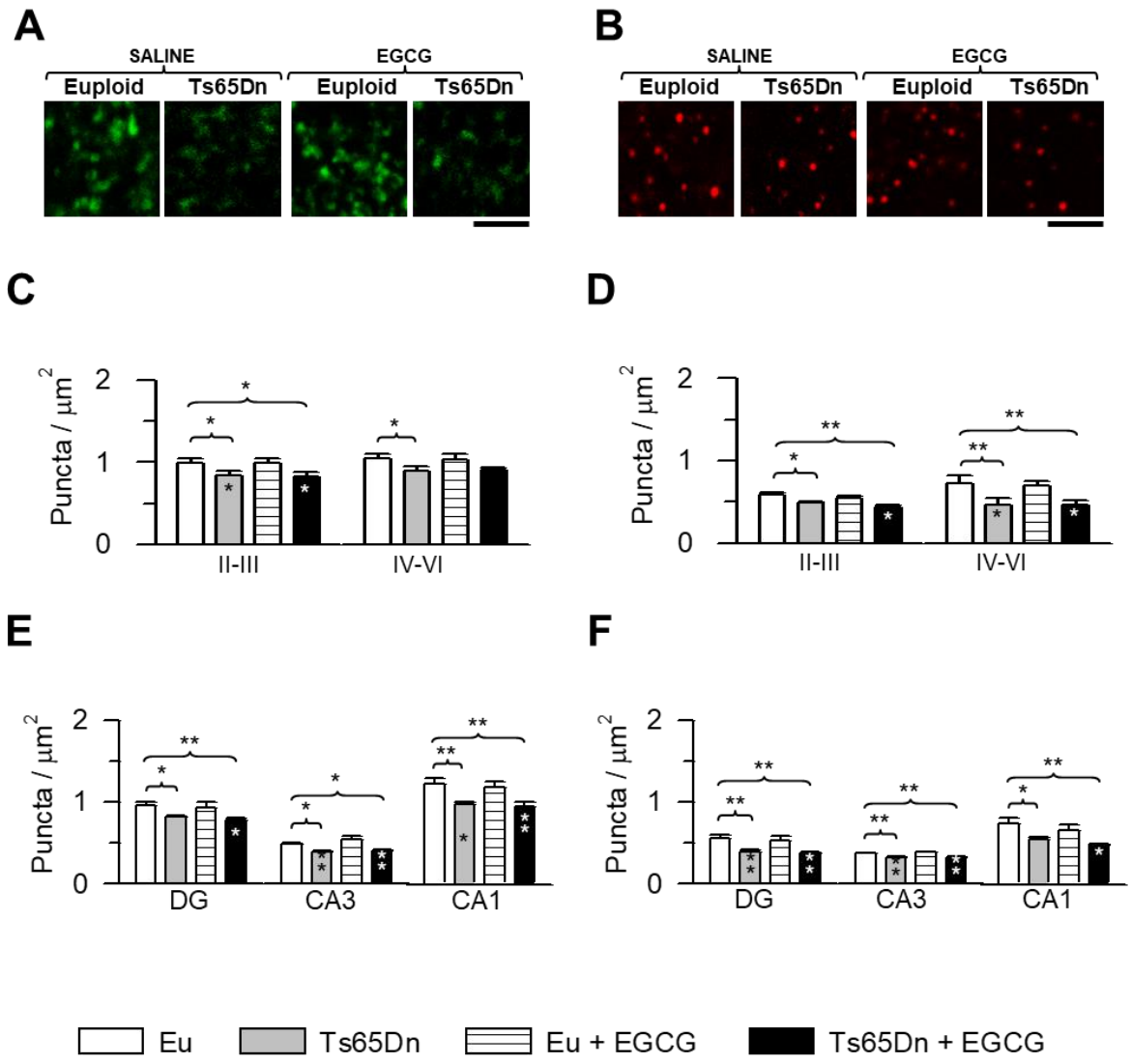

Figure 3.2.11. Effects of neonatal treatment with EGCG on number of synaptic puncta in P45 mice. A, B: Representative confocal microscope images of sections processed for SYN (A) and PSD-95 (B) immunofluorescence from the neocortex of an animal of each experimental group. Calibration bar=3 μm. C-F: Number of puncta per μm^2 exhibiting SYN and PSD-95 immunoreactivity in layers II-III and IV-VI of the neocortex (C: SYN; D: PSD-95), molecular layer of the dentate gyrus, stratum lucidum of field CA3, and stratum radiatum of field CA1 (E: SYN; F: PSD-95) of untreated and treated euploid and Ts65Dn mice (n=6: 3 males and 3 females for each of the four experimental groups). Values in C-F represent mean ± SE. * $p < 0.05$; ** $p < 0.01$; *** $p < 0.001$ (Fisher LSD after two-way ANOVA). Black asterisks in the gray bar indicate a difference between untreated Ts65Dn mice and treated euploid mice; white asterisks in the black bar indicate a difference between treated Ts65Dn mice and treated euploid mice. Abbreviations: Eu, euploid; DG, dentate gyrus; CA1 and CA3, hippocampal fields.

in neurons (Lin et al., 2009, Ruan et al., 2009), thereby inhibiting its activity. GSK3β is a serine/threonine kinase that plays a fundamental role in various biological processes (Jope and Johnson, 2004) at physiological levels. Altered GSK3β activity appears to be involved in neurodegenerative and neurological disturbances (Eldar-Finkelman and Martinez, 2011). In fact, when GSK3β is over-activated, it causes reduction in neurogenesis and impairment of synapse development (Eldar-Finkelman and Martinez, 2011, Kim and Snider, 2011). As previously shown in this thesis (see **Section 3.1**), in the hippocampus of P15 Ts65Dn mice GSK3β is dephosphorylated at ser9.

Based on these premises, we wondered whether treatment with EGCG affects the GSK3β phosphorylation state. Thus, we examined the levels of ser9 phosphorylated GSK3β (pGSK3β) and total GSK3β levels in hippocampal homogenates of P15 and P45 mice. In P15 mice, a two-way ANOVA on pGSK3β levels showed no genotype x treatment interaction, no significant effect of genotype, but a main effect of treatment [$F(1,20) = 33.75$, $p \leq 0.001$]. A *post hoc* Fisher LSD test confirmed (see **Section 3.1** of the thesis) that in the hippocampus of untreated Ts65Dn mice there were reduced levels of pGSK3β in comparison with euploid mice. Treatment with EGCG increased pGSK3β levels, that reached those of untreated euploid mice (**Fig. 3.2.12A,B**). A similar effect of EGCG treatment was also seen in euploid mice (**Fig. 3.2.12A,B**). A two-way ANOVA on total levels of GSK3β showed no genotype x treatment interaction, but did show a main effect of both genotype [$F(1,20) = 5.04$, $p \leq 0.05$] and treatment [$F(1,20) = 18.83$, $p \leq 0.001$]. A *post hoc* Fisher LSD test showed that while in untreated Ts65Dn mice there were higher total levels of GSK3β, in treated Ts65Dn mice levels of GSK3β underwent a large reduction (**Fig. 3.2.12A,C**). In P45 mice, a two-way ANOVA on pGSK3β levels showed no genotype x treatment interaction, a main effect of genotype [$F(1,20) = 12.90$, $p \leq 0.001$], but no effect of treatment. A *post hoc* Fisher LSD test showed that Ts65Dn mice exhibited reduced hippocampal levels of pGSK3β (**Fig. 3.2.12D,E**) in comparison with euploid mice also at P45. However, treated Ts65Dn mice aged 45 days did not exhibit any change in pGSK3β (**Fig. 3.2.12D,E**). A two-way ANOVA on total levels of GSK3β showed no

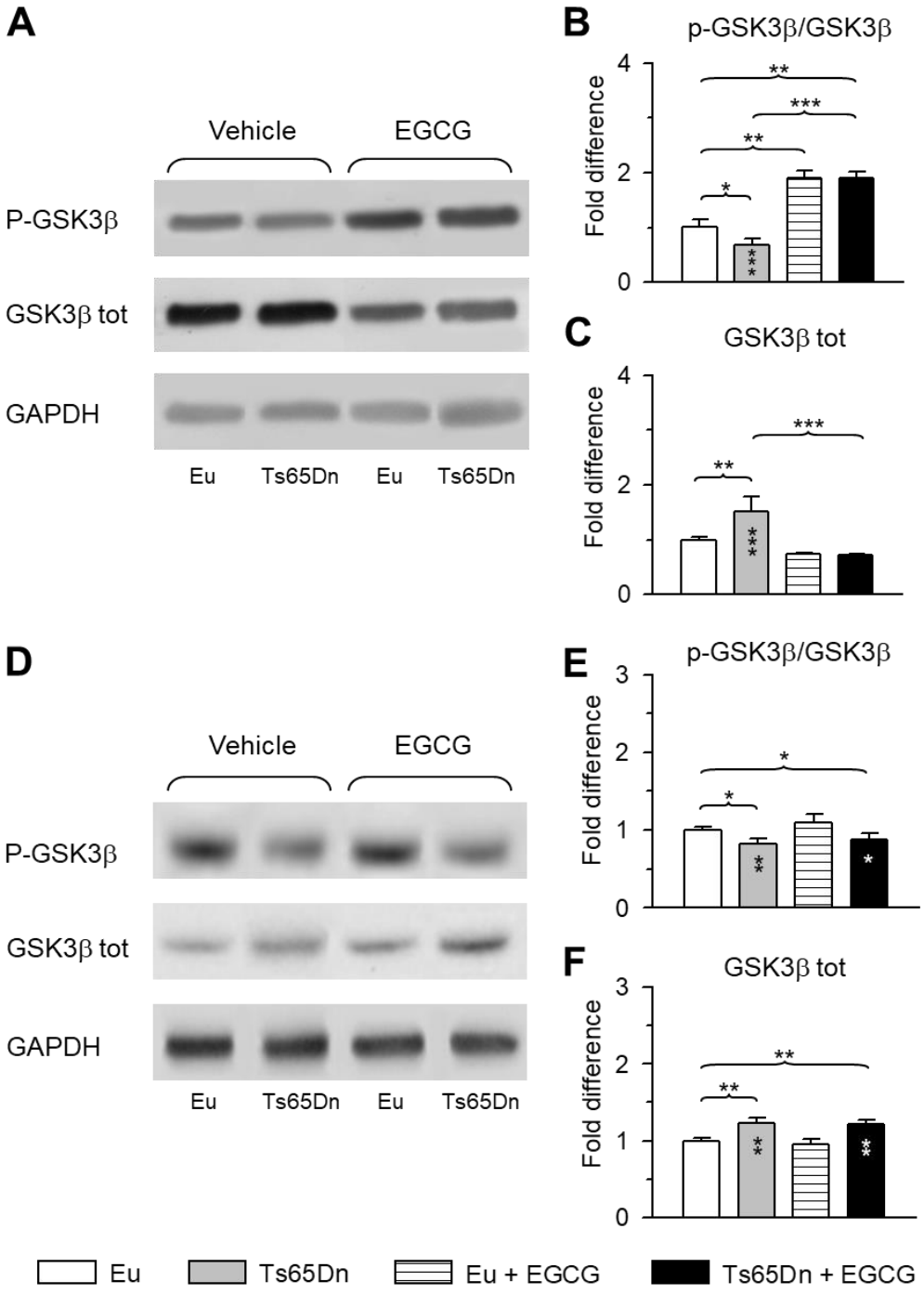

Figure 3.2.12. **Short- and long-term effects of neonatal treatment with EGCG on GSK3β protein expression in P15 and P45 Ts65Dn and euploid mice.** Western blot analysis of p-GSK3β, total GSK3β and GAPDH in the hippocampus of untreated and treated euploid and Ts65Dn mice at P15 (A-C) and P45 (D-F). At each age: n=6 (3 males and 3 females) for each experimental group. Western blots in (A, D) are examples from P15 (A) and P45 (D) animals from each experimental group. Histograms in (B, E) show p-GSK3β levels normalized to total GSK3β in P15 (B) and P45 (E) mice. Histograms in (C, F) show total GSK3β normalized to GAPDH in P15 (C) and P45 (F) mice. Values in (B, C, E, F) are expressed as fold difference in comparison with untreated euploid mice. Values in (B, C, E, F) are mean ± SE. * $p < 0.05$; ** $p < 0.01$; *** $p < 0.001$ (Fisher LSD test after two-way ANOVA). Black asterisks in the gray bar indicate a difference between untreated Ts65Dn mice and treated euploid mice; white asterisks in the black bar indicate a difference between treated Ts65Dn mice and treated euploid mice. Abbreviation: Eu, euploid.

genotype x treatment interaction, a main effect of genotype [$F(1,20) = 9.10$, $p \leq 0.01$], but no effect of treatment. A *post hoc* Fisher LSD test showed that Ts65Dn mice aged 45 days exhibited increased levels of total GSK3β (**Fig. 3.2.12D,F**) in comparison with euploid mice and that treatment had no effects in total levels of GSK3β in both euploid and Ts65Dn mice (**Fig. 3.2.12D,F**).

Effects of neonatal treatment with EGCG on hippocampus-dependent learning and memory

In order to explore the effects of a neonatal treatment with EGCG on hippocampus-dependent spatial learning and memory (Crawley, 2007), animals were subjected to behavioral tasks starting at P45, i.e. 25-30 days after treatment cessation. We used the Y-maze (YM) test and the Morris Water Maze (MWM) test.

Regarding the YM test, we compared the rate of spontaneous alternations and the number of arm entries for Ts65Dn and euploid mice. A two-way ANOVA revealed no genotype x treatment interaction, a main effect of genotype [$F(1,77) = 18.60$, $p \leq 0.0001$], but there was no significant effect of treatment. A *post hoc* Fisher LSD test showed that untreated Ts65Dn mice had a lower alternation rate in comparison with euploid mice (**Fig. 3.2.13A**). This defect was not improved by neonatal treatment with EGCG (**Fig. 3.2.13A**). The YM also provides estimation of spontaneous locomotor activity. A two-way ANOVA revealed no genotype x treatment interaction; a main effect of genotype [$F(1,77) = 5.50$, $p \leq 0.05$], but no effect of treatment. A *post hoc* Fisher LSD test showed that untreated and treated Ts65Dn had a larger number of entries in comparison with untreated euploid mice, although the difference was statistically significant only for treated mice (**Fig. 3.2.13B**). This evidence indicates that treatment did not improve either impaired working memory or enhanced spontaneous locomotor activity in Ts65Dn mice (Faizi et al., 2011).

A three-way mixed ANOVA, with genotype and treatment as grouping factors and day as a repeated measure revealed a genotype x day interaction [$F(4,316) = 5.73$, $p \leq 0.001$], a main effect of genotype [$F(1,79) = 104.99$, $p \leq 0.0001$] and day [$F(4,316) = 22.22$, $p \leq 0.0001$]. We found no genotype x treatment x day, genotype x treatment, treatment x day interactions or a main effect of treatment. A

post hoc Fisher LSD analysis showed that, on all of the examined days, untreated and treated Ts65Dn mice exhibited a poorer performance compared to untreated euploid mice (**Fig. 3.2.13C**). Similarly to Ts65Dn mice, in euploid mice treatment had no effect on the learning curve. A comparison of treated and untreated Ts65Dn mice showed no latency difference on days 1-4 but on day 5 treated Ts65Dn exhibited a latency reduction compared to untreated Ts65Dn mice ($p \leq 0.05$). Considering the absence of any genotype x treatment x day interaction (see above), it is possible that this difference is related to an "experiment-wise" error due to multiple comparisons across days rather than a learning improvement. Regarding the probe test, a two-way ANOVA revealed i) no genotype x treatment interaction, a main effect of genotype [$F(1,79) = 14.38$, $p \leq 0.001$], but no effect of treatment on latency; ii) no genotype x treatment interaction, a main effect of genotype [$F(1,79) = 15.78$, $p \leq 0.001$], but no effect of treatment on the percentage of time; and iii) no genotype x treatment interaction, a main effect of genotype [$F(1,79) = 17.00$ $p \leq 0.0001$] but no effect of treatment on the frequency. A *post hoc* Fisher LSD test revealed that untreated Ts65Dn mice performed worse than untreated euploid mice in all parameters analyzed in the probe test. In fact, they showed an increase in latency to enter the trained platform quadrant (**Fig. 3.2.13D**), a reduction in the time spent there (**Fig. 3.2.13E**), and a decrease in the frequency of entrances (**Fig. 3.2.13F**). In neonatally-treated euploid and Ts65Dn mice none of these parameters underwent an improvement in comparison with their untreated counterparts (**Fig. 3.2.13D-F**).

3.2.5 Discussion

In this study, we examined the effects of neonatal treatment with EGCG on hippocampal development in the Ts65Dn model of DS. The results show that pharmacotherapy with EGCG in the first two postnatal weeks fully rescues neural precursor cell proliferation and cellularity, as well as synapse development in Ts65Dn pups. However, these effects vanish with time and do not lead to an improvement in hippocampus-dependent long-term memory in young adult mice. Thus, therapy with

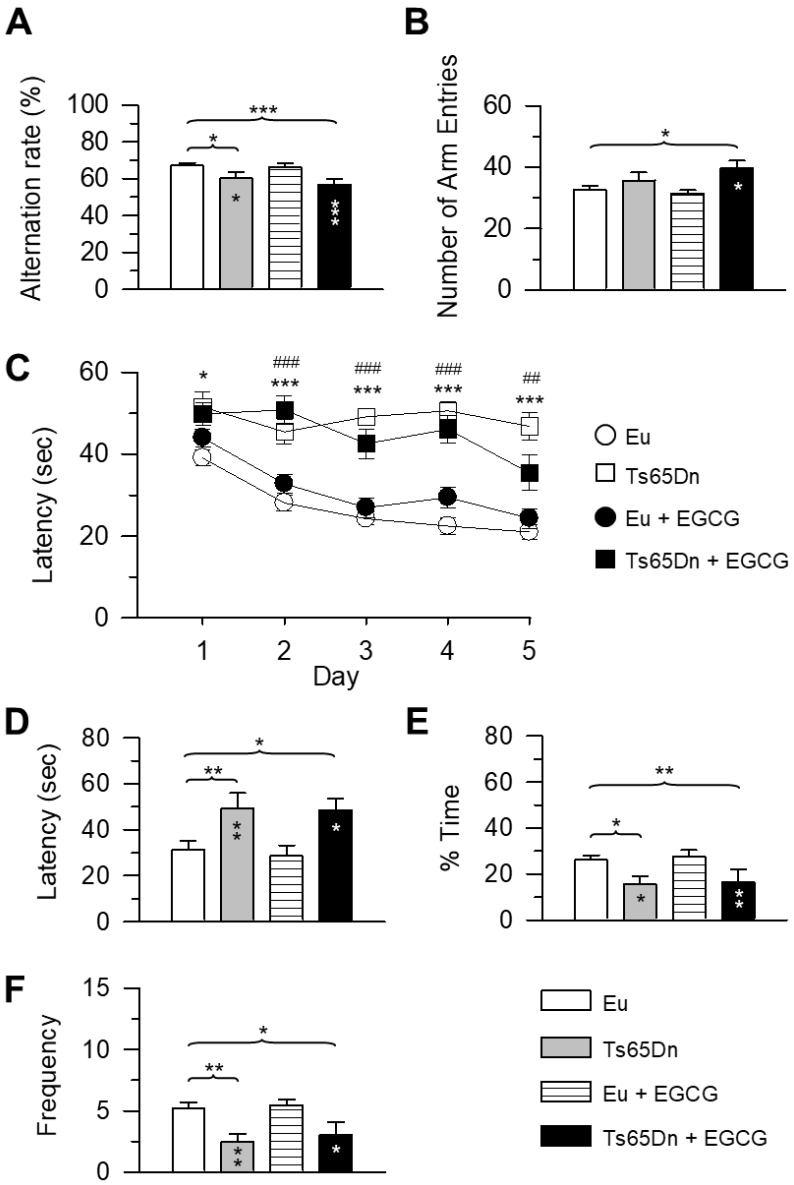

Figure 3.2.13. Long-term effects of neonatal treatment with EGCG on spatial learning in Ts65Dn and euploid mice. These mice received either saline or EGCG in the period P3-P15 and were behaviorally tested starting from 9 days before reaching 45-50 days of age (i.e. from 36-41 days old, for 9 days). A, B: Working memory performance in the Y-maze. Percentage of spontaneous alternations (A) and number of arm entries (B) in the Y-maze test in untreated euploid mice (n=37: 17 males and 20 females), untreated Ts65Dn mice (n=9: 5 males and 4 females), treated euploid mice (n=25: 12 males and 13 females), and treated Ts65Dn mice (n=10: 5 males and 5 females). C-F: Spatial learning and memory assessed with the Morris Water Maze in untreated euploid mice (n=38: 17 males and 21 females), untreated Ts65Dn mice (n=10: 5 males and 5 females), treated euploid mice (n=25: 12 males and 13 females), and treated Ts65Dn mice (n=10: 5 males and 5 females). The learning curves (C) reports data of euploid mice that received either saline (empty circle) or EGCG (filled circle) and Ts65Dn mice that received either saline (empty square) or EGCG (filled square). The symbols * and # indicate a difference between untreated euploid and untreated Ts65Dn mice, and between untreated euploid and treated Ts65Dn mice, respectively. Values represent mean ± SE. * $p < 0.05$; ** $p< 0.01$; *** $p < 0.001$; ## $p < 0.01$; ### $p < 0.001$ (Fisher LSD test after ANOVA). Black asterisks in the gray bar indicate a difference between untreated Ts65Dn mice and treated euploid mice; white asterisks in the black bar indicate a difference between treated Ts65Dn mice and treated euploid mice. Abbreviation: Eu, euploid; sec, seconds.

EGCG even during a particularly critical period for development of the hippocampus has no enduring effects on trisomic brain physiology.

Early treatment with EGCG restores hippocampal development in Ts65Dn pups

Neurogenesis failure and neuronal maturation are the major neurodevelopmental defects of the trisomic brain (reviewed by (Bartesaghi et al., 2011, Dierssen, 2012)). Among the triplicated genes, *Dyrk1A* is likely to play a key role in disrupting neurodevelopment. Some studies have already shown that treatment with EGCG, an inhibitor of DYRK1A and other kinases (see (Aranda et al., 2011)), restores hippocampus-dependent learning in adult Ts65Dn mice (De la Torre et al., 2014), even though there is no evidence regarding the neuroanatomical substrate of the positive effects of EGCG in the Ts65Dn mouse. Moreover, no study has investigated the effect of early treatment with EGCG in the Ts65Dn mouse. We found that neonatal treatment with EGCG restores i) the pool of proliferating NPCs (Ki-67-positive cells) in the SVZ and SGZ, with no effect on cell death (caspase-3-positive cells); ii) the number of cells in the S-phase of the cell cycle (BrdU-positive cells) in the DG; iii) the number of granule neurons in the hippocampal DG; iv) development of hippocampal as well as of neocortical synapses in trisomic pups.

In Ts65Dn mice aged 15 and 45 days p21 hippocampal levels were higher in comparison with euploid mice. In P15 Ts65Dn mice, treatment largely reduced p21 levels, suggesting that this effect may play a role in the restoration of neurogenesis. In contrast, in treated P45 Ts65Dn mice p21 protein levels returned to be high. This may explain the disappearance of the improvement in proliferation potency seen in P15 Ts65Dn mice. Since expression of p21 is regulated in a p53-dependent and independent manner (Macleod et al., 1995, Jung et al., 2010), EGCG may modulate p21 levels by inhibiting the DYRK1A-p53 pathway (Park et al., 2010). Importantly, restoration of NPCs proliferation in P15 mice translated into an increase in total granule cell number, indicating that an early treatment with EGCG may is able to restore the typical hypotrophy of the DG of the trisomic brain.

There is a number of evidence that green tea catechins up-regulates synaptic plasticity-related proteins

(Li et al., 2007, Rodrigues et al., 2013). Consistently with these effects of catechins, EGCG treatment in Ts65Dn pups increased the number of SYN and PSD-95 immunoreactive puncta, indicating an effect on maturation of pre- and post-synaptic terminals. Importantly, we observed these effects not only in the hippocampus but also in the neocortex, indicating that EGCG has a widespread effect on synapse development. As reported in **Section 3.1**, altered GSK3β signaling may underlie connectivity alterations in DS. We found that in trisomic pups EGCG restored the levels of GSK3β as well as its phosphorylation status, suggesting that this effect may contribute to the positive effect of EGCG on synapse plasticity. GSK3β can be phosphorylated (inactivated) at ser9 by several kinases, including Akt, protein kinase A, and protein kinase C (Jope and Johnson, 2004), that are in turn activated by EGCG (Levites et al., 2003, Mandel et al., 2004, Schroeter et al., 2007, Kelsey et al., 2010). This may explain the increased phosphorylation of GSK3β following EGCG treatment.

EGCG only transiently restore*s *the developmental alterations of the trisomic brain

The reduced neurogenesis of the trisomic brain has been shown to be due to both cell cycle elongation and precocious exit from the cell cycle (Chakrabarti et al., 2007, Contestabile et al., 2007, Contestabile et al., 2009, Dierssen, 2012). We found here that neonatal treatment with EGCG restores the number of cells in the S-phase of the cell cycle (BrdU-positive cells) and the total pool of proliferating NPCs (Ki-67-positive cells). It remains to be established whether treatment with EGCG impacts on both cell cycle kinetics and cell cycle exit. Whatever the mechanisms, it may be expected that treatments that are able to expand the reduced pool of NPCs during the critical windows of maximum neurogenesis, could lead to an enduring neurogenesis rescue. For this reason, we envisaged that the positive impact of EGCG on neurogenesis could outlast treatment cessation. Unfortunately, in Ts65Dn mice, the proliferation potency of granule cell precursors was reverted to untreated trisomic mice levels. The lack of enduring effects was also observed for phenotype acquisition, number of granule neurons and density of synaptic terminals in the hippocampal region and neocortex. Consistently with the lack of long-term effects of EGCG on brain neuroanatomy, treated

Ts65Dn mice exhibited poorer memory in comparison with untreated euploid mice one month after treatment cessation. This finding is consistent with the observation that EGCG improves cognitive performance in adolescents with DS but that this effect decreases with time (De la Torre et al., 2014). The disappearance with time of the beneficial effects on neurogenesis and connectivity following treatment with EGCG suggests that continuous administration of EGCG may be necessary in order to prevent the disappearance of its effects.

In both euploid and Ts65Dn mice, following treatment discontinuation there was a reduction in the levels of synaptic proteins in some of the examined brain regions when mice were 45 days old (**Fig. 3.2.10-11**). In addition, in treated Ts65Dn mice there was a reduction in the number of Ki-67-positive cells per unit area in comparison with their untreated counterparts (**Fig. 3.2.9B**), and in treated euploid mice there was a reduction in granule cell numerical density (**Fig. 3.2.9F**). Taken together, these findings suggest that treatment may leave a negative trace in the brain after its discontinuation.

3.3 Section 3

“Pharmacotherapy with 7,8-dihydroxiflavone, a BDNF mimetic, in the Ts65Dn mouse model of Down syndrome”

Information reported in this section refers to:

“A flavonoid agonist of the TrkB receptor for BDNF improves hippocampal neurogenesis and hippocampus-dependent memory in the Ts65Dn mouse model of DS”. Stagni F, **Giacomini A**, Guidi S, Emili M, Uguagliati B, Salvalai ME, Bortolotto V, Grilli M, Rimondini R, Bartesaghi R. (Stagni and Giacomini contributed equally to the article). *Experimental Neurology* (2017) 298 (Pt A):79-96.

3.3.1 Abstract

Reduced neurogenesis and impaired neuron maturation are considered major determinants of altered brain function in DS. Since the DS brain is impaired starting from the earliest fetal life stages, attempts to rescue neurogenesis and neuron maturation should take place as soon as possible. The brain-derived neurotrophic factor (BDNF) is a neurotrophin that plays a key role in brain development by specifically binding to the TRKB receptor. Systemic BDNF administration is impracticable because BDNF has a poor blood-brain barrier penetration. 7,8-dihydroxyflavone (7,8-DHF), a flavone present in plants, is a recently found small-molecule that crosses the blood-brain barrier and mimics the BDNF activity by binding the TRKB receptor. The goal of this study was to establish whether it is possible to restore brain development in the Ts65Dn mouse model of DS by targeting the TRKB receptor with 7,8-DHF. Ts65Dn mice, treated with 7,8-DHF in the neonatal period P3-P15, exhibited a large increase in the number of neural precursor cells in the dentate gyrus, restoration of granule cell number, and restoration of spine density. In order to establish the functional outcome of treatment, mice were treated with 7,8-DHF from P3 to adolescence (P45-50) and were tested with the Morris Water Maze test, in order to examine hippocampus-dependent learning and memory. Treated Ts65Dn mice exhibited restoration of learning and memory, indicating that the recovery of the hippocampal anatomy translated into a functional rescue. Ts65Dn mice aged 4 months, treated with 7,8-DHF for one month, exhibited no restoration of neurogenesis, but they showed an improvement in hippocampus-dependent learning and memory, indicating that treatment at advanced life stages, unlike at early life stages, is unable to completely rescue the trisomy-linked brain defects. Our study provides novel evidence that treatment with 7,8-DHF during the early postnatal period restores trisomy-linked neurodevelopmental defects, suggesting that targeting BDNF/TRKB pathway may represent a possible breakthrough for DS.

3.3.2 Introduction

Most of the brain neurons are produced in the prenatal period, with the notable exception of those involved in the formation of the hippocampus, where neurogenesis continues postnatally and throughout life (Seress et al., 2001, Rice and Barone, 2010, Stiles and Jernigan, 2010). After the critical periods of neurogenesis and synaptogenesis the brain can undergo relatively limited plastic changes. Thus, the perinatal period represents a window of opportunity for therapies aimed at improving the neurodevelopmental alterations of DS. Since the DS brain starts at a disadvantage, attempts to rescue neurogenesis and neuron maturation should take place as soon as possible.

The brain-derived neurotrophic factor (BDNF) is a neurotrophin that plays a key role in brain plasticity by specifically binding to the tropomyosin-related kinase receptor B (TRKB) (Haniu et al., 1997). This binding causes dimerization and autophosphorylation of the TRKB receptor, which triggers the activity of several intracellular pathways, thereby favoring neurogenesis, neuritogenesis and spine growth (see (Vilar and Mira, 2016)). In the DS brain, BDNF levels are already reduced at fetal life stages (Guedj et al., 2009, Toiber et al., 2010) and reduced BDNF levels have been shown in various brain regions of the Ts65Dn mouse (Bimonte-Nelson et al., 2003, Bianchi et al., 2010b, Fukuda et al., 2010, Begenisic et al., 2015).

In view of the role of the BDNF-TRKB system in neurogenesis and dendritic morphogenesis, it is conceivable that interventions targeted to the BDNF-TRKB system may be exploited in order to improve the trisomy-linked neurodevelopmental defects. Systemic administration of BDNF is impracticable because BDNF has a poor blood-brain barrier penetration. This obstacle could be circumvented by using TRKB agonists that can enter the brain. Recent screening of a chemical library has identified a flavone derivative, 7,8-dihydroxyflavone (7,8-DHF), as the first small-molecule compound that binds with high affinity and specificity to the TRKB receptor, activates its downstream signaling cascade (Liu et al., 2010), and penetrates the blood brain barrier (Liu et al., 2013). Administration of 7,8-DHF enhances the activation of phosphorylated TRKB and increases spine

density in several brain regions (Zeng et al., 2012), promotes neurogenesis in the dentate gyrus (Liu et al., 2010), fosters neurite outgrowth (Tsai et al., 2013) and exerts therapeutic efficacy in various animal disease models that are related to deficient BDNF signaling (Liu et al., 2016).

Various pharmacotherapies have been attempted in DS mouse models (Bartesaghi et al., 2011, Costa and Scott-McKean, 2013, Gardiner, 2015). A comparison of the effects of different therapies in mouse models shows that many of them were effective (Stagni et al., 2015a). It should be noted, however, that some of the used drugs may be not devoid of side effects, and/or have ephemeral effects, which diminishes their translational impact. The therapeutic potential of TRKB agonists for neurogenesis improvement in DS has never been examined. Considering the important role of the BDNF-TRKB receptor system on neurogenesis, we expect that by acting upon this system by exploiting the flavonoid 7,8-DHF it may be possible to positively impact the DS brain. Moreover, considering that flavonoids are natural substances, it seems likely that their administration at appropriate doses may be devoid of side effects. Based on these premises, we deemed it important to investigate whether treatment with 7,8-DHF is able to restore hippocampal development and hippocampus-dependent memory in the Ts65Dn mouse model of DS.

3.3.3 Materials and Methods

Colony

Ts65Dn mice were generated by mating B6EiC3Sn a/A-Ts(17^16)65Dn females with C57BL/6JEiJ x C3H/HeSnJ (B6EiC3Sn) F1 hybrid males. This parental generation was provided by Jackson Laboratories (Bar Harbor, ME, USA). To maintain the original genetic background, the mice used were of the first generation of this breeding. Animals were genotyped as previously described (Reinholdt et al., 2011). The day of birth was designated postnatal day zero (P0). The animals' health and comfort were controlled by the veterinary service. The animals had access to water and food ad libitum and lived in a room with a 12:12 h light/dark cycle. Experiments were performed in

accordance with the European Communities Council Directive of 24 November 1986 (86/609/EEC) for the use of experimental animals and were approved by Italian Ministry of Public Health (813/2016-PR). In this study, all efforts were made to minimize animal suffering and to keep the number of animals used to a minimum.

In the current study, treatment with either 7,8-DHF or vehicle began on postnatal day 3 (P3). All mice that survived in the P0 to P3 period entered this study, with no specific selection criteria. A total of 185 mice entered the study (96 males and 89 females). The number of vehicle-treated and 7,8-DHF treated mice was 96 and 89, respectively. Seven vehicle-treated (7.3%) and five 7,8-DHF-treated (5.6%) mice died before weaning, in the P6-P22 period. The similarity in the mortality rate across groups suggests that treatment has no adverse effects on the health of mice.

Experimental protocol

Pilot experiment. In a pilot study we tested the effects of different doses of 7,8-DHF on the proliferation rate in the subgranular zone (SGZ) of the dentate gyrus (DG) of Ts65Dn mice. Mice received a daily subcutaneous injection of 7,8-DHF (2.5, 5.0, or 10.0 mg/kg in PBS with 1% DMSO) from postnatal day 3 (P3) to P15. On P15, mice received an intraperitoneal injection (150 μg/g body weight) of BrdU (5-bromo-2-deoxyuridine; Sigma) in TrisHCl 50 mM 2h before being killed and the number of BrdU-positive cells in the SGZ was evaluated. We found that the optimum dose was 5.0 mg/kg (see **Fig. 3.3.4A**). Therefore, this study (Experiment 1, Experiment 2, and Experiment 3) was carried out using a 5.0 mg/kg dose.

Experiment 1. Euploid and Ts65Dn mice received a daily subcutaneous injection (at 9-10am) of 7,8-DHF (5.0 mg/kg in vehicle: PBS with 1% DMSO) or vehicle from postnatal day 3 (P3) to postnatal day 15 (**Fig. 3.3.1A**). Mice that received 7,8-DHF will be called “treated mice” (treated euploid mice: n=25; treated Ts65Dn mice: n=15). Mice that received the vehicle will be called “untreated mice” (untreated euploid mice: n=35; untreated Ts65Dn mice: n=21). On P15, mice received an intraperitoneal injection (150 μg/g body weight) of BrdU in TrisHCl 50 mM 2h before being killed

(**Fig. 3.3.1A**). The brains were excised and cut along the midline. The left hemisphere of a group of mice was fixed by immersion in PFA 4% and frozen, and the left hemisphere of another group of mice was used for Golgi staining. The right hemispheres of all mice was kept at –80°C and used for western blotting.

Experiment 2. Euploid and Ts65Dn mice received a daily subcutaneous injection (at 9-10am) of 7,8-DHF (5.0 mg/kg in vehicle) or vehicle from postnatal day 3 (P3) to postnatal day P45-P50 (**Fig. 3.3.2A**). At the end of treatment, mice were subjected to behavioural experiments (MWM), using the same protocol as that used in **Section 3.2**. Because C3H/HeSnJ mice carry a recessive mutation that leads to retinal degeneration, animals used for the behavioral study were genotyped by standard PCR to screen out all mice carrying this gene. Mice that did not carry a recessive mutation that leads to retinal degeneration entered the behavioral study (untreated euploid mice: n=19; untreated Ts65Dn mice: n=14; treated euploid mice: n=17; treated Ts65Dn mice: n=16). These mice will be called here P45 mice. Mice were behaviorally tested in the 6 days that preceded the day of sacrifice (**Fig. 3.3.2A**). The body weight of mice of all groups was recorded prior to sacrifice and the brain weight was recorded immediately after its removal. The number of animals used for each experimental procedure is specified in the figure legends and in **Table 3.3.1**.

Experiment 3. A total of 38 adult male mice were used. Mice aged 4 months received a daily i.p. injection of i) vehicle (0.9% NaCl; n=13 euploid and n=11 Ts65Dn mice) or ii) 7,8-DHF (5.0 mg/kg) dissolved in the vehicle (n=7 euploid and n=7 Ts65Dn mice) for 41 days (**Fig. 3.3.3A**). During the last 11 days of treatment mice were behaviorally tested with the Morris Water Maze (MWM) test. Adult mice underwent a longer MWM in order to detect, if present, age-dependent cognitive decline. These mice will be called here 5 month-old mice. At the end of behavioral testing mice were killed, the brain was removed, fixed by immersion in PFA 4% and frozen.

Histological procedures

The frozen brains of P15 and 5 month-old mice were cut with a freezing microtome into 30-μm-thick

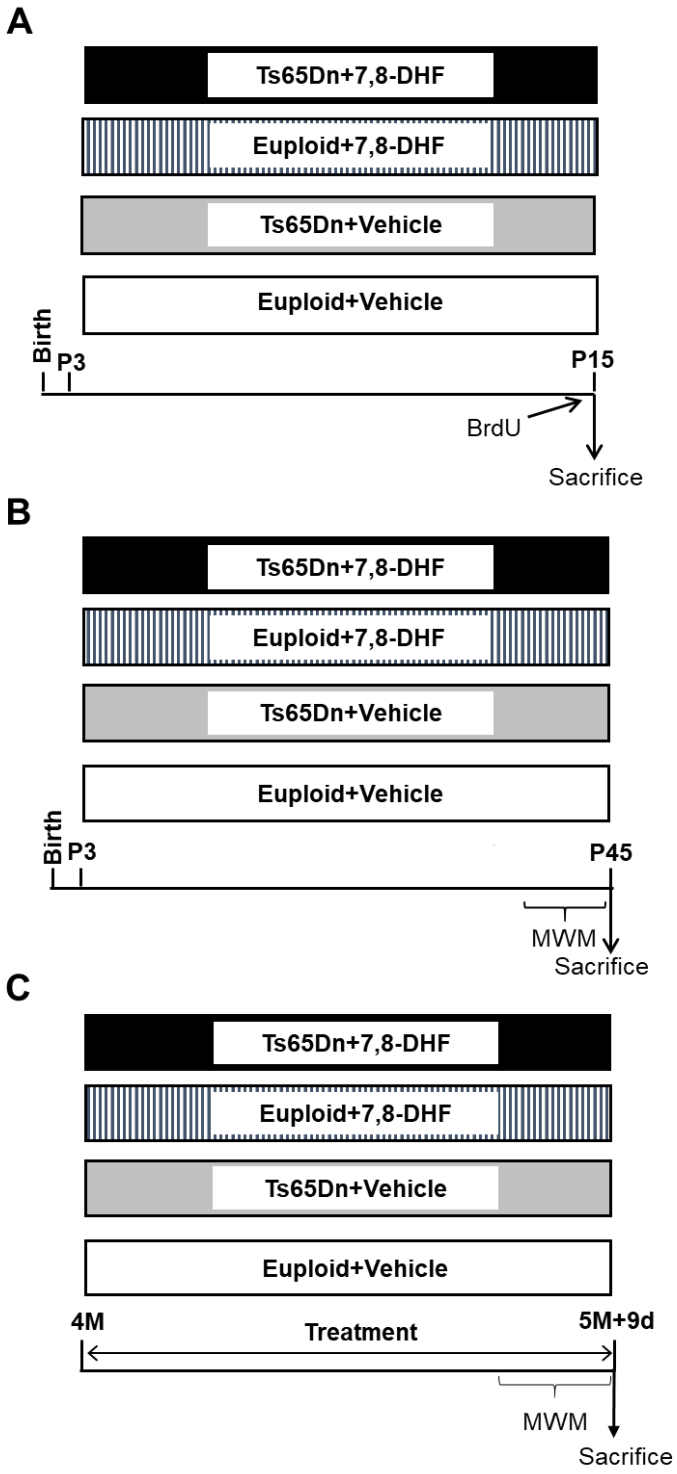

Figure 3.3.1. Experimental protocols. A: Euploid and Ts65Dn pups received one daily injection of either vehicle or 7,8-DHF (5.0 mg/kg) from postnatal day 3 (P3) to P15. At P15, mice received one injection of BrdU, and were killed after 2 h in order to evaluate the number of cells in the S-phase of the cell cycle. B: Euploid and Ts65Dn mice received one daily injection of either vehicle or 7,8-DHF (5.0 mg/kg) from postnatal day P3 to P45-50. These mice were tested with the Morris Water Maze test 6 days before being killed. C: Euploid and Ts65Dn mice received one daily injection of either vehicle or 7,8-DHF (5.0 mg/kg) from 4 months to 5 months + 9 days of age. These mice were tested with the Morris Water Maze test 9 days before being killed. Abbreviations: 7,8-DHF, 7,8-dihydroxyflavone; BrdU, bromodeoxyuridine; d, days; Eu, euploid; MWM, Morris Water Maze, P, postnatal.

Table 3.3.1 Number of mice included and excluded from the analyses.

	Euploid + Vehicle			Ts65Dn + Vehicle			Euploid + 7,8-DHF			Ts65Dn + 7,8-DHF		
	N. of mice entered in the experiment	N. of mice excluded from the analysis	N. of mice used for statistical analysis	N. of mice entered in the experiment	N. of mice excluded from the analysis	N. of mice used for statistical analysis	N. of mice entered in the experiment	N. of mice excluded from the analysis	N. of mice used for statistical analysis	N. of mice entered in the experiment	N. of mice excluded from the analysis	N. of mice used for statistical analysis
Brain Weight P15	35	-	35	21	-	21	25	-	25	15	-	15
Body Weight P15	35	-	35	21	-	21	25	-	25	15	-	15
Brain Weight P45	19	-	19	14	-	14	17	-	17	16	-	16
Body Weight P45	19	-	19	14	-	14	17	-	17	16	-	16
BrdU+Cells (DG)	7	-	7	8	-	8	3	-	3	5	-	5
N. of granule cells (DG)	4	-	4	4	-	4	4	-	4	5	-	5
Spine density (ML)	4	-	4	4	-	4	4	-	4	4	-	4
SYN (Hippocampus)	10	-	10	10	-	10	5	-	5	6	-	6
BDNF (Hippocampus)	21	1	20	21	-	21	5	-	5	6	-	6
TrkB-FL (Hippocampus)	21	2	19	21	2	19	5	-	5	6	-	6
p-TrkB (Hippocampus)	17	2	15	17	1	16	5	-	5	6	-	6
TrkB-T1 (Hippocampus)	21	2	19	21	-	21	5	-	5	6	-	6
p-ERK1(Hippocampus)	12	2	10	13	1	12	5	-	5	6	-	6
ERK1 tot (Hippocampus)	12	2	10	13	2	11	5	-	5	6	-	6
p-ERK2 (Hippocampus)	12	2	10	13	1	12	5	-	5	6	-	6
ERK2 tot (Hippocampus)	12	1	11	13	1	12	5	-	5	6	-	6
MWM (Learning+Probe)	19	3	16	14	-	14	17	1	16	16	1	15

Abbreviations: 7,8-DHF, 7,8-dihydroxyflavone; DG, dentate gyrus; ML, molecular layer of the dentate gyrus; N., number; P, post-natal day

coronal sections that were serially collected in anti-freezing solution (30% glycerol; 30% ethylen-glycol; 10% PBS10X; sodium azide 0.02%; MilliQ to volume). Slices from P15 brains were used for BrdU immunofluorescence; slices from 5 month-old brains were used for doublecortin (DCX) immunofluorescence.

Immunohistochemistry

The antibodies for immunohistochemistry, with their dilution and purpose are summarized in **Table 3.3.2**.

BrdU immunohistochemistry in P15 mice. One out of six free-floating sections (n=15-18 sections) from the hippocampal formation of P15 mice was processed for BrdU immunohistochemistry as described in **Section 3.1**. Slices were incubated with a rat anti-BrdU antibody (mouse monoclonal 1:100, Roche Applied Science, Mannheim, Germany). Detection was performed with a Cy3-conjugated anti rat-secondary antibody as indicated in **Table 3.3.2**.

DCX Immunohistochemistry in 5 month-old mice. One out of six free-floating sections from the hippocampal formation (n=10 sections) of 5 months old mice were processed for DCX immunohistochemistry, using the methods described in (Guidi et al., 2013). Quantification of DCX-positive cells in the DG was conducted in every 6^{th} section using a fluorescence microscope (Nikon Eclipse TE 2000-S inverted microscope; Nikon Corp., Kawasaki, Japan; objective: x 20, 0.50 NA; final magnification: x 200), equipped with a Nikon digital camera DS 2MBWc. DCX positive-cells were counted along the whole length of the granule cell layer and their number was expressed as number of cells for 100 µm of linear length.

Golgi staining

Brains of P15 mice were Golgi stained using the FD Rapid Golgi Stain ^{TM} Kit (FD NeuroTechnologies, Inc.). Brains were immersed in the impregnation solution containing mercuric chloride, potassium dichromate and potassium chromate and stored at room temperature in darkness

Table 3.3.2. Antibodies used for immunohistochemistry and western blot.

Antigen	Application	Antibody Dilution- Manufactures
α-Tubulin	**WB**	**Primary**: mouse monoclonal 1:1000 (Clone B-5-1-2) (Sigma-Aldrich, T5168) **Secondary:** HRP-conjugated anti-mouse 1:20000 (Jackson Immunoresearch, 115-035-003)
BDNF	**WB**	**Primary**: rabbit polyclonal 1:500 (N-20) (Santa Cruz Biotechnology, cs-546) **Secondary:** HRP-conjugated anti-rabbit 1:10000 (Jackson Immunoresearch, 111-035-003)
5-bromo-2-deoxyuridine (BrdU)	**IHC**	**Primary:** rat monoclonal 1:200 (BioRad, OBT0030) **Secondary:** Cy3-conjugated anti-rat IgG 1:200 (Jackson Immunoresearch, 112-165-143)
Extracellular signal-regulated kinase (ERK1/2)	**WB**	**Primary**: mouse monoclonal 1:1000 (3A7) (Cell Signaling, 9107) Technology **Secondary:** HRP-conjugated anti-mouse 1:10000(Jackson Immunoresearch, 115-035-003)
phosphorylated ERK (p-ERK1/2)	**WB**	**Primary**: rabbit polyclonal 1:1000 (Cell Signaling Technology, 9101) **Secondary:** HRP-conjugated anti-rabbit 1:10000 (Jackson Immunoresearch, 111-035-003)
GAPDH	**WB**	**Primary**: rabbit polyclonal 1:5000 (Sigma-Aldrich, G9545) **Secondary:** HRP-conjugated anti-rabbit 1:10000 (Jackson Immunoresearch, 111-035-003)
Synaptophysin (SYN)	**WB**	**Primary:** rabbit polyclonal 1:1000(Abcam, ab 14692) **Secondary:** HRP-conjugated anti-rabbit 1:10000 (Jackson Immunoresearch, 111-035-003)
Tropomyosin receptor kinase (Trk) B Full Length (FL) and TrkB truncated (T1)	**WB**	**Primary:** rabbit monoclonal 1:1000 (Cell Signaling Technology, 80E3) **Secondary:** HRP-conjugated anti-rabbit 1:10000 (Jackson Immunoresearch, 111-035-003)
phosphorylated TrkB-FL (p-TrkB-FL)	**WB**	**Primary:** rabbit polyclonal 1:1000 (Millipore, ABN1381) **Secondary:** HRP-conjugated anti-rabbit 1:10000 (Jackson Immunoresearch, 111-035-003)

Abbreviations: IHC, immunohistochemistry; WB, Western blotting.

for 3 weeks. Hemispheres were cut with a microtome in 90-µm-thick coronal sections that were mounted on gelatin-coated slides and were air dried at room temperature in the dark for one day. After drying, sections were rinsed with distilled water and subsequently stained in a developing solution (FD Rapid Golgi Stain Kit).

Measurements

Image acquisition. Immunofluorescence images were taken with a Nikon Eclipse TE 2000-S inverted microscope (Nikon Corp., Kawasaki, Japan), equipped with a Nikon digital camera DS 2MBWc. Measurements were carried out using the software Image Pro Plus (Media Cybernetics, Silver Spring, MD 20910, USA). Bright field images were taken on a light microscope (Leitz) equipped with a motorized stage and focus control system and a Coolsnap-Pro color digital camera (Media Cybernetics, Silver Spring, MD, USA).

BrdU-positive cells in P15 mice. BrdU-positive cells in the DG of P15 mice were detected using a fluorescence microscope (Eclipse; objective: x 40, 0.75 NA; final magnification: x 400). Quantification of BrdU-labeled nuclei was conducted in every 6^{th} section using a modified unbiased stereology protocol that has previously been reported as successfully quantifying BrdU labeling (Malberg et al., 2000, Kempermann and Gage, 2002, Tozuka et al., 2005). All BrdU-labeled cells located in the granule cell and subgranular layers were counted in their entire z axis (1 µm steps) in each section. To avoid oversampling errors, nuclei intersecting the uppermost focal plane were excluded. The total number of BrdU-labeled cells per animal was determined and multiplied by six to obtain the total estimated number of cells per DG.

Spine density in P15 mice. In Golgi-stained sections from the DG of P15 mice, spines of granule cells were counted using a 100x oil immersion objective lens (1.4 NA). Spines were counted in dendritic segments in the inner and outer half of the molecular layer. For each neuron, 2-3 segments were analyzed in the outer and inner half of the molecular layer, respectively. For each animal, spines were counted in at least 8 neurons. The length of each sampled dendritic segment was determined by

tracing its profile and the number of spines was counted manually. The linear spine density was calculated by dividing the total number of spines by the length of the dendritic segment. Spine density was expressed as number of spines per 100 μm dendrite.

Stereology of the DG in P15 mice. Unbiased stereology was performed on Hoechst-stained sections from P15 mice. The protocol used for stereology of the DG is the same as that used in **Section 3.1**.

Number of DCX positive cells in 5 month-old mice. Quantification of DCX positive cells in the DG was conducted in every 6th section using a fluorescence microscope (Nikon Eclipse TE 2000-S inverted microscope; Nikon Corp., Kawasaki, Japan; objective: x 20, 0.50 NA; final magnification: x 200), equipped with a Nikon digital camera DS 2MBWc. DCX positive cells were counted along the whole length of the granule cell layer and their number was expressed as number of cells for 100 μm of linear length.

Western blotting

In homogenates of the hippocampal formation of P15 mice, total proteins were obtained as described in **Section 3.1** of this thesis. Equivalent amount of proteins (50 μg) were subjected to electrophoresis on a Bolt 4-12% NuPAGE Bis-Tris Precast Gel (Novex, Life Technologies, Ltd, Paisley, UK) and transferred to a Hybond ECL nitrocellulose membrane (Amersham Life Science). The levels of the following proteins were evaluated: BDNF, TrkB full length (TrkB-FL), phosphorylated TRKB (p-TRKB), the truncated form 1 of the TRKB receptor (TRKB-T1), phosphorylated ERK1 (p-ERK1), phosphorylated ERK2 (p-ERK2), ERK1, ERK2, SYN, GAPDH and α-Tubulin using the antibodies reported in **Table 3.3.2**. Densitometric analysis of digitized images with ChemiDoc XRS+ was performed with Image Lab software (Bio-Rad Laboratories, Hercules, CA, USA) and intensity for each band was normalized to the intensity of the corresponding GAPDH or α-Tubulin band.

Behaviorioral testing

Morris Water Maze (MWM). The MWM protocol and apparatus used for P45 mice were the same as

those used in **Section 3.2**. Since we have not made YM in this study, we evaluated more parameters for MWM because in comparison with those analysed in Section 3.2. For the learning phase, we evaluated the latency to find the hidden platform, time in periphery, percentage of time in periphery, path length, proximity to the platform, and swimming speed. Retention was assessed with one trial (probe trial), on the sixth day, 24 h after the last acquisition trial, using the same starting point for all mice. For the probe trial, the latency of the first entrance in the trained platform zone, the frequency of entrances in the trained quadrant, the proximity to the trained platform position (Gallagher's test), the percentage of time spent at the periphery (thigmotaxis), the swimming speed and the percentage of time spent in each quadrant were employed as measures of retention of acquired spatial preference. The following number of mice were tested. Untreated euploid mice: n=19; untreated Ts65Dn mice: n=14; 7,8-DHF-treated euploid mice: n=17; 7,8-DHF-treated Ts65Dn mice: n=16. Three untreated euploid mice (yielding n=16), one 7,8-DHF-treated euploid mouse (yielding n=16) and one 7,8-DHF-treated Ts65Dn mouse (yielding n=15) were excluded from MWM analysis due to thigmotaxis for a whole recording session.

For adult (5-month-old) mice, the apparatus and the experimental condition of the MWM test was the same as those for P45 mice, with the exception of the learning phase duration. Learning phase was organized as follows. Days 1-8: learning sessions; day 9: probe test. During the learning phase mice were subjected to 4 trials on day one and to two blocks of 4 trials separated by an interval of 45 minutes on days 2-8. Mice were tested longer than in the other MWM protocols reported in the dissertation because we sought to establish whether Ts65Dn mice have cognitive decline at five months of age and whether treatment could prevent this condition.

Statistical analysis

Results are presented as mean ± standard error of the mean (SE). Data were analyzed with the IBM SPSS 22.0 software. Distribution of data and the homogeneity of variances were evaluated with Shapiro-Wilk test and Levene's test respectively. Statistical analysis was carried out using either a

one-way ANOVA or a two-way ANOVA with genotype (euploid, Ts65Dn) and treatment (vehicle, 7,8-DHF), as factors. *Post hoc* multiple comparisons were carried out using the Fisher least significant difference (LSD) test. For the learning phase of the MWM test, statistical analysis was performed using a three-way mixed ANOVA, with genotype and treatment as grouping factors and days as a repeated measure. For the probe test of MWM, we used a two-way ANOVA with genotype and treatment as factors followed by the Fisher LSD *post hoc* test for the latency of the first entrance in the trained platform zone, the frequency of entrances in the trained quadrant, the proximity to the trained platform position, the percentage of time spent in the periphery, and the swimming speed. For the percentage of time spent in quadrants, the percentage of time spent in the NW, NE and SE quadrants was compared to the percentage of time spent in the trained platform quadrant (SW), respectively, with a paired-samples t-test. Based on the "Box plot" tool available in SPSS Descriptive Statistics we excluded from each analysis the extremes, i.e. values that were larger than 3 times the IQ range [$x \geq Q3 + 3 * (IQ)$; $x \leq Q1 - 3 * (IQ)$]. Figure legends report the number of mice used for statistical analysis. A probability level of $p \leq 0.05$ was considered to be statistically significant.

3.3.4 Results

Effect of treatment with 7,8-DHF in P15 mice: general results

The Ts65Dn strain is characterized by a high mortality rate during gestation and before weaning (Roper and Reeves, 2006). In view of the fragility of this strain, we sought to establish whether treatment with 7,8-DHF has adverse effects on the outliving of Ts65Dn mice. In the current study, treatment with either 7,8-DHF or vehicle began on postnatal day 3 (P3). All mice that survived in the P0 to P3 period entered this study. A total of 185 mice entered the study (96 males and 89 females). The number of vehicle- and 7,8-DHF-treated mice was 96 and 89, respectively. Seven vehicle-treated (7.3%) and five 7,8-DHF-treated (5.6%) mice died before weaning, in the first two postnatal weeks. The mortality rate is similar between groups treated with either vehicle or 7,8-DHF, suggesting that

the treatment has no adverse effects on the health of mice.

We evaluated the body and brain weight of P15 mice in order to establish the effect of treatment on gross growth parameters. A two-way ANOVA on the body weight of P15 mice showed no genotype x treatment interaction [$F(1,92) = 0.63$, $p = 0.431$], no main effect of treatment but a main effect of genotype [$F(1,92) = 14.78$, $p < 0.001$]. A *post hoc* Fisher LSD test confirmed well-established evidence that Ts65Dn mice have a reduced body weight in comparison with euploid mice. Multiple comparisons revealed that treatment did not negatively affect the body weight of Ts65Dn mice (**Fig. 3.3.2A**). A two-way ANOVA on the brain weight of P15 mice showed no genotype x treatment interaction [$F(1,92) = 1.09$, $p = 0.300$], a main effect of genotype [$F(1,92) = 7.73$, $p = 0.007$] and a main effect of treatment [$F(1,92) = 6.18$, $p = 0.015$]. A *post hoc* Fisher LSD test showed that Ts65Dn mice had a reduced brain weight in comparison with euploid mice and that treatment did not cause a further brain weight reduction (**Fig. 3.3.2B**). Surprisingly, treated euploid mice showed a little but significant brain weight reduction in comparison with their untreated counterparts (**Fig. 3.3.2B**).

Effect of neonatal treatment with 7,8-DHF on neural precursor proliferation in the hippocampal dentate gyrus of Ts65Dn mice

Recent work has evaluated the effect of 7,8-DHF in mouse models of Alzheimer disease. A dose of 5.0 mg/kg has been shown to have no toxic effects, to restore cognitive performance, and to increase the proliferation rate of neural precursor cells of the DG (Liu et al., 2010). In order to establish whether this is the optimal dose for proliferation enhancement in our model, we treated pups with vehicle, 2.5 mg/kg, 5.0 mg/kg or 10.0 mg/kg of 7,8-DHF in the period P3-P15. Two hours after the last treatment, mice received one injection of BrdU (150 mg/Kg) and were killed after 2 h in order to examine the outcome of a thirteen days treatment on proliferation rate. A one-way ANOVA on the number of BrdU-positive cells in the dentate gyrus (DG) of Ts65Dn pups showed a significant effect of treatment [$F(3,20) = 4.15$, $p = 0.019$]. A *post hoc* Fisher LSD test showed that the 2.5 mg/kg was not effective on proliferation rate in comparison with vehicle-treated mice, while both the 5.0 mg/kg

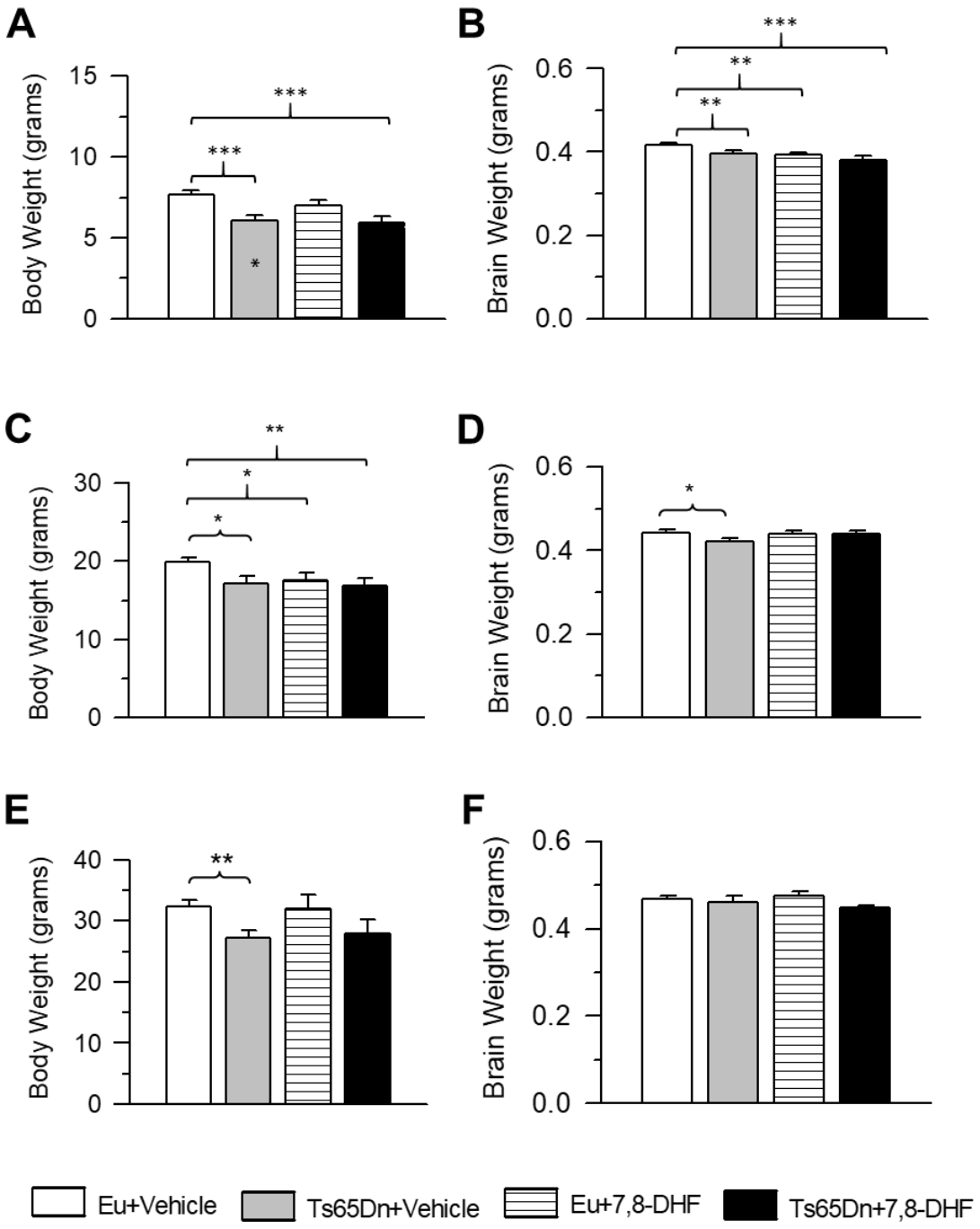

Figure 3.3.2. Body and brain weight of euploid and Ts65Dn mice treated with either vehicle or 7,8-DHF. A,B: Body (A) and brain (B) weight (mean ± SE) in grams of P15 euploid (n=35) and Ts65Dn (n=21) mice that received vehicle and euploid (n=25) and Ts65Dn (n=15) mice that received 7,8-DHF (5.0 mg/kg) in the period P3-P15. C,D: Body (C) and brain (D) weight (mean ± SE) in grams of P45 euploid (n=19) and Ts65Dn (n=14) mice that received vehicle and euploid (n=17) and Ts65Dn (n=16) mice that received 7,8-DHF (5.0 mg/kg) in the period P3-P45. E,F: Body (E) and brain (F) weight (mean ± SE) in grams of 5 month-old euploid (n=13) and Ts65Dn (n=11) mice that received vehicle and euploid (n=7) and Ts65Dn (n=7) mice that received 7,8-DHF (5.0 mg/kg) in the period 4M-5M+9d. * $p < 0.05$; ** $p < 0.01$; *** $p < 0.001$ (Fisher LSD test after two-way ANOVA). Black asterisk in the gray bar indicate a difference between untreated Ts65Dn mice and treated euploid mice. Abbreviations: 7,8-DHF, 7,8-dihydroxyflavone; BrdU, bromodeoxyuridine; Eu, euploid; MWM, Morris Water Maze, P, postnatal.

and the 10.0 mg/kg doses increased the number of BrdU-positive cells in Ts65Dn mice. In absolute terms, the 5.0 mg/kg dose had a higher pro-proliferative effect than the 10.0 mg/kg dose (**Fig. 3.3.3A**). Based on the preliminary experiments reported above, we chose a dose of 5.0 mg/kg dose for the experiments of this study. In order to establish the effects of 7,8-DHF on proliferation rate of neural progenitor cells (NPCs) of the DG, Ts65Dn mice and their euploid littermates were daily injected with 5.0 mg/kg of 7,8-DHF in the period P3-P15. At the end of treatment, mice were injected with BrdU and the number of BrdU-positive cells in the subgranular zone (SGZ) of the DG was evaluated. A two-way ANOVA on the total number of BrdU-positive cells showed a genotype x treatment interaction [$F(1,19) = 8.53$, $p = 0.009$], a main effect of genotype [$F(1,19) = 21.25$, $p < 0.001$], but no effect of treatment. A *post hoc* Fisher LSD test showed that untreated Ts65Dn mice had fewer proliferating cells in comparison with untreated euploid mice (total number per DG in Ts65Dn mice: n=7166±337, in euploid mice: n=10281±111). The number of proliferating cells after treatment in Ts65Dn mice underwent an increase (n=8963±449), becoming greater than that of their untreated counterparts, but already slightly lower in comparison with untreated euploid mice (**Fig. 3.3.3B,C**). BrdU-positive cells did not change in treated euploid mice (**Fig. 3.3.3B,C**). These results show that treatment greatly enhances cell proliferation in trisomic mice, although the number of proliferating cells does not reach the levels of euploid mice.

Effect of 7,8-DHF on the number of granule neurons in the dentate gyrus of Ts65Dn mice

Since treatment induced an increase in the proliferation potency of neural precursor cells in the DG of Ts65Dn mice, we expected this effect to lead to improvement of the defective cellularity proper of the DG of trisomic mice (Bianchi et al., 2010b). In order to answer this question, we stereologically counted the total number of granule cells in treated and untreated mice. A two-way ANOVA on total number of granule cells showed a genotype x treatment interaction [$F(1,13) = 6.71$, $p = 0.022$], but no main effect of either genotype or treatment. A *post hoc* Fisher LSD test showed that untreated Ts65Dn mice had fewer granule neurons in comparison with euploid mice. In treated Ts65Dn mice

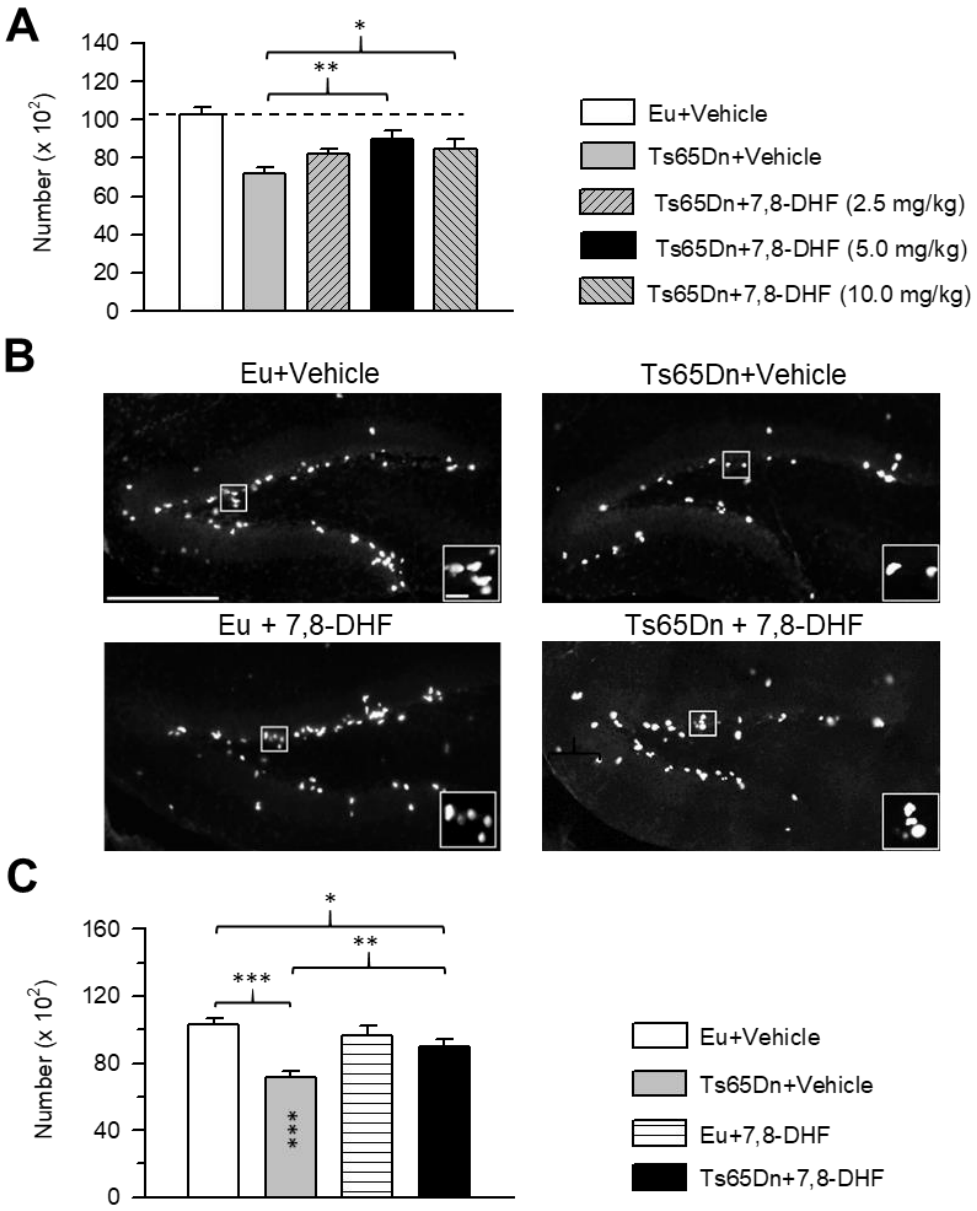

Figure 3.3.3. Effects of neonatal treatment with 7,8-DHF on the size of the population of cells in the S-phase of the cell cycle in the dentate gyrus of P15 Ts65Dn and euploid mice. A: In pilot experiments Ts65Dn mice received a daily injection of vehicle (n=8) or 7,8-DHF (2.5 mg/kg, n=4; 5.0 mg/kg, n=5; 10.0 mg/kg, n=7) in the period P3-P15. At P15, they were injected with BrdU and killed after 2 h. The histograms show the number of BrdU-positive cells in the DG of Ts65Dn mice treated with either vehicle or the indicated doses of 7,8-DHF. The number of BrdU-positive cells in euploid mice reported in (C) that received the vehicle is shown for comparison. B: Representative images of sections immunostained for BrdU from the DG of untreated euploid and Ts65Dn mice and euploid and Ts65Dn mice that were daily treated with 5.0 mg/kg of 7,8-DHF in the period P3-P15. Calibration bar=200 μm. The insets show zoomed images of the boxed area with examples of individual BrdU-positive cells. Calibration bar=20 μm. C: Total number of BrdU-positive cells in the DG of untreated euploid (n=7) and Ts65Dn (n=8) mice and euploid (n=3) and Ts65Dn (n=5) mice treated with 5.0 mg/kg of 7,8-DHF. Values (mean ± SE) in (A) and (C) refer to one hemisphere. * $p < 0.05$; ** $p < 0.01$; *** $p < 0.001$ (Fisher LSD test after two-way ANOVA). Black asterisks in the gray bar indicate a difference between untreated Ts65Dn mice and treated euploid mice. Abbreviation: 7,8-DHF, 7,8-dihydroxyflavone; Eu, euploid.

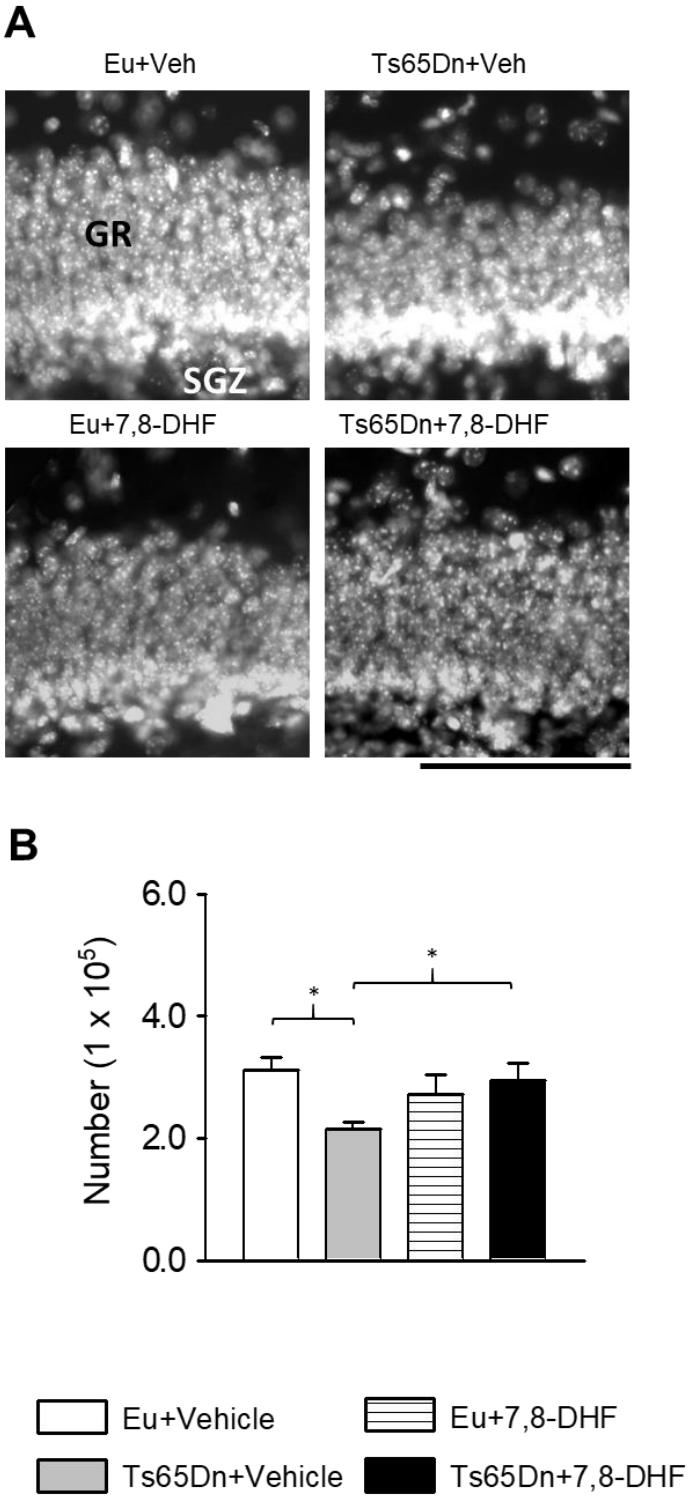

Figure 3.3.4. Effects of neonatal treatment with 7,8-DHF on granule cell number in the dentate gyrus of P15 Ts65Dn and euploid mice. A: Representative images of Hoechst-stained sections showing the granule cell layer of an animal from each experimental group. Calibration bar=100 μm. B: Total number of granule cells of untreated euploid (n=4) and Ts65Dn (n=4) mice and euploid (n=4) and Ts65Dn mice (n=5) treated with 5.0 mg/kg 7,8-DHF. Values (mean ± SE) refer to one DG. * $p < 0.05$ (Fisher LSD test after two-way ANOVA). Abbreviations: 7,8-DHF, 7,8-dihydroxyflavone; Eu, euploid; GR, granule cell layer; SGZ, subgranular zone; Veh, vehicle.

the number of granule cells became similar to that of untreated euploid mice (**Fig. 3.3.4A,B**). In euploid mice treatment had no effect on total number of granule cells (**Fig. 3.3.4A,B**).

Effect of 7,8-DHF on dendritic spine density in the dentate gyrus of Ts65Dn mice

Spine density reduction is a typical feature of the trisomic brain (Benavides-Piccione et al., 2004, Guidi et al., 2013) that, in conjunction with hypocellularity, is probably a critical determinant of intellectual disability. In order to establish whether 7,8-DHF improves this defects, in Golgi-stained brains we evaluated dendritic spine density of DG granule neurons. A two-way ANOVA on spine density showed a genotype x treatment interaction [$F(1,12) = 13.23$, $p = 0.003$], a main effect of genotype [$F(1,12) = 19.93$, $p = 0.001$] and a main effect of treatment [$F(1,12) = 42.30$, $p < 0.001$]. A *post hoc* Fisher LSD test showed that untreated Ts65Dn had a considerably reduced spine density in comparison with untreated euploid mice (**Fig. 3.3.5C**). Treatment with 7,8-DHF restored the number of spines of Ts65Dn mice (**Fig. 3.3.5C**), indicating that treatment fully rescues spine development. No effect of treatment were observed on spine density in euploid mice (**Fig. 3.3.5C**).

Effect of 7,8-DHF on synaptophysin levels in the hippocampal formation of Ts65Dn mice

The trisomic brain is characterized by altered synaptic circuitry that, in conjunction with reduced neurogenesis and dendritic pathology, largely contributes to impairment of signal processing (Bartesaghi et al., 2011). Since circuit formation is critically shaped in the early postnatal period throughout the brain we tried to establish whether neonatal treatment with 7,8-DHF had an effect on synapse development, examining the expression levels of SYN in the hippocampus of P15 mice.

A two-way ANOVA on the levels of SYN showed no genotype x treatment interaction [$F(1,27) = 0.82$, $p = 0.372$], no main effect of genotype, but a main effect of treatment [$F(1,27) = 6.62$, $p = 0.016$]. Confirming previous evidence (Stagni et al., 2013), a *post hoc* Fisher LSD test showed that untreated Ts65Dn mice had reduced SYN levels in comparison with untreated euploid mice, although the difference was marginally significant. Treatment with 7,8-DHF increased SYN levels in Ts65Dn

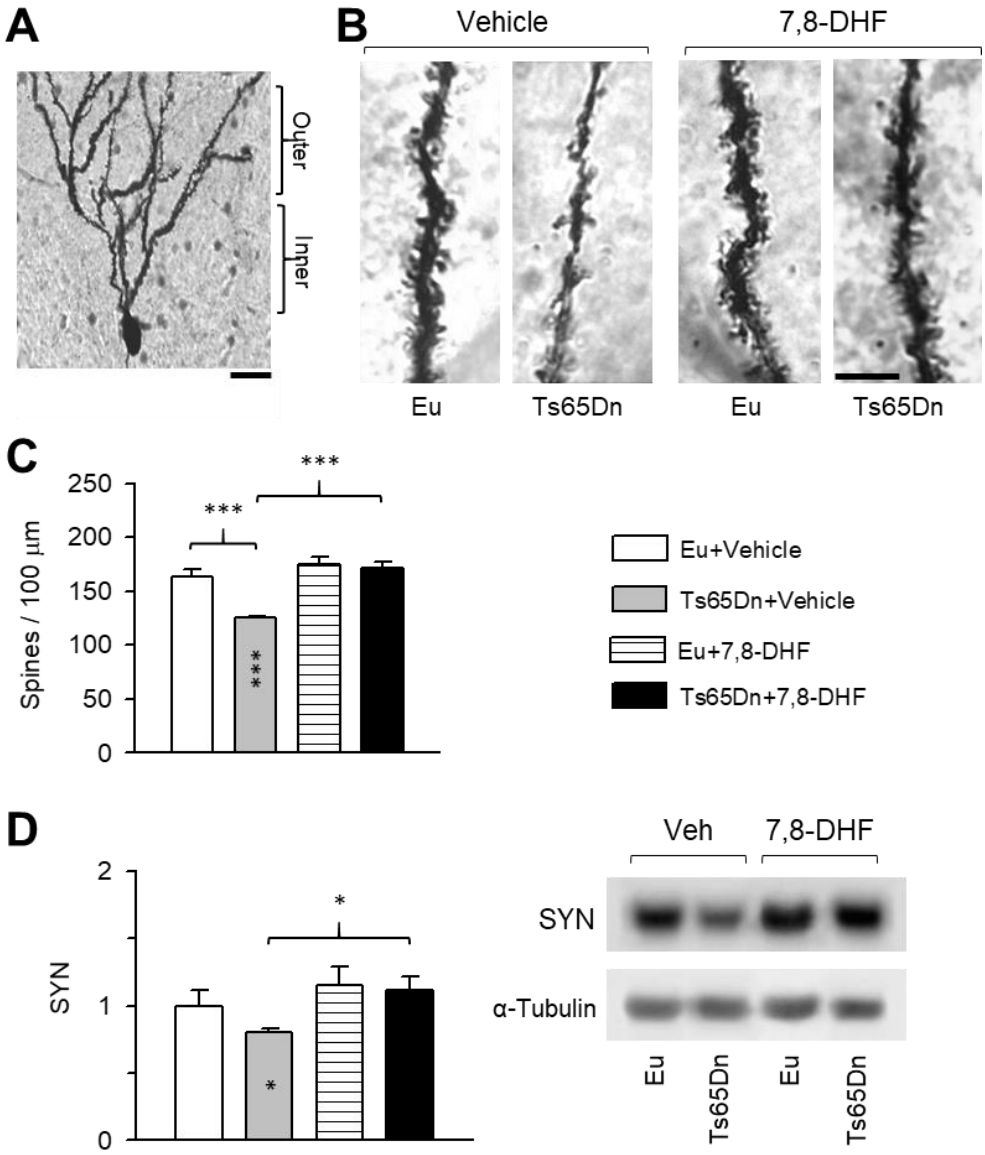

Figure 3.3.5. Effects of neonatal treatment with 7,8-DHF on dendritic spine density and synaptophysin levels in the dentate gyrus of P15 Ts65Dn and euploid mice. A: The photomicrograph shows a Golgi-stained granule cell. Dendritic spines were counted in the inner and outer half of the dendritic arbor of the granule cells. Calibration bar=10 µm. B: Photomicrograph of Golgi-stained granule cell dendrites showing spines on distal dendritic branches in an animal from each experimental groups. Calibration bar=5 µm. C: Spine density on the dendritic arbor of the granule cells of untreated euploid (n=4) and Ts65Dn mice (n=4) and euploid (n=4) and Ts65Dn (n=4) mice treated with 7,8-DHF. D: Western blot analysis of the expression levels of synaptophysin (SYN) in hippocampal homogenates of untreated euploid (n=10) and Ts65Dn (n=10) mice and treated euploid (n=5) and Ts65Dn (n=6) mice. SYN levels were normalized to α-Tubulin and expressed as fold difference in comparison with untreated euploid mice. Representative western blots are shown on the right. Values in (C,D) are mean ± SE. (*) $p < 0.06$; * $p < 0.05$; *** $p < 0.001$ (Fisher LSD test after two-way ANOVA). Black asterisks in the gray bar indicate a difference between untreated Ts65Dn mice and treated euploid mice. Abbreviations: 7,8-DHF, 7,8-dihydroxyflavone; Eu, euploid; SYN, synaptophysin; Veh, Vehicle.

(similar levels to those of untreated euploid mice) and in euploid mice (**Fig. 3.3.5D**). These findings suggest that treatment with 7,8-DHF restores development of hippocampal synapses in Ts65Dn mice and enhances synaptic development in euploid mice.

Effect of 7,8-DHF on the BDNF-TrkB receptor system in the hippocampal formation of Ts65Dn mice

BDNF signaling is elicited when it binds to TRKB, resulting in the receptor dimerization and autophosphorylation. The BDNF/TRKB signaling pathway is essential for normal brain function (Bibel et al., 1999). The TRKB full-length receptor (TRKB-FL) possesses an intracellular tyrosine kinase domain that mediates the crucial effects of BDNF. By contrast, the truncated form 1 of the TRKB receptor (TRKB-T1) lacks tyrosine kinase domain and, hence, the normal BDNF-mediated activity. However, TRKB-T1 appears to mediate inositol-1,4,5-trisphosphate-dependent calcium release (Rose et al., 2003). In order to establish the effect of genotype and treatment on the BDNF/TRKB system, we examined the protein levels of BDNF and TRKB receptors in the hippocampus of P15 euploid and Ts65Dn mice.

A two-way ANOVA on the BDNF levels showed no genotype x treatment interaction [$F(1,48) = 0.86$, $p = 0.359$], no main effect of genotype, but a main effect of treatment [$F(1,48) = 8.76$, $p = 0.005$]. A *post hoc* Fisher LSD test showed that Ts65Dn mice had similar BDNF protein levels as euploid mice (**Fig. 3.3.6B**). Treatment with 7,8-DHF caused a reduction in BDNF levels both in euploid and Ts65Dn mice although the difference was statistically significant for the latter only (**Fig. 3.3.6B**). A two-way ANOVA on the levels of TRKB-FL receptor showed no genotype x treatment interaction [$F(1,45) = 2.17$, $p = 0.148$] , a main effect of genotype [$F(1,45) = 5.71$, $p = 0.021$], and no effect of treatment. A *post hoc* Fisher LSD test showed no difference between untreated euploid and Ts65Dn mice in the levels of TRKB-FL (**Fig. 3.3.6A,C**). In Ts65Dn, but not in euploid mice, treatment with 7,8-DHF caused a reduction in the levels of TRKB-FL (**Fig. 3.3.6A,C**). A two-way ANOVA on the levels of the phosphorylated (active) form of the TRKB receptor (p-TRKB-FL)

showed no genotype x treatment interaction [F(1,39) = 0.03, p = 0.865], no main effect of genotype, but a main effect of treatment [F(1,39) = 10.88, p = 0.002]. A *post hoc* Fisher LSD test showed that in untreated Ts65Dn mice the levels of p-TRKB-FL were similar to those of euploid mice. In both genotypes, treatment with 7,8-DHF caused an increase in the levels of p-TRKB-FL (**Fig. 3.3.6A,D**). A two-way ANOVA on the levels of the TRKB-T1 receptor showed a genotype x treatment interaction [F(1,47) = 6.04, p = 0.018], but no main effect of either genotype or treatment. A *post hoc* Fisher LSD test showed that untreated Ts65Dn mice has similar levels of TRKB-T1 as untreated euploid mice. Treated Ts65Dn mice underwent a reduction in the levels of TRKB-T1 in comparison with their untreated counterparts and untreated euploid mice (**Fig. 3.3.6A,E**). These data suggest that treatment with 7,8-DHF stimulates the BDNF-signaling pathway. When the TRKB-FL receptor is activated, it interacts and activates a number of proteins that, in turn, trigger a signaling cascade to gene transcription. One of the main target of the BDNF/TRKB system is the RAS/ERK signaling pathway. Since RAS/ERK signaling is involved in cell proliferation and differentiation, we examined the effects of treatment on the activation of ERK1/2 in the hippocampus of Ts65Dn and euploid mice. A two-way ANOVA on p-ERK1 levels showed no genotype x treatment interaction [F(1,29) = 0.78, p = 0.385], but a main effect of both genotype [F(1,29) = 7.21, p = 0.012] and treatment [F(1,29) = 4.64, p = 0.040]. A *post hoc* Fisher LSD test showed no differences between untreated Ts65Dn and euploid mice and that treatment increased p-ERK1 levels of Ts65Dn mice in comparison with untreated Ts65Dn mice as well as untreated euploid mice (**Fig. 3.3.7A,C**). A two-way ANOVA on p-ERK2 levels showed no genotype x treatment interaction [F(1,29) = 1.73, p = 0.199], a main effect of genotype [F(1,29) = 8.92, p = 0.006] but no main effect of treatment. A *post hoc* Fisher LSD test showed that treated Ts65Dn mice underwent an increase in p-ERK2 levels in comparison with untreated euploid mice (**Fig. 3.3.87A,C**), but not with Ts65Dn mice. A two-way ANOVA on the levels of total ERK1 showed no genotype x treatment interaction [F(1,28) = 0.815, p = 0.374] and no main effect of either genotype or treatment. A *post hoc* Fisher LSD test showed that treated Ts65Dn mice underwent an increase in total ERK1 levels in comparison with untreated Ts65Dn mice (**Fig.**

3.3.7B,C). A two-way ANOVA on the levels of total ERK2 showed no genotype x treatment interaction [$F(1,30) = 0.065$, $p = 0.801$], no main effect of genotype, but a main effect of treatment [$F(1,30) = 13.76$, $p = 0.001$]. A *post hoc* Fisher LSD test showed that Ts65Dn mice treated with 7,8-DHF underwent an increase in total ERK2 levels in comparison with untreated euploid and Ts65Dn mice (**Fig. 3.3.7B,C**). An increase in total ERK2 levels also took place in treated euploid mice in comparison with their untreated counterparts (**Fig. 3.3.7B,C**). There is evidence that ERK2 is approximately four time more abundant than ERK1 in various brain regions and that alteration of the stoichiometry of the two isoform of ERK may have adverse effects (Lefloch et al., 2008). Therefore, we examined the relative abundance of ERK2/ERK1 and p-ERK2/p-ERK1 in treated and untreated mice. We found that in the hippocampal region of untreated euploid and Ts65Dn mice the ratio between ERK2 and ERK1 was approximately 3:1 and the ratio between p-ERK2 and p-ERK1 was approximately 2:1. Although in absolute terms treatment increased the levels of ERK1/2 and p-ERK1/2 in Ts65Dn mice (**Fig. 3.3.7A-C**), it did not affect their stoichiometry.

Effect of treatment with 7,8-DHF in P45 mice: general results

A two-way ANOVA on the body weight of P45 mice showed no genotype x treatment interaction [$F(1,62) = 1.57$, $p = 0.215$], a main effect of genotype [$F(1,62) = 4.98$, $p = 0.029$], but no main effect of treatment. A *post hoc* Fisher LSD test showed that Ts65Dn mice retained a reduced body weight in comparison with euploid mice and that treatment did not affect their body weight (**Fig. 3.3.2C**). In contrast, treated euploid mice underwent a body weight reduction in comparison with their untreated counterparts (**Fig. 3.3.2C**). A two-way ANOVA on the brain weight of P45 mice showed no genotype x treatment interaction [$F(1,62) = 2.06$, $p = 0.156$], and no main effect of both genotype and treatment. A *post hoc* Fisher LSD test showed that untreated Ts65Dn mice had a reduced brain weight in comparison with untreated euploid mice and that treatment restored this defect (**Fig. 3.3.2D**).

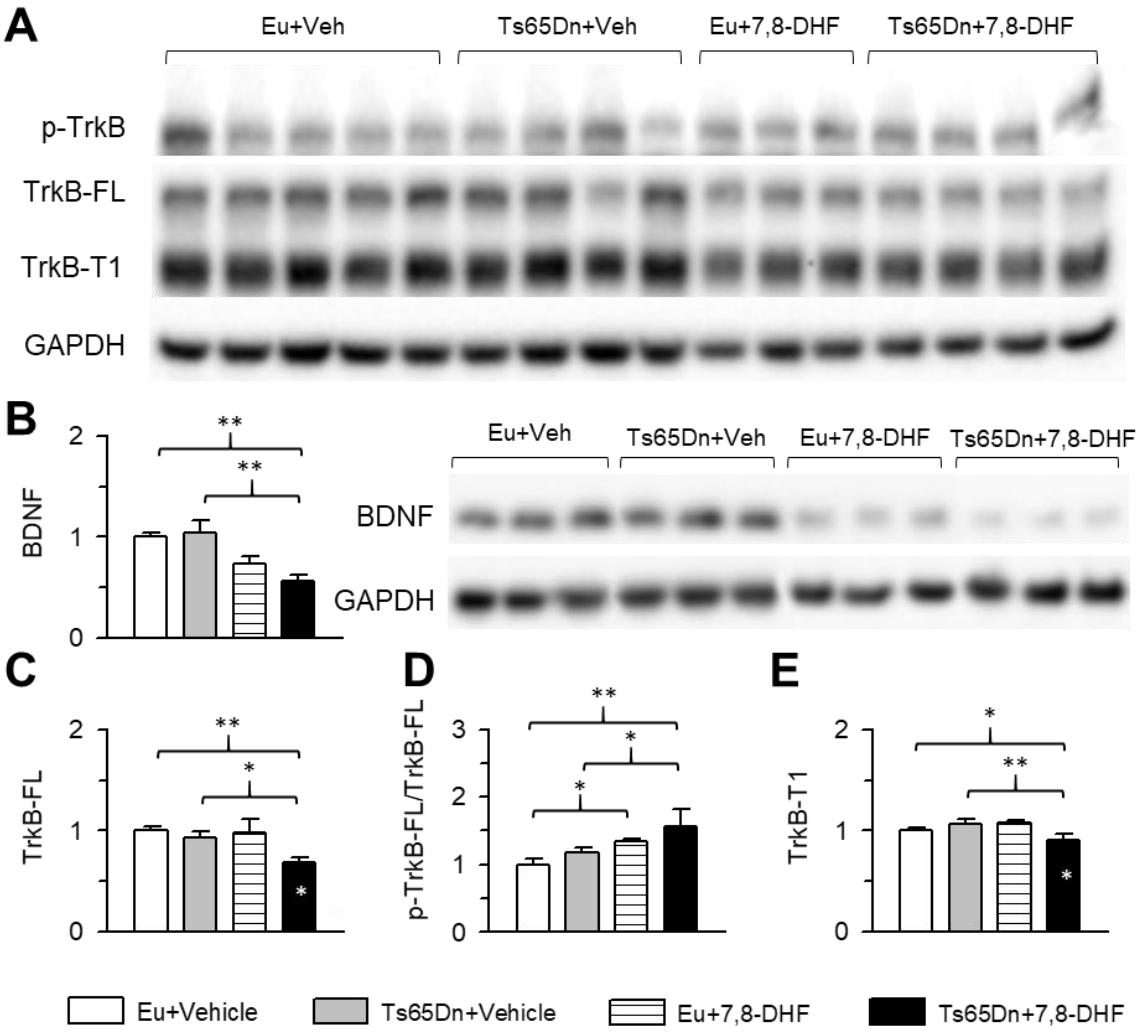

Figure 3.3.6. Effects of neonatal treatment with 7,8-DHF on the BDNF/TRKB receptor system in the hippocampal formation of P15 Ts65Dn and euploid mice. Western blot analysis of the BDNF/TRKB receptor system in the hippocampal formation of P15 Ts65Dn and euploid mice that received either vehicle or 7,8-DHF in the postnatal period P3-P15. A: representative western blots showing immunoreactivity for the phosphorylated TRKB receptor (p-TRKB), the full length TRKB receptor (TRKB-FL), the truncated TRKB receptor (TRKB-T1), and the housekeeping gene GAPDH. B: Levels of BDNF (untreated euploid mice: n=20; untreated Ts65Dn mice: n=21; treated euploid mice: n=5; treated Ts65Dn mice: n=6) and representative western blots showing immunoreactivity for BDNF and the housekeeping gene GAPDH. C: Levels of TRKB-FL (untreated euploid mice: n=19; untreated Ts65Dn mice: n=19; treated euploid mice: n=5; treated Ts65Dn mice: n=6). D: Levels of p-TRKB-FL (untreated euploid mice: n=15; untreated Ts65Dn mice: n=16; treated euploid mice: n=5; treated Ts65Dn mice: n=6). E: levels of TRKB-T1 (untreated euploid mice: n=19; untreated Ts65Dn mice: n=21; treated euploid mice: n=5; treated Ts65Dn mice: n=6). Data in (B, C, E) were normalized to GAPDH; data in (D) were normalized to TRKB-FL. Protein levels (mean ± SE) are expressed as fold difference in comparison with untreated euploid mice. * $p < 0.05$; ** $p < 0.01$; *** $p < 0.001$ (Fisher LSD test after two-way ANOVA). White asterisks in the black bar indicate a difference between treated Ts65Dn mice and treated euploid mice. Abbreviations: 7,8-DHF, 7,8-dihydroxyflavone; Eu, euploid; Veh, vehicle.

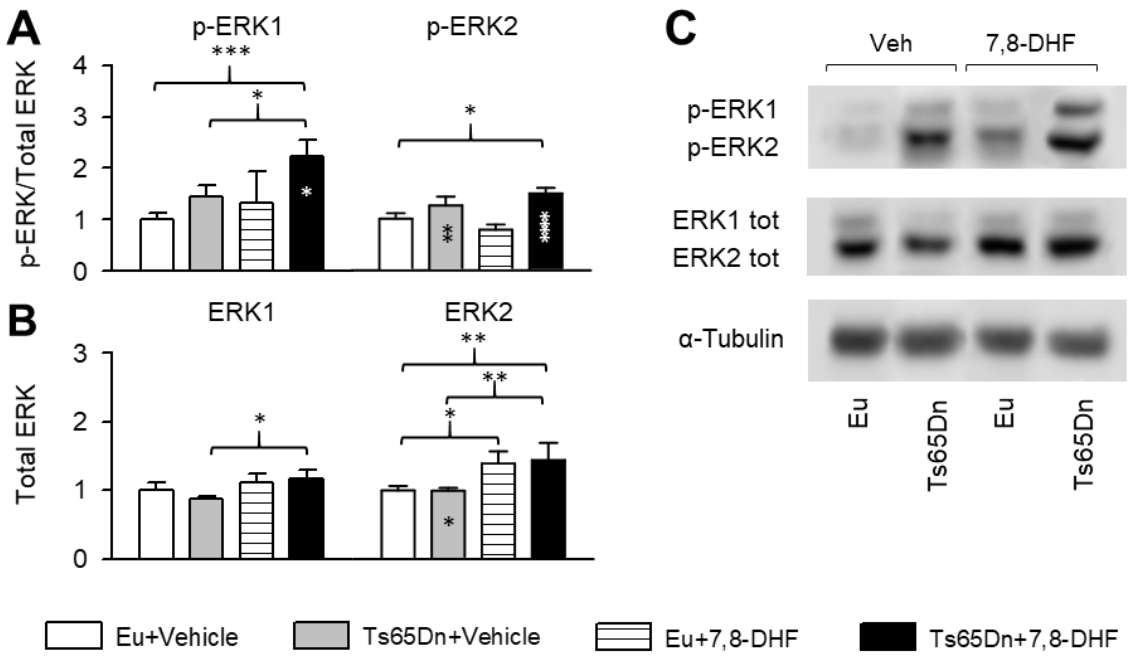

Figure 3.3.7. Effects of neonatal treatment with 7,8-DHF on the BDNF/TRKB receptor targets ERK1/2 in the hippocampal formation of P15 Ts65Dn and euploid mice. Data refer to P15 Ts65Dn and euploid mice that received either vehicle or 7,8-DHF in the postnatal period P3-P15. A,B: Western blot analysis of p-ERK1/p-ERK2 (untreated euploid mice: n=10; untreated Ts65Dn mice: n=12; treated euploid mice: n=5; treated Ts65Dn mice: n=6) (A) and total ERK1/ERK2 levels (untreated euploid mice: n=11; untreated Ts65Dn mice: n=11; treated euploid mice: n=5; treated Ts65Dn mice: n=6) (B) and representative western blots (C) showing immunoreactivity for p-ERK1, p-ERK2, ERK1, ERK2 and for the housekeeping protein α-Tubulin. Data in (B) were normalized to α-Tubulin; data in (A) were normalized to total ERK1 and total ERK2, respectively. Protein levels (mean ± SE) are expressed as fold difference in comparison with untreated euploid mice. * $p < 0.05$; ** $p < 0.01$; *** $p < 0.001$ (Fisher LSD test after two-way ANOVA). Black asterisks in the gray bar indicate a difference between untreated Ts65Dn mice and treated euploid mice. White asterisks in the black bar indicate a difference between treated Ts65Dn mice and treated euploid mice. Abbreviations: 7,8-DHF, 7,8-dihydroxyflavone; Eu, euploid; Veh, vehicle.

Effect of 7,8-DHF on hippocampus-dependent learning and memory in P45 mice

At the age of P45, mice can be behaviorally tested with tasks that explore hippocampus-dependent learning and memory (Guidi et al., 2014). In order to establish whether positive effects of treatment on brain morphology translates in a functional amelioration, we treated euploid and Ts65Dn mice from P3 to P45-50 and examined their behavior with the Morris Water Maze (MWM) test. The learning phase of the test lasted 5 days and on day six mice were subjected to the probe test in order to evaluate spatial memory. For the learning phase, the following variables were evaluated: escape latency, time in periphery, percentage of time in periphery, path length, proximity, and swimming speed. We carried out a three-way mixed ANOVA for all variables followed by *post hoc* Fisher LSD test. Results of ANOVA are reported hereafter and results of the *post hoc* test are summarized in **Table 3.3.3**.

A three-way mixed ANOVA on escape latency, with genotype and treatment as grouping factors and day as a repeated measure revealed no effect of genotype x treatment x day [$F(4,228) = 1.52$, $p = 0.196$]. We found a genotype x day interaction [$F(4,228) = 3.10$, $p = 0.016$], a treatment x day interaction [$F(4,228) = 2.77$, $p = 0.028$], no genotype x treatment interaction [$F(1,57) = 0.03$, $p = 0.874$], a main effect of genotype [$F(1,57) = 42.58$, $p < 0.001$], a main effect of treatment [$F(1,57) = 10.14$, $p = 0.002$], and a main effect of day [$F(4,228) = 21.75$, $p < 0.001$]. In accordance with previous findings, euploid mice exhibited a fast learning improvement with time, while untreated Ts65Dn mice exhibited a very scarce learning improvement and the latency to reach the platform did not decrease throughout the test (**Fig. 3.3.8A, Table 3.3.3**). In contrast, treatment improved learning in Ts65Dn mice and, save for day 3, their performance was similar to that of untreated euploid mice (**Fig. 3.3.8A**, **Table 3.3.3**). Treatment with 7,8-DHF induced an improvement in the latency of euploid mice in comparison with their untreated counterpart (**Fig. 3.3.8A**), although the difference was statistically significant on day 2 only (**Table 3.3.3**).

A three-way mixed ANOVA on the time spent in the periphery zone (thigmotaxis) revealed an effect of genotype x treatment x day [$F(4,228) = 2.88$, $p = 0.023$]. We found no genotype x day interaction

[F(4,228) = 0.99, p = 0.412], a treatment x day interaction [F(4,228) = 3.31, p = 0.012], no genotype x treatment interaction [F(1,57) = 0.001, p = 0.992], a main effect of genotype [F(1,57) = 19.63, p < 0.001], a main effect of treatment [F(1,57) = 8.07, p = 0.006], and a main effect of day [F(4,228) = 27.72, p < 0.001]. A *post hoc* Fisher LSD test showed that while untreated Ts65Dn mice spent more time in the periphery than untreated euploid mice, Ts65Dn mice treated with 7,8-DHF spent a similar time as euploid mice (**Fig. 3.3.8B**, **Table 3.3.3**), suggesting an improvement in the searching strategy. A reduction in thigmotaxis was also shown by euploid mice treated with 7,8-DHF.

A three-way mixed ANOVA on the percentage of time spent in the periphery showed an effect of genotype x treatment x day [F(4,228) = 3.01, p = 0.019]. We found a genotype x day interaction [F(4,228) = 2.47, p = 0.045], a treatment x day interaction [F(4,228) = 7.76, p < 0.001], no genotype x treatment interaction [F(1,57) = 1.48, p = 0.229], a main effect of genotype [F(1,57) = 11.71, p = 0.001], a main effect of treatment [F(1,57) = 8.04, p = 0.006], and a main effect of day [F(4,228) = 23.88, p < 0.001]. A *post hoc* Fisher LSD test showed that the time spent in the periphery by untreated Ts65Dn mice, expressed as percentage of the total latency, was similar to that of untreated euploid mice (**Fig. 3.3.8C, Table 3.3.3**). This means that the proportion of time spent in the periphery and outside the periphery was similar in euploid and Ts65Dn mice. Since in Ts65Dn mice the total latency to reach the platform was longer than in euploid mice, this means that Ts65Dn mice spent more time swimming in the periphery as well as outside the periphery. This implies that their longer escape latency can be attributable to both higher thigmotaxis levels and poorer spatial learning. In treated Ts65Dn mice the percentage of time in thigmotaxis underwent a reduction in comparison with their untreated counterparts (**Fig. 3.3.8C**, **Table 3.3.3**), suggesting an improvement in spatial learning.

A three-way mixed ANOVA on path length revealed no effect of genotype x treatment x day [F(4,228) = 2.09, p = 0.082]. We found a genotype x day interaction [F(4,228) = 7.80, p < 0.001], no treatment x day interaction [F(4,228) = 0.54 p = 0.707], no genotype x treatment interaction [F(1,57) = 0.05, p = 0.819], no main effect of genotype, no main effect of treatment but a main effect of day [F(4,228) = 43.74, p < 0.001]. In all groups, the path length decreased from day 1 to day 5 (**Fig.**

3.3.8D, Table 3.3.3). Until day 4, all four groups the path length was similar, even though in untreated Ts65Dn mice, the reduction was smaller than in untreated euploid mice. On day 5, the path length of untreated Ts65Dn mice was significantly larger in comparison with untreated euploid mice (**Fig. 3.3.8D, Table 3.3.3**). In contrast, on day 5 the path length of treated Ts65Dn mice was equal to that of treated and untreated euploid mice, suggesting an improvement in the searching strategy.

A three-way mixed ANOVA on the mean distance to the trained platform position (Gallagher's test; proximity) revealed an effect of genotype x treatment x day [$F(4,228) = 2.59$, $p = 0.038$]. We found a genotype x day interaction [$F(4,228) = 3.93$, $p = 0.004$], a treatment x day interaction [$F(4,228) = 4.79$, $p < 0.001$], no genotype x treatment interaction [$F(1,57) = 1.12$, $p = 0.295$], a main effect of genotype [$F(1,57) = 9.66$, $p = 0.003$], a main effect of treatment [$F(1,57) = 12.91$, $p = 0.001$], and a main effect of day [$F(4,228) = 13.39$, $p < 0.001$]. **Fig. 3.3.8E** shows that while in untreated euploid mice the proximity to the platform position increased from day 1 to day 5, untreated Ts65Dn mice underwent no improvement. Treated Ts65Dn mice underwent an improvement and on day 5 their proximity was significantly larger than their untreated counterparts and similar to that of untreated and treated euploid mice (**Fig. 3.3.8E, Table 3.3.3**), indicating a better swimming strategy to locate the platform.

A three-way mixed ANOVA on swimming speed revealed an effect of genotype x treatment x day [$F(4,228) = 3.20$, $p = 0.014$]. We found no genotype x day interaction [$F(4,228) = 0.71$, $p = 0.584$] , no treatment x day interaction [$F(4,228) = 1.98$, $p = 0.098$], no genotype x treatment interaction [$F(1,57) = 0.09$, $p = 0.760$], a main effect of genotype [$F(1,57) = 5.27$, $p = 0.025$], no main effect of treatment, but a main effect of day [$F(4,228) = 20.05$, $p < 0.001$]. A *post hoc* Fisher LSD test showed that in untreated Ts65Dn mice the swimming speed was similar to that the others three experimental groups throughout the learning phase (**Fig. 3.3.8F, Table 3.3.3**), suggesting that their longer escape latency was not due to speed reduction. Treated Ts65Dn mice had a reduced speed in comparison with untreated euploid mice on day 1, 2, and 3 but this condition disappeared in days 4 and 5, suggesting that their reduced escape latency was not due to an improvement in swimming speed.

Treated euploid mice had a reduced speed in comparison with untreated euploid mice on day 1, but a similar speed on days 2-5 (**Fig. 3.3.8F, Table 3.3.3**).

In the probe test, we considered the following parameters as an index of spatial memory: i) latency to enter the trained platform zone (latency), ii) frequency of entrances in the trained quadrant (frequency), iii) proximity to the trained platform position (Gallagher's test; proximity), iv) percentage of time spent at the periphery (thigmotaxis); v) swimming speed; vi) percentage of time spent in each quadrant. For all the parameters analyzed in the probe test, with the exclusion of the percentage of time spent in each quadrant, we conducted a two-way ANOVA, with genotype and treatment as independent variables, followed by a *post hoc* Fisher LSD test. A two-way ANOVA on the latency showed no genotype x treatment interaction [$F(1,57) = 0.87$, $p = 0.356$], but a main effect of genotype [$F(1,57) = 10.24$, $p = 0.002$] and a main effect of treatment [$F(1,57) = 4.60$, $p = 0.036$]. A *post hoc* Fisher LSD test showed that untreated Ts65Dn mice exhibited a larger latency than euploid mice. Treatment with 7,8-DHF caused a notable reduction in the latency of Ts65Dn mice that became similar to that of untreated euploid mice (**Fig. 3.3.9A**). A two-way ANOVA on the frequency showed no genotype x treatment interaction [$F(1,57) = 0.001$, $p = 0.992$], but a main effect of genotype [$F(1,57) = 10.06$, $p = 0.002$] and a main effect of treatment [$F(1,57) = 7.46$, $p = 0.008$]. A *post hoc* Fisher LSD test showed that untreated Ts65Dn mice exhibited a reduced frequency of entrances than euploid mice. In treated Ts65Dn mice, there was an increase in the frequency, that became similar to that of untreated euploid mice (**Fig. 3.3.9B**), although this effects was only marginally significant. A large increase in the frequency of entrances took place in treated euploid mice (**Fig. 3.3.9B**). This effect is in line with the reduction in the percentage of time they spent at the periphery (**Fig. 3.3.9F**). A two-way ANOVA on the proximity showed no genotype x treatment interaction [$F(1,57) = 1.60$, $p = 0.211$], but a main effect of genotype [$F(1,57) = 4.81$, $p = 0.032$] and a main effect of treatment [$F(1,57) = 7.05$, $p = 0.010$]. A *post hoc* Fisher LSD test showed that untreated Ts65Dn mice swam at a larger distance from the trained platform zone in comparison with untreated euploid mice **(Fig. 3.3.9C**). Treated Ts65Dn mice swam closer to the trained platform zone and their performance

became similar to that of untreated euploid mice (**Fig. 3.3.9C**).

A two-way ANOVA on the percentage of time spent in the periphery showed no genotype x treatment interaction [$F(1,57) = 0.62$, $p = 0.436$], no main effect of genotype but a main effect of treatment [$F(1,57) = 12.03$, $p = 0.001$]. A *post hoc* Fisher LSD test showed that in untreated Ts65Dn mice the percentage of time spent in the periphery was similar to that of untreated euploid mice (**Fig. 3.3.9D**). This indicates that Ts65Dn mice spent the same proportion of time in and outside the periphery as euploid mice. In treated Ts65Dn mice the percentage of time spent in the periphery was reduced in comparison with their untreated counterparts mice (**Fig. 3.3.9D**), suggesting that improvement in thigmotaxis contributes to the shorter latency to reach the trained platform zone. A reduction in the percentage of time in the periphery was also exhibited by treated vs. untreated euploid mice (**Fig. 3.3.9D**).

As during the learning phase, two-way ANOVA on the swimming speed showed no genotype x treatment interaction [$F(1,57) = 0.44$, $p = 0.511$], no main effect of genotype and no main effect of treatment and a *post hoc* Fisher LSD test showed no differences between groups (**Fig. 3.3.9E**).

A paired samples t-test showed that untreated Ts65Dn mice exhibited no differences in the time spent in the trained platform quadrant in comparison with the other quadrants (**Fig. 3.3.9F**). In contrast, treated Ts65Dn mice spent significantly more time in the trained platform quadrant in comparison with the NE quadrant [$t(14) = 2.49$; $p = 0.026$] and with the SE quadrant although the latter difference was only marginally significant [$t(14) = 2.05$; $p = 0.059$] (**Fig. 3.3.9F**). Untreated euploid mice spent significantly more time in the trained platform quadrant in comparison with the NE [$t(15) = 3.09$; $p = 0.008$] and SE quadrant [$t(15) = 2.16$; $p = 0.047$] quadrants (**Fig. 3.3.9F**). Likewise, treated euploid mice spent significantly more time in the trained platform quadrant in comparison with the NE [$t(15) = 3.85$; $p = 0.002$] and SE quadrant [$t(15) = 6.02$; $p < 0.001$] quadrants (**Fig. 3.3.9F**).

Taken together, these results show that Ts65Dn mice are impaired in spatial learning and memory. Treatment with 7,8-DHF indices an amelioration in Ts65Dn mice day by day in all parameters of the learning phase, although not to a significant level. At day 5, however, the performance of Ts65Dn

mice underwent a significant improvement in comparison with their untreated counterparts and was similar to that of untreated euploid mice. Importantly, in the probe test the behavior of treated Ts65Dn mice was similar to that of untreated euploid mice. This evidence suggests a complete restoration of hippocampus dependent memory.

Effect of treatment with 7,8-DHF in 5 month-old mice: general results

A two-way ANOVA on the body weight of 5 month-old mice showed no genotype x treatment interaction [$F(1,34) = 2.64$, $p = 0.114$], and no main effect of either genotype or treatment. A *post hoc* Fisher LSD test showed that Ts65Dn mice retained a reduced body weight in comparison with euploid mice and that treatment slightly increased their body weight (**Fig. 3.3.2E**). No effects of treatment on body weight were detectable in euploid mice (**Fig. 3.3.2E**). A two-way ANOVA on the brain weight of P45 mice showed no genotype x treatment interaction [$F(1,34) = 0.24$, $p = 0.626$], and no main effect of both genotype and treatment. A *post hoc* Fisher LSD test showed no difference in brain weight among groups (**Fig. 3.3.2F**).

Effect of 7,8-DHF on hippocampus-dependent learning and memory in 5 month-old mice

We examined the behavior of mice that had received 7,8-DHF or vehicle starting from four months of age. Behavioral testing started when mice were 5 month-old and lasted 11 days. Treatment was continued during behavioral testing. For the learning phase, we evaluated: escape latency, percentage of time at the periphery, path length, and swimming speed.

A three-way mixed ANOVA, with genotype and treatment as grouping factors and day as a repeated measure, on the escape latency revealed no effect of genotype x treatment x day. We found no genotype x day interaction, a treatment x day interaction [$F(7,238) = 2.23$, $p = 0.032$], no genotype x treatment interaction, a main effect of genotype [$F(1,34) = 20.63$, $p < 0.001$], no main effect of treatment but a main effect of day [$F(7,238) = 24.67$, $p < 0.001$]. While euploid mice exhibited a fast learning improvement with time, untreated Ts65Dn mice exhibited a very scarce learning

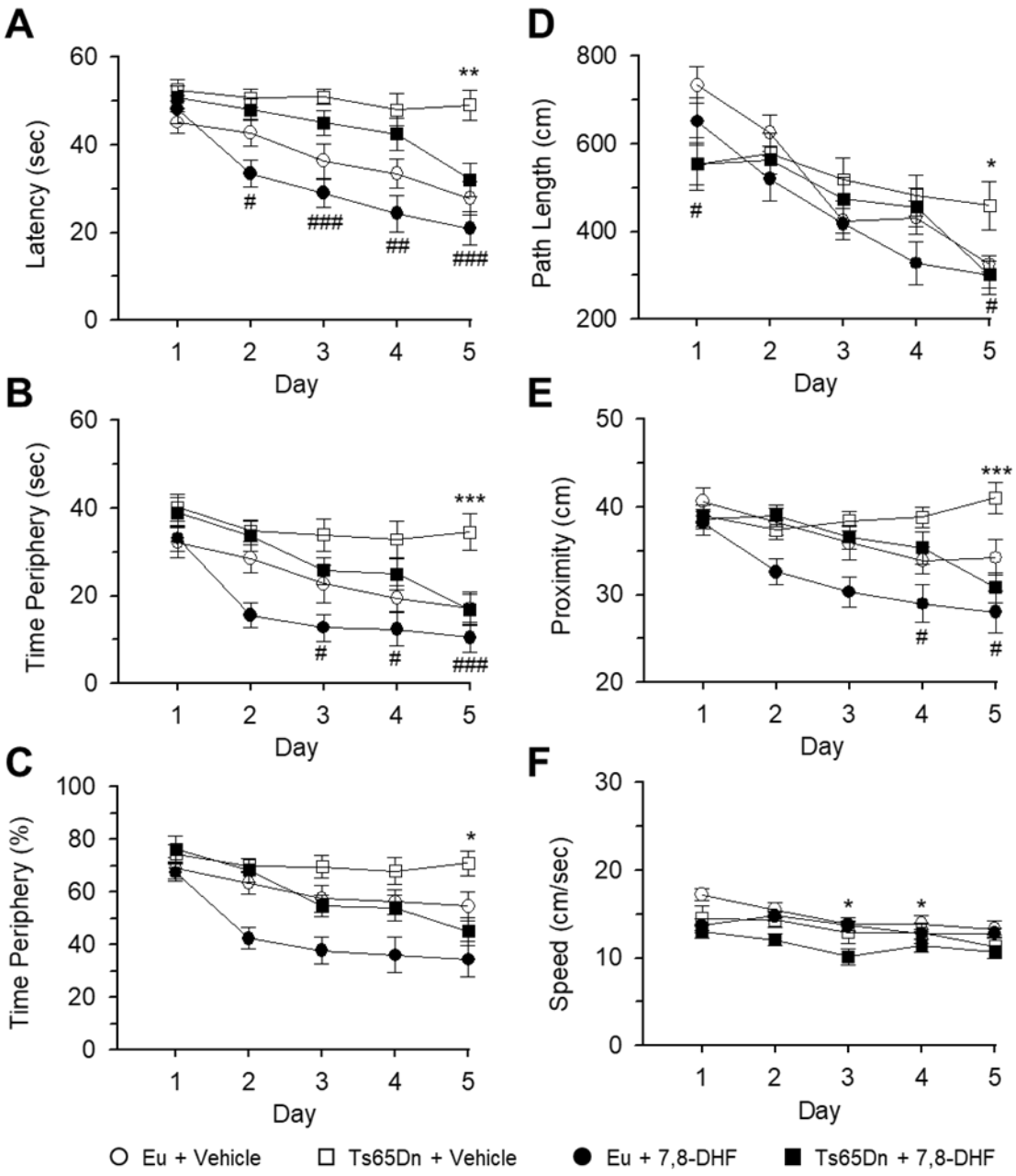

Figure 3.3.8. Effect of treatment with 7,8-DHF on spatial learning in young adult Ts65Dn and euploid mice. Mice received either vehicle or 7,8-DHF in the period P3-P45-50 and were behaviorally tested with the MWM starting from 6 days before reaching 45-50 days of age (untreated euploid mice: n=16; untreated Ts65Dn mice: n=14; treated euploid mice: n=16; treated Ts65Dn mice: n=15). The curves in (A-F) report data of euploid mice that received either vehicle (empty circle) or 7,8-DHF (filled circle) and Ts65Dn mice that received either vehicle (empty square) or 7,8-DHF (filled square). A-E: Learning phase of the MWM evaluated as latency to reach the platform (A), time spent in the periphery (thigmotaxis) (B), percentage of time spent in the periphery (C), path length (D), and proximity to the platform zone (E). F: Swimming speed. B-D: Values represent mean ± SE. Statistical analyses for: untreated Ts65Dn vs Treated Ts65Dn, * $p < 0.05$; ** $p < 0.01$; *** $p < 0.001$; untreated euploid mice vs untreated Ts65Dn mice, # $p < 0.05$; ## $p < 0.01$; ### $p < 0.001$ (Fisher LSD test after two-way ANOVA). Detailed statistical analysis is reported in Table 3.3.3. Abbreviations: 7,8-DHF, 7,8-dihydroxyflavone; cm, centimeters; Eu, euploid; sec, seconds.

Table 3.3.3. P values of the Fisher LSD test for the indicated variables of P45 mice.

Morris Water Maze																					
Learning Phase																					
		Latency					Time Periphery (sec)					Time Periphery (%)									
		D1	D2	D3	D4	D5	D1	D2	D3	D4	D5	D1	D2	D3	D4	D5					
Eu+Veh	Ts+Veh	.054	**.041**	**.001**	**.006**	**< .001**	.081	.140	**.028**	**.011**	**.001**	.258	.472	.242	.123	.094					
	Eu+7,8-DHF	.415	**.013**	.083	.068	.171	.837	**.002**	**.041**	.152	.177	.784	**< .001**	**.007**	**.013**	**.009**					
	Ts+7,8-DHF	.127	.162	**.045**	.078	.412	.131	.215	.532	.273	.939	.152	.189	.799	.983	.634					
Ts+Veh	Eu+7,8-DHF	.246	**< .001**	**< .001**	**< .001**	**< .001**	.120	**< .001**	**< .001**	**< .001**	**< .001**	.384	**< .001**	**< .001**	**< .001**	**< .001**					
	Ts+7,8-DHF	.665	.491	.181	.284	**.002**	.787	.796	.111	.133	**.001**	.783	.569	.363	.124	**.036**					
Eu+7,8-DHF	Ts+7,8-DHF	.461	**< .001**	**< .001**	**.001**	**.033**	.190	**< .001**	**.009**	**.014**	.210	.243	**< .001**	**.004**	**.016**	**.034**					
		Path Lenght					Proximity					Swim speed									
		D1	D2	D3	D4	D5	D1	D2	D3	D4	D5	D1	D2	D3	D4	D5					
Eu+Veh	Ts+Veh	**.022**	.473	.129	.449	**.028**	.382	.620	.325	**.050**	**.012**	.055	.297	.474	.402	.140					
	Eu+7,8-DHF	.269	.103	.905	.111	.660	.180	**.003**	**.006**	**.037**	**.017**	**.010**	.514	.776	.344	.705					
	Ts+7,8-DHF	**.020**	.342	.413	.712	.685	.293	.719	.877	.557	.245	**.003**	**.003**	**.006**	.056	.051					
Ts+Veh	Eu+7,8-DHF	.208	.383	.103	.024	**.010**	.669	**.014**	**< .001**	**< .001**	**< .001**	.550	.677	.328	.939	.263					
	Ts+7,8-DHF	.996	.830	.475	.697	**.011**	.874	.404	.411	.162	**.001**	.299	**.048**	**.042**	.296	.652					
Eu+7,8-DHF	Ts+7,8-DHF	.198	.504	.350	.054	.978	.786	**.001**	**.005**	**.009**	.215	.639	**.015**	**.003**	.315	.111					

Abbreviations: 7,8-DHF, 7,8-dihydroxyflavone; Eu, euploid; sec, seconds; Ts, Ts65Dn; Veh, vehicle.

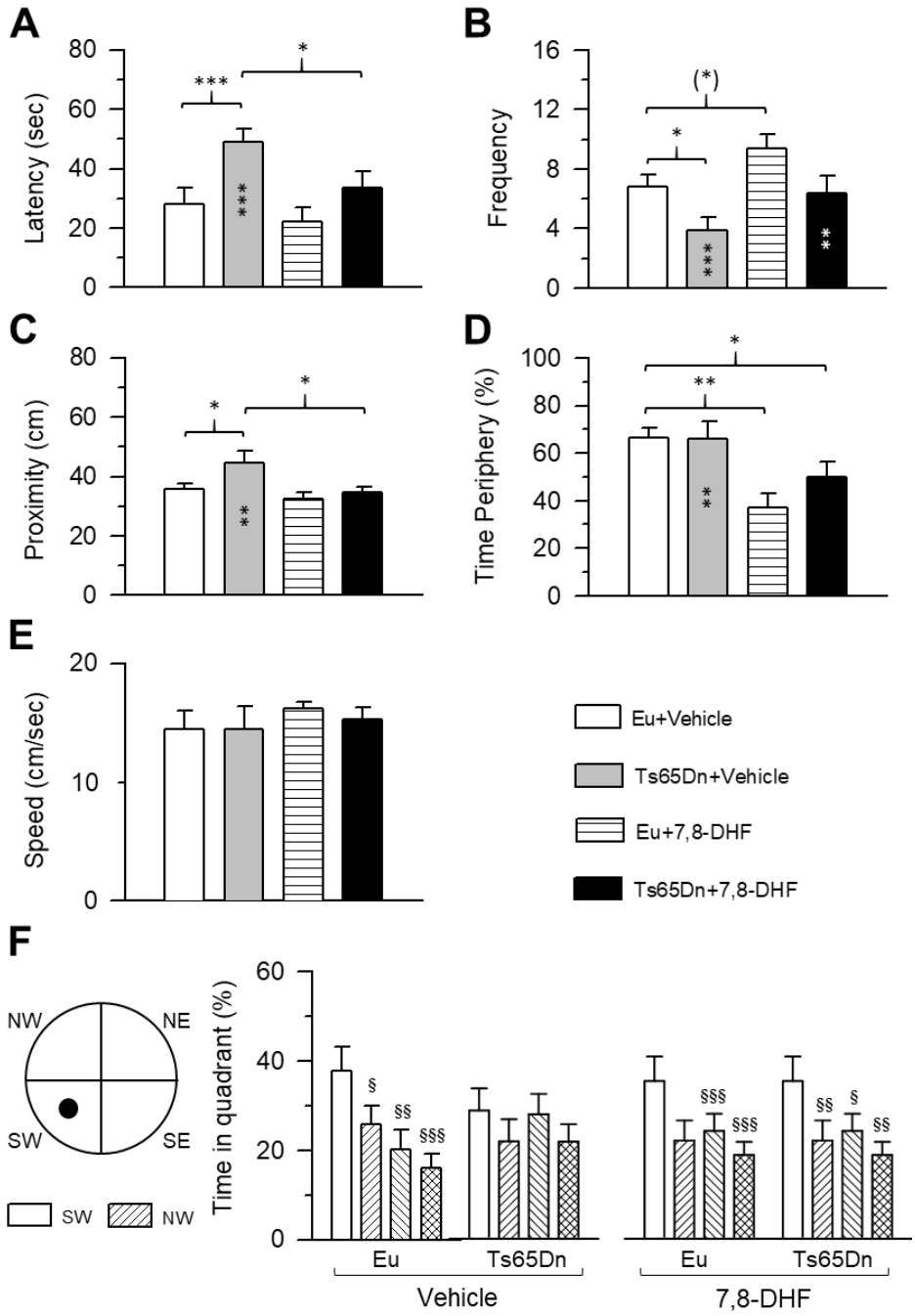

Figure 3.3.9. Effect of treatment with 7,8-DHF on spatial memory in young adult Ts65Dn and euploid mice. Spatial memory was assessed in the probe test after spatial learning (same mice as in Fig. 3.3.7). In the probe test, memory was assessed as latency to reach the trained platform zone (A), number of crossings (frequency) over the trained platform quadrant (B), proximity to the trained platform zone (C), percentage of time spent in the periphery (D), percentage of time spent in quadrants (F). E: Swimming speed during the probe test. Values represent mean ± SE. (*) $p < 0.06$; * $p < 0.05$; ** $p < 0.01$; *** $p < 0.001$; (Fisher LSD test after ANOVA). Black asterisks in the gray bar indicate a difference between untreated Ts65Dn mice and treated euploid mice; white asterisks in the black bar indicate a difference between treated Ts65Dn mice and treated euploid mice. The symbol § in (F) indicates a difference between each individual quadrant and the trained platform quadrant (see key on the left). for each experimental group. § $p < 0.05$; §§ $p < 0.01$; §§§ $p < 0.001$; (two-sample paired t-test). Abbreviations: 7,8-DHF, 7,8-dihydroxyflavone; Eu, euploid; NE, north-east; NW, north-west; SE, south-east; SW, south-west; sec, seconds.

improvement and the latency to reach the platform did not decrease throughout the test (**Fig. 3.3.10A, Table 3.3.4**). Likewise, Ts65Dn mice treated with 7,8-DHF showed a scarce learning improvement and their performance was not statistically different from that of untreated Ts65Dn mice (**Fig. 3.3.10A, Table 3.3.4**). In euploid mice treated with 7,8-DHF the latency was reduced in comparison with that of untreated euploid mice starting from day 5 (**Fig. 3.3.10A, Table 3.3.4**), although the difference was not statistically significant.

Three-way mixed ANOVA on the percentage of time spent in the periphery revealed an interaction of genotype x treatment x day [$F(7,238) = 2.140$, $p = 0.04$]. We found a genotype x day interaction [$F(7,238) = 3.28$, $p = 0.003$], no treatment x day interaction, no genotype x treatment interaction, and no main effects of genotype, treatment and day. A *post hoc* Fisher LSD test showed no differences among groups in the percentage of time spent in the periphery, with the exception of the first day, on which treated euploid mice explored more than the other groups (**Fig. 3.3.10B, Table 3.3.4**).

Three-way mixed ANOVA on the path length showed no effect of genotype x treatment x day. We found a genotype x day interaction [$F(7,238) = 2.21$, $p = 0.034$], no treatment x day interaction, no genotype x treatment interaction, a main effect of genotype [$F(1,34) = 4.22$, $p = 0.048$], a main effect of treatment [$F(1,34) = 14.11$, $p = 0.001$], and a main effect of day [$F(7,238) = 13.33$, $p < 0.001$]. A *post hoc* Fisher LSD test showed that path length decreased throughout the test for all experimental groups. Untreated euploid and Ts65Dn mice made the same path length over the entire test, with slight but not significant differences (**Fig. 3.3.10C, Table 3.3. 4**). In treated euploid mice the path length decreased day by day faster than in their untreated counterpart, suggesting a positive effect on the search strategy (**Fig. 3.3.10C, Table 3.3.4**). The path length also decreased faster in treated Ts65Dn in comparison with untreated Ts65Dn mice, and on days 3, 6, and 7 this decrement reached statistical significance (**Fig. 3.3.10D, Table 3.3.4**). This indicates that treated Ts65Dn have a better strategy to reach the platform in comparison with their untreated counterpart. Three-way mixed ANOVA on the path length showed no effect of genotype x treatment x day. We found no genotype x day interaction, no treatment x day interaction, no genotype x treatment interaction, no main effects

of either genotype or treatment, but a main effect of day [$F(7,238) = 8.49$, $p < 0.001$]. A *post hoc* Fisher LSD test showed no differences among groups in swimming speed and this parameter decreased day by day for all experimental groups (**Fig. 3.3.10D, Table 3.3. 4**). Treated Ts65Dn had a reduced swimming speed in comparison with the other groups every day of the test, although this difference was not statistically significant (**Fig. 3.3.10E, Table 3.3.4**).

In the probe test, we considered the following parameters as an index of spatial memory: i) latency to enter the trained platform zone (latency), ii) frequency of entrances in the trained platform zone (frequency), iii) proximity to the trained platform position (Gallagher's test; proximity), iv) percentage of time spent in the periphery (thigmotaxis), v) swimming speed, vi) percentage of time spent in quadrants. A two-way ANOVA on the latency showed no genotype x treatment interaction, no main effect of treatment but a main effect of genotype [$F(1,32) = 5,59$, $p = 0.024$]. A *post hoc* Fisher LSD test showed that untreated Ts65Dn mice exhibited a longer latency than untreated and treated euploid mice, although this difference was statistically significant in comparison with untreated euploid mice only, and that treatment did not improve latency (**Fig. 3.3.11A**). A two-way ANOVA on the frequency showed no genotype x treatment interaction, no main effect of treatment but a main effect of genotype [$F(1,32) = 6.44$, $p = 0.016$]. A *post hoc* Fisher LSD test showed that untreated Ts65Dn mice exhibited a reduced frequency of entrances than untreated euploid mice and that treatment did not cause a frequency increase (**Fig. 3.3.11B**). A two-way ANOVA on the proximity showed no genotype x treatment interaction, but a main effect of genotype [$F(1,32) = 5.08$, $p = 0.031$] and a main effect of treatment [$F(1,32) = 6.54$, $p = 0.016$]. A *post hoc* Fisher LSD test showed that untreated Ts65Dn mice swam at a larger distance from the trained platform zone in comparison with untreated and treated euploid mice, although this difference was statistically significant vs. the latter only (**Fig. 3.3.11C**). In treated Ts65Dn mice, the distance from the trained platform zone was not different in comparison with that of untreated euploid mice, although it was not different also in comparison with Ts65Dn mice (**Fig. 3.3.11C**). This indicates an improvement in searching strategy of treated Ts65Dn mice, and this result is in agreement with that obtained on path

length during learning phase (see **Fig. 3.3.10C**). A two-way ANOVA on thigmotaxis showed no genotype x treatment interaction, no main effect of both genotype and treatment. In agreement with evidence for the learning phase, a *post hoc* Fisher LSD test showed that in the probe test there were no differences in thigmotaxis among experimental groups, even though treated and untreated euploid mice spent more time in the center of the pool in comparison with Ts65Dn mice (**Fig. 3.3.11D**).

Two-way ANOVA on the swimming speed showed no genotype x treatment interaction, no main effect of both genotype and treatment. A *post hoc* Fisher LSD test no differences among groups, with the only exception of treated Ts65Dn mice that had a lower swimming speed in comparison with untreated euploid mice (**Fig. 3.3.11E**).

A paired samples t-test showed that untreated Ts65Dn mice exhibited no differences in the time spent in the trained platform quadrant in comparison with the other quadrants (**Fig. 3.3.11F**). Like their untreated counterparts, treated Ts65Dn mice did not discern among quadrants (**Fig. 3.3.11F**). Untreated euploid mice spent significantly more time in the trained platform quadrant in comparison with the NE [$t(11) = 2.98$; $p = 0.013$], SE quadrant [$t(11) = 3.43$; $p = 0.006$] and NW [$t(11) = 2.23$; $p = 0.047$] quadrants (**Fig. 3.3.11F**). Likewise, treated euploid mice spent significantly more time in the trained platform quadrant in comparison with the SE [$t(6) = 3.52$; $p = 0.013$] quadrant but not with the other two (**Fig. 3.3.11F**).

Taken together, data from learning phase and probe test show that treatment with 7,8-DHF administered from 4 to 5 months of age improves only partially spatial hippocampal skills in the Ts65Dn mouse. Indeed, in contrast to what we observed in P45 mice, there were no effects of treatment on latency to reach the platform neither in learning phase nor in the probe test, although Ts65Dn mice treated with 7,8-DHF had a reduced swim path and swam closer to the trained platform zone in comparison with untreated Ts65Dn mice. These discrepancies between P45 and 5 month-old mice suggest that there is an effect of age in Ts65Dn mice that changes their response to BDNF mimetics, such as 7,8-DHF. It remains to be established whether other doses of 7,8-DHF would be able to ameliorate more strongly hippocampus-dependent behavior in adult Ts65Dn mice.

Interestingly, 5 month-old euploid mice treated with 7,8-DHF showed an improvement in almost all parameters of the learning phase (but not of the probe test) analysed in this study in comparison with their untreated counterpart. Indeed, although there is no statistical differences (see **Table 3.3.4**), treated euploid mice had a reduced latency to reach the platform, spent less time at the periphery, and had a shorter swim path. These data indicates that a molecule that stimulate the BDNF/TRKB pathway increases learning abilities in adult healthy mice.

Effect of 7,8-DHF on neurogenesis in 5 month-old Ts65Dn and euploid mice

Immature granule neurons express doublecortin (DCX) during the period of neurite elongation (from one to four weeks after neuron birth) (Couillard-Despres et al., 2005), which allows evaluation of total number of new granule cells. In order to establish whether treatment with 7,8-DHF enhances hippocampal neurogenesis, brain sections of mice treated for one month with saline or 7,8-DHF were subjected to immunohistochemistry for DCX. A two-way ANOVA on the number of DCX-positive cells showed no genotype x treatment interaction but a significant effect of genotype [$F(1,14) = 24.83$, $p < 0.001$] and no effect of treatment. In agreement with previous evidence, untreated Ts65Dn mice had a reduced number of new granule cells in comparison with untreated euploid mice (**Fig. 3.3.12A,B**). Treatment with 7,8-DHF did not increase the number of new granule cells that remained reduced in comparison with control euploid mice (**Fig. 3.3.12A,B**). In euploid mice treatment with either vehicle or 7,8-DHF did not affect the number of proliferating cells (**Fig. 3.3.12A,B**).

Effect of 7,8-DHF on the phosphorylation levels of the TRKB receptor in 5 month- old Ts65Dn and euploid mice

Binding of BDNF or its mimetic 7,8-DHF to the TRKB full length receptor (TRKB-FL), that possesses an intracellular tyrosine kinase domain, causes receptor dimerization and autophosphorylation. By contrasts, the truncated form of the TRKB receptor (TRKB-T1) lacks tyrosine kinase activity. In order to establish the effect of 7,8-DHF on the expression levels and

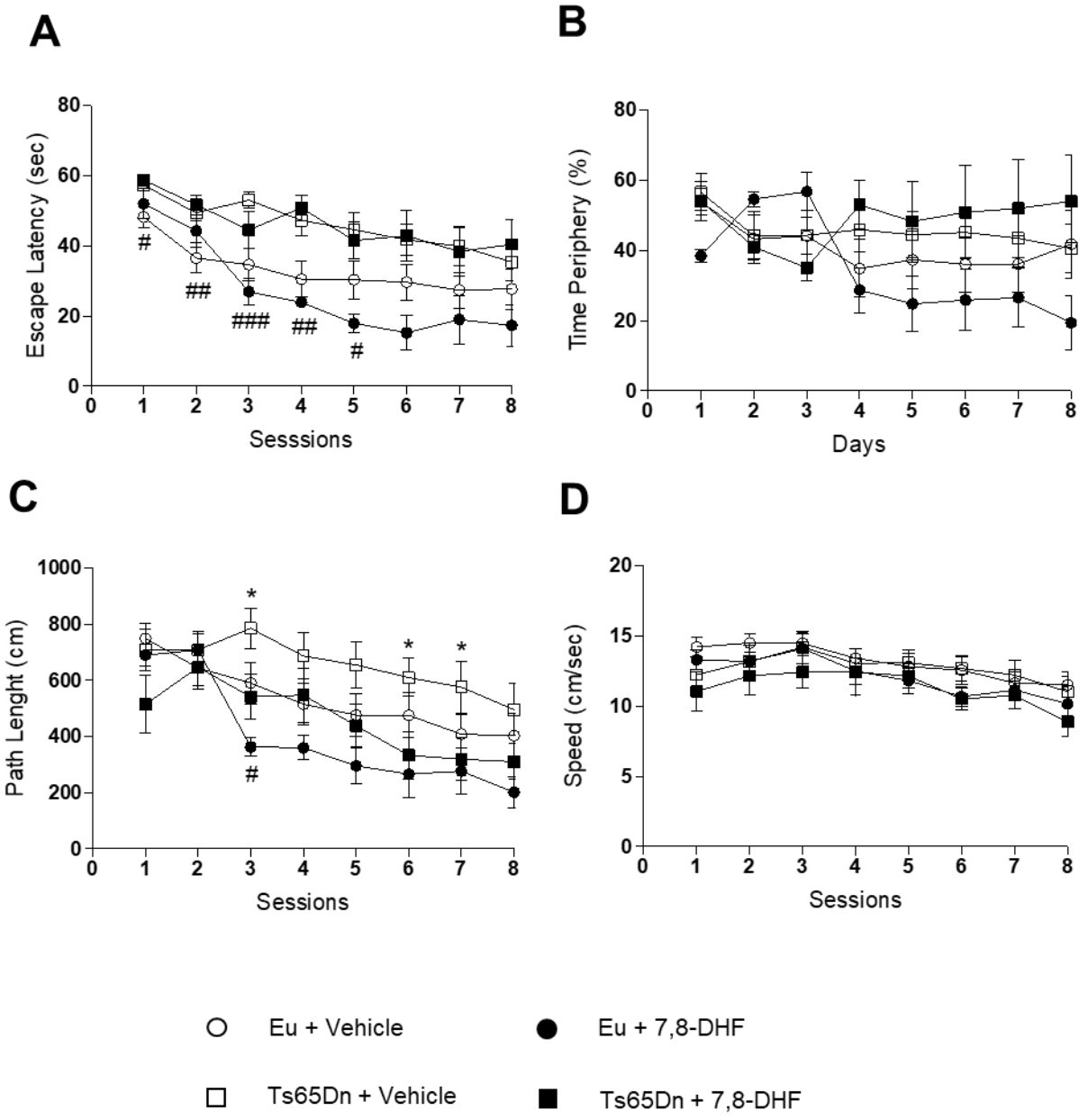

Figure 3.3.10. Effect of treatment with 7,8-DHF on spatial learning in 5 month-old Ts65Dn and euploid mice. Mice received either vehicle or 7,8-DHF in the period 4M-5M+9 days and were behaviorally tested with the MWM during the last 9 days of treatment (untreated euploid mice: n=13; untreated Ts65Dn mice: n=11; treated euploid mice: n=7; treated Ts65Dn mice: n=7). The curves in (A-D) report data of euploid mice that received either vehicle (empty circle) or 7,8-DHF (filled circle) and Ts65Dn mice that received either vehicle (empty square) or 7,8-DHF (filled square). A-C: Learning phase of the MWM evaluated as latency to reach the platform (A), percentage of time spent in the periphery (B), path length (C). D: Swimming speed. Values in (B-D) represent mean ± SE. Statistical analyses for: untreated Ts65Dn vs Treated Ts65Dn, * $p < 0.05$; untreated euploid mice vs untreated Ts65Dn mice, # $p < 0.05$; ## $p < 0.01$; ### $p < 0.001$ (Fisher LSD test after two-way ANOVA). Detailed statistical analysis is reported Table 3.3.4. Abbreviations: 7,8-DHF, 7,8-dihydroxyflavone; Eu, euploid; sec, seconds.

Table 3.3.4. P values of the Fisher LSD test for the indicated variables of 5 month-old mice.

		Latency (s)							
		D1	**D2**	**D3**	**D4**	**D5**	**D6**	**D7**	**D8**
Eu+Veh	**Eu+7,8-DHF**	0.296	0.135	0.170	0.281	0.078	0.051	0.293	0.209
	Ts65Dn+Veh	**0.017**	**0.006**	**0.001**	**0.003**	**0.022**	0.060	0.079	0.282
	Ts65Dn+7,8-DHF	**0.018**	**0.005**	0.083	**0.002**	0.108	0.073	0.174	0.194
Eu+7,8-DHF	**Ts65Dn+Veh**	0.283	0.331	**≤ 0.001**	**0.001**	**0.001**	**0.001**	**0.015**	**0.037**
	Ts65Dn+7,8-DHF	0.217	0.204	**0.008**	**≤ 0.001**	**0.004**	**0.002**	**0.038**	**0.029**
Ts65Dn+Veh	**Ts65Dn+7,8-DHF**	0.767	0.659	0.144	0.585	0.668	0.882	0.852	0.722
		Time at the periphery (%)							
		D1	**D2**	**D3**	**D4**	**D5**	**D6**	**D7**	**D8**
Eu+Veh	**Eu+7,8-DHF**	**0.016**	0.215	0.159	0.559	0.293	0.414	0.459	0.096
	Ts65Dn+Veh	0.617	0.907	0.980	0.234	0.490	0.405	0.516	0.917
	Ts65Dn+7,8-DHF	0.975	0.805	0.312	0.093	0.359	0.237	0.225	0.357
Eu+7,8-DHF	**Ts65Dn+Veh**	**0.007**	0.269	0.178	0.119	0.113	0.139	0.209	0.125
	Ts65Dn+7,8-DHF	**0.032**	0.194	**0.038**	**0.050**	0.088	0.084	0.091	**0.026**
Ts65Dn+Veh	**Ts65Dn+7,8-DHF**	0.693	0.735	0.317	0.519	0.758	0.653	0.525	0.328
		Path Lenght (m)							
		D1	**D2**	**D3**	**D4**	**D5**	**D6**	**D7**	**D8**
Eu+Veh	**Eu+7,8-DHF**	0.531	0.739	**0.030**	0.166	0.107	0.067	0.259	0.085
	Ts65Dn+Veh	0.620	0.447	**0.033**	0.082	0.070	0.175	0.105	0.361
	Ts65Dn+7,8-DHF	**0.018**	0.979	0.627	0.773	0.725	0.206	0.441	0.420
Eu+7,8-DHF	**Ts65Dn+Veh**	0.850	0.746	**≤ 0.001**	**0.007**	**0.003**	**0.005**	**0.016**	**0.017**
	Ts65Dn+7,8-DHF	0.111	0.787	0.129	0.144	0.262	0.601	0.749	0.407
Ts65Dn+Veh	**Ts65Dn+7,8-DHF**	0.054	0.535	**0.024**	0.225	0.062	**0.021**	**0.037**	0.124
		Swim speed (cm/s)							
		D1	**D2**	**D3**	**D4**	**D5**	**D6**	**D7**	**D8**
Eu+Veh	**Eu+7,8-DHF**	0.531	0.954	0.789	0.473	0.453	0.152	0.730	0.343
	Ts65Dn+Veh	0.620	0.292	0.821	0.749	0.815	0.929	0.654	0.689
	Ts65Dn+7,8-DHF	0.018	0.104	0.150	0.913	0.616	0.119	0.484	0.071
Eu+7,8-DHF	**Ts65Dn+Veh**	0.477	0.401	0.947	0.670	0.356	0.144	0.476	0.559
	Ts65Dn+7,8-DHF	0.180	0.166	0.298	0.468	0.827	0.908	0.754	0.435
Ts65Dn+Veh	**Ts65Dn+7,8-DHF**	0.432	0.480	0.225	0.706	0.494	0.113	0.292	0.152

Abbreviations: 7,8-DHF, 7,8-dihydroxyflavone; Eu, euploid; Ts, Ts65Dn; Veh, vehicle.

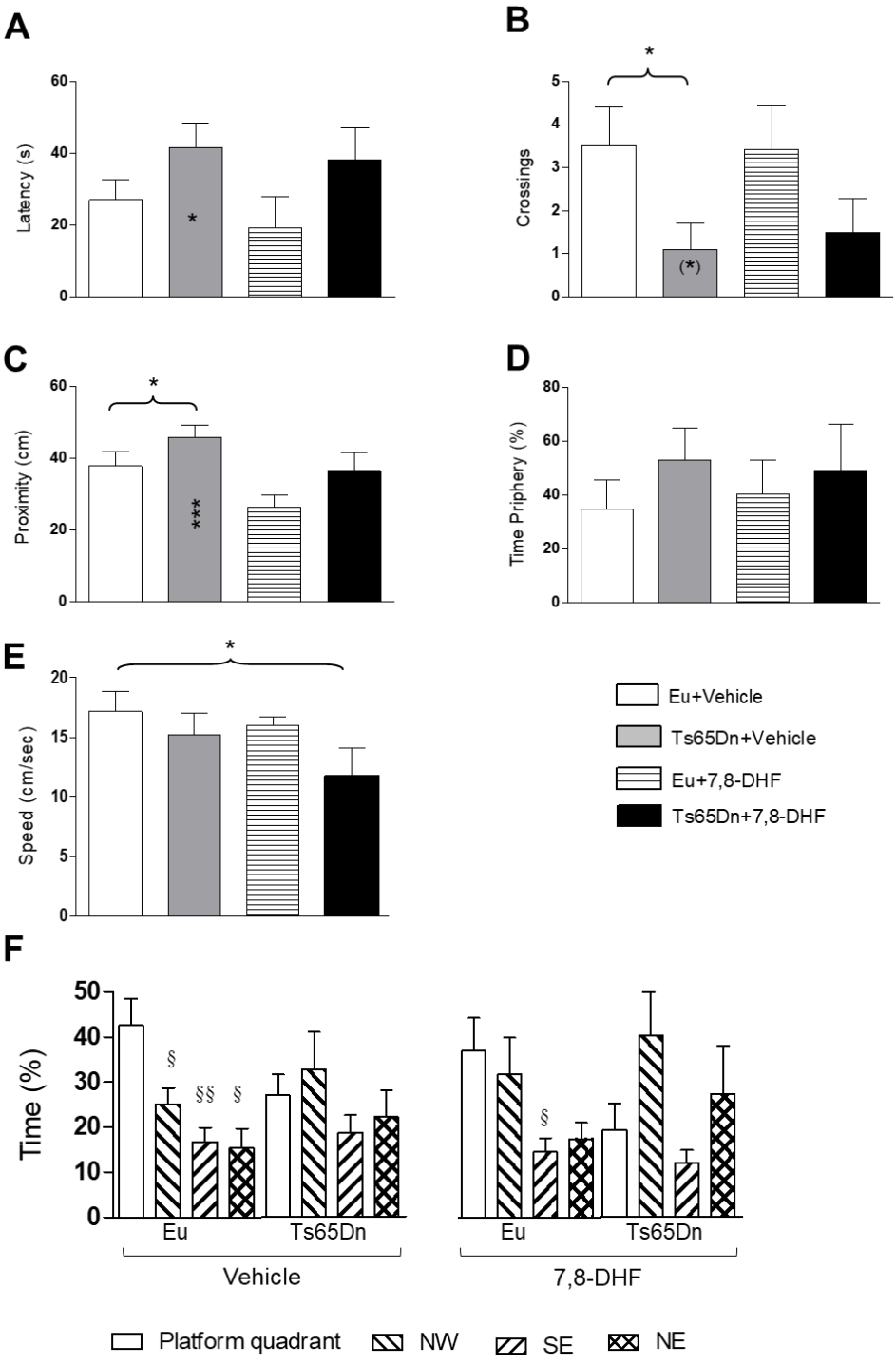

Figure 3.3.11. Effect of treatment with 7,8-DHF on spatial memory in 5 month-old Ts65Dn and euploid mice. Spatial memory was assessed in the probe test after spatial learning (same mice as in Fig. 3.3.10). In the probe test, memory was assessed as latency to reach the trained platform zone (A), number of crossings (frequency) over the trained platform zone (B), proximity to the trained platform zone (C), percentage of time spent in the periphery (D), percentage of time spent in quadrants (F). E: Swimming speed during the probe test. Values represent mean ± SE. (*) $p < 0.06$; * $p < 0.05$; *** $p < 0.001$ (Fisher LSD test after ANOVA). Black asterisks in the gray bar indicate a difference between untreated Ts65Dn mice and treated euploid mice. The symbol § in (F) indicates a difference between each individual quadrant and the trained platform quadrant (see key below). for each experimental group. (§) $p < 0.06$; § $p < 0.05$; §§ $p < 0.01$ (two-sample paired t-test). Abbreviations: 7,8-DHF, 7,8-dihydroxyflavone; Eu, euploid; NE, north-east; NW, north-west; SE, south-east sec, sec, seconds

activity of the TRKB receptor, hippocampal homogenates of treated and untreated mice were subjected to western blot analysis. A two-way ANOVA on the levels of BDNF showed no genotype x treatment interaction and no main effect of both genotype and treatment. Accordingly with data obtained in P15 mice, a post hoc Fisher LSD test did not reveal any difference in BDNF levels between untreated euploid and Ts65Dn mice aged 5 months (data not shown). Treatment with 7,8-DHF did not affect the levels of BDNF in euploid as well as Ts65Dn mice (data not shown).

A two-way ANOVA on the levels of TRKB-FL receptor showed no genotype x treatment interaction, no main effect of genotype but a main effect of treatment [$F(1,26) = 16.51$, $p < 0.001$]. A *post hoc* Fisher LSD test showed that untreated and Ts65Dn mice had reduced levels of the TRKB-FL receptor in comparison with untreated euploid mice (**Fig. 3.3.13B**). Treatment with 7,8-DHF caused an increase in the levels of the TRKB-FL receptor that became similar to those of untreated euploid mice. An increase in TRKB-FL receptor levels also took place in treated euploid mice in comparison with their untreated counterparts, although the difference was not statistically significant. A two-way ANOVA on the levels of the phosphorylated form of the TRKB receptor (p-TRKB) showed no genotype x treatment interaction, no main effect of genotype but a main effect of treatment [$F(1,23) = 5.31$, $p = 0.03$]. A *post hoc* Fisher LSD test showed that in untreated Ts65Dn mice the levels of p-TRKB were similar to those of euploid mice (**Fig. 3.3.13C**). In Ts65Dn mice, treatment with 7,8-DHF caused a reduction in the levels of p-TRKB in comparison with their untreated counterparts as well as in comparison with untreated euploid (**Fig. 3.3.13C**).

A two-way ANOVA on the levels of the TRKB-T1 receptor showed no genotype x treatment interaction and no main effect of either genotype or treatment. A *post hoc* Fisher LSD test showed that untreated Ts65Dn mice has similar levels of TRKB-T1 as untreated euploid mice. Treated Ts65Dn and euploid mice underwent an increase in the levels of TRKB-T1 in comparison with their untreated counterparts but the difference was not statistically significant (**Fig. 3.3.13D**).

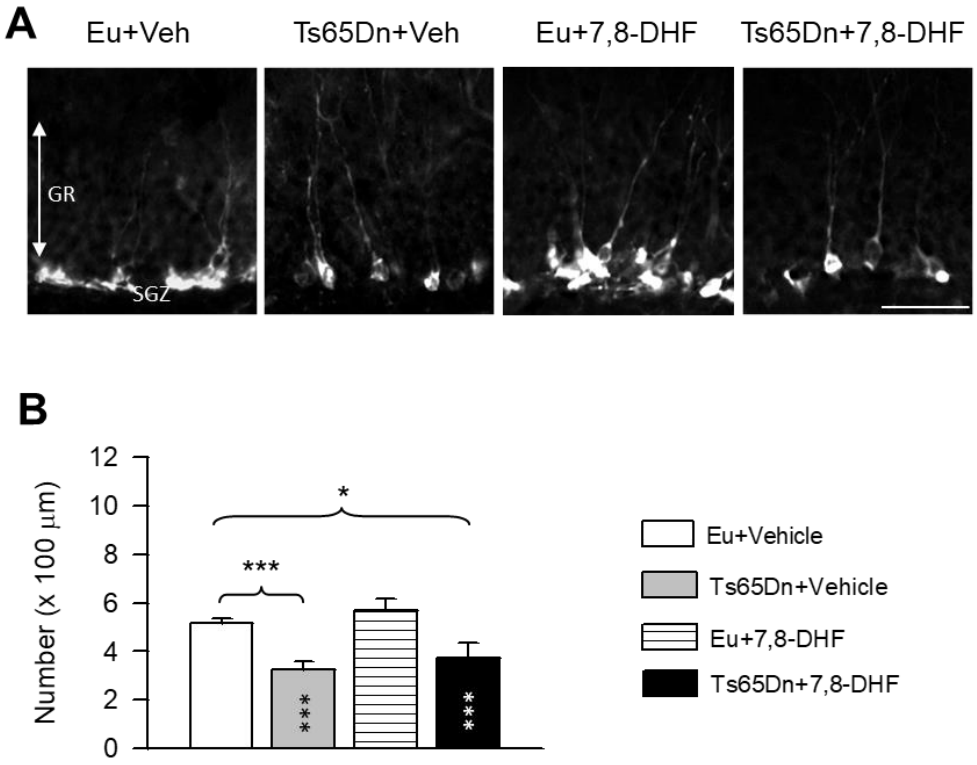

Figure 3.3.12. Effect of treatment with 7,8-DHF on the number of new granule cells in the dentate gyrus of 5 month-old mice. A: Examples of sections processed for fluorescence immunostaining for DCX from the DG of untreated and treated mice. Calibration bar: 50 µm. B: Number of DCX-positive cells in the DG of of untreated euploid (n=6) and Ts65Dn mice (n=6) and euploid (n=4) and Ts65Dn (n=4) mice treated with 7,8-DHF. Values represent mean ± SE. * $p < 0.05$; *** $p < 0.001$ (Fisher LSD test after two-way ANOVA). Black asterisks in the gray bar indicate a difference between untreated Ts65Dn mice and treated euploid mice; white asterisks in the black bar indicate a difference between treated euploid and treated Ts65Dn mice. Abbreviations: 7,8-DHF, 7,8-dihydroxyflavone; Eu, euploid; Gr, granule cell layer; SGZ, subgranular zone.

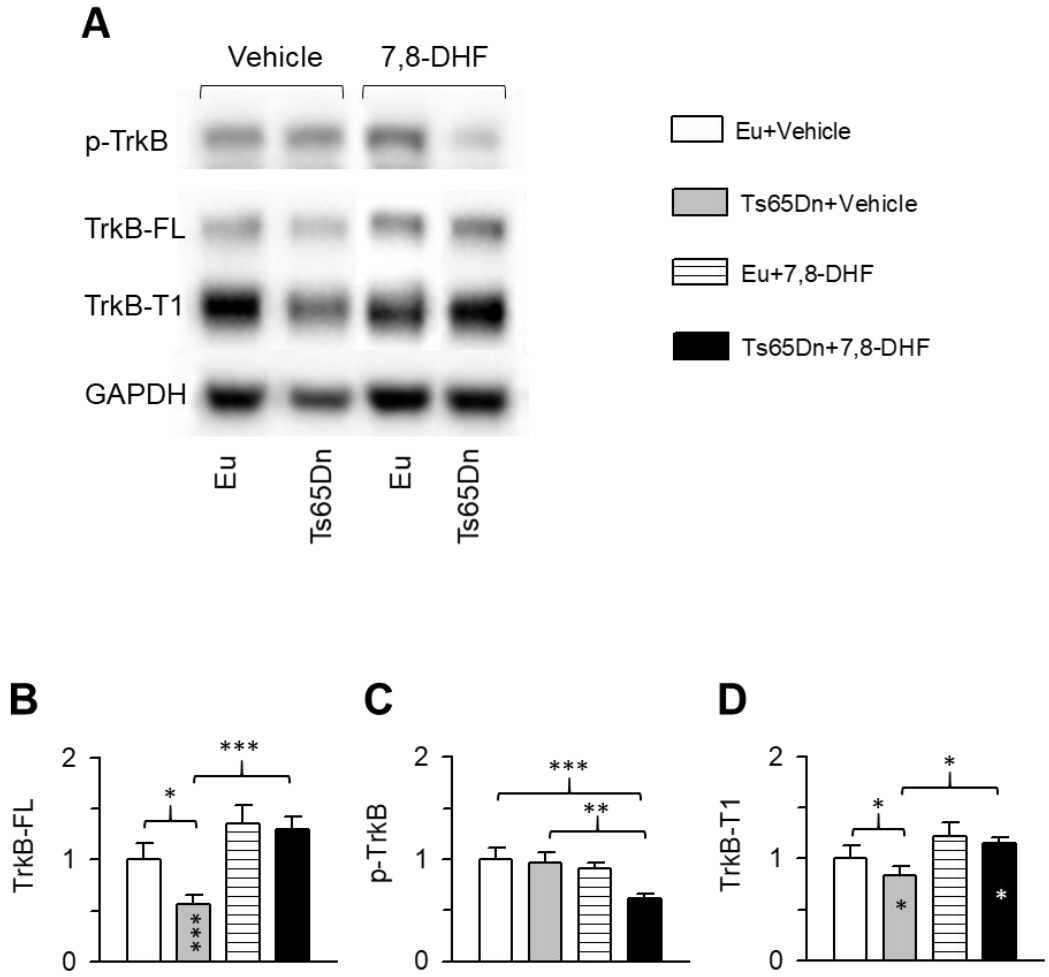

Figure 3.3.14. Effects of treatment with 7,8-DHF on the TRKB receptor. Western blot analysis of the TRKB receptor in hippocampal homogenates of treated and untreated mice. A: representative western blots showing immunoreactivity for the phosphorylated TRKB receptor (p-TRKB), the full length TRKB receptor (TRKB-FL), the truncated TRKB receptor (TRKB-T1), and the housekeeping gene GAPDH. B-D: Levels of TRKB-FL (B) p-TRKB (C) and TRKB-T1 (D) of untreated euploid (n=8) and Ts65Dn (n=9) and euploid (n=7) and Ts65Dn (n=7) mice treated with 7,8-DHF. Values represent mean ± SE. * $p < 0.05$; $p < 0.01$ *** $p < 0.001$ (Fisher LSD test after two-way ANOVA). Black asterisks in the gray bar indicate a difference between untreated Ts65Dn mice and treated euploid mice; white asterisks in the black bar indicate a difference between treated euploid and treated Ts65Dn mice. Abbreviations: 7,8-DHF, 7,8-dihydroxyflavone; Eu, euploid.

3.3.5 Discussion

Results show that treatment with a BDNF mimetic restores hippocampal neurogenesis and dendritic spine density in pups and largely improves behavior in young adult mice. In contrast, 7,8-DHF administration in adult mice is ineffective on neurogenesis and only partially improves behavior, suggesting that the magnitude of treatment effects may change with age.

Treatment with the BDNF mimetic 7,8-DHF positively impacts the major defects of hippocampal development in Ts65Dn mice

In disagreement with data obtained in adult Ts65Dn mice (Bimonte-Nelson et al., 2003, Fukuda et al., 2010, Begenisic et al., 2015), we did not find any reduction in BDNF protein levels in the hippocampus of P15 Ts65Dn mice, suggesting that BDNF expression may be differently regulated during different life stages. Although there were no differences of BDNF expression levels in neonate Ts65Dn in comparison with euploid mice, treatment with 7,8-DHF resulted in the recovery of neurogenesis reduction and dendritic pathology, consistently with the pivotal role played by BDNF in brain development.

We found that treatment with 7,8-DHF increased the number of proliferating cells in the SGZ of Ts65Dn mice. Indeed, while the number of dividing cells in untreated Ts65Dn mice was -30% in comparison with untreated euploid mice, in treated Ts65Dn mice their number was -13% (see **Fig. 3.3.3C**), indicating that 7,8-DHF causes a large improvement in proliferation potency. Importantly, although the number of dividing cells in the SGZ of Ts65Dn mice was not fully rescued after treatment, total granule cell number was fully restored. This result may be explained by an effect of 7,8-DHF on the process of phenotype acquisition, with a shift in the relative number of cells destined to become neurons. P15 Ts65Dn mice exhibited an impairment in the process of spinogenesis. The finding that their granule neurons had a reduced spine density indicates that this defect starts at early phases of hippocampal development. This spine defects implies a reduction in the number of

excitatory terminals and, consequently, reduced complexity of hippocampal circuitry. Consistently with this conclusion, an evaluation of the levels of the presynaptic protein SYN in Ts65Dn mice showed that the counterpart of the spine density reduction was a reduction in SYN levels. We showed that treatment with 7,8-DHF restored the number of dendritic spines of Ts65Dn mice as well as SYN levels, suggesting a treatment-induced restoration of the hippocampal circuitry.

Conflicting results are reported in the literature regarding the pro-proliferative effect of the BDNF/TRKB system in different species and cellular systems (Foltran and Diaz, 2016, Vilar and Mira, 2016). Many studies suggest that BDNF fosters neurogenesis and neuron maturation but not proliferation of NPCs. Our results suggest that in Ts65Dn mice activation of the TRKB receptor enhances NPCs proliferation, in addition to neurogenesis and neuron maturation. Although the effect on proliferation was less prominent than the effect on neurogenesis and neuron maturation, the outcome was restoration of the defective cellularity in the granule layer of the DG. It is of interest to observe that some of the neurogenesis-enhancing therapies attempted so far in mouse models of DS may present caveats for human use due to the risk of uncontrolled proliferation in peripheral tissues and, thus, have a cancerogenic effect (Bartesaghi et al., 2011, Gardiner, 2015). The finding that 7,8-DHF, in spite of its relatively moderate pro-proliferative activity, is able to restore the final number of granule neurons may render this molecule a good candidate for therapy in DS.

Treatment with 7,8-DHF rescues hippocampus-dependent behavior in young adult Ts65Dn mice

The granule cells of the DG are the first element of the hippocampal trisynaptic circuit, a circuit whose function is fundamental for long-term memory. The dendrites of the granule cells receive their major input from the entorhinal cortex that represents an interface between the hippocampal formation and the rest of the brain. Signals from polymodal association cortices sent by the entorhinal cortex to the DG are processed by the trisynaptic circuit and then sent back to the entorhinal cortex. Hippocampus-dependent learning and memory impairment is a consistent feature of DS and the Ts65Dn mouse model (Demas et al., 1996, Carlesimo et al., 1997, Vicari et al., 2000, Belichenko et

al., 2007, Salehi et al., 2009). We found here that in Ts65Dn mice treated with 7,8-DHF there was an improvement in hippocampus-dependent learning and a rescue in spatial memory, as assessed in the probe test, indicating that the effects of treatment on the hippocampal defects that characterize the trisomic condition translate into a behavioral benefit. It remains to be established whether after treatment cessation these effects are retained at further life stages.

Activation of the TRKB receptor by 7,8-DHF enhances the activity of TRKB receptor-dependent signaling

In the hippocampus of P15 Ts65Dn mice we found normal levels of BDNF, TRKB-FL, and TRKB-T1 receptors. Results showed a reduction in the levels of BDNF and TRKB-FL receptor in Ts65Dn mice after thirteen days of treatment with 7,8-DHF, suggesting a compensatory reduction of their transcription and/or an increase in their degradation. The absence of a similar reduction in treated euploid mice suggests that the mechanisms underlying degradation of the TRKB receptor may be more powerful in the trisomic brain. It must be noted that, although treatment induced an overall reduction in TRKB receptor levels, its phosphorylation increased, indicating that treatment activates TRKB receptor, and, hence, TRKB-dependent pathways. Accordingly, we found here that in treated Ts65Dn mice there was an increase in the levels of p-ERK1 and p-ERK2, which is consistent with the treatment-induced phosphorylation increase of the TRKB receptor. ERK activity is required for cell proliferation (Lefloch et al., 2008), and there is evidence that the BDNF/TRKB signaling-induced increase in spine density of hippocampal pyramidal neurons is ERK1/2 dependent (Alonso et al., 2004). Thus, we hypothesize that the increased activity of ERK1/2 after 7,8-DHF treatment may represent a key contributor to the rescue of hippocampal development in Ts65Dn mice.

Although much is now known regarding the role of ERK1/2, the mechanisms underlying their expression still need to be elucidated (Busca et al., 2016). We found here that treatment with 7,8-DHF increased both ERK1 and ERK2 levels. A recent study shows that the ratio between total ERK1 and ERK2 protein levels in different mouse brain regions is about 1:4, that the same ratio holds for

p-ERK1/2 and that derangement of these ratios has adverse effects on the brain (Lefloch et al., 2008). Importantly, in Ts65Dn mice, treatment caused an increase in ERK1/2 and p-ERK1/2 but their ratios remained similar to those of their untreated counterparts. This indicates that treatment enhances the activity of ERK1/2 without disrupting the important balance between the two ERK isoforms.

Treatment with 7,8-DHF has no adverse effects on viability and growth of Ts65Dn mice

In order to evaluate whether 7,8-DHF as adverse effects in Ts65Dn mice, we considered mice viability, body weight, and brain wheight. We found no effect of treatment on mice viability. There is evidence that in rodents treatment with BDNF causes a reduction in food intake and that activation of muscular TRKB by 7,8-DHF regulates energy metabolism in muscles (Gray et al., 2006, Chan et al., 2015). Conversely, rodent models with a reduction in BDNF/TRKB signaling exhibit hyperphagia and obesity (Chan et al., 2015). We found that a relatively short treatment with 7,8-DHF (13 days: from P3 to P15) as well as a more prolonged treatment (42-47 days: from P3 to P45-50) did not cause a body weight reduction in Ts65Dn mice. In addition, we did not found an adverse effect of treatment on the brain weight of Ts65Dn mice, but rather, a positive effect on brain growth. From these findings it appears that a chronic treatment with 7,8-DHF has a safe profile on the general health of Ts65Dn mice, suggestig a high translational impact of treatment with 7,8-DHF.

Treatment with 7,8-DHF does not rescue neurogenesis but leads to an improvement of behavior in adult Ts65Dn mice

In contrast with the positive effects of a treatment with 7,8-DHF seen in Ts65Dn pups, we found that 41 days of treatment with 7,8-DHF in adult Ts65Dn mice did not enhance hippocampal neurogenesis. Although with a different magnitude, treatment amelliorated hippocampus-dependent learning abilities as in young-adult as in adult Ts65Dn mice. There are evidence that treatment with 7,8-DHF in 5XFAD mice (a mouse model of familial AD) increases dendritic spine density in hippocampal neurons and rescues memory deficits (Zhang et al., 2014). Given that there was a lack of neurogenesis

enhancement in 5 month-old treated Ts65Dn mice, it would be reasonable that good effects of 7,8-DHF observed in learning phase of MWM may be related to an improvement in neuronal maturation (dendritic arbour/dendritic spines) of pre-existent hippocamapal granule cells. This could lead to an amelioration of hippocampal circuitry and, thus, hippocampal dependent behavior. Further studies should be conducted to settle this issue. These results in the Ts65Dn mouse model of DS are consistent with evidence obtained in models of other brain disorders, showing that treatment with 7,8-DHF, administered at the same dose (5.0 mg/kg) used in this study, ameliorates cognition (Jang et al., 2010, Liu et al., 2010, Andero et al., 2011, Andero et al., 2012, Devi and Ohno, 2012, Zeng et al., 2012, Zhang et al., 2014). Treatment with 7,8-DHF ameliorates motor function in a mouse model of Hungtington's disease (Jiang et al., 2013) and improves motor performance and neuronal survival in a mouse model of amyotrophic lateral sclerosis (Korkmaz et al., 2014). This is in contrast with our observation in Ts65Dn mice, where we observed a mild reduction in swimming speed during MWM in adult mice treated with 7,8-DHF.

The schedule of treatment used in the studies mentioned above ranged from a few days to months, suggesting that the lack of an effect on neurogenesis in Ts65Dn mice observed here is unlikely to be related to an insufficient duration of treatment. Different disorders of the nervous system may show common molecular signatures but also widely different molecular alterations, suggesting that the outcome of a given therapeutic approach may not be necessarily shared by different brain disorders. It seems reasonable to conclude that the reduced effects of treatment with 7,8-DHF on neurogenesis observed here in the Ts65Dn model may be related to differences in the molecular pathways that are perturbed in this model and in the models in which 7,8 DHF resulted effective. In this connection, it is of importance to observe that 5XFAD mouse model of AD shows reduction in both TRKB-FL and p-TRKB receptors and that treatment with 7,8-DHF for 12 days restores both TRKB-FL and p-TRKB receptor levels (Devi and Ohno, 2012). In the same model, treatment for 4 months increases p-TRKB (although not total TRKB) levels (Zhang et al., 2014). Aged rats, exhibit significant decreases in TRKB and p-TRKB levels in the hippocampus compared to young controls and administration of

7,8-DHF for 34 days enhances p-TRKB (but not total TRKB) levels (Zeng et al., 2012). Finally, in a mouse model of Hungtington's disease, treatment with 7,8-DHF from 6 to 20 weeks of age has been shown to increase p-TRKB levels (Jiang et al., 2013).

We found here that Ts65Dn mice exhibit reduced levels of the TRKB receptor but normal levels of its active form (p-TRKB). This is at variance with the 5XFAD mouse model and with aged rats that exhibit reduced levels of both the TRKB and p-TRKB receptors. In Ts65Dn mice treatment with 7,8-DHF largely increased the expression of the TRKB receptor that became twice as large as that of untreated Ts65Dn mice but, surprisingly, it reduced the relative levels of its active form (p-TRKB). The mechanisms underlying the treatment-induced increase in TRKB levels with a concomitant reduction in its relative phosphorylation form remain to be elucidated. It should be taken into account that, however, higher levels of TRKB-FL would lead to an increase in the number of receptors that can be phosphorylated and, in fact, we observed an increase of 32% in p-TRKB absolute levels (normalizing p-TRKB on GAPDH) in the hippocampus of Ts65Dn treated with 7,8-DHF (data not shown). Whatever the explanation, since the BDNF/TRKB receptor system plays an important role in the modulation of neurogenesis, deregulation of this pathway observed in Ts65Dn mice after treatment with 7,8-DHF may explain the lack of a beneficial effect on neurogenesis

4. GENERAL DISCUSSION AND CONCLUSIONS

4.1 Goal

In spite of the growing interest in the field of potential treatments for cognitive impairment in DS, there are **no effective therapies for DS so far**. The overall goal of my thesis work was to give a contribution to the discovery of effective pharmacotherapies for DS.

4.2 Model

To this purpose, I have used the **Ts65Dn mouse** model because, in spite of unavoidable limitations i) it is the model that most closely recapitulates the human condition and ii) most of the pharmacotherapies attempted so far have used this model, which allows a comparison across different interventions (see (Bartesaghi et al., 2011, Stagni et al., 2015a)).

4.3 Timing

Considering that neurogenesis and dendritogenesis defects occur at very early phases of brain development (Takashima et al., 1981, Becker, 1991, Vuksic et al., 2002, Contestabile et al., 2007, Guidi et al., 2008, Larsen et al., 2008, Guidi et al., 2011a, Lu et al., 2012), prenatal therapies should be the most appropriate choice in order to restore the trisomy-linked developmental defects of the brain. However, the prenatal period also represents a critical time for the development of the other organs forming the body. This aspect should be considered carefully and may raise concerns in the framework of potential treatments, unless their safety is granted. In rodents, the hippocampal dentate gyrus produces most of its neurons in the first two postnatal weeks (Brazel et al., 2003). Thus, the **neonatal period** appears to be an ideal time window in order to establish whether it is possible to correct neurogenesis and dendritogenesis defects with selected molecules and to establish the long-term effect (if any) of treatment. Information gained with early postnatal treatments may provide an answer to various key questions. 1) Is the selected molecule effective in correcting neurogenesis? 2)

Does the same molecule also correct dendritogenesis defects? 3) Does treatment elicit long-term effects? 4) Does treatment elicit adverse effects during treatment or after treatment cessation? This information may have a powerful translational impact at least in two directions. 1) Molecules effective and without side effects may be exploited in children with DS in order to IMPROVE their brain and cognitive performance. If clinical trials in children with DS will show a clear efficacy without side effects this outcome may suggest that it could be worthwhile to test the effective molecule during pregnancy and to run the risk of possible unpredictable side effects in the face of a potential full RESCUE of brain development.

4.4 Rationale for the chosen treatments and their effects

With this idea in mind, in this study I have examined the effects of three different molecules on development of the hippocampus. Which was the idea that lead to the selection of these molecules? The general idea was to act on pathways important for neurogenesis and dendritogenesis and that are known to be perturbed in DS.

APP is one of the triplicated genes that appears to be involved in several detrimental effects in the DS brain (see (Bartesaghi et al., 2011)). One of its cleavage products, AICD, strongly interferes with the SHH pathway, a pathway fundamental for morphogenesis and neurogenesis (Trazzi et al., 2011, Trazzi et al., 2013). In particular, AICD increases the transcription of *PTCH1* which, in turn, keeps the SHH pathway in a repressed state. The outcome of this inhibition is a reduction in the proliferation rate of NPCs and a reduced propensity to acquire a neuronal phenotype. Since AICD derives from the cleavage of the carboxy-terminal fragments of APP that is operated by the enzyme γ-secretase, inhibition of the activity of γ-secretase should reduce the formation of AICD. This should translate into a reduction on PTCH1 levels and disinhibition of the SHH pathway. We used the γ-secretase inhibitor **ELND006** (Basi et al., 2010) and found that neonatal treatment with this compound restored neurogenesis and neuron number in the DG and synaptic development in the hippocampal formation (DG and hippocampus) of Ts65Dn mice. Most of these effects were retained at one month after

treatment cessation and were accompanied by restoration of the synaptic function at the synapse between granule cells and field CA3 pyramidal neurons.

DYRK1A belongs to the triplicated genes that are considered to be strongly involved in neurogenesis impairment in DS (Chen et al., 2013). Many of the downstream targets of DYRK1A are associated with the control of cell growth and survival, especially in the nervous system (Hindley and Philpott, 2012, Chen et al., 2013). DYRK1A impairs cell cycle progression of embryonic progenitors through various mechanisms, suggesting that inhibition of its activity may restore neurogenesis in DS. Several small-molecule inhibitors of the protein kinase activity of DYRK1A are available. Many DYRK1A inhibitors also inhibit CDK-like kinase 1. **EGCG (**the major polyphenolic compound of green tea), however, has been identified as a specific DYRK1A inhibitor (Bain et al., 2003). Therefore, treatment with EGCG may be exploited in order to inhibit DYRK1A activity and, consequently, counteract the negative effects exerted by DIRK1A on neurogenesis in the DS brain. Indeed, green tea extracts appear to improve learning in the adult Ts65Dn mouse and exert some behavioral, although ephemeral, benefits in young adults with DS (De la Torre et al., 2014, de la Torre et al., 2016). It is possible that treatment with EGCG in the critical time window of hippocampal neurogenesis has more pronounced effects on hippocampal neurogenesis and that these effects are retained with time, which might lead to a long-lasting behavioral improvement. In order to clarify this issue, we have treated Ts65Dn mice in the neonatal period and examined the short- and long-term effects of treatment. We found that at the end of treatment there was full restoration of hippocampal neurogenesis, neuron number and synapse development. Unfortunately, at one month after treatment cessation, these effects had disappeared and there were no signs of behavioral improvement.

BDNF is a neurotrophin that plays a key role in brain plasticity by specifically binding to the TRKB teceptor. This binding triggers the activity of several intracellular pathways, thereby favoring neurogenesis, neuritogenesis and spine growth (Haniu et al., 1997). In the DS brain, BDNF levels are already reduced at fetal life stages and reduced BDNF levels have been shown in various brain regions of the Ts65Dn mouse (Bimonte-Nelson et al., 2003, Guedj et al., 2009, Bianchi et al., 2010a, Fukuda

et al., 2010, Toiber et al., 2010, Begenisic et al., 2015, Stagni et al., 2015b, Kazim et al., 2017, Villarroya et al., 2017). In view of the role of the BDNF-TRKB system in neurogenesis and dendritic morphogenesis, interventions targeted to the BDNF-TRKB system may be exploited in order to improve the trisomy-linked neurodevelopmental defects. Systemic administration of BDNF is impracticable because BDNF has a poor blood-brain barrier penetration. 7,8-dihydroxyflavone (7,8-DHF), however, is a flavone-derivative that penetrates the blood brain barrier, binds with high specificity to the TRKB receptor and activates its downstream signaling cascade (Liu et al., 2010, Liu et al., 2013, Liu et al., 2016). Administration of 7,8-DHF has been shown to exert therapeutic efficacy in various animal disease models that are related to deficient BDNF signaling. Based on these premises we sought to establish whether it is possible to restore neurogenesis in the Ts65Dn mouse by targeting the TRKB receptor with 7,8-DHF. We found that Ts65Dn mice, neonatally-treated with 7,8-DHF, underwent restoration of neurogenesis, granule cell number, and dendritic spine density. Mice that were treated with 7,8-DHF from postnatal day 3 to adolescence exhibited restoration of learning and memory, indicating that the recovery of the hippocampal anatomy translated into a functional rescue. No adverse effects were observed on the general health and growth of mice.

4.5 Potential translational impact of the study

From the viewpoint of the magnitude and duration of the effects, the use of **ELND006**, a selective inhibitor of γ-secretase, seems to be a promising strategy. However, we also found some adverse effects, possibly due to the fact that so called "selective inhibitors" of γ-secretase are not completely selective. Indeed, a clinical trial with ELND006 in individuals with Alzheimer's disease was interrupted due to toxicity. Therefore, the promising results of our study require that more selective inhibitors of γ-secretase and/or other means to prevent the transcriptional activity of AICD are created, in order to have a true translational impact for DS.

While **EGCG** may represent a good strategy for the restoration of the major trisomy-due brain defects, the disappearance of its effects with time implies that a schedule of continuous treatment

should be used in order to maintain the brain in its restored state. The advantage of natural compounds is that they have a long tradition in the history of the humankind and, therefore their use is considered to be safe (at appropriate doses). Taken together, the results of this study suggest that neonatal treatment with EGCG represents a good strategy for DS. The timing however is not all, because even neonatal treatment must not be discontinued or, at least, followed by additional treatment according to a schedule that needs to be identified. However, potential adverse effects of a prolonged EGCG treatment on the bone should be carefully considered.

Treatment with **7,8-DHF** during the early postnatal period restored neurogenesis and spinogenesis in the hippocampus of Ts65Dn mice and treatment until adolescence lead to full recue of hippocampus-dependent learning and memory. It remains to be established whether these effects are retained after treatment cessation. If so, targeting the BDNF/TRKB pathway may represent a good treatment for DS. Even if the effects of 7,8-DHF will be proven to be ephemeral, since it is a natural compound present in plants and has been shown to have no adverse effects on vital organs, such as the kidney and the liver, it seems likely that repeated treatment may be feasible and have no drawbacks.

A comparison of the three therapies used in this study indicates that although all are able to rescue neurogenesis, targeting the BDNF/TRKB pathway with 7,8-DHF may represent the treatment with the highest translational impact for children with DS because, it is effective and has the highest safety profile.

4.6 Future directions and challenges

In my study, I focused on the effects of treatments in the early postnatal period with the goal to identify molecules that can restore neurogenesis alterations in DS. I took advantage of the fact that in rodents hippocampal neurogenesis is very prominent in the early postnatal period. This makes it possible to treat mice and easily observe whether treatment is effective and has no patent adverse effects. Neurogenesis, however, is fundamentally a prenatal event. Therefore, the next step will be to establish whether prenatal treatments restore neurogenesis and cellularity throughout the brain. If so,

a generalized recovery of the functions that are impaired in DS may be expected. Preclinical demonstration that it is possible to pharmacologically prevent brain developmental alterations in a mouse model of DS with a variety of agents may stimulate the design of clinical trials during pregnancy with the molecule/s with the safest profile. Provided that the selected therapies elicit in fetuses with DS the same effects as in mice this would imply a drastic amelioration (restoration?) of intellectual disability. This is the challenge that faces the community of preclinical researchers interested in DS: to transform a dream into reality.

5. REFERENCES

Abraham H, Vincze A, Veszpremi B, Kravjak A, Gomori E, Kovacs GG, Seress L (2011) Impaired myelination of the human hippocampal formation in Down syndrome. Int J Dev Neurosci 30:147-158.

Adolphe C, Hetherington R, Ellis T, Wainwright B (2006) Patched1 functions as a gatekeeper by promoting cell cycle progression. Cancer Res 66:2081-2088.

Ahn KJ, Jeong HK, Choi HS, Ryoo SR, Kim YJ, Goo JS, Choi SY, Han JS, Ha I, Song WJ (2006) DYRK1A BAC transgenic mice show altered synaptic plasticity with learning and memory defects. Neurobiol Dis 22:463-472.

Aldridge K, Reeves RH, Olson LE, Richtsmeier JT (2007) Differential effects of trisomy on brain shape and volume in related aneuploid mouse models. Am J Med Genet A 143A:1060-1070.

Alonso M, Medina JH, Pozzo-Miller L (2004) ERK1/2 activation is necessary for BDNF to increase dendritic spine density in hippocampal CA1 pyramidal neurons. Learn Mem 11:172-178.

Altafaj X, Dierssen M, Baamonde C, Marti E, Visa J, Guimera J, Oset M, Gonzalez JR, Florez J, Fillat C, Estivill X (2001) Neurodevelopmental delay, motor abnormalities and cognitive deficits in transgenic mice overexpressing Dyrk1A (minibrain), a murine model of Down's syndrome. Hum Mol Genet 10:1915-1923.

Altman J (1982) Morphological development of the rat cerebellum and some of its mechanisms. Exp Brain Res Suppl. 6:8-49.

Altman J, Bayer S (1975) Postnatal development of the hippocampal dentate gyrus under normal and experimental conditions. In: Isaacson RL and Pribram KH, editors. The hippocampus, Vol 1. Plenum Press, New York and London. p 95-122. 95-122.

Altman J, Bayer SA (1990a) Migration and distribution of two populations of hippocampal granule cell precursors during the perinatal and postnatal periods. J Comp Neurol 301:365-381.

Altman J, Bayer SA (1990b) Mosaic organization of the hippocampal neuroepithelium and the multiple germinal sources of dentate granule cells. J Comp Neurol 301:325-342.

Altman J, Bayer SA (1990c) Prolonged sojourn of developing pyramidal cells in the intermediate zone of the hippocampus and their settling in the stratum pyramidale. J Comp Neurol 301:343-364.

Amano K, Sago H, Uchikawa C, Suzuki T, Kotliarova SE, Nukina N, Epstein CJ, Yamakawa K (2004) Dosage-dependent over-expression of genes in the trisomic region of Ts1Cje mouse model for Down syndrome. Hum Mol Genet 13:1333-1340.

Amaral DG, Witter MP (1995) Hippocampal formation. In: "The Rat Nervous System", G Paxinos, Academic Press, 443-492.

Amiel J, Sproat-Emison E, Garcia-Barcelo M, Lantieri F, Burzynski G, Borrego S, Pelet A, Arnold S, Miao X, Griseri P, Brooks AS, Antinolo G, de Pontual L, Clement-Ziza M, Munnich A, Kashuk C, West K, Wong KK, Lyonnet S, Chakravarti A, Tam PK, Ceccherini I, Hofstra RM, Fernandez R, Hirschsprung Disease C (2008) Hirschsprung disease, associated syndromes and genetics: a review. J Med Genet 45:1-14.

Andero R, Daviu N, Escorihuela RM, Nadal R, Armario A (2012) 7,8-dihydroxyflavone, a TrkB receptor agonist, blocks long-term spatial memory impairment caused by immobilization stress in rats. Hippocampus 22:399-408.

Andero R, Heldt SA, Ye K, Liu X, Armario A, Ressler KJ (2011) Effect of 7,8-dihydroxyflavone, a small-molecule TrkB agonist, on emotional learning. Am J Psychiatry 168:163-172.

Angot E, Loulier K, Nguyen-Ba-Charvet KT, Gadeau AP, Ruat M, Traiffort E (2008) Chemoattractive activity of sonic hedgehog in the adult subventricular zone modulates the number of neural precursors reaching the olfactory bulb. Stem Cells 26:2311-2320.

Antonarakis SE (2017) Down syndrome and the complexity of genome dosage imbalance. Nat Rev Genet 18:147-163.

Aracava Y, Pereira EF, Maelicke A, Albuquerque EX (2005) Memantine blocks alpha7* nicotinic acetylcholine receptors more potently than n-methyl-D-aspartate receptors in rat hippocampal neurons. J Pharmacol Exp Ther 312:1195-1205.

Arai Y, Ijuin T, Takenawa T, Becker LE, Takashima S (2002) Excessive expression of synaptojanin in brains with Down syndrome. Brain Dev 24:67-72.

Aranda S, Laguna A, de la Luna S (2011) DYRK family of protein kinases: evolutionary relationships, biochemical properties, and functional roles. Faseb J 25:449-462.

Arumugam A, Raja K, Venugopalan M, Chandrasekaran B, Kovanur Sampath K, Muthusamy H, Shanmugam N (2016) Down syndrome-A narrative review with a focus on anatomical features. Clin Anat 29:568-577.

Arya R, Kabra M, Gulati S (2011) Epilepsy in children with Down syndrome. Epileptic Disord 13:1-7.

Ash JA, Velazquez R, Kelley CM, Powers BE, Ginsberg SD, Mufson EJ, Strupp BJ (2014) Maternal choline supplementation improves spatial mapping and increases basal forebrain cholinergic neuron number and size in aged Ts65Dn mice. Neurobiol Dis 70:32-42.

Asim A, Kumar A, Muthuswamy S, Jain S, Agarwal S (2015) "Down syndrome: an insight of the disease". J Biomed Sci 22:41.

Aylward EH, Habbak R, Warren AC, Pulsifer MB, Barta PE, Jerram M, Pearlson GD (1997) Cerebellar volume in adults with Down syndrome. Arch Neurol 54:209-212.

Aylward EH, Li Q, Honeycutt NA, Warren AC, Pulsifer MB, Barta PE, Chan MD, Smith PD, Jerram M, Pearlson GD (1999) MRI volumes of the hippocampus and amygdala in adults with Down's syndrome with and without dementia. Am J Psychiatry 156:564-568.

Bahn S, Mimmack M, Ryan M, Caldwell MA, Jauniaux E, Starkey M, Svendsen CN, Emson P (2002) Neuronal target genes of the neuron-restrictive silencer factor in neurospheres derived from fetuses with Down's syndrome: a gene expression study. Lancet 359:310-315.

Bain J, McLauchlan H, Elliott M, Cohen P (2003) The specificities of protein kinase inhibitors: an update. Biochem J 371:199-204.

Barnes EA, Kong M, Ollendorff V, Donoghue DJ (2001) Patched1 interacts with cyclin B1 to regulate cell cycle progression. Embo J 20:2214-2223.

Bartesaghi R, Guidi S, Ciani E (2011) Is it possible to improve neurodevelopmental abnormalities in Down syndrome? Rev Neurosci 22:419-455.

Basi GS, Hemphill S, Brigham EF, Liao A, Aubele DL, Baker J, Barbour R, Bova M, Chen XH, Dappen MS, Eichenbaum T, Goldbach E, Hawkinson J, Lawler-Herbold R, Hu K, Hui T, Jagodzinski JJ, Keim PS, Kholodenko D, Latimer LH, Lee M, Marugg J, Mattson MN, McCauley S, Miller JL, Motter R, Mutter L, Neitzel ML, Ni H, Nguyen L, Quinn K, Ruslim L, Semko CM, Shapiro P, Smith J, Soriano F, Szoke B, Tanaka K, Tang P, Tucker JA, Ye XM, Yu M, Wu J, Xu YZ, Garofalo AW, Sauer JM, Konradi AW, Ness D, Shopp G, Pleiss MA, Freedman SB, Schenk D (2010) Amyloid precursor protein selective gamma-secretase inhibitors for treatment of Alzheimer's disease. Alzheimers Res Ther 2:36.

Baxter LL, Moran TH, Richtsmeier JT, Troncoso J, Reeves RH (2000) Discovery and genetic localization of Down syndrome cerebellar phenotypes using the Ts65Dn mouse. Hum Mol Genet 9:195-202.

Becker LE (1991) Synaptic dysgenesis. Can J Neurol Sci 18:170-180.

Becker LE, Armstrong DL, Chan F (1986) Dendritic atrophy in children with Down's syndrome. Ann Neurol 20:520-526.

Begenisic T, Baroncelli L, Sansevero G, Milanese M, Bonifacino T, Bonanno G, Cioni G, Maffei L, Sale A (2014) Fluoxetine in adulthood normalizes GABA release and rescues hippocampal synaptic plasticity and spatial memory in a mouse model of Down syndrome. Neurobiol Dis 63:12-19.

Begenisic T, Sansevero G, Baroncelli L, Cioni G, Sale A (2015) Early environmental therapy rescues brain development in a mouse model of Down syndrome. Neurobiology of disease 82:409-419.

Belichenko NP, Belichenko PV, Kleschevnikov AM, Salehi A, Reeves RH, Mobley WC (2009) The "Down syndrome critical region" is sufficient in the mouse model to confer behavioral, neurophysiological, and synaptic phenotypes characteristic of Down syndrome. J Neurosci 29:5938-5948.

Belichenko PV, Kleschevnikov AM (2011) Deficiency of Adult Neurogenesis in the Ts65Dn Mouse Model of Down Syndrome. In: Genetics and Etiology of Down Syndrome (Dey, S., ed), p Ch. 09 Rijeka: InTech.

Belichenko PV, Kleschevnikov AM, Salehi A, Epstein CJ, Mobley WC (2007) Synaptic and cognitive abnormalities in mouse models of Down syndrome: exploring genotype-phenotype relationships. J Comp Neurol 504:329-345.

Belichenko PV, Masliah E, Kleschevnikov AM, Villar AJ, Epstein CJ, Salehi A, Mobley WC (2004) Synaptic structural abnormalities in the Ts65Dn mouse model of Down Syndrome. J Comp Neurol 480:281-298.

Benavides-Piccione R, Ballesteros-Yanez I, de Lagran MM, Elston G, Estivill X, Fillat C, Defelipe J, Dierssen M (2004) On dendrites in Down syndrome and DS murine models: a spiny way to learn. Prog Neurobiol 74:111-126.

Benavides-Piccione R, Dierssen M, Ballesteros-Yanez I, Martinez de Lagran M, Arbones ML, Fotaki V, DeFelipe J, Elston GN (2005) Alterations in the phenotype of neocortical pyramidal cells in the Dyrk1A+/- mouse. Neurobiol Dis 20:115-122.

Bernert G, Nemethova M, Herrera-Marschitz M, Cairns N, Lubec G (1996) Decreased cyclin dependent kinase in brain of patients with Down syndrome. Neurosci Lett 216:68-70.

Best TK, Cramer NP, Chakrabarti L, Haydar TF, Galdzicki Z (2012) Dysfunctional hippocampal inhibition in the Ts65Dn mouse model of Down syndrome. Exp Neurol 233:749-757.

Best TK, Siarey RJ, Galdzicki Z (2007) Ts65Dn, a mouse model of Down syndrome, exhibits increased GABAB-induced potassium current. J Neurophysiol 97:892-900.

Bianchi P, Bettini S, Guidi S, Ciani E, Trazzi S, Stagni F, Ragazzi E, Franceschini V, Bartesaghi R (2014) Age-related impairment of olfactory bulb neurogenesis in the Ts65Dn mouse model of Down syndrome. Exp Neurol 251:1-11.

Bianchi P, Ciani E, Contestabile A, Guidi S, Bartesaghi R (2010a) Lithium restores neurogenesis in the subventricular zone of the Ts65Dn mouse, a model for Down syndrome. Brain Pathol 20:106-118.

Bianchi P, Ciani E, Guidi S, Trazzi S, Felice D, Grossi G, Fernandez M, Giuliani A, Calza L, Bartesaghi R (2010b) Early pharmacotherapy restores neurogenesis and cognitive performance in the Ts65Dn mouse model for Down syndrome. J Neurosci 30:8769-8779.

Bibel M, Hoppe E, Barde YA (1999) Biochemical and functional interactions between the neurotrophin receptors trk and p75NTR. EMBO J 18:616-622.

Bimonte-Nelson HA, Hunter CL, Nelson ME, Granholm AC (2003) Frontal cortex BDNF levels correlate with working memory in an animal model of Down syndrome. Behav Brain Res 139:47-57.

Blanchard J, Bolognin S, Chohan MO, Rabe A, Iqbal K, Grundke-Iqbal I (2011) Rescue of synaptic failure and alleviation of learning and memory impairments in a trisomic mouse model of down syndrome. J Neuropathol Exp Neurol 70:1070-1079.

Blehaut H, Mircher C, Ravel A, Conte M, de Portzamparc V, Poret G, de Kermadec FH, Rethore MO, Sturtz FG (2010) Effect of leucovorin (folinic acid) on the developmental quotient of children with Down's syndrome (trisomy 21) and influence of thyroid status. PLoS One 5:e8394.

Blomgren K, Leist M, Groc L (2007) Pathological apoptosis in the developing brain. Apoptosis 12:993-1010.

Boada R, Hutaff-Lee C, Schrader A, Weitzenkamp D, Benke TA, Goldson EJ, Costa AC (2012) Antagonism of NMDA receptors as a potential treatment for Down syndrome: a pilot randomized controlled trial. Transl Psychiatry 2:e141.

Bonni A, Sun Y, Nadal-Vicens M, Bhatt A, Frank DA, Rozovsky I, Stahl N, Yancopoulos GD, Greenberg ME (1997) Regulation of gliogenesis in the central nervous system by the JAK-STAT signaling pathway. Science 278:477-483.

Branca C, Sarnico I, Ruotolo R, Lanzillotta A, Viscomi AR, Benarese M, Porrini V, Lorenzini L, Calza L, Imbimbo BP, Ottonello S, Pizzi M (2014) Pharmacological targeting of the beta-amyloid precursor protein intracellular domain. Sci Rep 4:4618.

Braudeau J, Delatour B, Duchon A, Pereira PL, Dauphinot L, de Chaumont F, Olivo-Marin JC, Dodd RH, Herault Y, Potier MC (2011) Specific targeting of the GABA-A receptor alpha5 subtype by a selective inverse agonist restores cognitive deficits in Down syndrome mice. J Psychopharmacol 25:1030-1042.

Brazel CY, Romanko MJ, Rothstein RP, Levison SW (2003) Roles of the mammalian subventricular zone in brain development. Prog Neurobiol 69:49-69.

Bull MJ, Committee on G (2011) Health supervision for children with Down syndrome. Pediatrics 128:393-406.

Burbach JP (2011) What are neuropeptides? Methods Mol Biol 789:1-36.

Busca R, Pouyssegur J, Lenormand P (2016) ERK1 and ERK2 Map Kinases: Specific Roles or Functional Redundancy? Front Cell Dev Biol 4:53.

Busciglio J, Pelsman A, Helguera P, Ashur-Fabian O, Pinhasov A, Brenneman DE, Gozes I (2007) NAP and ADNF-9 protect normal and Down's syndrome cortical neurons from oxidative damage and apoptosis. Curr Pharm Des 13:1091-1098.

Busciglio J, Pelsman A, Wong C, Pigino G, Yuan M, Mori H, Yankner BA (2002) Altered metabolism of the amyloid beta precursor protein is associated with mitochondrial dysfunction in Down's syndrome. Neuron 33:677-688.

Buxhoeveden D, Fobbs A, Roy E, Casanova M (2002) Quantitative comparison of radial cell columns in children with Down's syndrome and controls. J Intellect Disabil Res 46:76-81.

Cao X, Sudhof TC (2001) A transcriptionally active complex of APP with Fe65 and histone acetyltransferase Tip60. Science 293:115-120.
Carducci F, Onorati P, Condoluci C, Di Gennaro G, Quarato PP, Pierallini A, Sara M, Miano S, Cornia R, Albertini G (2013) Whole-brain voxel-based morphometry study of children and adolescents with Down syndrome. Funct Neurol 28:19-28.
Carlesimo GA, Marotta L, Vicari S (1997) Long-term memory in mental retardation: evidence for a specific impairment in subjects with Down's syndrome. Neuropsychologia 35:71-79.
Catuara-Solarz S, Espinosa-Carrasco J, Erb I, Langohr K, Gonzalez JR, Notredame C, Dierssen M (2016) Combined Treatment With Environmental Enrichment and (-)-Epigallocatechin-3-Gallate Ameliorates Learning Deficits and Hippocampal Alterations in a Mouse Model of Down Syndrome. eNeuro 3.
Chakrabarti L, Best TK, Cramer NP, Carney RS, Isaac JT, Galdzicki Z, Haydar TF (2010) Olig1 and Olig2 triplication causes developmental brain defects in Down syndrome. Nat Neurosci 13:927-934.
Chakrabarti L, Galdzicki Z, Haydar TF (2007) Defects in embryonic neurogenesis and initial synapse formation in the forebrain of the Ts65Dn mouse model of Down syndrome. J Neurosci 27:11483-11495.
Chakrabarti L, Scafidi J, Gallo V, Haydar TF (2011) Environmental enrichment rescues postnatal neurogenesis defect in the male and female Ts65Dn mouse model of Down syndrome. Developmental neuroscience 33:428-441.
Chalifoux JR, Carter AG (2011) GABAB receptor modulation of voltage-sensitive calcium channels in spines and dendrites. J Neurosci 31:4221-4232.
Chan CB, Tse MC, Liu X, Zhang S, Schmidt R, Otten R, Liu L, Ye K (2015) Activation of muscular TrkB by its small molecular agonist 7,8-dihydroxyflavone sex-dependently regulates energy metabolism in diet-induced obese mice. Chem Biol 22:355-368.
Chan WY, Lorke DE, Tiu SC, Yew DT (2002) Proliferation and apoptosis in the developing human neocortex. Anat Rec 267:261-276.
Chapman RS, Hesketh LJ (2000) Behavioral phenotype of individuals with Down syndrome. Ment Retard Dev Disabil Res Rev 6:84-95.
Chatterjee A, Dutta S, Mukherjee S, Mukherjee N, Dutta A, Mukherjee A, Sinha S, Panda CK, Chaudhuri K, Roy AL, Mukhopadhyay K (2013) Potential contribution of SIM2 and ETS2 functional polymorphisms in Down syndrome associated malignancies. BMC Med Genet 14:12.
Chen C, Jiang P, Xue H, Peterson SE, Tran HT, McCann AE, Parast MM, Li S, Pleasure DE, Laurent LC, Loring JF, Liu Y, Deng W (2014) Role of astroglia in Down's syndrome revealed by patient-derived human-induced pluripotent stem cells. Nat Commun 5:4430.
Chen JY, Lin JR, Tsai FC, Meyer T (2013) Dosage of Dyrk1a shifts cells within a p21-cyclin D1 signaling map to control the decision to enter the cell cycle. Mol Cell 52:87-100.
Chohan MO, Li B, Blanchard J, Tung YC, Heaney AT, Rabe A, Iqbal K, Grundke-Iqbal I (2011) Enhancement of dentate gyrus neurogenesis, dendritic and synaptic plasticity and memory by a neurotrophic peptide. Neurobiol Aging 32:1420-1434.
Choong XY, Tosh JL, Pulford LJ, Fisher EM (2015) Dissecting Alzheimer disease in Down syndrome using mouse models. Front Behav Neurosci 9:268.
Clark S, Schwalbe J, Stasko MR, Yarowsky PJ, Costa AC (2006) Fluoxetine rescues deficient neurogenesis in hippocampus of the Ts65Dn mouse model for Down syndrome. Exp Neurol 200:256-261.
Colas D, Chuluun B, Garner CC, Heller HC (2017) Short-term treatment with flumazenil restores long-term object memory in a mouse model of Down syndrome. Neurobiol Learn Mem 140:11-16.
Colas D, Chuluun B, Warrier D, Blank M, Wetmore DZ, Buckmaster P, Garner CC, Heller HC (2013) Short-term treatment with the GABAA receptor antagonist pentylenetetrazole produces a sustained pro-cognitive benefit in a mouse model of Down's syndrome. Br J Pharmacol 169:963-973.
Colombo JA, Reisin HD, Jones M, Bentham C (2005) Development of interlaminar astroglial processes in the cerebral cortex of control and Down's syndrome human cases. Exp Neurol 193:207-217.
Contestabile A, Ciani E (2008) The place of choline acetyltransferase activity measurement in the "cholinergic hypothesis" of neurodegenerative diseases. Neurochem Res 33:318-327.
Contestabile A, Fila T, Bartesaghi R, Ciani E (2006) Choline acetyltransferase activity at different ages in brain of Ts65Dn mice, an animal model for Down's syndrome and related neurodegenerative diseases. J Neurochem.

Contestabile A, Fila T, Bartesaghi R, Ciani E (2008) Cell Cycle Elongation Impairs Proliferation of Cerebellar Granule Cell Precursors in the Ts65Dn Mouse, an Animal Model for Down Syndrome. Brain Pathol.

Contestabile A, Fila T, Bartesaghi R, Ciani E (2009) Cell cycle elongation impairs proliferation of cerebellar granule cell precursors in the Ts65Dn mouse, an animal model for Down syndrome. Brain Pathol 19:224-237.

Contestabile A, Fila T, Ceccarelli C, Bonasoni P, Bonapace L, Santini D, Bartesaghi R, Ciani E (2007) Cell cycle alteration and decreased cell proliferation in the hippocampal dentate gyrus and in the neocortical germinal matrix of fetuses with Down syndrome and in Ts65Dn mice. Hippocampus 17:665-678.

Contestabile A, Greco B, Ghezzi D, Tucci V, Benfenati F, Gasparini L (2013) Lithium rescues synaptic plasticity and memory in Down syndrome mice. J Clin Invest 123:348-361.

Cooper JD, Salehi A, Delcroix JD, Howe CL, Belichenko PV, Chua-Couzens J, Kilbridge JF, Carlson EJ, Epstein CJ, Mobley WC (2001) Failed retrograde transport of NGF in a mouse model of Down's syndrome: reversal of cholinergic neurodegenerative phenotypes following NGF infusion. Proc Natl Acad Sci U S A 98:10439-10444.

Coppede F (2016) Risk factors for Down syndrome. Arch Toxicol 90:2917-2929.

Corrales A, Martinez P, Garcia S, Vidal V, Garcia E, Florez J, Sanchez-Barcelo EJ, Martinez-Cue C, Rueda N (2013) Long-term oral administration of melatonin improves spatial learning and memory and protects against cholinergic degeneration in middle-aged Ts65Dn mice, a model of Down syndrome. J Pineal Res 54:346-358.

Corrales A, Vidal R, Garcia S, Vidal V, Martinez P, Garcia E, Florez J, Sanchez-Barcelo EJ, Martinez-Cue C, Rueda N (2014) Chronic melatonin treatment rescues electrophysiological and neuromorphological deficits in a mouse model of Down syndrome. J Pineal Res 56:51-61.

Corsi MM, Dogliotti G, Pedroni F, Palazzi E, Magni P, Chiappelli M, Licastro F (2006) Plasma nerve growth factor (NGF) and inflammatory cytokines (IL-6 and MCP-1) in young and adult subjects with Down syndrome: an interesting pathway. Neuro Endocrinol Lett 27:773-778.

Cossec JC, Lavaur J, Berman DE, Rivals I, Hoischen A, Stora S, Ripoll C, Mircher C, Grattau Y, Olivomarin JC, de Chaumont F, Lecourtois M, Antonarakis SE, Veltman JA, Delabar JM, Duyckaerts C, Di Paolo G, Potier MC (2012) Trisomy for synaptojanin1 in Down syndrome is functionally linked to the enlargement of early endosomes. Hum Mol Genet 21:3156-3172.

Costa AC, Scott-McKean JJ (2013) Prospects for improving brain function in individuals with down syndrome. CNS Drugs 27:679-702.

Costa AC, Scott-McKean JJ, Stasko MR (2008) Acute injections of the NMDA receptor antagonist memantine rescue performance deficits of the Ts65Dn mouse model of Down syndrome on a fear conditioning test. Neuropsychopharmacology 33:1624-1632.

Couillard-Despres S, Winner B, Schaubeck S, Aigner R, Vroemen M, Weidner N, Bogdahn U, Winkler J, Kuhn HG, Aigner L (2005) Doublecortin expression levels in adult brain reflect neurogenesis. Eur J Neurosci 21:1-14.

Crawley J (2007) What's wrong with my mouse? WILEY-INTERSCIENCE - A John Wiley & Sons, Inc., Publication.

Cummings JL, Mega M, Gray K, Rosenberg-Thompson S, Carusi DA, Gornbein J (1994) The Neuropsychiatric Inventory: comprehensive assessment of psychopathology in dementia. Neurology 44:2308-2314.

Cupers P, Orlans I, Craessaerts K, Annaert W, De Strooper B (2001) The amyloid precursor protein (APP)-cytoplasmic fragment generated by gamma-secretase is rapidly degraded but distributes partially in a nuclear fraction of neurones in culture. J Neurochem 78:1168-1178.

Dang V, Medina B, Das D, Moghadam S, Martin KJ, Lin B, Naik P, Patel D, Nosheny R, Wesson Ashford J, Salehi A (2014) Formoterol, a long-acting beta2 adrenergic agonist, improves cognitive function and promotes dendritic complexity in a mouse model of Down syndrome. Biol Psychiatry 75:179-188.

Das I, Park JM, Shin JH, Jeon SK, Lorenzi H, Linden DJ, Worley PF, Reeves RH (2013) Hedgehog agonist therapy corrects structural and cognitive deficits in a Down syndrome mouse model. Sci Transl Med 5:201ra120.

Davisson MT, Schmidt C, Reeves RH, Irving NG, Akeson EC, Harris BS, Bronson RT (1993) Segmental trisomy as a mouse model for Down syndrome. Prog Clin Biol Res 384:117-133.

de la Torre R, de Sola S, Hernandez G, Farre M, Pujol J, Rodriguez J, Espadaler JM, Langohr K, Cuenca-Royo A, Principe A, Xicota L, Janel N, Catuara-Solarz S, Sanchez-Benavides G, Blehaut H, Duenas-Espin I, Del Hoyo L, Benejam B, Blanco-Hinojo L, Videla S, Fito M, Delabar JM, Dierssen M, group Ts

(2016) Safety and efficacy of cognitive training plus epigallocatechin-3-gallate in young adults with Down's syndrome (TESDAD): a double-blind, randomised, placebo-controlled, phase 2 trial. Lancet Neurol 15:801-810.

De la Torre R, De Sola S, Pons M, Duchon A, de Lagran MM, Farre M, Fito M, Benejam B, Langohr K, Rodriguez J, Pujadas M, Bizot JC, Cuenca A, Janel N, Catuara S, Covas MI, Blehaut H, Herault Y, Delabar JM, Dierssen M (2014) Epigallocatechin-3-gallate, a DYRK1A inhibitor, rescues cognitive deficits in Down syndrome mouse models and in humans. Mol Nutr Food Res 58:278-288.

Deidda G, Parrini M, Naskar S, Bozarth IF, Contestabile A, Cancedda L (2015) Reversing excitatory GABAAR signaling restores synaptic plasticity and memory in a mouse model of Down syndrome. Nat Med 21:318-326.

Demas GE, Nelson RJ, Krueger BK, Yarowsky PJ (1996) Spatial memory deficits in segmental trisomic Ts65Dn mice. Behav Brain Res 82:85-92.

Devi L, Ohno M (2012) 7,8-dihydroxyflavone, a small-molecule TrkB agonist, reverses memory deficits and BACE1 elevation in a mouse model of Alzheimer's disease. Neuropsychopharmacology : official publication of the American College of Neuropsychopharmacology 37:434-444.

Dey A, Bhowmik K, Chatterjee A, Chakrabarty PB, Sinha S, Mukhopadhyay K (2013) Down Syndrome Related Muscle Hypotonia: Association with COL6A3 Functional SNP rs2270669. Front Genet 4:57.

Dierssen M (2012) Down syndrome: the brain in trisomic mode. Nat Rev Neurosci 13:844-858.

Dierssen M, Benavides-Piccione R, Martinez-Cue C, Estivill X, Florez J, Elston GN, DeFelipe J (2003) Alterations of neocortical pyramidal cell phenotype in the Ts65Dn mouse model of Down syndrome: effects of environmental enrichment. Cereb Cortex 13:758-764.

Driscoll DA, Morgan MA, Schulkin J (2009) Screening for Down syndrome: changing practice of obstetricians. Am J Obstet Gynecol 200:459 e451-459.

Duchon A, Raveau M, Chevalier C, Nalesso V, Sharp AJ, Herault Y (2011) Identification of the translocation breakpoints in the Ts65Dn and Ts1Cje mouse lines: relevance for modeling Down syndrome. Mamm Genome 22:674-684.

Dykens EM, Hodapp RM, Evans DW (1994) Profiles and development of adaptive behavior in children with Down syndrome. Am J Ment Retard 98:580-587.

El Hajj N, Dittrich M, Bock J, Kraus TF, Nanda I, Muller T, Seidmann L, Tralau T, Galetzka D, Schneider E, Haaf T (2016) Epigenetic dysregulation in the developing Down syndrome cortex. Epigenetics 11:563-578.

Eldar-Finkelman H, Martinez A (2011) GSK-3 Inhibitors: Preclinical and Clinical Focus on CNS. Front Mol Neurosci 4:32.

Ellis J, Logan S, Pumphrey R, Tan HK, Henley W, Edwards V, Moy R, Gilbert R (2008) Inequalities in provision of the Disability Living Allowance for Down syndrome. Arch Dis Child 93:14-16.

Esbensen AJ, Hooper SR, Fidler D, Hartley SL, Edgin J, d'Ardhuy XL, Capone G, Conners FA, Mervis CB, Abbeduto L, Rafii MS, Krinsky-McHale SJ, Urv T, Group OMW (2017) Outcome Measures for Clinical Trials in Down Syndrome. Am J Intellect Dev Disabil 122:247-281.

Faber KM, Haring JH (1999) Synaptogenesis in the postnatal rat fascia dentata is influenced by 5-HT1a receptor activation. Brain Res Dev Brain Res 114:245-252.

Faizi M, Bader PL, Tun C, Encarnacion A, Kleschevnikov A, Belichenko P, Saw N, Priestley M, Tsien RW, Mobley WC, Shamloo M (2011) Comprehensive behavioral phenotyping of Ts65Dn mouse model of Down syndrome: activation of beta1-adrenergic receptor by xamoterol as a potential cognitive enhancer. Neurobiol Dis 43:397-413.

Fernandez F, Morishita W, Zuniga E, Nguyen J, Blank M, Malenka RC, Garner CC (2007) Pharmacotherapy for cognitive impairment in a mouse model of Down syndrome. Nat Neurosci 10:411-413.

Fernandez F, Trinidad JC, Blank M, Feng DD, Burlingame AL, Garner CC (2009) Normal protein composition of synapses in Ts65Dn mice: a mouse model of Down syndrome. J Neurochem 110:157-169.

Ferrando-Miguel R, Shim KS, Cheon MS, Gimona M, Furuse M, Lubec G (2003) Overexpression of Interferon α/β Receptor β Chain in Fetal Down Syndrome Brain. Neuroembryology and Aging 2:147-155.

Finkel SI (2004) Effects of rivastigmine on behavioral and psychological symptoms of dementia in Alzheimer's disease. Clin Ther 26:980-990.

Finsterwald C, Fiumelli H, Cardinaux JR, Martin JL (2010) Regulation of dendritic development by BDNF requires activation of CRTC1 by glutamate. J Biol Chem 285:28587-28595.

Fleisher AS, Raman R, Siemers ER, Becerra L, Clark CM, Dean RA, Farlow MR, Galvin JE, Peskind ER, Quinn JF, Sherzai A, Sowell BB, Aisen PS, Thal LJ (2008) Phase 2 safety trial targeting amyloid beta production with a gamma-secretase inhibitor in Alzheimer disease. Arch Neurol 65:1031-1038.

Foltran RB, Diaz SL (2016) BDNF isoforms: a round trip ticket between neurogenesis and serotonin? J Neurochem 138:204-221.

Fortress AM, Hamlett ED, Vazey EM, Aston-Jones G, Cass WA, Boger HA, Granholm AC (2015) Designer receptors enhance memory in a mouse model of Down syndrome. J Neurosci 35:1343-1353.

Freeman SB, Taft LF, Dooley KJ, Allran K, Sherman SL, Hassold TJ, Khoury MJ, Saker DM (1998) Population-based study of congenital heart defects in Down syndrome. Am J Med Genet 80:213-217.

Freeman SB, Torfs CP, Romitti PA, Royle MH, Druschel C, Hobbs CA, Sherman SL (2009) Congenital gastrointestinal defects in Down syndrome: a report from the Atlanta and National Down Syndrome Projects. Clin Genet 75:180-184.

Fukuda Y, Berry TL, Nelson M, Hunter CL, Fukuhara K, Imai H, Ito S, Granholm-Bentley AC, Kaplan AP, Mutoh T (2010) Stimulated neuronal expression of brain-derived neurotrophic factor by Neurotropin. Mol Cell Neurosci 45:226-233.

Gandolfi A, Horoupian DS, De Teresa RM (1981) Pathology of the auditory system in autosomal trisomies with morphometric and quantitative study of the ventral cochlear nucleus. J Neurol Sci 51:43-50.

Garcia-Cerro S, Martinez P, Vidal V, Corrales A, Florez J, Vidal R, Rueda N, Arbones ML, Martinez-Cue C (2014) Overexpression of Dyrk1A is implicated in several cognitive, electrophysiological and neuromorphological alterations found in a mouse model of Down syndrome. PLoS One 9:e106572.

Gardiner K, Costa AC (2006) The proteins of human chromosome 21. Am J Med Genet C Semin Med Genet 142C:196-205.

Gardiner KJ (2015) Pharmacological approaches to improving cognitive function in Down syndrome: current status and considerations. Drug Des Devel Ther 9:103-125.

Ghosal K, Stathopoulos A, Pimplikar SW (2010) APP intracellular domain impairs adult neurogenesis in transgenic mice by inducing neuroinflammation. PLoS One 5:e11866.

Giacomini A, Stagni F, Trazzi S, Guidi S, Emili M, Brigham E, Ciani E, Bartesaghi R (2015) Inhibition of APP gamma-secretase restores Sonic Hedgehog signaling and neurogenesis in the Ts65Dn mouse model of Down syndrome. Neurobiology of disease 82:385-396.

Golden JA, Hyman BT (1994) Development of the superior temporal neocortex is anomalous in trisomy 21. J Neuropathol Exp Neurol 53:513-520.

Gonzalez A, Moya-Alvarado G, Gonzalez-Billaut C, Bronfman FC (2016) Cellular and molecular mechanisms regulating neuronal growth by brain-derived neurotrophic factor. Cytoskeleton (Hoboken) 73:612-628.

Goodliffe JW, Olmos-Serrano JL, Aziz NM, Pennings JL, Guedj F, Bianchi DW, Haydar TF (2016) Absence of Prenatal Forebrain Defects in the Dp(16)1Yey/+ Mouse Model of Down Syndrome. J Neurosci 36:2926-2944.

Granholm AC, Ford KA, Hyde LA, Bimonte HA, Hunter CL, Nelson M, Albeck D, Sanders LA, Mufson EJ, Crnic LS (2002) Estrogen restores cognition and cholinergic phenotype in an animal model of Down syndrome. Physiol Behav 77:371-385.

Granholm AC, Sanders L, Seo H, Lin L, Ford K, Isacson O (2003) Estrogen alters amyloid precursor protein as well as dendritic and cholinergic markers in a mouse model of Down syndrome. Hippocampus 13:905-914.

Gray J, Yeo GS, Cox JJ, Morton J, Adlam AL, Keogh JM, Yanovski JA, El Gharbawy A, Han JC, Tung YC, Hodges JR, Raymond FL, O'Rahilly S, Farooqi IS (2006) Hyperphagia, severe obesity, impaired cognitive function, and hyperactivity associated with functional loss of one copy of the brain-derived neurotrophic factor (BDNF) gene. Diabetes 55:3366-3371.

Griffin WS, Sheng JG, McKenzie JE, Royston MC, Gentleman SM, Brumback RA, Cork LC, Del Bigio MR, Roberts GW, Mrak RE (1998) Life-long overexpression of S100beta in Down's syndrome: implications for Alzheimer pathogenesis. Neurobiol Aging 19:401-405.

Gropp A, Kolbus U, Giers D (1975) Systematic approach to the study of trisomy in the mouse. II. Cytogenet Cell Genet 14:42-62.

Guedj F, Sebrie C, Rivals I, Ledru A, Paly E, Bizot JC, Smith D, Rubin E, Gillet B, Arbones M, Delabar JM (2009) Green tea polyphenols rescue of brain defects induced by overexpression of DYRK1A. PLoS One 4:e4606.

Guidi S, Bianchi P, Alstrup AK, Henningsen K, Smith DF, Bartesaghi R (2011a) Postnatal neurogenesis in the hippocampal dentate gyrus and subventricular zone of the Gottingen minipig. Brain Res Bull 85:169-179.

Guidi S, Bianchi P, Stagni F, Giacomini A, Emili M, Trazzi S, Ciani E, Bartesaghi R (2016) Lithium Restores Age Related Olfactory Impairment in the Ts65Dn Mouse Model of Down Syndrome. CNS Neurol Disord Drug Targets.

Guidi S, Bonasoni P, Ceccarelli C, Santini D, Gualtieri F, Ciani E, Bartesaghi R (2008) Neurogenesis impairment and increased cell death reduce total neuron number in the hippocampal region of fetuses with Down syndrome. Brain Pathol 18:180-197.

Guidi S, Ciani E, Bonasoni P, Santini D, Bartesaghi R (2011b) Widespread proliferation impairment and hypocellularity in the cerebellum of fetuses with down syndrome. Brain Pathol 21:361-373.

Guidi S, Emili M, Giacomini A, Stagni F, Bartesaghi R (2017) NEUROANATOMICAL ALTERATIONS IN THE TEMPORAL CORTEX OF HUMAN FETUSES WITH DOWN SYNDROME. "Paving the Way for Therapy" 2nd International Conference of the Trisomy 21 Research Society, June 7-11, 2017, Feinberg Conference Center, Northwestern Memorial Hospital, Chicago, IL USA.

Guidi S, Stagni F, Bianchi P, Ciani E, Giacomini A, De Franceschi M, Moldrich R, Kurniawan N, Mardon K, Giuliani A, Calza L, Bartesaghi R (2014) Prenatal pharmacotherapy rescues brain development in a Down's syndrome mouse model. Brain 137:380-401.

Guidi S, Stagni F, Bianchi P, Ciani E, Ragazzi E, Trazzi S, Grossi G, Mangano C, Calza L, Bartesaghi R (2013) Early pharmacotherapy with fluoxetine rescues dendritic pathology in the Ts65Dn mouse model of Down syndrome. Brain Pathol 23:129-143.

Guihard-Costa AM, Khung S, Delbecque K, Menez F, Delezoide AL (2006) Biometry of Face and Brain in Fetuses With Trisomy 21. Pediatr Res.

Haas M, Bell D, Slender M, Lana-Elola E, Watson-Scales S, Fisher E, Tybulewicz V, Guillemot F (2013) Alterations to dendritic spine morphology, but not dendrite patterning, of cortical projection neurons in Tc1 and Ts1Rhr mouse models of Down syndrome. PLoSOne 8:e78561.

Hamill OP, Marty A, Neher E, Sakmann B, Sigworth FJ (1981) Improved patch-clamp techniques for high-resolution current recording from cells and cell-free membrane patches. Pflugers Archiv : European journal of physiology 391:85-100.

Hamlett ED, Boger HA, Ledreux A, Kelley CM, Mufson EJ, Falangola MF, Guilfoyle DN, Nixon RA, Patterson D, Duval N, Granholm AC (2016) Cognitive Impairment, Neuroimaging, and Alzheimer Neuropathology in Mouse Models of Down Syndrome. Curr Alzheimer Res 13:35-52.

Hammerle B, Elizalde C, Galceran J, Becker W, Tejedor FJ (2003) The MNB/DYRK1A protein kinase: neurobiological functions and Down syndrome implications. J Neural Transm Suppl 129-137.

Hammerle B, Ulin E, Guimera J, Becker W, Guillemot F, Tejedor FJ (2011) Transient expression of Mnb/Dyrk1a couples cell cycle exit and differentiation of neuronal precursors by inducing p27KIP1 expression and suppressing NOTCH signaling. Development 138:2543-2554.

Haniu M, Montestruque S, Bures EJ, Talvenheimo J, Toso R, Lewis-Sandy S, Welcher AA, Rohde MF (1997) Interactions between brain-derived neurotrophic factor and the TRKB receptor. Identification of two ligand binding domains in soluble TRKB by affinity separation and chemical cross-linking. The Journal of biological chemistry 272:25296-25303.

Hanney M, Prasher V, Williams N, Jones EL, Aarsland D, Corbett A, Lawrence D, Yu LM, Tyrer S, Francis PT, Johnson T, Bullock R, Ballard C, researchers Mt (2012) Memantine for dementia in adults older than 40 years with Down's syndrome (MEADOWS): a randomised, double-blind, placebo-controlled trial. Lancet 379:528-536.

Harashima C, Jacobowitz DM, Stoffel M, Chakrabarti L, Haydar TF, Siarey RJ, Galdzicki Z (2006) Elevated expression of the G-protein-activated inwardly rectifying potassium channel 2 (GIRK2) in cerebellar unipolar brush cells of a Down syndrome mouse model. Cell Mol Neurobiol 26:719-734.

Hardy O, Worley G, Lee MM, Chaing S, Mackey J, Crissman B, Kishnani PS (2004) Hypothyroidism in Down syndrome: screening guidelines and testing methodology. Am J Med Genet A 124A:436-437.

Hart SJ, Visootsak J, Tamburri P, Phuong P, Baumer N, Hernandez MC, Skotko BG, Ochoa-Lubinoff C, Liogier D'Ardhuy X, Kishnani PS, Spiridigliozzi GA (2017) Pharmacological interventions to improve cognition and adaptive functioning in Down syndrome: Strides to date. Am J Med Genet A 173:3029-3041.

Hartley D, Blumenthal T, Carrillo M, DiPaolo G, Esralew L, Gardiner K, Granholm AC, Iqbal K, Krams M, Lemere C, Lott I, Mobley W, Ness S, Nixon R, Potter H, Reeves R, Sabbagh M, Silverman W, Tycko

B, Whitten M, Wisniewski T (2015) Down syndrome and Alzheimer's disease: Common pathways, common goals. Alzheimers Dement 11:700-709.
Hattori M, Fujiyama A, Taylor TD, Watanabe H, Yada T, Park HS, Toyoda A, Ishii K, Totoki Y, Choi DK, Groner Y, Soeda E, Ohki M, Takagi T, Sakaki Y, Taudien S, Blechschmidt K, Polley A, Menzel U, Delabar J, Kumpf K, Lehmann R, Patterson D, Reichwald K, Rump A, Schillhabel M, Schudy A, Zimmermann W, Rosenthal A, Kudoh J, Schibuya K, Kawasaki K, Asakawa S, Shintani A, Sasaki T, Nagamine K, Mitsuyama S, Antonarakis SE, Minoshima S, Shimizu N, Nordsiek G, Hornischer K, Brant P, Scharfe M, Schon O, Desario A, Reichelt J, Kauer G, Blocker H, Ramser J, Beck A, Klages S, Hennig S, Riesselmann L, Dagand E, Haaf T, Wehrmeyer S, Borzym K, Gardiner K, Nizetic D, Francis F, Lehrach H, Reinhardt R, Yaspo ML (2000) The DNA sequence of human chromosome 21. Nature 405:311-319.
He Z, Cai J, Lim J-W, Kroll K, Ma L (2011) A novel KRAB domain-containing zinc finger transcription factor ZNF431 directly represses Patched1 transcription. The Journal of biological chemistry 286:7279-7289.
Hefti E, Blanco JG (2017) Pharmacotherapeutic Considerations for Individuals with Down Syndrome. Pharmacotherapy 37:214-220.
Heinen M, Hettich MM, Ryan DP, Schnell S, Paesler K, Ehninger D (2012) Adult-onset fluoxetine treatment does not improve behavioral impairments and may have adverse effects on the Ts65Dn mouse model of Down syndrome. Neural Plast 2012:467251.
Hewitt CA, Ling KH, Merson TD, Simpson KM, Ritchie ME, King SL, Pritchard MA, Smyth GK, Thomas T, Scott HS, Voss AK (2010) Gene network disruptions and neurogenesis defects in the adult Ts1Cje mouse model of Down syndrome. PLoS One 5:e11561.
Hibaoui Y, Grad I, Letourneau A, Sailani MR, Dahoun S, Santoni FA, Gimelli S, Guipponi M, Pelte MF, Bena F, Antonarakis SE, Feki A (2014) Modelling and rescuing neurodevelopmental defect of Down syndrome using induced pluripotent stem cells from monozygotic twins discordant for trisomy 21. EMBO Mol Med 6:259-277.
Hindley C, Philpott A (2012) Co-ordination of cell cycle and differentiation in the developing nervous system. Biochem J 444:375-382.
Holtzman DM, Bayney RM, Li YW, Khosrovi H, Berger CN, Epstein CJ, Mobley WC (1992) Dysregulation of gene expression in mouse trisomy 16, an animal model of Down syndrome. Embo J 11:619-627.
Holtzman DM, Santucci D, Kilbridge J, Chua-Couzens J, Fontana DJ, Daniels SE, Johnson RM, Chen K, Sun Y, Carlson E, Alleva E, Epstein CJ, Mobley WC (1996) Developmental abnormalities and age-related neurodegeneration in a mouse model of Down syndrome. Proc Natl Acad Sci U S A 93:13333-13338.
Hopkins CR (2010) ACS chemical neuroscience molecule spotlight on semagacestat (LY450139). ACS Chem Neurosci 1:533-534.
Hopkins CR (2011) ACS chemical neuroscience molecule spotlight on ELND006: another gamma-secretase inhibitor fails in the clinic. ACS Chem Neurosci 2:279-280.
Hu G, Bidel S, Jousilahti P, Antikainen R, Tuomilehto J (2007) Coffee and tea consumption and the risk of Parkinson's disease. Mov Disord 22:2242-2248.
Huang GJ, He Z, Ma L (2012) ZFP932 suppresses cellular Hedgehog response and Patched1 transcription. Vitamins and hormones 88:309-332.
Hunter CL, Bachman D, Granholm AC (2004a) Minocycline prevents cholinergic loss in a mouse model of Down's syndrome. Ann Neurol 56:675-688.
Hunter CL, Bimonte-Nelson HA, Nelson M, Eckman CB, Granholm AC (2004b) Behavioral and neurobiological markers of Alzheimer's disease in Ts65Dn mice: effects of estrogen. Neurobiol Aging 25:873-884.
Incerti M, Horowitz K, Roberson R, Abebe D, Toso L, Caballero M, Spong CY (2012) Prenatal treatment prevents learning deficit in Down syndrome model. PLoS One 7:e50724.
Incerti M, Toso L, Vink J, Roberson R, Nold C, Abebe D, Spong CY (2011) Prevention of learning deficit in a Down syndrome model. Obstet Gynecol 117:354-361.
Insausti AM, Megias M, Crespo D, Cruz-Orive LM, Dierssen M, Vallina IF, Insausti R, Florez J (1998) Hippocampal volume and neuronal number in Ts65Dn mice: a murine model of Down syndrome. Neurosci Lett 253:175-178.
Ishihara K, Amano K, Takaki E, Shimohata A, Sago H, Epstein CJ, Yamakawa K (2010) Enlarged brain ventricles and impaired neurogenesis in the Ts1Cje and Ts2Cje mouse models of Down syndrome. Cereb Cortex 20:1131-1143.

Ivanov A, Esclapez M, Ferhat L (2009) Role of drebrin A in dendritic spine plasticity and synaptic function: Implications in neurological disorders. Commun Integr Biol 2:268-270.
Jang SW, Liu X, Yepes M, Shepherd KR, Miller GW, Liu Y, Wilson WD, Xiao G, Blanchi B, Sun YE, Ye K (2010) A selective TrkB agonist with potent neurotrophic activities by 7,8-dihydroxyflavone. Proc Natl Acad Sci U S A 107:2687-2692.
Jernigan TL, Bellugi U, Sowell E, Doherty S, Hesselink JR (1993) Cerebral morphologic distinctions between Williams and Down syndromes. Arch Neurol 50:186-191.
Jiang M, Peng Q, Liu X, Jin J, Hou Z, Zhang J, Mori S, Ross CA, Ye K, Duan W (2013) Small-molecule TrkB receptor agonists improve motor function and extend survival in a mouse model of Huntington's disease. Hum Mol Genet 22:2462-2470.
Jin Y, Sui HJ, Dong Y, Ding Q, Qu WH, Yu SX, Jin YX (2012) Atorvastatin enhances neurite outgrowth in cortical neurons in vitro via up-regulating the Akt/mTOR and Akt/GSK-3beta signaling pathways. Acta Pharmacol Sin 33:861-872.
Jope RS, Johnson GV (2004) The glamour and gloom of glycogen synthase kinase-3. Trends Biochem Sci 29:95-102.
Jung YS, Qian Y, Chen X (2010) Examination of the expanding pathways for the regulation of p21 expression and activity. Cell Signal 22:1003-1012.
Karmiloff-Smith A, Al-Janabi T, D'Souza H, Groet J, Massand E, Mok K, Startin C, Fisher E, Hardy J, Nizetic D, Tybulewicz V, Strydom A (2016) The importance of understanding individual differences in Down syndrome. F1000Res 5.
Kates WR, Folley BS, Lanham DC, Capone GT, Kaufmann WE (2002) Cerebral growth in Fragile X syndrome: review and comparison with Down syndrome. Microsc Res Tech 57:159-167.
Katoh Y, Katoh M (2009) Hedgehog target genes: mechanisms of carcinogenesis induced by aberrant hedgehog signaling activation. Curr Mol Med 9:873-886.
Kazemi M, Salehi M, Kheirollahi M (2016) Down Syndrome: Current Status, Challenges and Future Perspectives. Int J Mol Cell Med 5:125-133.
Kazim SF, Blanchard J, Bianchi R, Iqbal K (2017) Early neurotrophic pharmacotherapy rescues developmental delay and Alzheimer's-like memory deficits in the Ts65Dn mouse model of Down syndrome. Sci Rep 7:45561.
Kelley CM, Ash JA, Powers BE, Velazquez R, Alldred MJ, Ikonomovic MD, Ginsberg SD, Strupp BJ, Mufson EJ (2016) Effects of Maternal Choline Supplementation on the Septohippocampal Cholinergic System in the Ts65Dn Mouse Model of Down Syndrome. Curr Alzheimer Res 13:84-96.
Kelley CM, Powers BE, Velazquez R, Ash JA, Ginsberg SD, Strupp BJ, Mufson EJ (2014) Maternal choline supplementation differentially alters the basal forebrain cholinergic system of young-adult Ts65Dn and disomic mice. J Comp Neurol 522:1390-1410.
Kelsey NA, Wilkins HM, Linseman DA (2010) Nutraceutical antioxidants as novel neuroprotective agents. Molecules 15:7792-7814.
Kempermann G, Gage FH (2002) Genetic influence on phenotypic differentiation in adult hippocampal neurogenesis. Brain Res Dev Brain Res 134:1-12.
Kenney AM, Rowitch DH (2000) Sonic hedgehog promotes G(1) cyclin expression and sustained cell cycle progression in mammalian neuronal precursors. Molecular and cellular biology 20:9055-9067.
Kesslak JP, Nagata SF, Lott I, Nalcioglu O (1994) Magnetic resonance imaging analysis of age-related changes in the brains of individuals with Down's syndrome. Neurology 44:1039-1045.
Kim HC, Quon MJ, Kim J (2014) New insights into the mechanisms of polyphenols beyond antioxidant properties; lessons from the green tea polyphenol, epigallocatechin 3-gallate. Redox Biology 2:187-195.
Kim WY, Snider WD (2011) Functions of GSK-3 Signaling in Development of the Nervous System. Front Mol Neurosci 4:44.
Kimura M, Cao X, Skurnick J, Cody M, Soteropoulos P, Aviv A (2005) Proliferation dynamics in cultured skin fibroblasts from Down syndrome subjects. Free Radic Biol Med 39:374-380.
Kishnani PS, Heller JH, Spiridigliozzi GA, Lott I, Escobar L, Richardson S, Zhang R, McRae T (2010) Donepezil for treatment of cognitive dysfunction in children with Down syndrome aged 10-17. Am J Med Genet A 152A:3028-3035.
Kishnani PS, Sommer BR, Handen BL, Seltzer B, Capone GT, Spiridigliozzi GA, Heller JH, Richardson S, McRae T (2009) The efficacy, safety, and tolerability of donepezil for the treatment of young adults with Down syndrome. Am J Med Genet A 149A:1641-1654.

Kishnani PS, Sullivan JA, Walter BK, Spiridigliozzi GA, Doraiswamy PM, Krishnan KR (1999) Cholinergic therapy for Down's syndrome. Lancet 353:1064-1065.
Kleschevnikov AM, Belichenko PV, Gall J, George L, Nosheny R, Maloney MT, Salehi A, Mobley WC (2012) Increased efficiency of the GABAA and GABAB receptor-mediated neurotransmission in the Ts65Dn mouse model of Down syndrome. Neurobiol Dis 45:683-691.
Korkmaz OT, Aytan N, Carreras I, Choi JK, Kowall NW, Jenkins BG, Dedeoglu A (2014) 7,8-Dihydroxyflavone improves motor performance and enhances lower motor neuronal survival in a mouse model of amyotrophic lateral sclerosis. Neurosci Lett 566:286-291.
Kuehn BM (2016) Treating trisomies: Prenatal Down's syndrome therapies explored in mice. Nat Med 22:6-7.
Kurabayashi N, Nguyen MD, Sanada K (2015) DYRK1A overexpression enhances STAT activity and astrogliogenesis in a Down syndrome mouse model. EMBO Rep 16:1548-1562.
Kurt MA, Davies DC, Kidd M, Dierssen M, Florez J (2000) Synaptic deficit in the temporal cortex of partial trisomy 16 (Ts65Dn) mice. Brain Res 858:191-197.
Kurt MA, Kafa MI, Dierssen M, Davies DC (2004) Deficits of neuronal density in CA1 and synaptic density in the dentate gyrus, CA3 and CA1, in a mouse model of Down syndrome. Brain Res 1022:101-109.
Kwon M, Fernandez JR, Zegarek GF, Lo SB, Firestein BL (2011) BDNF-promoted increases in proximal dendrites occur via CREB-dependent transcriptional regulation of cypin. J Neurosci 31:9735-9745.
Larsen KB, Laursen H, Graem N, Samuelsen GB, Bogdanovic N, Pakkenberg B (2008) Reduced cell number in the neocortical part of the human fetal brain in Down syndrome. Ann Anat 190:421-427.
Latchney SE, Jaramillo TC, Rivera PD, Eisch AJ, Powell CM (2015) Chronic P7C3 treatment restores hippocampal neurogenesis. Neurosci Lett 591:86-92.
Lefloch R, Pouyssegur J, Lenormand P (2008) Single and combined silencing of ERK1 and ERK2 reveals their positive contribution to growth signaling depending on their expression levels. Mol Cell Biol 28:511-527.
Levites Y, Amit T, Mandel S, Youdim MB (2003) Neuroprotection and neurorescue against Abeta toxicity and PKC-dependent release of nonamyloidogenic soluble precursor protein by green tea polyphenol (-)-epigallocatechin-3-gallate. Faseb J 17:952-954.
Li Z, Yu T, Morishima M, Pao A, LaDuca J, Conroy J, Nowak N, Matsui S, Shiraishi I, Yu YE (2007) Duplication of the entire 22.9 Mb human chromosome 21 syntenic region on mouse chromosome 16 causes cardiovascular and gastrointestinal abnormalities. Hum Mol Genet 16:1359-1366.
Lin CL, Chen TF, Chiu MJ, Way TD, Lin JK (2009) Epigallocatechin gallate (EGCG) suppresses beta-amyloid-induced neurotoxicity through inhibiting c-Abl/FE65 nuclear translocation and GSK3 beta activation. Neurobiol Aging 30:81-92.
Liogier d'Ardhuy X, Edgin JO, Bouis C, de Sola S, Goeldner C, Kishnani P, Noldeke J, Rice S, Sacco S, Squassante L, Spiridigliozzi G, Visootsak J, Heller J, Khwaja O (2015) Assessment of Cognitive Scales to Examine Memory, Executive Function and Language in Individuals with Down Syndrome: Implications of a 6-month Observational Study. Front Behav Neurosci 9:300.
Liu C, Chan CB, Ye K (2016) 7,8-dihydroxyflavone, a small molecular TrkB agonist, is useful for treating various BDNF-implicated human disorders. Translational neurodegeneration 5:2.
Liu X, Chan C-B, Jang S-W, Pradoldej S, Huang J, He K, Phun LH, France S, Xiao G, Jia Y, Luo HR, Ye K (2010) A synthetic 7,8-dihydroxyflavone derivative promotes neurogenesis and exhibits potent antidepressant effect. Journal of medicinal chemistry 53:8274-8286.
Liu X, Qi Q, Xiao G, Li J, Luo HR, Ye K (2013) O-methylated metabolite of 7,8-dihydroxyflavone activates TrkB receptor and displays antidepressant activity. Pharmacology 91:185-200.
Livingstone N, Hanratty J, McShane R, Macdonald G (2015) Pharmacological interventions for cognitive decline in people with Down syndrome. Cochrane Database Syst Rev CD011546.
Lobaugh NJ, Karaskov V, Rombough V, Rovet J, Bryson S, Greenbaum R, Haslam RH, Koren G (2001) Piracetam therapy does not enhance cognitive functioning in children with down syndrome. Arch Pediatr Adolesc Med 155:442-448.
Lockrow J, Prakasam A, Huang P, Bimonte-Nelson H, Sambamurti K, Granholm AC (2009) Cholinergic degeneration and memory loss delayed by vitamin E in a Down syndrome mouse model. Exp Neurol 216:278-289.
Lockstone HE, Harris LW, Swatton JE, Wayland MT, Holland AJ, Bahn S (2007) Gene expression profiling in the adult Down syndrome brain. Genomics 90:647-660.

Lopez-Hidalgo R, Ballestin R, Vega J, Blasco-Ibanez JM, Crespo C, Gilabert-Juan J, Nacher J, Varea E (2016) Hypocellularity in the Murine Model for Down Syndrome Ts65Dn Is Not Affected by Adult Neurogenesis. Front Neurosci 10:75.

Lorenzi HA, Reeves RH (2006) Hippocampal hypocellularity in the Ts65Dn mouse originates early in development. Brain Res 1104:153-159.

Lott IT (2012) Neurological phenotypes for Down syndrome across the life span. Prog Brain Res 197:101-121.

Lott IT, Dierssen M (2010) Cognitive deficits and associated neurological complications in individuals with Down's syndrome. Lancet Neurol 9:623-633.

Lu HE, Yang YC, Chen SM, Su HL, Huang PC, Tsai MS, Wang TH, Tseng CP, Hwang SM (2013) Modeling neurogenesis impairment in Down syndrome with induced pluripotent stem cells from Trisomy 21 amniotic fluid cells. Exp Cell Res 319:498-505.

Lu J, Lian G, Zhou H, Esposito G, Steardo L, Delli-Bovi LC, Hecht JL, Lu QR, Sheen V (2012) OLIG2 over-expression impairs proliferation of human Down syndrome neural progenitors. Hum Mol Genet 21:2330-2340.

Ly PT, Wu Y, Zou H, Wang R, Zhou W, Kinoshita A, Zhang M, Yang Y, Cai F, Woodgett J, Song W (2013) Inhibition of GSK3beta-mediated BACE1 expression reduces Alzheimer-associated phenotypes. J Clin Invest 123:224-235.

Lysenko LV, Kim J, Henry C, Tyrtyshnaia A, Kohnz RA, Madamba F, Simon GM, Kleschevnikova NE, Nomura DK, Ezekowitz RA, Kleschevnikov AM (2014) Monoacylglycerol lipase inhibitor JZL184 improves behavior and neural properties in Ts65Dn mice, a model of down syndrome. PLoS One 9:e114521.

Machold R, Hayashi S, Rutlin M, Muzumdar MD, Nery S, Corbin JG, Gritli-Linde A, Dellovade T, Porter JA, Rubin LL, Dudek H, McMahon AP, Fishell G (2003) Sonic hedgehog is required for progenitor cell maintenance in telencephalic stem cell niches. Neuron 39:937-950.

Macleod KF, Sherry N, Hannon G, Beach D, Tokino T, Kinzler K, Vogelstein B, Jacks T (1995) p53-dependent and independent expression of p21 during cell growth, differentiation, and DNA damage. Genes Dev 9:935-944.

Malberg JE, Eisch AJ, Nestler EJ, Duman RS (2000) Chronic antidepressant treatment increases neurogenesis in adult rat hippocampus. J Neurosci 20:9104-9110.

Mandel S, Weinreb O, Amit T, Youdim MB (2004) Cell signaling pathways in the neuroprotective actions of the green tea polyphenol (-)-epigallocatechin-3-gallate: implications for neurodegenerative diseases. J Neurochem 88:1555-1569.

Mandel SA, Amit T, Kalfon L, Reznichenko L, Weinreb O, Youdim MB (2008) Cell signaling pathways and iron chelation in the neurorestorative activity of green tea polyphenols: special reference to epigallocatechin gallate (EGCG). J Alzheimers Dis 15:211-222.

Mann DM, Yates PO, Marcyniuk B, Ravindra CR (1985) Pathological evidence for neurotransmitter deficits in Down's syndrome of middle age. J Ment Defic Res 29 (Pt 2):125-135.

Marin-Padilla M (1976) Pyramidal cell abnormalities in the motor cortex of a child with Down's syndrome. A Golgi study. J Comp Neurol 167:63-81.

Martinez-Cue C, Martinez P, Rueda N, Vidal R, Garcia S, Vidal V, Corrales A, Montero JA, Pazos A, Florez J, Gasser R, Thomas AW, Honer M, Knoflach F, Trejo JL, Wettstein JG, Hernandez MC (2013) Reducing GABAA alpha5 receptor-mediated inhibition rescues functional and neuromorphological deficits in a mouse model of down syndrome. J Neurosci 33:3953-3966.

Mazur-Kolecka B, Golabek A, Kida E, Rabe A, Hwang YW, Adayev T, Wegiel J, Flory M, Kaczmarski W, Marchi E, Frackowiak J (2012) Effect of DYRK1A activity inhibition on development of neuronal progenitors isolated from Ts65Dn mice. J Neurosci Res 90:999-1010.

Megias M, Verduga R, Dierssen M, Florez J, Insausti R, Crespo D (1997) Cholinergic, serotonergic and catecholaminergic neurons are not affected in Ts65Dn mice. Neuroreport 8:3475-3478.

Memmi EM, Sanarico AG, Giacobbe A, Peschiaroli A, Frezza V, Cicalese A, Pisati F, Tosoni D, Zhou H, Tonon G, Antonov A, Melino G, Pelicci PG, Bernassola F (2015) p63 Sustains self-renewal of mammary cancer stem cells through regulation of Sonic Hedgehog signaling. Proceedings of the National Academy of Sciences of the United States of America 112:3499-3504.

Meraviglia V, Ulivi AF, Boccazzi M, Valenza F, Fratangeli A, Passafaro M, Lecca D, Stagni F, Giacomini A, Bartesaghi R, Abbracchio MP, Ceruti S, Rosa P (2016) SNX27, a protein involved in down syndrome, regulates GPR17 trafficking and oligodendrocyte differentiation. Glia 64:1437-1460.

Minichiello L (2009) TrkB signalling pathways in LTP and learning. Nat Rev Neurosci 10:850-860.
Mito T, Becker LE (1993) Developmental changes of S-100 protein and glial fibrillary acidic protein in the brain in Down syndrome. Exp Neurol 120:170-176.
Moldrich RX, Dauphinot L, Laffaire J, Vitalis T, Herault Y, Beart PM, Rossier J, Vivien D, Gehrig C, Antonarakis SE, Lyle R, Potier MC (2009) Proliferation deficits and gene expression dysregulation in Down's syndrome (Ts1Cje) neural progenitor cells cultured from neurospheres. J Neurosci Res 87:3143-3152.
Moller RS, Kubart S, Hoeltzenbein M, Heye B, Vogel I, Hansen CP, Menzel C, Ullmann R, Tommerup N, Ropers HH, Tumer Z, Kalscheuer VM (2008) Truncation of the Down syndrome candidate gene DYRK1A in two unrelated patients with microcephaly. Am J Hum Genet 82:1165-1170.
Moon J, Chen M, Gandhy SU, Strawderman M, Levitsky DA, Maclean KN, Strupp BJ (2010) Perinatal choline supplementation improves cognitive functioning and emotion regulation in the Ts65Dn mouse model of Down syndrome. Behav Neurosci 124:346-361.
Murakami N, Bolton D, Hwang YW (2009) Dyrk1A binds to multiple endocytic proteins required for formation of clathrin-coated vesicles. Biochemistry 48:9297-9305. doi: 9210.1021/bi9010557.
Nadel L (2003) Down's syndrome: a genetic disorder in biobehavioral perspective. Genes Brain Behav 2:156-166.
Najas S, Arranz J, Lochhead PA, Ashford AL, Oxley D, Delabar JM, Cook SJ, Barallobre MJ, Arbones ML (2015) DYRK1A-mediated Cyclin D1 Degradation in Neural Stem Cells Contributes to the Neurogenic Cortical Defects in Down Syndrome. EBioMedicine 2:120-134.
Nakano-Kobayashi A, Awaya T, Kii I, Sumida Y, Okuno Y, Yoshida S, Sumida T, Inoue H, Hosoya T, Hagiwara M (2017) Prenatal neurogenesis induction therapy normalizes brain structure and function in Down syndrome mice. Proc Natl Acad Sci U S A 114:10268-10273.
Nalivaeva NN, Turner AJ (2013) The amyloid precursor protein: a biochemical enigma in brain development, function and disease. FEBS Lett 587:2046-2054.
Necchi D, Lomoio S, Scherini E (2008) Axonal abnormalities in cerebellar Purkinje cells of the Ts65Dn mouse. Brain Res 1238:181-188.
Neri G, Opitz JM (2009) Down syndrome: comments and reflections on the 50th anniversary of Lejeune's discovery. Am J Med Genet A 149A:2647-2654.
Netzer WJ, Powell C, Nong Y, Blundell J, Wong L, Duff K, Flajolet M, Greengard P (2010) Lowering beta-amyloid levels rescues learning and memory in a Down syndrome mouse model. PLoS One 5:e10943.
Noble D (2008) Computational models of the heart and their use in assessing the actions of drugs. J Pharmacol Sci 107:107-117.
Nowakowski RS, Lewin SB, Miller MW (1989) Bromodeoxyuridine immunohistochemical determination of the lengths of the cell cycle and the DNA-synthetic phase for an anatomically defined population. J Neurocytol 18:311-318.
O'Doherty A, Ruf S, Mulligan C, Hildreth V, Errington ML, Cooke S, Sesay A, Modino S, Vanes L, Hernandez D, Linehan JM, Sharpe PT, Brandner S, Bliss TV, Henderson DJ, Nizetic D, Tybulewicz VL, Fisher EM (2005) An aneuploid mouse strain carrying human chromosome 21 with Down syndrome phenotypes. Science 309:2033-2037.
Olmos-Serrano JL, Tyler WA, Cabral HJ, Haydar TF (2016) Longitudinal measures of cognition in the Ts65Dn mouse: Refining windows and defining modalities for therapeutic intervention in Down syndrome. Experimental neurology 279:40-56.
Olson LE, Roper RJ, Baxter LL, Carlson EJ, Epstein CJ, Reeves RH (2004) Down syndrome mouse models Ts65Dn, Ts1Cje, and Ms1Cje/Ts65Dn exhibit variable severity of cerebellar phenotypes. Dev Dyn 230:581-589.
Olson LE, Roper RJ, Sengstaken CL, Peterson EA, Aquino V, Galdzicki Z, Siarey R, Pletnikov M, Moran TH, Reeves RH (2007) Trisomy for the Down syndrome 'critical region' is necessary but not sufficient for brain phenotypes of trisomic mice. Hum Mol Genet 16:774-782.
Ortiz-Abalia J, Sahun I, Altafaj X, Andreu N, Estivill X, Dierssen M, Fillat C (2008) Targeting Dyrk1A with AAVshRNA attenuates motor alterations in TgDyrk1A, a mouse model of Down syndrome. Am J Hum Genet 83:479-488.
Papavassiliou P, York TP, Gursoy N, Hill G, Nicely LV, Sundaram U, McClain A, Aggen SH, Eaves L, Riley B, Jackson-Cook C (2009) The phenotype of persons having mosaicism for trisomy 21/Down syndrome reflects the percentage of trisomic cells present in different tissues. Am J Med Genet A 149A:573-583.

Parisotto EB, Vidal V, Garcia-Cerro S, Lantigua S, Wilhelm Filho D, Sanchez-Barcelo EJ, Martinez-Cue C, Rueda N (2016) Chronic Melatonin Administration Reduced Oxidative Damage and Cellular Senescence in the Hippocampus of a Mouse Model of Down Syndrome. Neurochem Res 41:2904-2913.

Park J, Oh Y, Yoo L, Jung MS, Song WJ, Lee SH, Seo H, Chung KC (2010) Dyrk1A phosphorylates p53 and inhibits proliferation of embryonic neuronal cells. J Biol Chem 285:31895-31906.

Park J, Yang EJ, Yoon JH, Chung KC (2007) Dyrk1A overexpression in immortalized hippocampal cells produces the neuropathological features of Down syndrome. Mol Cell Neurosci 36:270-279.

Perez-Cremades D, Hernandez S, Blasco-Ibanez JM, Crespo C, Nacher J, Varea E (2010) Alteration of inhibitory circuits in the somatosensory cortex of Ts65Dn mice, a model for Down's syndrome. J Neural Transm 117:445-455.

Perez-Nunez R, Barraza N, Gonzalez-Jamett A, Cardenas AM, Barnier JV, Caviedes P (2016) Overexpressed Down Syndrome Cell Adhesion Molecule (DSCAM) Deregulates P21-Activated Kinase (PAK) Activity in an In Vitro Neuronal Model of Down Syndrome: Consequences on Cell Process Formation and Extension. Neurotox Res 30:76-87.

Perluigi M, Butterfield DA (2011) The identification of protein biomarkers for oxidative stress in Down syndrome. Expert Rev Proteomics 8:427-429.

Pieper AA, Xie S, Capota E, Estill SJ, Zhong J, Long JM, Becker GL, Huntington P, Goldman SE, Shen CH, Capota M, Britt JK, Kotti T, Ure K, Brat DJ, Williams NS, MacMillan KS, Naidoo J, Melito L, Hsieh J, De Brabander J, Ready JM, McKnight SL (2010) Discovery of a proneurogenic, neuroprotective chemical. Cell 142:39-51.

Pinter JD, Brown WE, Eliez S, Schmitt JE, Capone GT, Reiss AL (2001a) Amygdala and hippocampal volumes in children with Down syndrome: a high-resolution MRI study. Neurology 56:972-974.

Pinter JD, Eliez S, Schmitt JE, Capone GT, Reiss AL (2001b) Neuroanatomy of Down's syndrome: a high-resolution MRI study. Am J Psychiatry 158:1659-1665.

Pollonini G, Gao V, Rabe A, Palminiello S, Albertini G, Alberini CM (2008) Abnormal expression of synaptic proteins and neurotrophin-3 in the Down syndrome mouse model Ts65Dn. Neuroscience 156:99-106.

Pons-Espinal M, Martinez de Lagran M, Dierssen M (2013) Environmental enrichment rescues DYRK1A activity and hippocampal adult neurogenesis in TgDyrk1A. Neurobiol Dis 60:18-31.

Popov VI, Kleschevnikov AM, Klimenko OA, Stewart MG, Belichenko PV (2011) Three-dimensional synaptic ultrastructure in the dentate gyrus and hippocampal area CA3 in the Ts65Dn mouse model of down syndrome. J Comp Neurol 519:1338-1354.

Priller C, Bauer T, Mitteregger G, Krebs B, Kretzschmar HA, Herms J (2006) Synapse formation and function is modulated by the amyloid precursor protein. J Neurosci 26:7212-7221.

Rachidi M, Lopes C (2008) Mental retardation and associated neurological dysfunctions in Down syndrome: a consequence of dysregulation in critical chromosome 21 genes and associated molecular pathways. Eur J Paediatr Neurol 12:168-182.

Rafii MS, Skotko BG, McDonough ME, Pulsifer M, Evans C, Doran E, Muranevici G, Kesslak P, Abushakra S, Lott IT, Group EDS (2017) A Randomized, Double-Blind, Placebo-Controlled, Phase II Study of Oral ELND005 (scyllo-Inositol) in Young Adults with Down Syndrome without Dementia. J Alzheimers Dis 58:401-411.

Raz N, Torres IJ, Briggs SD, Spencer WD, Thornton AE, Loken WJ, Gunning FM, McQuain JD, Driesen NR, Acker JD (1995) Selective neuroanatomic abnormalities in Down's syndrome and their cognitive correlates: evidence from MRI morphometry. Neurology 45:356-366.

Reeves R (1995) A mouse model for Down syndrome exhibits learning and behaviour deficits. Nat Genet 11:177-184.

Reinholdt LG, Ding Y, Gilbert GJ, Czechanski A, Solzak JP, Roper RJ, Johnson MT, Donahue LR, Lutz C, Davisson MT (2011) Molecular characterization of the translocation breakpoints in the Down syndrome mouse model Ts65Dn. Mamm Genome 22:685-691.

Rice D, Barone S (2010) Critical periods of vulnerabiliy for the developing nervpus system: evidence from humans and animal models. Environ Health Perspect 108, Suppl 3:511-533.

Risser D, Lubec G, Cairns N, Herrera-Marschitz M (1997) Excitatory amino acids and monoamines in parahippocampal gyrus and frontal cortical pole of adults with Down syndrome. Life Sci 60:1231-1237.

Rodrigues J, Assuncao M, Lukoyanov N, Cardoso A, Carvalho F, Andrade JP (2013) Protective effects of a catechin-rich extract on the hippocampal formation and spatial memory in aging rats. Behav Brain Res 246:94-102.

Roncace V, Burattini C, Stagni F, Guidi S, Giacomini A, Emili M, Aicardi G, Bartesaghi R (2017) Neuroanatomical alterations and synaptic plasticity impairment in the perirhinal cortex of the Ts65Dn mouse model of Down syndrome. Neurobiol Dis 106:89-100.

Roper RJ, Baxter LL, Saran NG, Klinedinst DK, Beachy PA, Reeves RH (2006) Defective cerebellar response to mitogenic Hedgehog signaling in Down [corrected] syndrome mice. Proc Natl Acad Sci U S A 103:1452-1456.

Roper RJ, Reeves RH (2006) Understanding the basis for Down syndrome phenotypes. PLoS Genet 2:e50.

Roper RJ, VanHorn JF, Cain CC, Reeves RH (2009) A neural crest deficit in Down syndrome mice is associated with deficient mitotic response to Sonic hedgehog. Mech Dev 126:212-219.

Rose CR, Blum R, Pichler B, Lepier A, Kafitz KW, Konnerth A (2003) Truncated TrkB-T1 mediates neurotrophin-evoked calcium signalling in glia cells. Nature 426:74-78.

Rotmensch S, Goldstein I, Liberati M, Shalev J, Ben-Rafael Z, Copel JA (1997) Fetal transcerebellar diameter in Down syndrome. Obstet Gynecol 89:534-537.

Rozier RG, Sutton BK, Bawden JW, Haupt K, Slade GD, King RS (2003) Prevention of early childhood caries in North Carolina medical practices: implications for research and practice. J Dent Educ 67:876-885.

Ruan H, Yang Y, Zhu X, Wang X, Chen R (2009) Neuroprotective effects of (+/-)-catechin against 1-methyl-4-phenyl-1,2,3,6-tetrahydropyridine (MPTP)-induced dopaminergic neurotoxicity in mice. Neurosci Lett 450:152-157.

Rueda N, Florez J, Martinez-Cue C (2008a) Chronic pentylenetetrazole but not donepezil treatment rescues spatial cognition in Ts65Dn mice, a model for Down syndrome. Neurosci Lett 433:22-27.

Rueda N, Florez J, Martinez-Cue C (2008b) Effects of chronic administration of SGS-111 during adulthood and during the pre- and post-natal periods on the cognitive deficits of Ts65Dn mice, a model of Down syndrome. Behav Brain Res 188:355-367.

Rueda N, Florez J, Martinez-Cue C (2012) Mouse models of Down syndrome as a tool to unravel the causes of mental disabilities. Neural Plast 2012:584071.

Rueda N, Llorens-Martin M, Florez J, Valdizan E, Banerjee P, Trejo JL, Martinez-Cue C (2010) Memantine normalizes several phenotypic features in the Ts65Dn mouse model of Down syndrome. J Alzheimers Dis 21:277-290.

Rui Y, Myers KR, Yu K, Wise A, De Blas AL, Hartzell HC, Zheng JQ (2013) Activity-dependent regulation of dendritic growth and maintenance by glycogen synthase kinase 3beta. Nat Commun 4:2628.

Ruparelia A, Pearn ML, Mobley WC (2013) Aging and intellectual disability: insights from mouse models of Down syndrome. Dev Disabil Res Rev 18:43-50.

Russo C, Salis S, Dolcini V, Venezia V, Song XH, Teller JK, Schettini G (2001) Amino-terminal modification and tyrosine phosphorylation of [corrected] carboxy-terminal fragments of the amyloid precursor protein in Alzheimer's disease and Down's syndrome brain. Neurobiol Dis 8:173-180.

Sago H, Carlson EJ, Smith DJ, Kilbridge J, Rubin EM, Mobley WC, Epstein CJ, Huang TT (1998) Ts1Cje, a partial trisomy 16 mouse model for Down syndrome, exhibits learning and behavioral abnormalities. Proc Natl Acad Sci U S A 95:6256-6261.

Sago H, Carlson EJ, Smith DJ, Rubin EM, Crnic LS, Huang TT, Epstein CJ (2000) Genetic dissection of region associated with behavioral abnormalities in mouse models for Down syndrome. Pediatr Res 48:606-613.

Salehi A, Faizi M, Colas D, Valletta J, Laguna J, Takimoto-Kimura R, Kleschevnikov A, Wagner SL, Aisen P, Shamloo M, Mobley WC (2009) Restoration of norepinephrine-modulated contextual memory in a mouse model of Down syndrome. Sci Transl Med 1:7ra17.

Schmidt-Sidor B, Wisniewski KE, Shepard TH, Sersen EA (1990) Brain growth in Down syndrome subjects 15 to 22 weeks of gestational age and birth to 60 months. Clin Neuropathol 9:181-190.

Scholzen T, Gerdes J (2000) The Ki-67 protein: from the known and the unknown. J Cell Physiol 182:311-322.

Schroeter H, Bahia P, Spencer JP, Sheppard O, Rattray M, Cadenas E, Rice-Evans C, Williams RJ (2007) (-)Epicatechin stimulates ERK-dependent cyclic AMP response element activity and up-regulates GluR2 in cortical neurons. J Neurochem 101:1596-1606. Epub 2007 Feb 1597.

Schulz E, Scholz B (1992) [Neurohistological findings in the parietal cortex of children with chromosome aberrations]. J Hirnforsch 33:37-62.

Scott-McKean JJ, Costa AC (2011) Exaggerated NMDA mediated LTD in a mouse model of Down syndrome and pharmacological rescuing by memantine. Learn Mem 18:774-778.
Seress L, Abraham H, Tornoczky T, Kosztolanyi G (2001) Cell formation in the human hippocampal formation from mid-gestation to the late postnatal period. Neuroscience 105:831-843.
Severi S, Guidi S, Ciani E, Bartesaghi R (2005) Sex differences in the stereological parameters of the hippocampal dentate gyrus of the guinea-pig before puberty. Neuroscience 132:375-387.
Shapiro BL (1997) Whither Down syndrome critical regions? Hum Genet 99:421-423.
Shichiri M, Yoshida Y, Ishida N, Hagihara Y, Iwahashi H, Tamai H, Niki E (2011) Alpha-Tocopherol suppresses lipid peroxidation and behavioral and cognitive impairments in the Ts65Dn mouse model of Down syndrome. Free Radic Biol Med 50:1801-1811.
Shim KS, Lubec G (2002) Drebrin, a dendritic spine protein, is manifold decreased in brains of patients with Alzheimer's disease and Down syndrome. Neurosci Lett 324:209-212.
Siarey RJ, Carlson EJ, Epstein CJ, Balbo A, Rapoport SI, Galdzicki Z (1999) Increased synaptic depression in the Ts65Dn mouse, a model for mental retardation in Down syndrome. Neuropharmacology 38:1917-1920.
Sillitoe RV, Joyner AL (2007) Morphology, molecular codes, and circuitry produce the three-dimensional complexity of the cerebellum. Annu Rev Cell Dev Biol 23:549-577.
Smigielska-Kuzia J, Bockowski L, Sobaniec W, Sendrowski K, Olchowik B, Cholewa M, Lukasiewicz A, Lebkowska U (2011) A volumetric magnetic resonance imaging study of brain structures in children with Down syndrome. Neurologia i neurochirurgia polska 45:363-369.
Soppa U, Schumacher J, Florencio Ortiz V, Pasqualon T, Tejedor FJ, Becker W (2014) The Down syndrome-related protein kinase DYRK1A phosphorylates p27(Kip1) and Cyclin D1 and induces cell cycle exit and neuronal differentiation. Cell Cycle 13:2084-2100.
Souchet B, Guedj F, Penke-Verdier Z, Daubigney F, Duchon A, Herault Y, Bizot JC, Janel N, Creau N, Delatour B, Delabar JM (2015) Pharmacological correction of excitation/inhibition imbalance in Down syndrome mouse models. Front Behav Neurosci 9:267.
Spencer JP (2009) The impact of flavonoids on memory: physiological and molecular considerations. Chem Soc Rev 38:1152-1161. doi: 1110.1039/b800422f. Epub 802009 Jan 800420.
Spiridigliozzi GA, Hart SJ, Heller JH, Schneider HE, Baker JA, Weadon C, Capone GT, Kishnani PS (2016) Safety and efficacy of rivastigmine in children with Down syndrome: A double blind placebo controlled trial. Am J Med Genet A 170:1545-1555.
Stagni F, Giacomini A, Emili M, Guidi S, Bartesaghi R (2017) Neurogenesis impairment: An early developmental defect in Down syndrome. Free Radic Biol Med.
Stagni F, Giacomini A, Emili M, Trazzi S, Guidi S, Sassi M, Ciani E, Rimondini R, Bartesaghi R (2016) Short- and long-term effects of neonatal pharmacotherapy with epigallocatechin-3-gallate on hippocampal development in the Ts65Dn mouse model of Down syndrome. Neuroscience 333:277-301.
Stagni F, Giacomini A, Guidi S, Ciani E, Bartesaghi R (2015a) Timing of therapies for Down syndrome: the sooner, the better. Front Behav Neurosci 9:265.
Stagni F, Giacomini A, Guidi S, Ciani E, Ragazzi E, Filonzi M, De Iasio R, Rimondini R, Bartesaghi R (2015b) Long-term effects of neonatal treatment with fluoxetine on cognitive performance in Ts65Dn mice. Neurobiol Dis 74C:204-218.
Stagni F, Magistretti J, Guidi S, Ciani E, Mangano C, Calza L, Bartesaghi R (2013) Pharmacotherapy with Fluoxetine Restores Functional Connectivity from the Dentate Gyrus to Field CA3 in the Ts65Dn Mouse Model of Down Syndrome. PLoS One 8:e61689.
Starbuck JM, Dutka T, Ratliff TS, Reeves RH, Richtsmeier JT (2014) Overlapping trisomies for human chromosome 21 orthologs produce similar effects on skull and brain morphology of Dp(16)1Yey and Ts65Dn mice. Am J Med Genet A 164A:1981-1990.
Stern Y (2012) Cognitive reserve in ageing and Alzheimer's disease. Lancet Neurol 11:1006-1012.
Stiles J, Jernigan TL (2010) The basics of brain development. Neuropsychol Rev 20:327-348.
Stringer M, Abeysekera I, Dria KJ, Roper RJ, Goodlett CR (2015a) Low dose EGCG treatment beginning in adolescence does not improve cognitive impairment in a Down syndrome mouse model. Pharmacol Biochem Behav.
Stringer ME, Abeysekera I, Roper RJ, Goodlett CR (2015b) Deficits in a radial-arm maze spatial pattern separation task in a mouse model for Down Syndrome. Program No 68102 2015 Neuroscience Meeting Planner, Washington, DC: Society for Neuroscience, 2015 Online.

Sudarov A, Joyner AL (2007) Cerebellum morphogenesis: the foliation pattern is orchestrated by multi-cellular anchoring centers. Neural Dev 2:26.

Suetsugu M, Mehraein P (1980) Spine distribution along the apical dendrites of the pyramidal neurons in Down's syndrome. A quantitative Golgi study. Acta Neuropathol 50:207-210.

Suzuki S, Numakawa T, Shimazu K, Koshimizu H, Hara T, Hatanaka H, Mei L, Lu B, Kojima M (2004) BDNF-induced recruitment of TrkB receptor into neuronal lipid rafts: roles in synaptic modulation. J Cell Biol 167:1205-1215.

Sylvester PE (1983) The hippocampus in Down's syndrome. J Ment Defic Res 27 (Pt 3):227-236.

Takahashi-Yanaga F, Sasaguri T (2008) GSK-3beta regulates cyclin D1 expression: a new target for chemotherapy. Cell Signal 20:581-589.

Takashima S, Becker LE, Armstrong DL, Chan F (1981) Abnormal neuronal development in the visual cortex of the human fetus and infant with down's syndrome. A quantitative and qualitative Golgi study. Brain Res 225:1-21.

Takashima S, Ieshima A, Nakamura H, Becker LE (1989) Dendrites, dementia and the Down syndrome. Brain Dev 11:131-133.

Takizawa CG, Morgan DO (2000) Control of mitosis by changes in the subcellular location of cyclin-B1-Cdk1 and Cdc25C. Curr Opin Cell Biol 12:658-665.

Tanzi RE, Gusella JF, Watkins PC, Bruns GA, St George-Hyslop P, Van Keuren ML, Patterson D, Pagan S, Kurnit DM, Neve RL (1987) Amyloid beta protein gene: cDNA, mRNA distribution, and genetic linkage near the Alzheimer locus. Science (New York, N Y) 235:880-884.

Teipel SJ, Hampel H (2006) Neuroanatomy of Down syndrome in vivo: a model of preclinical Alzheimer's disease. Behav Genet 36:405-415.

ten Donkelaar HJ, Lammens M, Wesseling P, Thijssen HO, Renier WO (2003) Development and developmental disorders of the human cerebellum. J Neurol 250:1025-1036.

Tesla R, Wolf HP, Xu P, Drawbridge J, Estill SJ, Huntington P, McDaniel L, Knobbe W, Burket A, Tran S, Starwalt R, Morlock L, Naidoo J, Williams NS, Ready JM, McKnight SL, Pieper AA (2012) Neuroprotective efficacy of aminopropyl carbazoles in a mouse model of amyotrophic lateral sclerosis. Proc Natl Acad Sci U S A 109:17016-17021.

Thomazeau A, Lassalle O, Iafrati J, Souchet B, Guedj F, Janel N, Chavis P, Delabar J, Manzoni OJ (2014) Prefrontal deficits in a murine model overexpressing the down syndrome candidate gene dyrk1a. J Neurosci 34:1138-1147.

Toiber D, Azkona G, Ben-Ari S, Toran N, Soreq H, Dierssen M (2010) Engineering DYRK1A overdosage yields Down syndrome-characteristic cortical splicing aberrations. Neurobiol Dis 40:348-359.

Tozuka Y, Fukuda S, Namba T, Seki T, Hisatsune T (2005) GABAergic excitation promotes neuronal differentiation in adult hippocampal progenitor cells. Neuron 47:803-815.

Trazzi S, Fuchs C, De Franceschi M, Mitrugno V, Bartesaghi R, Ciani E (2014) APP-dependent alteration of GSK3ß activity impairs neurogenesis in the Ts65Dn mouse model of Down syndrome. Neurobiol Dis doi: 10.1016/j.nbd.2014.03.003. [Epub ahead of print].

Trazzi S, Fuchs C, Valli E, Perini G, Bartesaghi R, Ciani E (2013) The amyloid precursor protein (APP) triplicated gene impairs neuronal precursor differentiation and neurite development through two different domains in the Ts65Dn mouse model for Down syndrome. J Biol Chem 288:20817-20829.

Trazzi S, Mitrugno VM, Valli E, Fuchs C, Rizzi S, Guidi S, Perini G, Bartesaghi R, Ciani E (2011) APP-dependent up-regulation of Ptch1 underlies proliferation impairment of neural precursors in Down syndrome. Hum Mol Genet 20:1560-1573.

Tsai T, Klausmeyer A, Conrad R, Gottschling C, Leo M, Faissner A, Wiese S (2013) 7,8-Dihydroxyflavone leads to survival of cultured embryonic motoneurons by activating intracellular signaling pathways. Mol Cell Neurosci 56:18-28.

Turner BJ, Lopes EC, Cheema SS (2003) The serotonin precursor 5-hydroxytryptophan delays neuromuscular disease in murine familial amyotrophic lateral sclerosis. Amyotroph Lateral Scler Other Motor Neuron Disord 4:171-176.

Vacca RA, Valenti D, Caccamese S, Daglia M, Braidy N, Nabavi SM (2016) Plant polyphenols as natural drugs for the management of Down syndrome and related disorders. Neurosci Biobehav Rev 71:865-877.

Vacik T, Ort M, Gregorova S, Strnad P, Blatny R, Conte N, Bradley A, Bures J, Forejt J (2005) Segmental trisomy of chromosome 17: a mouse model of human aneuploidy syndromes. Proc Natl Acad Sci U S A 102:4500-4505.

Valenti D, de Bari L, de Rasmo D, Signorile A, Henrion-Caude A, Contestabile A, Vacca RA (2016) The polyphenols resveratrol and epigallocatechin-3-gallate restore the severe impairment of mitochondria in hippocampal progenitor cells from a Down syndrome mouse model. Biochim Biophys Acta 1862:1093-1104.

Vazey EM, Aston-Jones G (2014) Designer receptor manipulations reveal a role of the locus coeruleus noradrenergic system in isoflurane general anesthesia. Proc Natl Acad Sci U S A 111:3859-3864.

Velazquez R, Ash JA, Powers BE, Kelley CM, Strawderman M, Luscher ZI, Ginsberg SD, Mufson EJ, Strupp BJ (2013) Maternal choline supplementation improves spatial learning and adult hippocampal neurogenesis in the Ts65Dn mouse model of Down syndrome. Neurobiol Dis 58:92-101.

Vicari S (2006) Motor development and neuropsychological patterns in persons with Down syndrome. Behav Genet 36:355-364.

Vicari S, Bellucci S, Carlesimo GA (2000) Implicit and explicit memory: a functional dissociation in persons with Down syndrome. Neuropsychologia 38:240-251.

Vilar M, Mira H (2016) Regulation of Neurogenesis by Neurotrophins during Adulthood: Expected and Unexpected Roles. Frontiers in neuroscience 10:26.

Villar AJ, Belichenko PV, Gillespie AM, Kozy HM, Mobley WC, Epstein CJ (2005) Identification and characterization of a new Down syndrome model, Ts[Rb(12.1716)]2Cje, resulting from a spontaneous Robertsonian fusion between T(171)65Dn and mouse chromosome 12. Mamm Genome 16:79-90.

Villarroya O, Ballestin R, Lopez-Hidalgo R, Mulet M, Blasco-Ibanez JM, Crespo C, Nacher J, Gilabert-Juan J, Varea E (2017) Morphological alterations in the hippocampus of the Ts65Dn mouse model for Down Syndrome correlate with structural plasticity markers. Histol Histopathol 11894.

von Rotz RC, Kohli BM, Bosset J, Meier M, Suzuki T, Nitsch RM, Konietzko U (2004) The APP intracellular domain forms nuclear multiprotein complexes and regulates the transcription of its own precursor. J Cell Sci 117:4435-4448.

Vorhees CV, Williams MT (2006) Morris water maze: procedures for assessing spatial and related forms of learning and memory. Nat Protoc 1:848-858.

Vuksic M, Petanjek Z, Rasin MR, Kostovic I (2002) Perinatal growth of prefrontal layer III pyramids in Down syndrome. Pediatr Neurol 27:36-38.

Wang MH, Chang WJ, Soung HS, Chang KC (2012) (-)-Epigallocatechin-3-gallate decreases the impairment in learning and memory in spontaneous hypertension rats. Behav Pharmacol 23:771-780.

Weis S, Weber G, Neuhold A, Rett A (1991) Down syndrome: MR quantification of brain structures and comparison with normal control subjects. AJNR Am J Neuroradiol 12:1207-1211.

Weitzdoerfer R, Dierssen M, Fountoulakis M, Lubec G (2001) Fetal life in Down syndrome starts with normal neuronal density but impaired dendritic spines and synaptosomal structure. J Neural Transm Suppl 61:59-70.

West MJ, Gundersen HJ (1990) Unbiased stereological estimation of the number of neurons in the human hippocampus. J Comp Neurol 296:1-22.

Whitaker-Azmitia PM (2001) Serotonin and brain development: role in human developmental diseases. Brain Res Bull 56:479-485.

Winter TC, Ostrovsky AA, Komarniski CA, Uhrich SB (2000) Cerebellar and frontal lobe hypoplasia in fetuses with trisomy 21: usefulness as combined US markers. Radiology 214:533-538.

Wiseman FK, Alford KA, Tybulewicz VL, Fisher EM (2009) Down syndrome--recent progress and future prospects. Hum Mol Genet 18:R75-83.

Wisniewski KE (1990) Down syndrome children often have brain with maturation delay, retardation of growth, and cortical dysgenesis. Am J Med Genet Suppl 7:274-281.

Wisniewski KE, Schmidt-Sidor B (1989) Postnatal delay of myelin formation in brains from Down syndrome infants and children. Clin Neuropathol 8:55-62.

Workman AD, Charvet CJ, Clancy B, Darlington RB, Finlay BL (2013) Modeling transformations of neurodevelopmental sequences across mammalian species. The Journal of neuroscience : the official journal of the Society for Neuroscience 33:7368-7383.

Xavier AC, Taub JW (2010) Acute leukemia in children with Down syndrome. Haematologica 95:1043-1045.

Xie W, Ramakrishna N, Wieraszko A, Hwang YW (2008) Promotion of neuronal plasticity by (-)-epigallocatechin-3-gallate. Neurochem Res 33:776-783.

Yang EJ, Ahn YS, Chung KC (2001) Protein kinase Dyrk1 activates cAMP response element-binding protein during neuronal differentiation in hippocampal progenitor cells. J Biol Chem 276:39819-39824.

Yu T, Li Z, Jia Z, Clapcote SJ, Liu C, Li S, Asrar S, Pao A, Chen R, Fan N, Carattini-Rivera S, Bechard AR, Spring S, Henkelman RM, Stoica G, Matsui S, Nowak NJ, Roder JC, Chen C, Bradley A, Yu YE (2010a) A mouse model of Down syndrome trisomic for all human chromosome 21 syntenic regions. Hum Mol Genet 19:2780-2791.

Yu T, Liu C, Belichenko P, Clapcote SJ, Li S, Pao A, Kleschevnikov A, Bechard AR, Asrar S, Chen R, Fan N, Zhou Z, Jia Z, Chen C, Roder JC, Liu B, Baldini A, Mobley WC, Yu YE (2010b) Effects of individual segmental trisomies of human chromosome 21 syntenic regions on hippocampal long-term potentiation and cognitive behaviors in mice. Brain Res 1366:162-171.

Zeng Y, Liu Y, Wu M, Liu J, Hu Q (2012) Activation of TrkB by 7,8-dihydroxyflavone prevents fear memory defects and facilitates amygdalar synaptic plasticity in aging. J Alzheimers Dis 31:765-778.

Zhang L, Meng K, Jiang X, Liu C, Pao A, Belichenko PV, Kleschevnikov AM, Josselyn S, Liang P, Ye P, Mobley WC, Yu YE (2014) Human chromosome 21 orthologous region on mouse chromosome 17 is a major determinant of Down syndrome-related developmental cognitive deficits. Hum Mol Genet 23:578-589.

Zhou F, Gong K, Song B, Ma T, van Laar T, Gong Y, Zhang L (2012) The APP intracellular domain (AICD) inhibits Wnt signalling and promotes neurite outgrowth. Biochim Biophys Acta 1823:1233-1241.